Effects of electrical stimulation by cochlear implants on residual acoustic hearing

Attila Fráter

A thesis submitted for the degree of Doctor of Philosophy

UCL Ear Institute

University College London

June 2019

I, Attila Frater confirm that the work presented in this thesis is my own. Where information has been derived from other sources, I confirm that this has been indicated in the thesis.

Abstract

The objective of the project is the investigation of the mechanical changes and acoustic-electric interactions in the cochlea with an implanted cochlear prosthesis to aid stimulation strategy design and propose techniques for detecting those interactions in users of cochlear implants (CI) with residual hearing, benefitting from electro acoustic stimulation (EAS) strategies.

The effects of a CI electrode, inserted into the scala tympani, on the travelling wave are investigated by a modelling study. A three-dimensional finite element box model of the cochlea with an inserted CI is implemented and the changes in the travelling wave due to the CI electrode are examined while varying the parameters of the implant and its location. Attenuation and basal shift of the travelling wave peak was minimal under conditions where the electrode was not in the region of the travelling wave peak.

Acoustic-electric interactions in the hearing cochlea are explored via in vivo physiology studies. A first set of experiments were conducted to establish a link between the electrophonic response and the electrically evoked otoacoustic emissions (EEOAE). Indications for a possible connection were found. A second set of experiments were carried out to investigate the interaction between electrophonic and acoustic response. A beating phenomenon between the electrophonic response and an acoustic pure tone evoked response was shown and, additionally, a modulation of the direct electric response due to the acoustic stimulus was revealed.

Findings of the modelling study may be considered for acoustic stimulation design in EAS CIs. Results of the electrophysiological studies point towards the application of EEOAEs and the beating phenomenon as non-invasive clinical tests to detect electrophonic response in humans. In addition, a diagnostic test is proposed to reveal the effect that acoustic stimulation might have on the direct electric stimulation that might produce unwanted distortion of the desired electric responses.

Impact Statement

Cochlear implants (CI) are arguably the most successful sensory prosthetic devices today that provide hearing sensation to deaf people. Recent advantages in surgical techniques and novel electrode array designs extend the eligibility of recipients to patients with a residual low frequency hearing. Patients with residual hearing are stimulated by acoustic and electric signals simultaneously and the interaction of these modalities have a crucial impact on the perception of sounds.

The first part of the present research investigated the passive mechanical effect of the presence of a CI in the scala tympani on the acoustic travelling wave via a finite element modelling study. Results demonstrated that the acoustic travelling may be altered due to the foreign object within the cochlear duct. The findings of this study, that were presented in scientific conferences and communicated to the industry, may aid the design of future CI electrode arrays as well as the development of speech processing strategies for hybrid devices.

The second part of the work examined the interaction of acoustic and electric stimulation with a focus on a method development for detecting the presence of electrophonic responses in a hearing cochlea by using various physiological methodologies. Electrophonic responses are likely to have a negative impact on hybrid devices, as they might interact with the residual hearing of their users. The results were disseminated in several conferences, within the UK and across the globe, and discussed with experts from the cochlear implant industry. In a first approach, electrophonic responses were attempted to be linked to electrically evoked otoacoustic emissions (EEOAE), which can be measured non-invasively with a probe microphone in the ear canal and could serve as an objective tool to indicate the presence of electrophonic responses in CI users. Results have shown a somewhat unexpected weak relationship between EEOAEs and electrophonics that offers a great possibility to investigate these phenomena further in the future. The second approach demonstrated a possible beating effect between electrophonic and acoustic responses. This acousto-electric beat may be perceived by CI users with residual hearing hence, may be applied as a non-invasive tool for detecting electrophonic responses in humans. Furthermore, an interaction of a low frequency acoustic travelling wave with the electric stimulation was also discovered, which has a possible impact on hybrid CI users, who usually require highly amplified acoustic stimulation. Thus, its detection is of utmost importance, and the proposed test, again based on a perceptual beating effect, might be developed into a non-invasive diagnostic tool to identify such interaction.

Acknowledgements

First and foremost, I would like to thank my principal supervisor Torsten Marquardt for all his help during the years of my PhD. I am grateful for having the opportunity to work under your guidance. I could have not asked for a better mentor and I am truly looking forward to collaborating with you in the future.

I would like to thank Oticon Medical for partly funding my studies. Many thanks to Søren Riis and Patrick Maas, my external supervisors, who kept continuous interest in my research and always gave invaluable feedback on my work.

I am thankful for having been part of the Ear Institute at UCL, an exceptionally inspiring working environment. In the initial stage of my project, I had the possibility to conduct a cochlear modelling study, in which Daniel Zackon gave a great help and was always open to fruitful discussions. Soon my interest shifted to physiological experimentation and learnt the basic surgical skills from Lucy Anderson, I will always be thankful for her immense help. I must also thank Nick Lesica, who not only allowed me to work under his project licence, but when needed, also provided equipment for my research. I am grateful for the guidance of Jonathan Ashmore, Andy Forge and Dan Jagger in experimental pharmacology. Ultimately, I would like to thank Debi Vickers for giving me the opportunity to present my results at Improving Cochlear Implant Performance meetings.

I would like to thank my viva examiners, Jennifer Linden and Waldo Nogueira, for taking time reading this thesis. I hope you find it intriguing and we will have a great discussion.

Of course, the past four years would have not been possible without my friends and family. Thank you for always standing by my side and for your continuous support.

Table of contents

List of figures

List of tables

Introduction

Among the human sensory systems, the system of hearing amazes by its extreme capabilities. The huge dynamic range of hearing allows us to perceive sounds as faint as the rattle of leaves in a breeze and as loud as a rocket launch. Sounds are also processed over a wide spectral range. During the solo performance of a drummer, we can both appreciate the deep thundering sound of the bass drum as well as the high, cutting tone of the tiny splash cymbals. In addition to the vast range in loudness and spectrum, the precision of the auditory system also makes it possible to sense the miniscule differences in both sound intensity and frequency.

Hearing also evolved to differentiate sounds coming from various directions, an essential capability for everyday life. The fast and accurate localization of sounds helped our ancestors to identify danger in good time and today helps us e.g. to direct our attention on the scene in the theatre. The separation of important parts of a sound scape is also effortless for the normal hearing. Recognition of the voice of a friend in a crowd or paying attention to someone during the babble of a group discussion is natural and comes without additional effort.

1 The ear

To be able to achieve these astonishing properties, nature constructed an intricate and complex organ pair, our ears. Pressure waves generated by a sound source are arriving at the observer to be captured by the pinna, the entering points to the external most stage of the auditory system, the outer ear. The pinna guides the pressure waves to the ear canal that ends at the tympanic membrane. The pressure wave generated vibrations of the tympanic membrane continue their way into the middle ear in the form of structural vibrations along the chain of the three small ossicles, the malleus, incus and stapes. The footplate of the stapes abuts the oval window, an opening to the inner ear, the cochlea. The main components of the ear, aiding the propagation of a sound from its source to the inner ear, are illustrated in Figure 1.1.

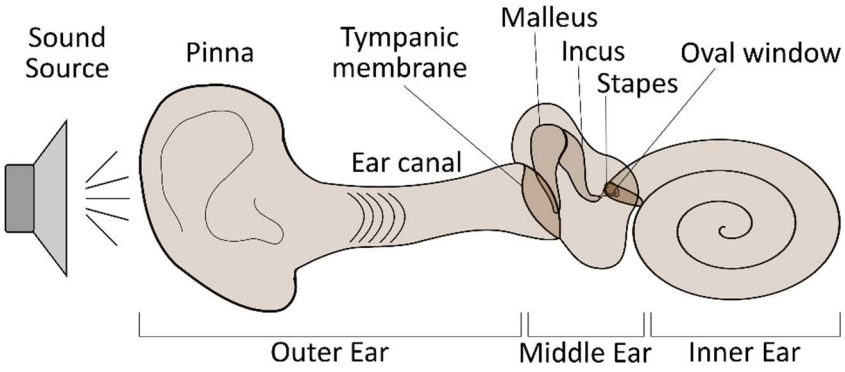

Figure 1.1 Propagation of sound from a sound source to the inner ear.

The cochlea is a spiralling structure that consists of fluid filled ducts, the scala tympani, the scala vestibuli and the scala media. These ducts are following the spiral of the cochlea and are separated by membranes. The scala vestibuli and media are separated by the Reissner's membrane and the scala media is separated by the basilar membrane from the scala tympani. The scala tympani and scala vestibuli are joined at the apex of the cochlea by the helicotrema and filled by the sodium rich fluid, the perilymph. The scala media is filled by the potassium rich endolymph and exhibits an approximately +80 mV potential compared to the perilymph [Békésy, 1952].

The oval window is an opening to the scala vestibuli and its vibration generates a pressure wave in the perilymph that results in a frequency specific travelling wave along the basilar membrane that was first observed by Békésy György [Békésy, 1928, 1960]. The fluid pressure is released at the round window, an opening on the cochlear wall to the scala tympani at the cochlear base, so that the cochlea is actually not compressed, but displaces the basilar membrane. Figure 1.2 illustrates the uncoiled cochlea with the travelling wave on the basilar membrane.

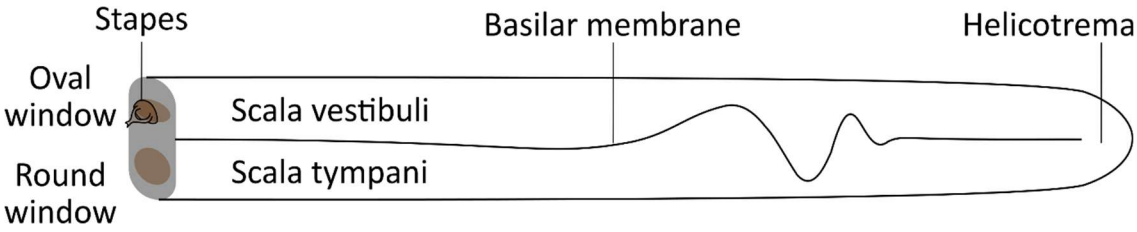

Figure 1.2 Schematic of the uncoiled cochlea and the travelling wave on the basilar membrane.

On top of the basilar membrane lies a highly organized structure of cells, the Organ of Corti, as illustrated in Figure 1.3. The Organ of Corti is the home of the sensory cells, the hair cells. The hair cells are sheltered by the tectorial membrane and can be separated into two distinct types, the inner and outer hair cells. These cells share common morphological properties, such as consisting of a cell body with a bundle of stereocilia on its apical surface. However, their role is different. The inner hair cells are organized in a single row along the cochlea and serve as the primary input to the afferent auditory

nerves, which innervate the basal end of these cells. The outer hair cells are organized in 3 rows and act as the active amplifier of the cochlea, playing a major role in shaping the sensory input [Dallos, 1992]. Outer hair cells are mainly innervated by efferent nerve fibres.

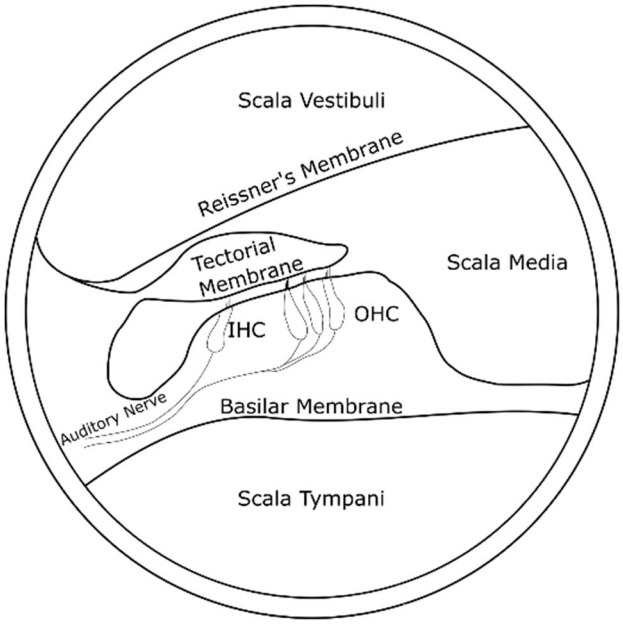

Figure 1.3 Cochlear cross-section illustrating the Organ of Corti on top of the basilar membrane.

The travelling wave along the basilar membrane results in the deflection of hair cell stereocilia. The deflection of hair cell stereocilia results in the membrane potential change of the cell as shown in Figure 1.4 [Hudspeth & Corey, 1977]. The depolarisation of an inner hair cell can cause a release of vesicles into the synaptic cleft at the base of the cell. A vesicle at the afferent auditory nerve's peripheral synapse triggers an action potential, a voltage discharge that propagates through the nerve and serves as a communication signal towards the brain.

The auditory nerves project to the cochlear nucleus from which the auditory information is transferred directly or through the superior olivary complex to the inferior colliculus (IC). The IC consists of distinct parts, such as the central nucleus of the IC (ICC), the dorsal cortex and the external nucleus. The IC is mostly excited by contralateral sounds and only the ICC is organized tonotopically in a dorsoventral direction for low to high frequencies. From the IC, the auditory pathway continues to the medial geniculate body in the thalamus and eventually information is transferred to the auditory cortex.

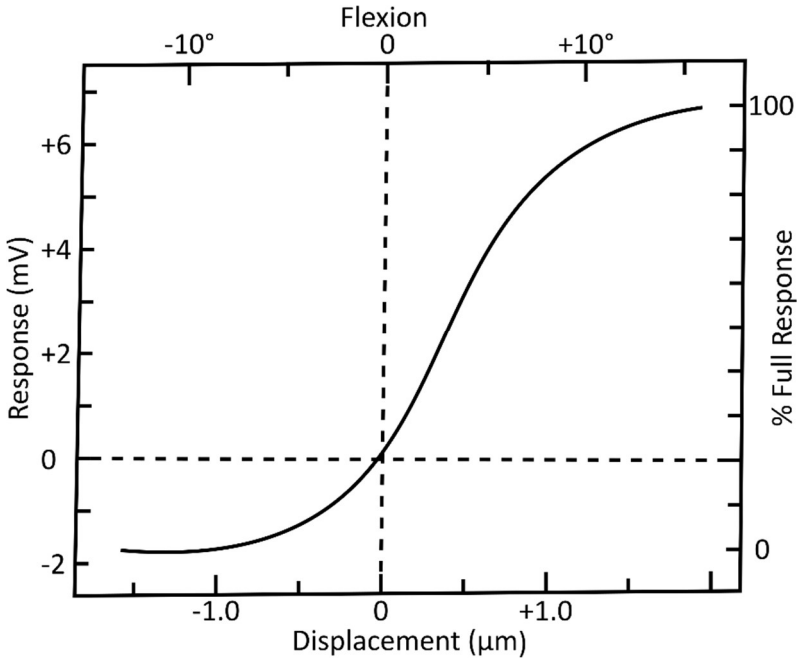

Figure 1.4 Receptor potential change of bullfrog saccular hair cell in response to stereocilia displacement. Redrawn from [Hudspeth & Corey, 1977].

2 Hearing loss

The sophisticated system of our hearing can easily be damaged, leading to a certain amount of hearing loss. The damage is usually measured by the elevation in threshold levels i.e. the elevation of the lowest sound pressure level within a frequency band that can be detected by the patient. Based on the nature of the problem, various types of hearing losses can be distinguished.

Besides being unilateral or bilateral, depending on whether one or both ears are affected, hearing loss can generally be categorised based on severity that is determined by the amount of increase in hearing thresholds. A hearing loss is considered to be mild if the threshold is elevated by 25 to 40 dB, moderate if elevation is between 40 and 70 dB, severe if elevated by 70 to 90 dB and profound if the threshold is increased beyond 90 dB [Clark, 1981]. Depending on the cause of the hearing loss, it can be hereditary or acquired. An acquired hearing loss can be further categorized as sudden or progressive.

From a physiological point of view, a hearing loss can be conductive or sensorineural. Conductive hearing loss is caused by the obstruction of the sound in the outer or middle ear, preventing it from propagating to the inner ear. Sensorineural hearing loss involves the loss of sensory cells or auditory nerves at the level of the inner ear.

Indeed, one of the most widespread health issues of the modern world is related to hearing. According to the World Health organization, around 5% of the world's population suffer from some form of a hearing disorder [World Health Organization, 2013].

Furthermore, the population of the world is aging fast, e.g. the approximated population of 962 million people over 60 years is expected to grow to 2.1 billion [United Nations, 2017], making age-related hearing loss to become more prevalent.

3 Treatment of hearing loss

Conductive hearing loss can usually be treated by the removal of the blockage causing the problem. When the blockage cannot be removed, e.g. in case of middle ear infection (otitis media mesotympanalis, cochleostoma) or fixation of the middle ear ossicles (otosclerosis) [Zahnert, 2011], a bone conductive hearing aid can serve as a solution. This device is attached to the temporal bone and transmits vibrations to the cochlea directly.

Treatment of sensorineural hearing loss by the regeneration of sensory hair cells or auditory nerves is currently not established [Revuelta et al., 2017]. Depending on the severity of the sensorineural hearing loss, various medical devices are used to restore hearing sensation. In the case of a mild to moderate hearing loss, residual hair cells are still present in the cochlea and a hearing aid is prescribed for the patient. The working principle of hearing aids is based on the amplification of the incoming sound to compensate for the level of hearing loss. If the loss of hearing is profound, the inner hair cells are usually assumed to be completely absent and a cochlear implant is suggested for hearing rehabilitation and now used by over 600000 patients worldwide [Roland & Tobey, 2013; The Ear Foundation, 2016]. A cochlear implant is a device that is designed to bypass the inner hair cells and electrically stimulate the auditory nerves by the aid of electrodes implanted inside the cochlea.

4 Cochlear implants

Probably the first experiment on electric stimulation of the ear was conducted by Volta in the dawn of the 19th century. By closing an electrical circuit with metal bars placed into his ear canals, he described the sensation of a sudden jolt followed by a noise, resembling the boiling of a viscous liquid while the circuit was closed. Not surprisingly, due to his sensible fear of the damaging nature of the experiment, he did not continue with further investigations.

Since the experiment of Volta, an enormous amount of research is oriented towards the applicability of electric stimulation to restore hearing for the profoundly deaf. The first application of electric stimulation to restore hearing sensation dates back to 1957 in Paris when Djourno and Eyriès successfully implanted a device that was capable of stimulating

the auditory nerves and provide the sensation of environmental sounds [Wilson & Dorman, 2008].

The first real predecessors of modern cochlear implants were developed and implanted in the beginning of the 1960s by Dr. William F. House. These early devices had one stimulating electrode contact implanted into the scala tympani and a return electrode attached to the temporal muscle. The capability of these implants to successfully complement lip reading gave the initial kick and set off the astonishing wave of cochlear implant development over the past few decades.

The general design of contemporary devices is shown in Figure 4.1. The sound is captured by a microphone or a microphone array, the signal of which is processed by an external behind the ear speech processor. The processed signal is transferred through the skin by a tele coil to an implanted unit embedded into the temporal bone. This implant eventually delivers current to the contacts of an array of electrodes positioned inside the scala tympani. The application of multiple electrodes makes it possible to stimulate the cochlea at various loci, thus mimicking the frequency analyser function of the basilar membrane.

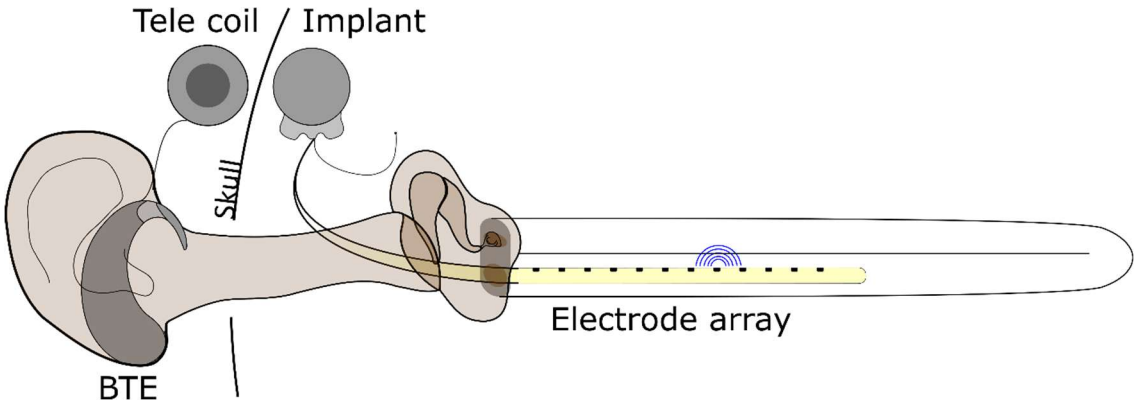

Figure 4.1 Schematic of a cochlear implant with its electrode array inserted into the scala tympani. BTE – Behind the ear speech processor.

Along with the improvements in the structural design, the signal processing strategies applied in cochlear implants also went through major refinements. The interested reader is referred to the thorough review of Loizou (1998) on the evolution of the signal processing strategies.

Simplistically, today's devices first split the acquired signal into N frequency bands that are assigned to the intracochlear electrode contacts, then the signal of most prominent N band is selected, the strategy known as 'NofM' [Seligman & McDermott, 1995], and converted to electrical pulses on these N channels only. The processing is conducted on a frame by frame basis and the electrical pulses are modulated either in amplitude or width to restore loudness sensation. Eventually, the electrical pulses are delivered to the

associated contacts on the electrode array in an interleaved manner, known as the continuous interleaved sampling (CIS) method [Wilson et al., 1991]. The 'NofM' and CIS methods were introduced to minimize the interference of electrical fields generated by the neighbouring electrodes and contributed greatly to enhance speech understanding by cochlear implant users [Wilson et al., 1991].

5 Electro-Acoustic Stimulation

There is a small, but growing population [Gstoettner et al., 2008; Von Ilberg et al., 2011] of patients with a restricted amount of residual hair cells that is insufficient for achieving satisfactory speech intelligibility when stimulated acoustically by a hearing aid.

The improvements in cochlear implant electrode array design and surgical procedures [Gstöttner et al., 2004; Adunka et al., 2009] led to the mitigation of implantation criteria in the past two decades [Gstöttner et al., 2004; Kiefer et al., 2004; Sampaio et al., 2011]. Patients with residual hearing are now eligible for receiving a cochlear implant and can also benefit from the additional application of a hearing aid in the same ear. This hybrid stimulation type that simultaneously applies both electric and acoustic signals in the same ear is usually referred to as the electro acoustic stimulation (EAS).

A typical EAS patient often possesses moderate to severe hearing loss in the low frequencies that gradually becomes severe towards the higher frequencies. This pathology is often referred to as a ski-slope type hearing loss [Gstoettner et al., 2008]. The residual hearing in the low frequency range offers the possibility of augmentation of the cochlear implant with a conventional hearing aid as illustrated in Figure 5.1.

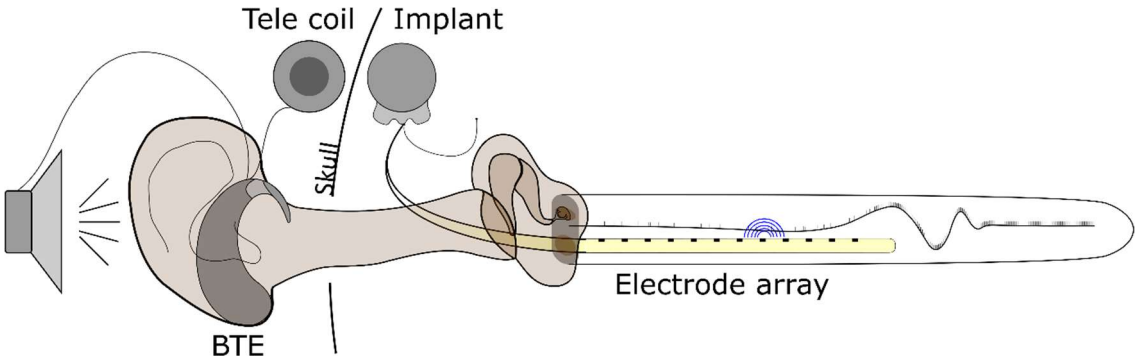

Figure 5.1 Schematic of electro-acoustic stimulation (EAS) using a hybrid device.

The working principle of the combined stimulation is based on the excitation of separate cochlear regions by the acoustic and the electric stimuli. The apical, low frequency end of the cochlea, that retains hearing, is stimulated acoustically by the hearing aid. The basal, high frequency part of the cochlea, where hearing loss is profound, is stimulated electrically by the cochlear implant.

Patients are shown to benefit from combined acoustic and electric stimulation [Turner et al., 2004; Gantz et al., 2005]. Achieved performance in speech intelligibility with the combined stimulus is superior to the performance achieved either by acoustic or electric stimulation alone [Von Ilberg et al., 1999; Kiefer et al., 2005; Büchner et al., 2009]. Compared to normal cochlear implant users, EAS users also benefit from better speech understanding in noisy environments [Gifford et al., 2013] and also score higher in pitch perception [Gantz et al., 2005; Skarzynski et al., 2006; Adunka et al., 2013; Irving et al., 2014]. Furthermore, EAS users were also shown to outperform conventional cochlear implant users in song and instrument recognition tasks [Gfeller et al., 2006]. However, despite the promising initial outcomes of EAS, several questions are raised by the application of this technology. The questions mainly revolve around the used surgical approach, electrode design, stimulation strategies and the interaction of stimulus modalities. The main goal of the PhD project at hand was the investigation of acousto-electric interactions by physiological studies.

Stimulation of the same ear with different modalities imposes high demand on the applied signal processing and fitting strategies. The acoustic and electric stimulation pathways possess different delays that should be accounted for to achieve precise synchrony of the stimulation modalities. Although the different signal processing delays in the cochlear implant and the hearing aid can be compensated by delaying the faster device, the frequency-dependent acoustic propagation delay within the cochlea is scarcely if ever taken into account [Francart & McDermott, 2013].

Besides signal processing delays, another unsettled dispute concerns the frequency allocation of the acoustic and electric stimulation. Although there is no established method for electrode frequency mapping for EAS [Incerti et al., 2013], Francart and colleagues provided a good overview of the available possibilities [Francart & McDermott, 2013]. Among others, they differentiate a ‘standard mapping’ and ‘no overlap’ procedure for frequency allocation. In the ‘standard mapping’ procedure the complete spectrum of the acoustic stimulus is split into distinct bands and the split signal is routed to the channels of the cochlear implant. In the ‘no overlap’ procedure a crossover frequency (see next section) is defined and only the frequency content of the sound above the limit of residual hearing is mapped to the cochlear implant channels, and only for the channels with tonotopic contact location above this limit are activated. An interesting point that the review highlights is the preference of non-overlapping map over a standard electrode mapping [C. J. James et al., 2006; Fraysse et al., 2006] by EAS patients. This thesis will show that if the aim is to avoid interference between electric and acoustic stimulation, additionally to the separation of modalities during frequency

allocation, the overlap in the frequency content of the acoustic and electric stimulation should also be kept in mind.

To define a limit that separates the acoustically and electrically stimulated regions such that the modalities do not interfere adversely, usually a crossover frequency is selected. Pure tone audiometry is often used for identifying the crossover frequency by selecting the frequency where the patient's hearing loss exceeds an arbitrary limit, that is usually selected to be between 65 and 85 dB HL [Krüger et al., 2017]. However, the approach of selecting a crossover frequency is likely suboptimal since the spread of electrical excitation may still affect the residual hearing as illustrated in Figure 5.2.

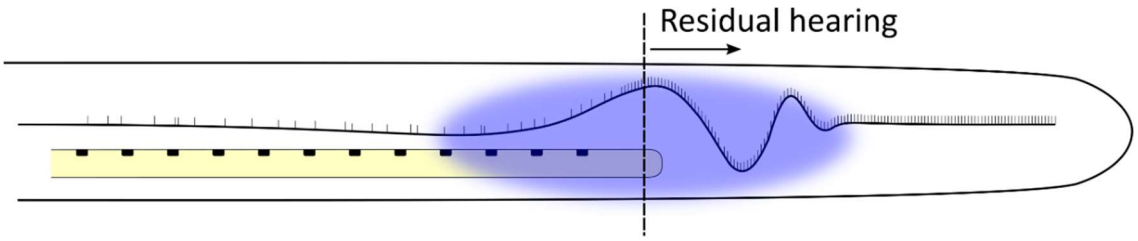

Figure 5.2 Electrical spread of the cochlear implant (blue shaded area) may reach the residual hearing part of the implanted cochlea.

Additionally to the electric-acoustic interactions in the residual hearing range, modality interference may also appear at more basal regions. As illustrated in Figure 5.3, the acoustic travelling wave travels through the place of electric stimulation and may interfere with it.

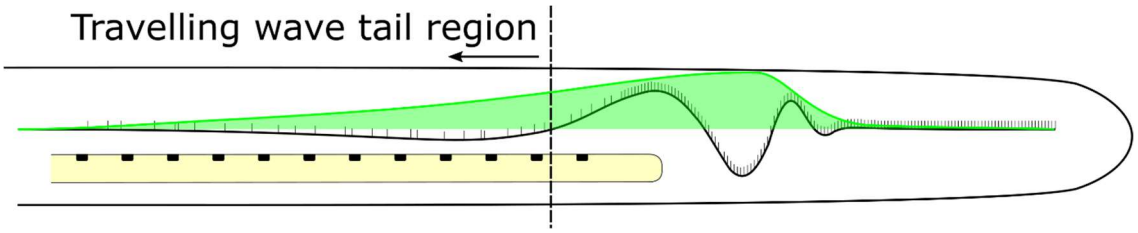

Figure 5.3 Interference of acoustic and electric stimulation in the basal part of the cochlea due to the tail of the travelling wave. The envelope of the travelling wave is indicated by a green line and green shading indicates the area below it.

To gain better understanding of electric-acoustic interactions in ears with residual hearing, recent research demonstrated masking effects between the modalities using psychophysical [Lin et al., 2011; Krüger et al., 2017; Imsiecke et al., 2018; Saoji et al., 2018] and electrophysiological experiments [Koka & Litvak, 2017].

Although EAS patients are assumed to be profoundly deaf in the region of electrical stimulation, the outer hair cells may still be present and have electromotile response to the electrical stimulation by the implant and induce mechanical responses that might interact with the residual acoustic hearing. Indeed, the cochlear microphonic, a potential

generated mostly by outer hair cells [Dallos & Cheatham, 1976], is present in EAS users, furthermore it is used as a marker for monitoring cochlear health during hearing preservation surgeries [Choudhury et al., 2012; Fitzpatrick et al., 2014; Formeister et al., 2015; Adunka et al., 2016; O'Connell et al., 2017; Riggs et al., 2017; Giardina et al., 2018; Haumann et al., 2019]. Part B, the main report in this thesis will describe the physiological experiments, which investigated the acousto-electric interactions that may originate from outer hair cells.

Preservation of residual hearing after surgical intervention is a key to the success of EAS [Adunka et al., 2013; Causon et al., 2015]. Additional hearing loss during the first 6 to 12 month after implantation is usually in the range of 18 to 34 dB at 500 Hz and below [Incerti et al., 2013]. Post-operative hearing loss is often associated with cochlear damage caused by the CI electrode array, e.g. translocation of the CI electrode from the scala tympani to the scala vestibuli, that in turn may result in fibrosis and ossification [Ishiyama et al., 2016, 2019]. One of the key elements of surgery is the approach to accessing the interior of the cochlea. In one approach the round window membrane is removed to allow for the insertion of the cochlear implant electrode array into the scala tympani. In another method, the scala tympani is accessed by drilling a small hole, a cochleostomy, in the round window niche. The debate around the surgical approach, whether preparing a cochleostomy or opening the round window, remains unsettled [Havenith et al., 2013]. Cochleostomy is usually accused of imposing an unnecessary trauma due to drilling the cochlear wall [Addams-Williams et al., 2011]. On the positive side, the cochleostomy technique provides an access to the scala tympani that supports an insertion angle that follows the turn of the scala thus leads to a less likely damage to the cochlear partition compared to an insertion through the round window [Adunka & Buchman, 2007]. Additionally, the cochleostomy approach assures an intact round window. Hence its natural pressure release role, that is essential for effective acoustic stimulation, remains undisturbed. On the other hand, round window insertion offers a safe and reliable insertion that poses less risk of damaging the cochlea by strong mechanical vibration compared to the drilling of a cochleostomy [Skarzynski et al., 2007; Gudis et al., 2012].

The design of electrode carriers is of special interest when hearing preservation is desired. Besides the implantation of a conventional electrode array, also the option of choosing a short array, designed to reduce the possibility of damage to the low frequency residual hearing range, is available for EAS candidates. The short carrier design offers a less traumatic insertion, yielding a better chance of hearing preservation after surgery [Gantz & Turner, 2003]. On the other hand, it also carries the possibility of an unfavourable re-implantation, should the residual hearing become lost. The short

electrode array does not reach the low frequency cochlear region, thus a replacement with a longer array is necessary to achieve a complete cochlear coverage and restore the ability of hearing through its complete range [Gstoettner et al., 2006; Turner et al., 2008]. Due to the uncertainty of losing residual hearing, the implantation of conventional, long electrode array design is nowadays chosen as a more secure option. Hearing preservation was also shown to be possible with electrodes covering extensively the cochlear length [Adunka et al., 2004; Helbig et al., 2011; Skarzynski et al., 2011]. In case of the loss of residual hearing, a long electrode array can later be used to electrically stimulate the entire cochlea and avoid the necessity of a re-implantation [Prentiss et al., 2010]. To promote an atraumatic insertion, with a long electrode array, an often-discussed property of the carrier is its diameter and flexibility [Briggs et al., 2006; Hochmair et al., 2015]. A thinner electrode may provide a less traumatic insertion compared to a thicker array [Helbig et al., 2016], on the cost of losing the electrode's structural rigidity that may lead to a more cumbersome insertion procedure and occasional electrode carrier fold-over.

Additionally to the surgical consequences of electrode dimensions, one should also bear in mind the effects that an implanted electrode may impose on the acoustically evoked travelling wave. Even with a successfully inserted electrode (i.e. preserved residual hearing and assuming that the electrode does not contact the basilar membrane), the presence of a foreign body within the scala tympani may alter the acoustically evoked fluid velocity field and in turn distort the travelling wave. Although often debated, past research gave little insight to these effects, thus it served as an excellent topic to study in the beginning of the project. The details of the relevant work will be discussed in a short report (Part A) at the beginning of the thesis.

Part A Exploring the effects of a cochlear implant electrode within the scala tympani on the passive cochlear travelling wave

A1 Introduction

It is often postulated that the insertion of a cochlear implant into the scala tympani (ST), disturbs the intricate acoustic conditions inside the cochlea by altering the acoustic travelling wave. This can obviously become a problem if the residual hearing of the patient is utilised by the use of a device with EAS strategy as it might affect their perception of acoustic sounds. Thus, a detailed investigation of these effects is desirable.

The cochlear travelling wave can be studied by various methods. In vivo and in vitro experiments often utilize a laser Doppler velocimetry technique [Nuttall et al., 1991], that requires the placement of reflective beads onto the basilar membrane and a clear view of these beads. To study the effect of a cochlear implant electrode array on the travelling wave, the in vivo or in vitro studies are impractical because the view is blocked by the implant. In addition, one can only measure the basilar membrane movement within a very restricted spatial range and the exact position of the implant electrode is difficult to control. An alternative approach is the realistic representation of the cochlear environment by a computational model. Because powerful computers are nowadays readily available, a widely used method in recent years is the finite element model (FEM) representation of the cochlea. In an FEM model, the parameters of the cochlea can be adjusted to match that of the realistic hearing organ and the parameters of a CI can easily be modified to represent various electrode types and positioning.

Previous FEM studies addressing this problem mostly focused on the effect of a CI that is in contact with the BM. Kiefer and colleagues (2006) used a realistic 3D model of the cochlea and simulated the presence of a CI by fixing a section of the BM, i.e. they did not model the electrode array itself, and showed the appearance of BM displacement peaks basal and apical to the fixed region, even if the characteristic place of the stimulation fell within the fixed region. Using a box model, Semmelbauer and colleagues (2018) investigated the effects of a cochlear implants with various lengths on the acoustic travelling wave and compared the cases in which the CIs were distant to the basilar membrane (BM) to cases representing a partial contact of the CI and the BM. They observed a damped BM displacement in the case with partial contact, but no major influence of an electrode array distant to the BM.

In our study, we applied the FEM approach to investigate the principles that underlie the effects that a foreign object in the ST may impose on the acoustic travelling wave. First, the effects of a long and a short electrode array are compared by means of their distance to the BM. Second, the effect of electrode diameter is investigated.

A2 Background to passive cochlear mechanics

The last stage of the middle ear's ossicular chain is the stapes that abuts the oval window, an opening into the cochlea. The vibrations of the stapes generate pressure waves in the perilymph, a fluid that fills the scala tympani (ST) and scala vestibuli (SV). Between the ducts of the ST and the SV lies the basilar membrane (BM)[1], a membrane constructed of radially[2] organized fibres that are loosely coupled longitudinally by soft tissue. The interaction of fluid mass and the BM stiffness results in a travelling wave along the BM [Ni et al., 2014] that was first revealed in the 1930s' by the experiments of Békésy György (1960). The amplitude of the travelling wave gradually builds up from the base, until its peak location and diminishes rapidly afterwards [Robles & Ruggero, 2001]. The location of the traveling wave peak is characteristic to the frequency of the stimulation and it is termed the characteristic place (CP). In turn, every place along the BM has its own characteristic frequency (CF). The unique frequency to place association of the BM, its so-called tonotopy, enables this membrane to be the frequency analyser of hearing. The mapping of frequencies along the cochlea was studied in detail by Greenwood [Greenwood, 1961], who defined a species independent formula for the assignment of frequencies to specific loci. It describes a gradual decrease in CFs from the base to the apex.

In a mechanical mass-spring system, when the mass reactance (1) and the stiffness reactance (2) cancel out, resonance occurs. Therefore, the resonance frequency of this system is defined by its stiffness and mass as written in equation (3):

$$X_m = 2\pi f m \tag{1}$$

$$X_k = -\frac{k}{2\pi f} \tag{2}$$

$$f = \frac{1}{2\pi}\sqrt{\frac{k}{m}} \quad , \tag{3}$$

[1] To be more precise, the ST and SV is separated by a third entity, the scala media (SM) that is bounded by the BM and the Reisnner's membrane. In modelling studies concerning passive cochlear mechanics the Reisnner's membrane is usually neglected due to its acoustic transparency [Böhnke & Arnold, 1999; Gelfand, 2010], thus the SV and the SM is represented as one fluid compartment.

[2] In the present study, the longitudinal axis refers to the axis that runs along the BM. The radial axis refers to the axis in the plane of the BM and perpendicular to the longitudinal axis. Ultimately, the vertical axis is defined as the axis normal to the plane of the BM.

where m is the mass, k is the stiffness and f is the resonance frequency of the system. In the cochlea, the resonance frequency is related to the CF of a BM location, the stiffness of the system is represented by the BM properties and the mass is represented by the effective mass of the fluid around the BM.

BM stiffness, that is mainly determined by the geometrical properties of the membrane, governs the tonotopical distribution of CFs [Greenwood, 1961]. The radial and vertical dimensions of the membrane are tapered along its longitudinal extent. BM thickness decreases and BM width increases from the basal to the apical end [Wada et al., 1998]. The dimensional changes in the BM establish the basis of the BM's negative stiffness gradient from base to apex. Additionally to the dimensional properties, the membrane's decreasing fibre density from base to apex also contributes to the negative stiffness gradient.

A3 Model description

The acoustic travelling wave is mainly governed by the previously described passive mechanisms of the cochlea, thus active mechanisms that contribute to secondary characteristics of the travelling wave e.g. compressive nonlinearity, increased sensitivity and sharper tuning, are not included in the model.

The Comsol Multiphysics finite element modelling software was selected as a working environment to investigate the principles of a CI electrode array in the ST on the acoustic travelling wave. The software can connect various physical systems, of which the presented model applies thermoacoustics and solid mechanics that were coupled to replicate the fluid-structure interaction between the cochlear fluid and the involved solids, namely the BM and the CI electrode. To examine the steady state response of the whole system to pure tones, the time-efficient frequency domain solver, that also considered viscous damping, was selected for conducting simulations.

The geometry of the model is shown in Figure A3.1. The cochlea was represented in an uncoiled form, parallel to the x-axis. To reduce the computational load, only half of the model was simulated by cutting the cochlea into half along its longitudinal axis. The ST and SV were simulated as fluid compartments separated by the BM (indicated by green colour) and conjoined at the apex by the helicotrema, that was represented by a third fluid compartment. The simulated material properties of the fluid were like those of water. The BM was modelled as an orthotropic solid, i.e. the stiffness coupling was stronger radially than longitudinally, to represent the radial organization of fibres within the membrane. The electrode array (shown as a blue object) was incorporated as a conical, homogeneous, isotropic solid object within the ST, positioned parallel to and aligned to

the middle of the BM. Our study did only address the effect of the electrode array on the basilar membrane motion. Therefore, the electrode array ended 1 mm apical to the round window so that the vibration of the round window remained unobstructed.

The surrounding boundaries are defined as walls with 'non-slip' condition (velocity is defined as u = 0) except for the y = 0 and the basal, x = 0 planes. Symmetry condition in the y = 0 plane was used. The symmetry condition allowed the fluid to flow along the plane, but not through it, i.e. the normal velocity at the plane was zero (n·u = 0). To mimic the vibration input by the stapes footplate on the oval window, a velocity was applied on the upper basal face (x = 0 and z > 0, indicated by red colour). To account for the pressure release at the round window, a no stress condition was used on the lower basal face (x = 0 and z < 0, indicated by cyan colour). The BM was fixed at its four edges. Viscous boundary layer was applied to the walls of the box, to the top and bottom faces of the BM and to the boundaries of the CI electrode.

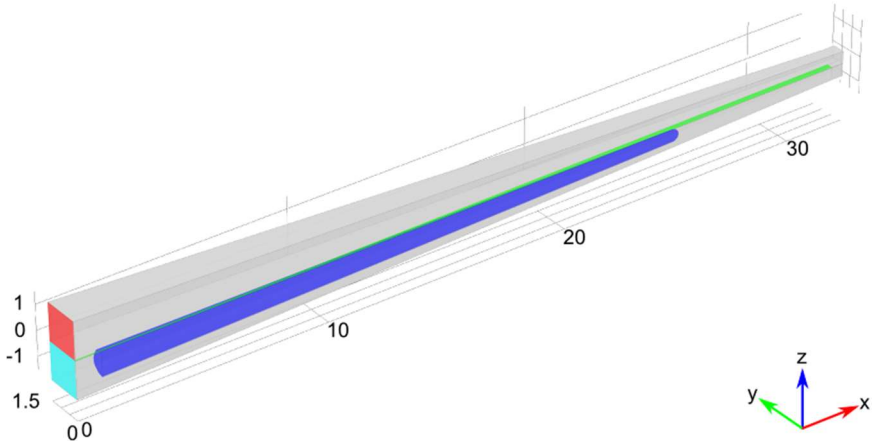

Figure A3.1 The geometry of the Comsol FEM model of a cochlea with an inserted electrode array. Red and cyan rectangles indicate the oval and round windows respectively, green colour marks the basilar membrane and blue colour highlights the CI electrode array.

After the definition of the geometry and the material properties, the constructed model was meshed. First, the BM was meshed as bricks by distributing 800, 8 and 2 node points along its x, y and z coordinates. The generated mesh faces were then sectioned diagonally to fit the automatically generated tetrahedral elements used for meshing the fluid compartments and the CI.

A4 Model without CI electrode: Tuning the tonotopy

The investigation of the effects of a CI on the cochlear mechanics requires a reasonably well-represented travelling wave and tonotopy along the BM. To model the stiffness

gradient of the BM, its width was increased from base to apex and the x, y and z components of Young's modulus of the partition was changed according to equation (4), (5) and (6) where E_0 is the Young's modulus at the base of the BM, and x is the distance from the base. Parameters b and c are controlling the curvature of the gradient of the Young's moduli. Note that orthotropy of the BM was implemented by $E_x = E_y/1000$.

$$E_x = \frac{E_y}{1000} \tag{4}$$

$$E_y = E_0\left(1 - \frac{x}{b}\right)^c; E_0 = 5 \times 10^7 \tag{5}$$

$$E_z = E_y \tag{6}$$

The models tonotopy was tested against Greenwood's function [Greenwood, 1990] at frequencies ranging from 125 to 8000Hz in octave steps. Displacement and phase results were extracted from the nodes along the midline of the BM (y=0, z=0). Figure A4.1 shows the simulation results in response to the tested frequencies.

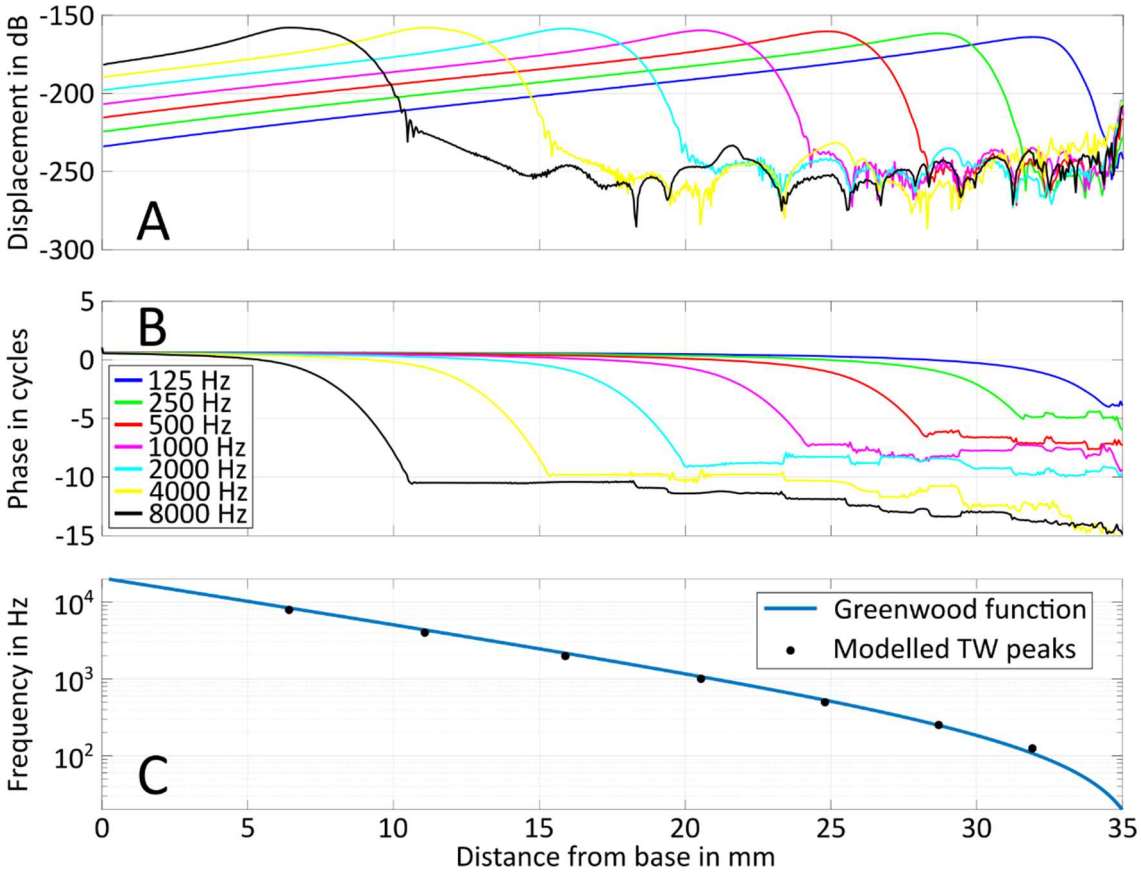

Figure A4.1 Simulation results of the travelling wave in response to frequencies between 125 and 8000Hz. Panel A shows the traveling wave envelopes expressed in arbitrary dB scale. Panel B shows the phase accumulation of the travelling waves expressed in cycles. Panel C shows the tonotopic match of simulation results (black dots) to the Greenwood function (blue line).

Panel A and B show the envelope and phase information of the travelling waves in response to a range of simulation frequencies. Envelope information is expressed in arbitrary dB scale and phase information is expressed in cycles. The simulation results

show the expected behaviour. The envelopes build up gradually until reaching their peak after which they sharply roll off. Panel C shows the reference Greenwood function as a blue line along with the extracted travelling wave envelope peak loci as black dots that show a reasonable fit.

A5 Effect of electrode to basilar membrane distance on the travelling wave

The effect of an inserted electrode array on the travelling wave with respect to its distance from the basilar membrane is investigated both in the presence of a long (24 mm) and a short (10 mm) array. The electrode array's upper surface was always parallel to the BM, i.e. the distance to the BM was constant along the entire length of the array. Simulations were run at 1 kHz and the electrode to BM distance was varied between 10 and 150 µm. Travelling wave envelopes expressed as vertical displacement and corresponding phase responses are extracted from the midline of the BM and shown in Figure A5.1 with the long array and in Figure A5.2 with the short array.

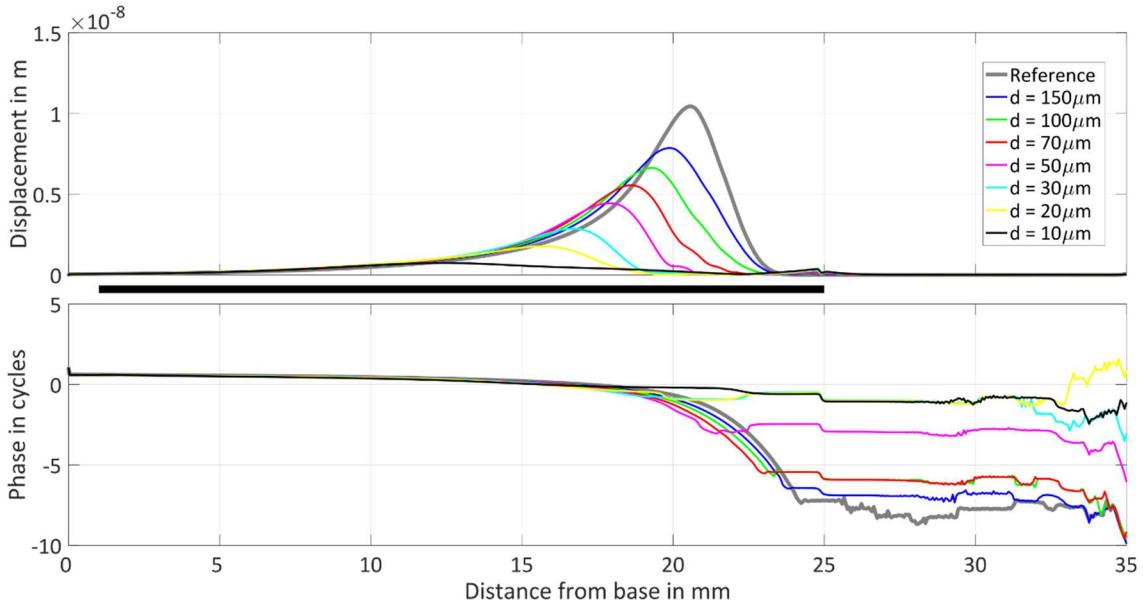

Figure A5.1 Travelling wave envelope and phase in the presence of a 24 mm long electrode array in the scala tympani at various distances (d) from the basilar membrane. Reference result without an inserted electrode is shown with a thick grey line. The location of the electrode array is indicated by the black bar between the panels.

In case of the simulations with the long electrode array, as the electrode to BM distance is decreased, a gradual reduction of peak displacement accompanied by a basal shift of

the characteristic place can be observed. Additionally, the reduced distance also results in the widening of the travelling wave peak. Similarly to the travelling wave peak, its phase accumulation also shows a basal shift with decreasing electrode to BM distance.

In case of the simulations with the sort electrode array, a slight reduction in the peak displacement is only visible with the electrode being 10 µm close to the BM, otherwise the travelling wave envelope is unaffected. The phase accumulation in this set of simulations is unaffected compared to the reference condition.

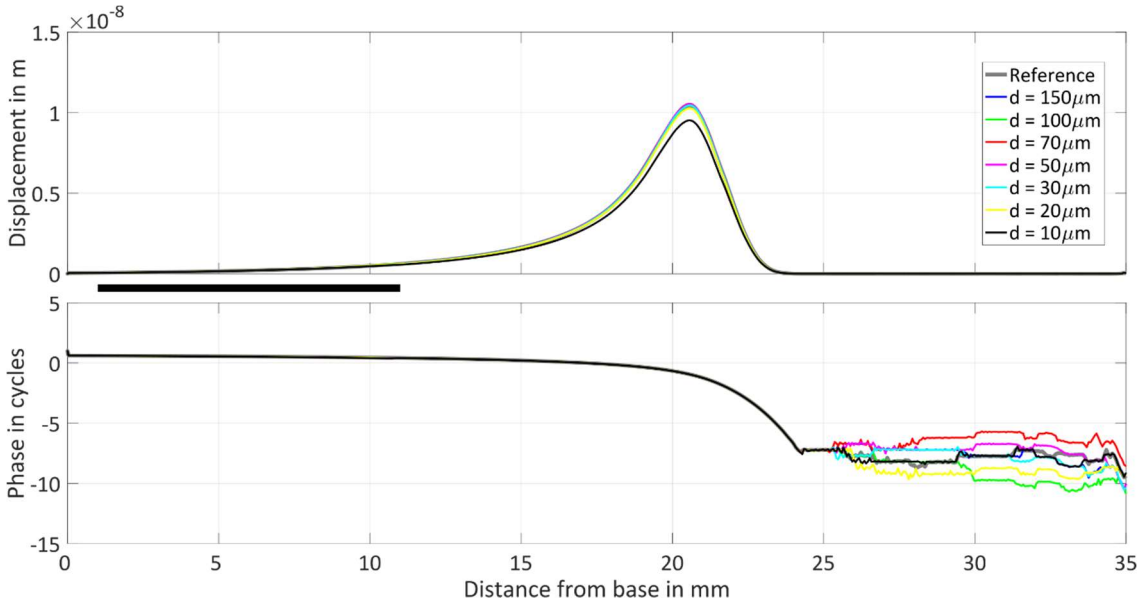

Figure A5.2 Travelling wave envelope and phase in the presence of a 10 mm long electrode array in the scala tympani at various distances (d) from the basilar membrane. Reference result without an inserted electrode is shown with a thick grey line. The location of the electrode array is indicated by the black bar between the panels.

A6 Effect of electrode radius on the travelling wave

In the previous section, the basal and apical radii of the electrode array were always 0.5 and 0.25 µm the electrode's volume was kept constant. To investigate the changes in the travelling wave in the presence of CI electrodes with various sizes, 1 kHz simulations were conducted, using a model with a long electrode array. The distance of the electrode from the BM was either 30 or 150 µm. The volume of the electrode was systematically changed by reducing the basal (r_b, from 0.5 mm to 0.1 mm) and apical radii ($r_a = r_b/2$). For comparison, simulations were also made by reduced ST volumes. The volume reductions accounted for the volume that would have been occupied by the electrode array. Reduction of ST volume was achieved by systematically reducing the height of the box representing the ST.

Results for the CI 30 µm and 150 µm away from the BM are shown in Figure A6.1 and Figure A6.2 and results for the simulations with various ST volume are presented in Figure A6.3. In all figures, the thick grey line represents the reference simulation condition without the CI and unmodified ST volume.

In case of the simulations with the electrode 30 µm away from the BM, with increasing electrode radius the amplitude of the travelling wave peak decreased, and the characteristic place shifted basally. Similarly to the characteristic place, the phase accumulation also shows a basal shift with increasing electrode radius.

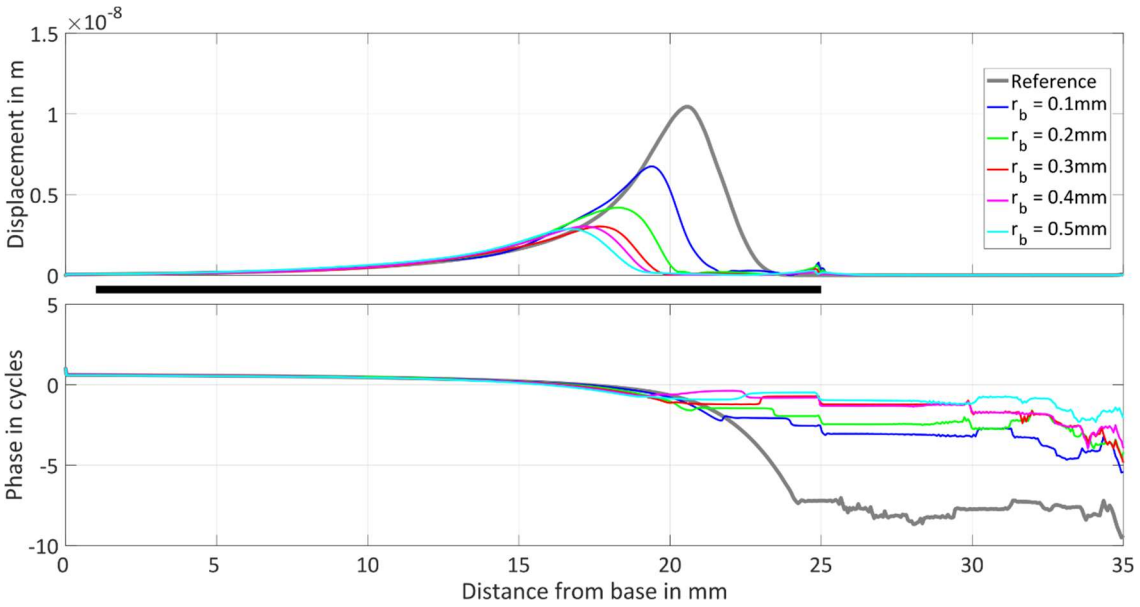

Figure A6.1 Travelling wave envelope and phase in the presence of a 24 mm long electrode array with various radii (r_b) in the scala tympani at 30 µm distances from the basilar membrane. Reference result without an inserted electrode is shown with a thick grey line. The location of the electrode array is indicated by the black bar between the panels.

In case of the simulations with the electrode 150 µm away from the BM, the increasing electrode radius resulted only in a slight travelling wave peak reduction and a slight basal shift of the characteristic place. Similarly to the characteristic place, the phase accumulation also shows a little basal shift with increasing electrode radius. These effects were considerably smaller than in the case with the electrode 30 µm close to the BM.

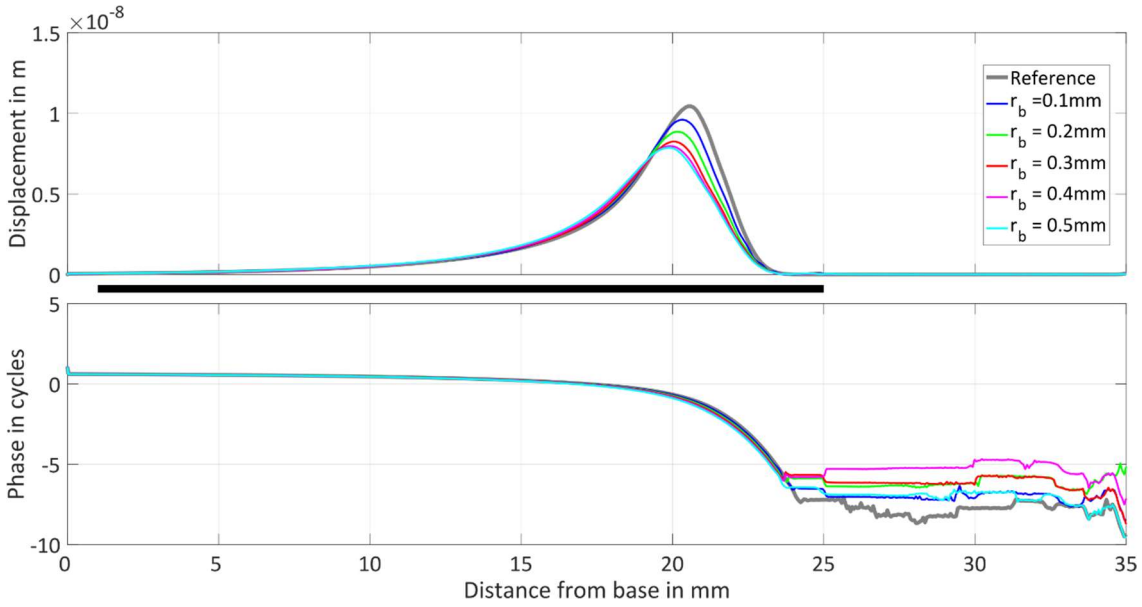

Figure A6.2 Travelling wave envelope and phase in the presence of a 24 mm long electrode array with various radii (r_b) in the scala tympani at 150 µm distances from the basilar membrane. Reference result without an inserted electrode is shown as a thick grey line. The location of the electrode array is indicated by the black bar between the panels.

The results of simulations with various ST volumes did not show a difference compared to the reference condition, neither in the envelope nor in the phase data.

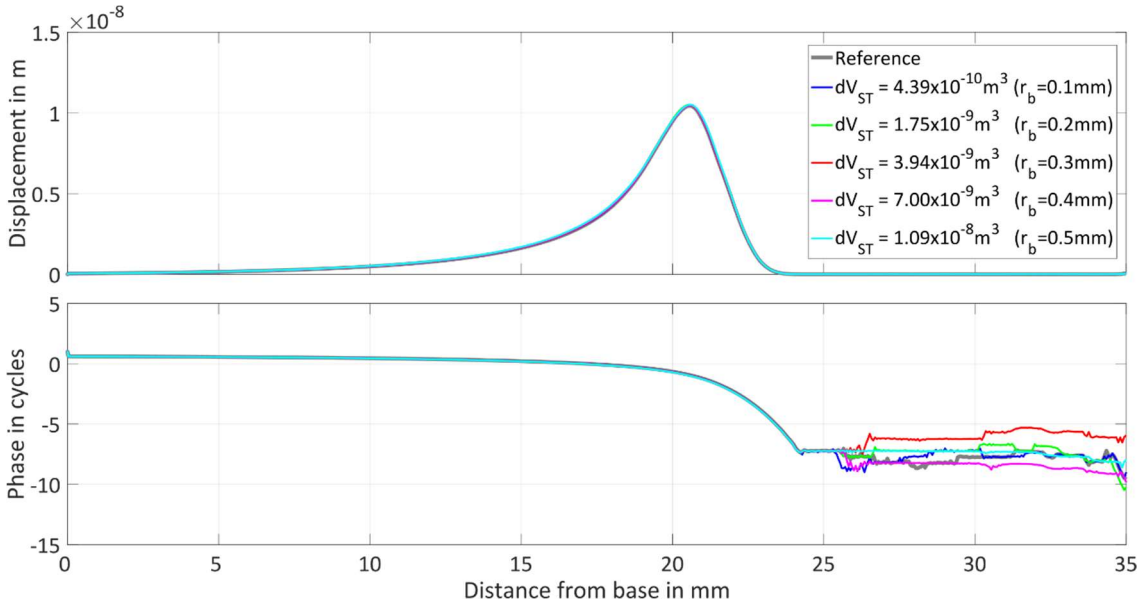

Figure A6.3 Travelling wave envelope and phase results for simulations with various scala tympani volumes (V_{ST}). Reference result with the original scala tympani dimensions is overlaid by the other lines because changes were minor.

A7 Discussion

In equation (1) to (3) it was shown that resonance of a mass and the spring system occurs when mass and stiffness reactance cancel out. Upon insertion of a CI electrode into the ST, a gap is created between the BM and the electrode, obstructing the fluid flow as illustrated in Figure A7.1. In this case, to displace the same amount of fluid as in the electrode free condition, within the same amount of time, a higher acceleration is required. The higher acceleration results in the increase of mass reactance X_m, that requires a higher stiffness reactance X_k to be cancelled out. X_k can be increased if the stiffness of the system increases. The BM stiffness increases towards the base, thus explaining the basal shift of the characteristic place.

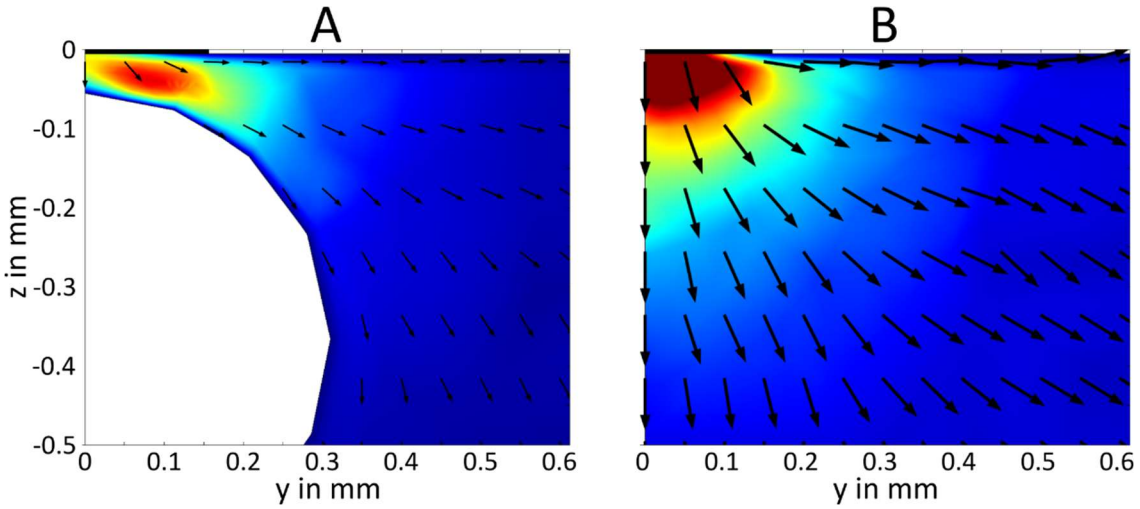

Figure A7.1 Illustration of fluid flow obstruction in the ST by a CI. Panels show a cross-section of the ST at x=20 mm in the proximity of the BM that is represented by a black bar in the top left corners. The magnitude of local fluid velocity is represented by colours and its directionality within the cross-section by the arrows. A – a CI obstructs the fluid flow. B – fluid can freely move.

In section A5, in the case of the long electrode array the gap between the electrode and the BM was gradually getting tighter, resulting in a gradual shift of the travelling pave pattern towards the base, which is explained by the increasing mass reactance. The phase results were also showing that the travelling wave required a shorter distance to build up as the CI electrode was getting closer to the BM. Additionally, the peak amplitude of the travelling wave also decreased gradually, that may be explained by the increased amount of viscous losses in the tightening gap between the CI electrode and the BM. At very small distances the shift of the characteristic place might be partly explained by the extremely high viscous losses, in other words, the travelling wave ran out of energy before reaching the resonance place.

In the case of the short electrode array, the characteristic place was apical to the electrode, thus the resonant system was unaffected. The slight decrease in the peak

amplitude, when the electrode was closest to the BM, may have been the result of energy loss in the travelling wave due to increased losses as the gap approached the viscous boundary layer thickness in the basally located gap. The phase results also confirmed this hypothesis as there was no change in phase accumulation in any of the conditions compared to the reference.

In section A6, changing the radius of the electrode, essentially resulted in the change in the width of the gap between the electrode and the BM. A thinner electrode corresponds to a shorter gap, and the fluid volume that has to be accelerated so that overall mass reactance decreased and resulting changes of the characteristic place and the travelling wave peak amplitude became smaller. The control simulations with the reduced ST height show that it is not simply the reduced volume of fluid in the scala tympani, which causes the observed effects, but the fluid flow near the BM.

A8 Conclusions and future work

A 3D FEM model was established that was incorporating viscous fluid damping and was capable of the realistic representation of the passive travelling wave for frequencies covering the 125 to 8000 Hz range.

In addition, CI electrode arrays were modelled as a conical object within the ST and their effect at various distances to the BM distance was investigated. Simulations with a short and a long electrode array demonstrated that the electrode array may disturb the fluid flow at the travelling wave peak, resulting in its suppression and basal shift. The simulations also showed that, presence of an electrode array influences the acoustic stimulation only if it is very close to the BM. Section A6 demonstrated that the size of the gap between the electrode array and the BM influences the travelling wave not the available ST cross-section area.

Based on the findings of the present modelling study, a short, lateral wall electrode array [Gantz & Turner, 2003] may be suggested for EAS users as this carrier type does not cover the apical region of the cochlea hence it does not interfere with the acoustic stimulation of the residual hearing range. However, the residual hearing of EAS patients may be lost over time [Talbot & Hartley, 2008; Adunka et al., 2013; Incerti et al., 2013], making the replacement of the short electrode array by a long one necessary in order to restore the low frequency hearing. To avoid reimplantation in the case of a delayed loss of hearing, EAS users may also be implanted by atraumatic long electrode arrays [Adunka et al., 2004; Helbig et al., 2011; Skarzynski et al., 2011]. If a long electrode array is used in an EAS condition, the attenuation and basal shift of the travelling wave peak

may need to be considered and compensated by pre-processing the acoustic signal in the speech processor.

Part B Acousto-electric interactions in the hearing ear due to electromotility

B1 Response of the normal hearing cochlea to electric stimulation – an overview

The main mechanisms playing a role in the electrically and acoustically stimulated inner ear with residual hearing, and possibly taking place during stimulation with EAS devices, are illustrated in Figure B1.1. Blue colour indicates mechanisms related to electric hearing and green colour indicates mechanisms related to normal, acoustic hearing. The figure shows the uncoiled cochlea with the basilar membrane located between scala vestibuli (above) and scala tympani (below), with residual hair cells on top of it. A cochlear implant is inserted into the scala tympani and it stimulates at the 5th electrode (counted from the apex). Acoustic stimulation is noted by the loudspeaker symbol to the left of the inner ear. Numbers above the cochlear duct indicate various positions along the organ and the corresponding cross-sections are shown below.

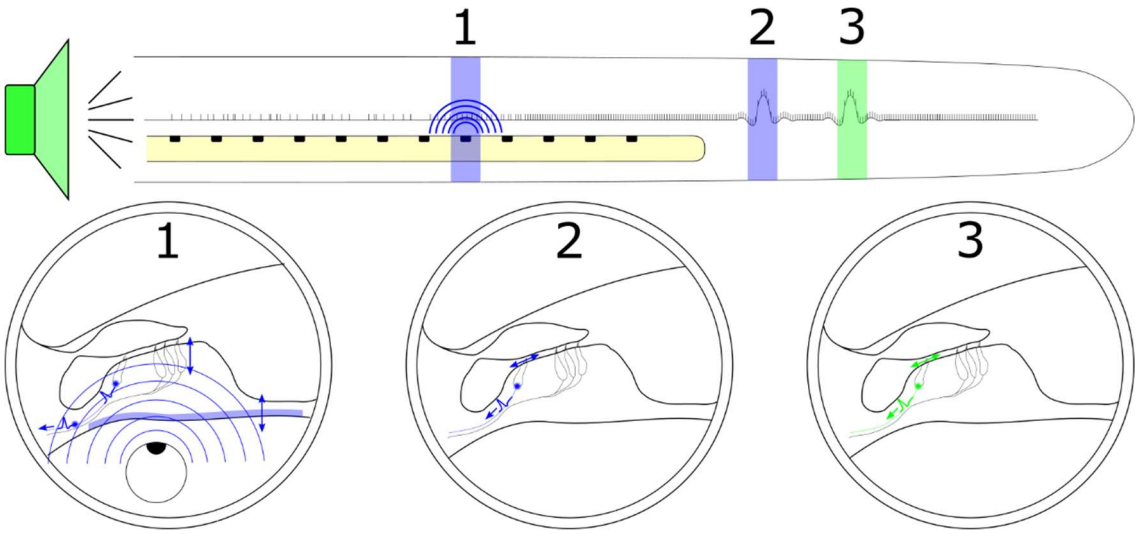

Figure B1.1 Mechanisms of hearing in the electrically or acoustically stimulated cochlea with residual hearing.1 – cochlear cross-section at the place of direct electric stimulation.
2 – cochlear cross-section at the place of electrically evoked travelling wave peak.
3 – cochlear cross-section at the place of acoustic travelling wave peak.

Acoustic response (3) results from the acoustically evoked travelling wave on the basilar membrane that excite the inner hair cells (IHC) and in turn the auditory nerve fibres (ANFs) at the characteristic place of the acoustic stimulus frequency.

Electric stimulation of the ANFs firstly takes place directly at the location of the stimulating electrode (1). At this direct electric stimulation place, the electrical field may excite various sites of the cochlear partition [Sato et al., 2017]. The electric field may

directly evoke action potentials at the ANFs or indirectly by a less probable depolarization of the IHCs [Moxon, 1971].

At the location of the stimulating electrode, an electrically-evoked mechanical response is also generated that results in an acoustic like response that travels along the basilar membrane to the characteristic place of the electric stimulus frequency (2). This electrically-evoked response has been termed the electrophonic response [Moxon, 1971]. The basilar membrane may be set into movement by forces originating either from OHC electromotility [Nuttall & Ren, 1995; Ren et al., 2009] or from an electrostatic interaction between the charged scala media (with ~80 mV endocochlear potential) and the stimulating electric field [Sato et al., 2017].

B1.1 Direct electric response

Direct electric stimulation of the auditory nerves is the mechanism employed in cochlear implants and properties of it were investigated extensively both in deaf [Stypulkowski & van den Honert, 1984; van den Honert & Stypulkowski, 1984; Shepherd et al., 1993; Shepherd & Javel, 1997, 1999; Miller et al., 1998; Javel & Shepherd, 2000] and hearing ears [Moxon, 1971; Miller et al., 2006]. In deafened ears (by induced IHC and OHC death, but remaining ANFs), electrical stimulus was shown to generate a broad excitation pattern with small dynamic range and short response latency. Compared to deafened conditions, direct electric stimulation of a hearing cochlea is shown to have a lower threshold and a wider dynamic range [Sato et al., 2016].

B1.2 Outer hair cell motility

In the 1980s, outer hair cells (OHC) were shown to exhibit motile responses to electric stimulation in vitro [Brownell et al., 1985; Ashmore, 1987]. Electromotility of the outer hair cell was further characterised by Santos-Sacchi [Santos-Sacchi, 1989]. Depolarization of the membrane potential results in the reduction of cell length and hyperpolarization leads to elongation as shown in Figure B1.2. Later, electromotility was also shown to follow the electric stimulation frequencies up to 100 kHz both in vitro [Frank et al., 1999] and in vivo [Grosh et al., 2004].

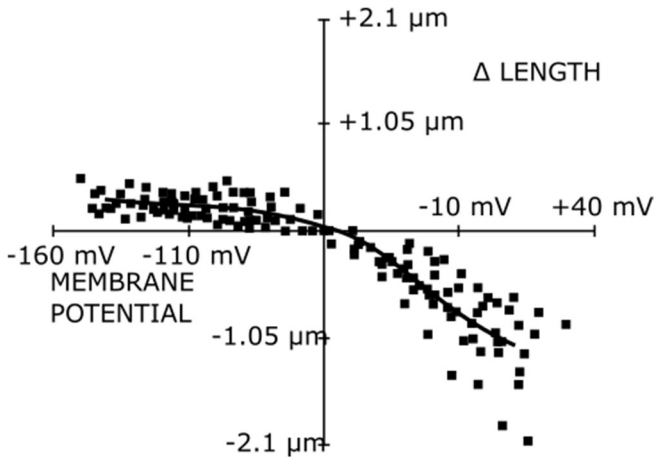

Figure B1.2 Change of OHC length with respect to the OHC membrane potential. Adapted from [Santos-Sacchi, 1989].

Depending on the current injection site, the current resulting in electromotility, may pass through the transduction channels of the OHC (scala media injection) or the basolateral membrane of the cell (scala tympani or extra-cochlear injection) [Jiefu et al., 2006].

B1.3 Electrically evoked otoacoustic emissions (EEOAEs)

Preceding the discovery of OHC electromotility, Hubbard and Mountain (1983) measured acoustic emissions from the ear canal in response to electric stimulation, so-called electrically evoked otoacoustic emissions (EEOAE) . Since the discovery of OHC electromotility, EEOAEs are often associated with OHCs and used for studying their electromotility in vivo. EEOAEs were shown to follow the stimulus frequency [Hubbard & Mountain, 1983] and to grow linearly with increasing current levels [Murata et al., 1991; Ren & Nuttall, 1995]. The frequency response of the emissions exhibit a stimulation-site-dependent low pass characteristic in guinea pigs [Murata et al., 1991; Kirk & Yates, 1996] as shown in Figure B1.3. EEOAEs in response to sinusoidal stimulation are represented by solid lines with filled markers (lines with empty markers show the enhancement of EEOAEs with an additional acoustic tone that is the topic of chapter B4 and will be discussed there in detail). The frequency characteristics of EEOAEs obtained for the second and third turn stimulations show a flat response up to slightly below the characteristic frequency of the stimulation sites and then sharply roll off. This indicates that due to the mechanical impedance mismatch, electro-motility is ineffective in generating an EEOAE if the stimulation frequency is above the tuning of the BM. But roll-off is not indefinitely steep and EEOAE are still present at frequencies higher than the characteristic frequency of the stimulation site. In agreement with Nakajima et al. (1994), Kirk and Yates (1996) argue that due to the spread of electric excitation, the generation

site of EEOAEs is spatially distributed. The spread of excitation allows for the generation of EEOAEs at frequencies with a characteristic place basal to the stimulation site. Furthermore, the spatial distribution of EEOAEs generation also explains the peaks and notches of the first turn results by the spatially distributed generation site. The measured EEOAE in the ear canal is the vector sum of the responses originating from various locations that can differ in phase thus suppress or enhance each other. Nuttall's group also confirmed these findings for electrical stimulation delivered to the scala tympani and also demonstrated the bandpass characteristics of EEOAEs from this cochlear location as shown in Figure B1.4 [Nuttall et al., 2001].

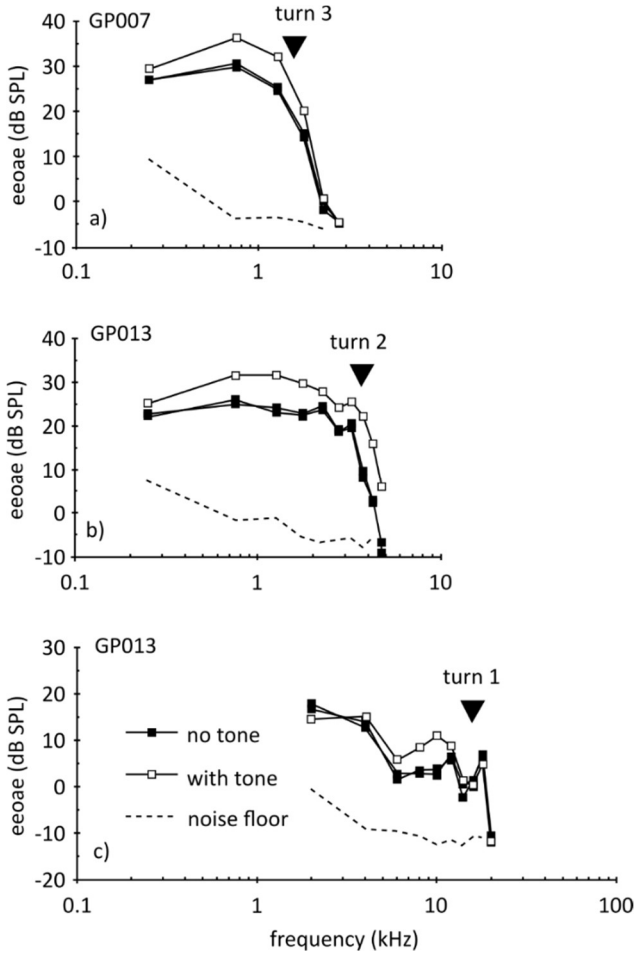

Figure B1.3 Frequency tuning of EEOAE generated by stimulation at various cochlear turns in the guinea pig. The curves with filled markers in the 'no tone' condition show the frequency tuning of EEOAEs measured before and after an EEOAE measurement that was conducted in the presence of an additional acoustic tone – the 'with tone' condition represented by empty markers. Dashed lines show the noise floor of the measurements. Bold arrowhead markers indicate the characteristic frequency of the stimulation site. Adapted from [Kirk & Yates, 1996].

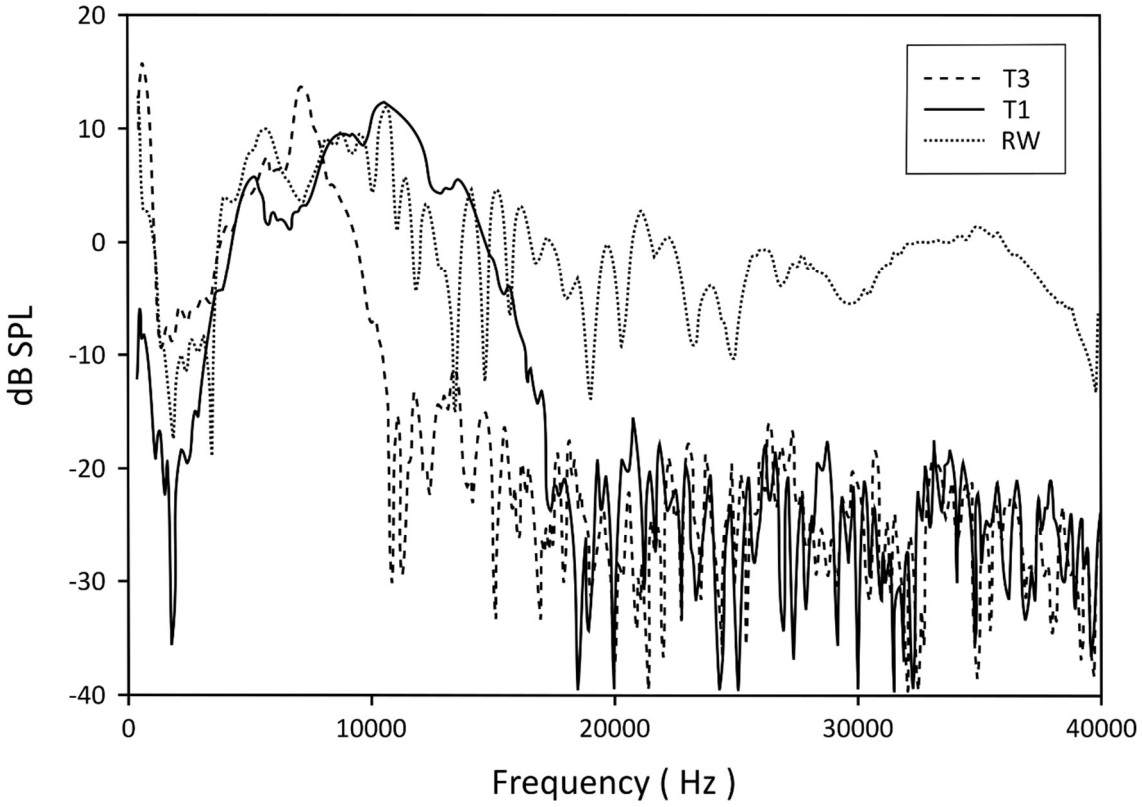

Figure B1.4 Band-pass characteristics of EEOAE transfer functions evoked by an electrode positioned in the first (T1), third (T3) turn of the scala tympani or at the round window (RW) of the guinea pig. Adapted from [Nuttall et al., 2001].

B1.4 Electrophonic response

Properties of the electrophonic response were studied by various physiological techniques. Using single fibre auditory nerve recordings, Moxon (1971) was the first to report electophonic responses. His observation that, compared to a direct electric stimulation, the electrophonic response exhibits a longer latency that can be associated with both the travelling wave delay and an IHC synaptic delay was later also confirmed by Lusted and Simmons (1988). Electrophonic responses were also observed in BM displacement measurements in guinea pigs [Nuttall & Ren, 1995]. Nuttall and Ren (1995) demonstrated that electric stimulation of the hearing cochlea evokes a BM motion similar to the motion evoked by acoustic stimulation, namely a travelling wave. By the application of an acoustic forward masking paradigm of the electrically evoked compound action potential (ECAP), the frequency selectivity of electrophonic response to extracochlear sinusoidal electrical stimulation was shown by Ren and colleagues (2009). Using multi-channel recording along the tonotopy of the inferior colliculus, also Sato and colleagues (2016) showed in guinea pigs, that the electrophonic response travels down to the characteristic place of the electrical stimulation frequency, similarly to the acoustic travelling wave.

One might assume that the mechanical drive underlying electrophonic responses is the same as that underlying EEOAEs, namely OHC motility. But this is still to be shown and own attempts will be reported in chapters B4 and B5.

B1.5 Electro acoustic interactions

As cochlear implantation with hearing preservation started to spread towards the end of the 20th century [Von Ilberg et al., 1999], the demand for basic animal physiology research about acousto-electric interactions also increased. Some of the first investigations showed the suppression of ECAP, in response to monopolar electrical pulses, by broadband acoustic noise [Nourski et al., 2005, 2007]. Applying the opposite paradigm, Stronks and colleagues demonstrated that acoustically evoked compound action potentials (ACAP), in response to tones, can also be suppressed by monopolar electrical pulse trains [Stronks et al., 2010, 2011]. Stronks et al. (2010) also pointed out that the suppression of ACAP was the strongest at frequencies corresponding to the spectral peak of the electrical stimulation, and therefore linked the suppressive mechanism to the electrophonic response. Interaction between electrophonic and acoustic responses will be one of the main topics of chapter B6 in this thesis.

To gain better understanding of electric-acoustic interactions in human ears with residual hearing, recent research investigated masking effects between the modalities using psychophysical [Lin et al., 2011; Krüger et al., 2017; Imsiecke et al., 2018; Saoji et al., 2018] and electrophysiological experiments [Koka & Litvak, 2017].

Psychophysical masking effects in EAS patients were attempted to be linked to electrophysiological measures by Koka and Litvak (2017). They measured cochlear microphonic responses to acoustic stimulus alone and to acoustic stimulus in the presence of an electric masker pulse train. The difference in the cochlear microphonic responses were compared to behavioural acoustic threshold elevations during electric masking tests. Although the change in cochlear microphonics qualitatively reflected the psychophysical threshold elevations, quantitatively the behavioural change was larger. The authors argued that the quantitative difference in the measures may have been due conducting the tests at different stimulus levels.

The masking of an acoustic probe by electric stimulation was shown to be dependent both on the distance between the cochlear loci of the electrical stimulation site and the best place of the acoustic stimulus [Krüger et al., 2017] as well as the temporal delay between the masker and the probe [Imsiecke et al., 2018]. Electric masking effects were shown to decrease with increasing spatial and temporal separation between the modalities. Interestingly, these studies have also shown that spatiotemporal dependency

of masking was missing in the acoustic masking paradigm. Although, the difference between the electric and acoustic masking effects may be explained by central masking effect instead of peripheral mechanisms, as suggested by the investigators and by the results of contralateral masking studies [C. James et al., 2001], the present study may shine a new light on these findings (see chapter B6).

B2 General Physiology Methods

Preceding experimentation, specialised experimental hardware had to be trialled, software written and tested. The details of the finally applied equipment and the used surgical procedure are discussed in the following sections.

B2.1 Experimental setup

The block diagram of the experimental setup is presented in Figure B2.1. Experiments were conducted inside a triple-walled soundproof booth. All equipment inside the booth (within the dashed rectangle in Figure B2.1) was operated by their own battery to avoid ground loops.

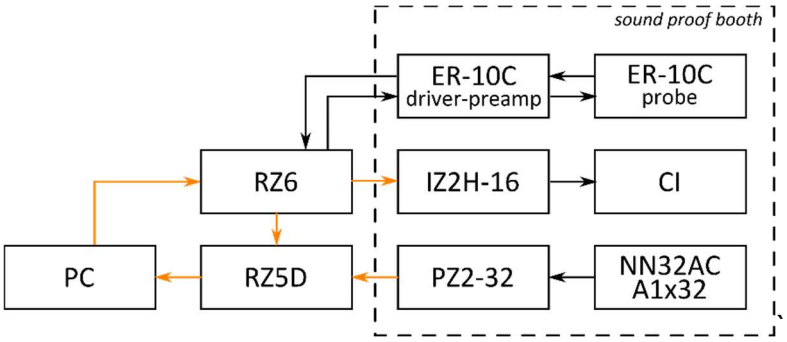

Figure B2.1 Schematic of experimental setup. Orange arrows represent optical connection, for detailed explanation see text.

The complete system was controlled from outside the soundproof booth by a personal computer (PC, running MS Windows 7), using custom-made Matlab (Mathworks, Natick, MA) software for signal generation and OpenEx (TDT, Alachua, FL) circuit for signal acquisition.

B2.1.1 Stimulus generation

The Matlab generated waveforms were loaded to an RZ6 multi-processor (TDT, Alachua, FL). This unit was responsible for the synchronous presentation of acoustic and electric stimuli at a sampling rate of 100 kHz.

Acoustic stimuli were presented by one of the two loudspeakers of the otoacoustic emission probe (ER10C, Etymotic Research, Elk Grove Village, IL). Tight coupling of the acoustic stimulus to the ear canal was achieved by snugly fitting the probe's eartip tube (ER10C-02) into the hollow interior of the right ear cone (see section B2.2).

Electric stimulation current was generated by an optically isolated current source (IZ2H-16, TDT, Alachua, FL)) that was controlled by the RZ6 and delivered the electrical stimulation currents to the cochlea via an animal CI electrode array (provided by Oticon

Medical, Vallauris, France). The diameter of electrode array was 0.3 or 0.4 mm and consisted of 4 or 6 contacts with a spacing of 0.7 mm (see panel D in Figure B2.2). The mode of stimulation, if not otherwise stated, was bipolar, using the two most apical electrodes.

B2.1.2 Acoustic calibration

Acoustic calibration of the ER10C speaker was completed with a short silicone tube, simulating a guinea pig ear canal. Into one end of the tube, a B&K 4138 1/8th inch microphone (Brüel & Kjær, Nærum, Denmark) was inserted and the other end of the tube was attached to the tip of ear cone that contained the ER10C probe. The distance between microphone and cone tip was 5 mm. The B&K 4138 microphone was calibrated by a B&K 4231 calibrator and the signal of the microphone was amplified by a B&K 2669 microphone preamplifier. The B&K microphone signal was fed through a B&K 2636 preamplifier that forwarded the amplified signal to the TDT RZ6. For the calibration of the ER10C microphone, the silicone tube that simulated the ear canal was pierced in approximately the middle by a short, 1 mm plastic tube to which an insert earphone (ER4, Etymotic Research, Elk Grove Village, IL) was attached that produced a wideband calibration noise. This configuration ensured that, at least to the lowest resonance within the silicone tube, both microphones received the same sound pressure, and so the frequency response of the ER10C microphone could be obtained for the off-line compensation of the recorded acoustic signals.

B2.1.3 Signal recording

Acquisition of acoustic and neural signals was performed by the TDT RZ6 and RZ5D multi-processors, respectively. An optical connection between these units, in a communication loop that included the controlling PC, ensured clock-synchronized recordings across both devices.

Acoustic signal recording was completed by the microphone of the ER-10C probe. To utilize the maximum dynamic range at the input of the RZ6 (10 V_{peak}), the signal was amplified by 20 dB with the ER-10C preamplifier and by a further 20 dB with the onboard amplifier of the RZ6. The analog signal was eventually sampled at a 100 kHz rate by the RZ6 unit.

Acoustic calibration of the ER10C microphone was done with a similar setup as the calibration of the ER10C loudspeaker. An ER4 (Etymotic Research) speaker, driven by the RZ6 multiprocessor, was additionally inserted into the tube through a tight gap to serve as a sound source for the calibration.

Neural signals were recorded by a 32-channel linear, single shank probe (A1x32, NeuroNexus, Ann Arbor, MI). To minimize crosstalk from the strong electric stimulation in the cochlea, differential recording mode, using the available reference electrode on the shank, was applied. The recording probe was attached to a high impedance headstage (NN32AC, TDT). To minimize electric artefacts, the grounding wire of the head stage was attached to the temporal muscle by a micro crocodile clip as close as possible to the craniotomy (see section B2.2). The neural signals were transmitted from the headstage to a 32-channel TDT PZ2 preamplifier that sampled the electrical signals at a 25 kHz rate and transferred them via optical cables to the RZ5D multiprocessor outside the booth.

B2.2 Surgical procedure

Male Duncan-Hartley guinea pigs were used in the in-vivo physiological experiments. This rodent is widely used in hearing research, thus offering us a possibility for a research comparable to others work. Additionally, cochlear size of guinea pigs allows the insertion of a cochlear implant while maintaining an intact/residual hearing. Lastly, the ease of access to this rodent's midbrain makes neural recordings from the auditory pathway possible.

Preceding surgery, anaesthesia was induced by intraperitoneal injection of 6-6.9 ml/kg Urethane (20%). Analgesia was initiated by intra muscular injection of 0.2 ml Hypnorm or 0.4 ml Fentadon and was maintained by injection of half dose throughout the procedure as indicated by pedal reflex, or blood oxygen level which was monitored with an oximeter. To prevent mucous and saliva secretion, 0.2 ml Atropine was delivered subcutaneously. Lignocaine was locally applied upon indication during surgery.

Depth of anaesthesia was examined regularly by testing the paw withdrawal and blink reflexes (by the touch of eyelashes). Physiological state of the animal (heart rate, breathing rate and SpO2 level) was monitored by a custom-made software (Matlab) that analysed data of the oximeter (Nonin, developer's kit, Plymuth, MN) attached to the front paw. The body temperature of the animal was monitored and maintained by a closed loop system (Harvard apparatus, Holliston, MA) that collected data from a rectal probe and controlled a heating blanket that the subject was placed on.

After establishment of a deep anaesthesia, the animal was shaved where further surgical steps required clear surface (proximity of ear canals, top of the head and at the throat). Both tragi were removed, and ear canals were cleaned of wax to ensure blockage free sound delivery and recording. A tracheotomy was prepared, and the trachea was cannulated to promote effortless breathing. The head of the animal was secured in a

stereotaxic frame by using hollow ear cones for clear access to the ear canals. The scalp was opened along the midline and the temporal muscle was detached from the skull to prepare a clean surface for the ~5×5 mm craniotomy that was made at the line of ear canals, 2-3 mm lateral to the midline (see panel A in Figure B2.2) on the contralateral side to the stimulated right ear. Finally, the dura was removed.

For CI insertion, the cochlea was accessed caudally. First, an opening at the bulla was prepared. In a second step, a cochleostomy was scraped proximal to the round window (see panel C in Figure B2.2) to prepare for scala tympani insertion of an animal CI electrode array (Oticon Medical, Vallauris, France, see panel D in Figure B2.2). As a concluding step, the electrode array was inserted into the scala and advanced apically following the curvature of the first cochlear turn, with having at least the two most apical electrode contacts inside the scala tympani to allow bipolar stimulation.

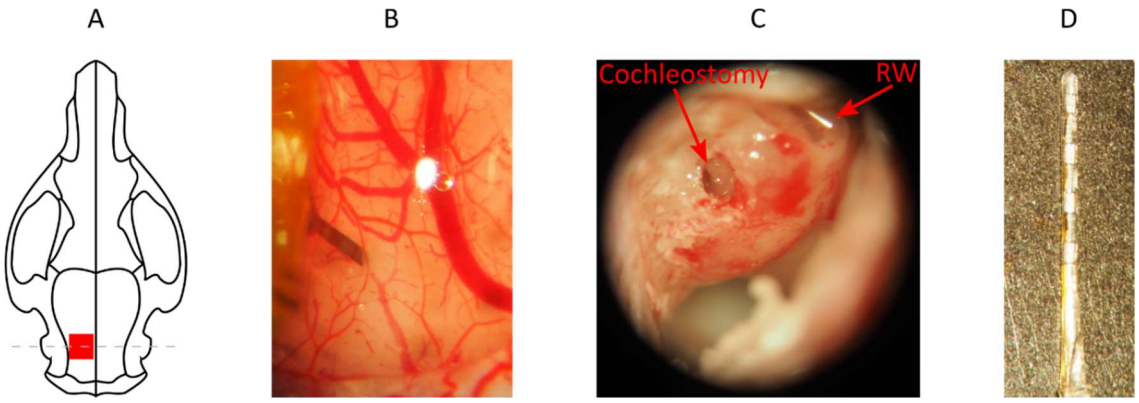

Figure B2.2 Illustration of surgical landmarks and the CI electrode. A – Typical position of craniotomy. B – Typical insertion site of the recording electrode. Note the characteristic blood vessel that branches in Y-shape and served as a landmark for insertion. C – Typical position of cochleostomy while looking rostral through the bulla opening. RW – Round Window. D – Animal cochlear implant electrode with 0.3 mm diameter and 4 contacts.

All procedures were approved under the United Kingdom Animal (Scientific Procedures) Act of 1986.

B2.3 Insertion of the neural recording electrode

The 32-channel neural recording probe was inserted into the brain with a 30° angle inwards the sagittal plane to run along the tonotopic axis of the inferior colliculus (IC). Characteristic blood vessels as landmarks (see panel B in Figure B2.2) aided the process of searching for the low-frequency midbrain region that was usually found within 5 to 10 attempts. After positioning the neural probe with its tip abutting the brain surface, presentation of 300 ms long wide-band acoustic noise bursts with 300 ms gaps at a level of approximately 40 dBSPL was started. The recording probe was slowly advanced to

deeper brain regions using a micromanipulator (SM-5, Luigs & Neuman, Ratingen, Germany) and the signal from the tip electrode of the array was monitored audio-visually. Upon observation of an auditory response, signal presentation was changed to pure tones with frequencies and levels dynamically adjusted on a 2D plane by computer-mouse movements, using a custom Matlab graphical interface. In case of identification of a tuned neural response to a satisfactorily low frequency tone (satisfactory was defined by the actual experimental procedure, typically < 500 Hz), the probe was further advanced, until responses were observed along the whole recording array, covering the typical range of 500 to 16000 Hz. In case of initially finding with the tip electrode an IC region responding already to too high stimulation frequencies, the neural probe was not further advanced, but immediately retraced and repositioned for another track in order to reduce mechanical damage to the mid-brain.

An acoustic response area measurement (see section B2.4), with responses ranging typically between 500 Hz and 16000 Hz, confirmed the correct recording electrode placement in the IC. Acoustic response measurement was repeated after opening of the bulla. A decrease in response threshold was typical at this point due to release of middle ear pressure that could build up during the surgical procedure. To monitor hearing sensitivity, acoustic response area measurement was also repeated following the preparation of the cochleostomy and the insertion of the CI. Hearing sensitivity usually remained unchanged after the cochleostomy and the rare cases of damaged cochlea (e.g. cracked cochlear wall), the experimental results were not included in further analysis. Following the CI insertion, the high-frequency thresholds sometimes increased and in case of extensive hearing loss, the experimental results were excluded from later analysis.

B2.4 Determining the recording electrode to frequency map

To confirm correct positioning of the electrode along the tonotopic axis of the IC, an automated procedure that recorded neural responses to randomized acoustic pure tones with various levels (30 to 70 dB SPL) across the entire frequency range (0.2 to 16.6kHz) was applied. Activity in response to the stimuli was plotted as seen in Figure B2.3. Each plot represents the acoustic response area of an electrode contact. It shows the power within the neural signal, coded as colour, as a function of tone frequency and level. The detailed description of how neural power was determined can be found in Appendix BA. A gradual shift of the activation pattern form the dorsolateral (Ch-1) to the ventromedial

(Ch-32) electrodes can be observed, which describes the tonotopic gradient of the central nucleus of the IC [Lim & Anderson, 2007; Schnupp et al., 2015].

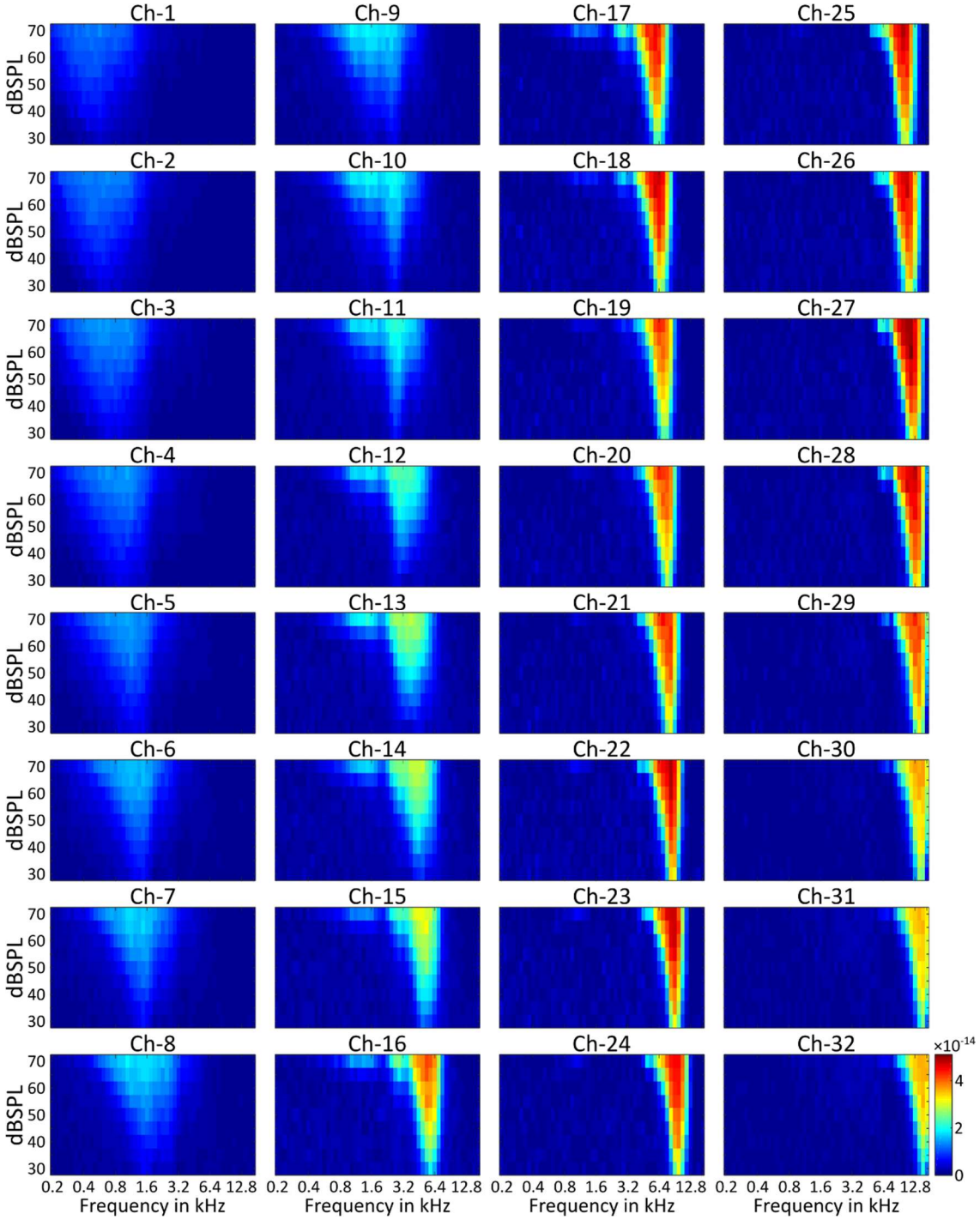

Figure B2.3 Example frequency response area plots confirming proper electrode positioning within the IC (362B1)[3].The title of the panels indicate the number of the recording electrodes in an ascending order that follows a dorsoventral progression of the IC. The stimulus frequency and level are indicated in the x- and y-axis and the neural response strength is visualized by the colour scale.

[3] 362B1 is the identifier of the experiment. The first three digits identify the experimental animal and the digits following the letter 'B' (B stand for 'Block', the format used for data storage) identify the experiment number. This identifier is noted below all figures corresponding to experimental data throughout the thesis.

Instead of plotting the response area at every electrode, the response along the spatial extent of the linear electrode array to a single frequency can be constructed (Figure B2.4). These will be called the spatial tuning curves (STC) and examples for various tone frequencies are shown in Figure B2.5.

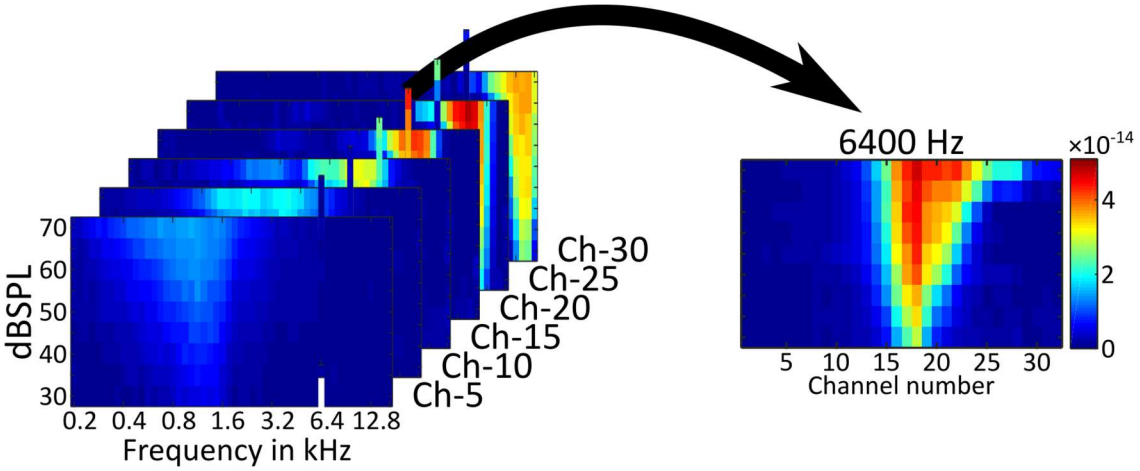

Figure B2.4 Response area to spatial tuning curve conversion.

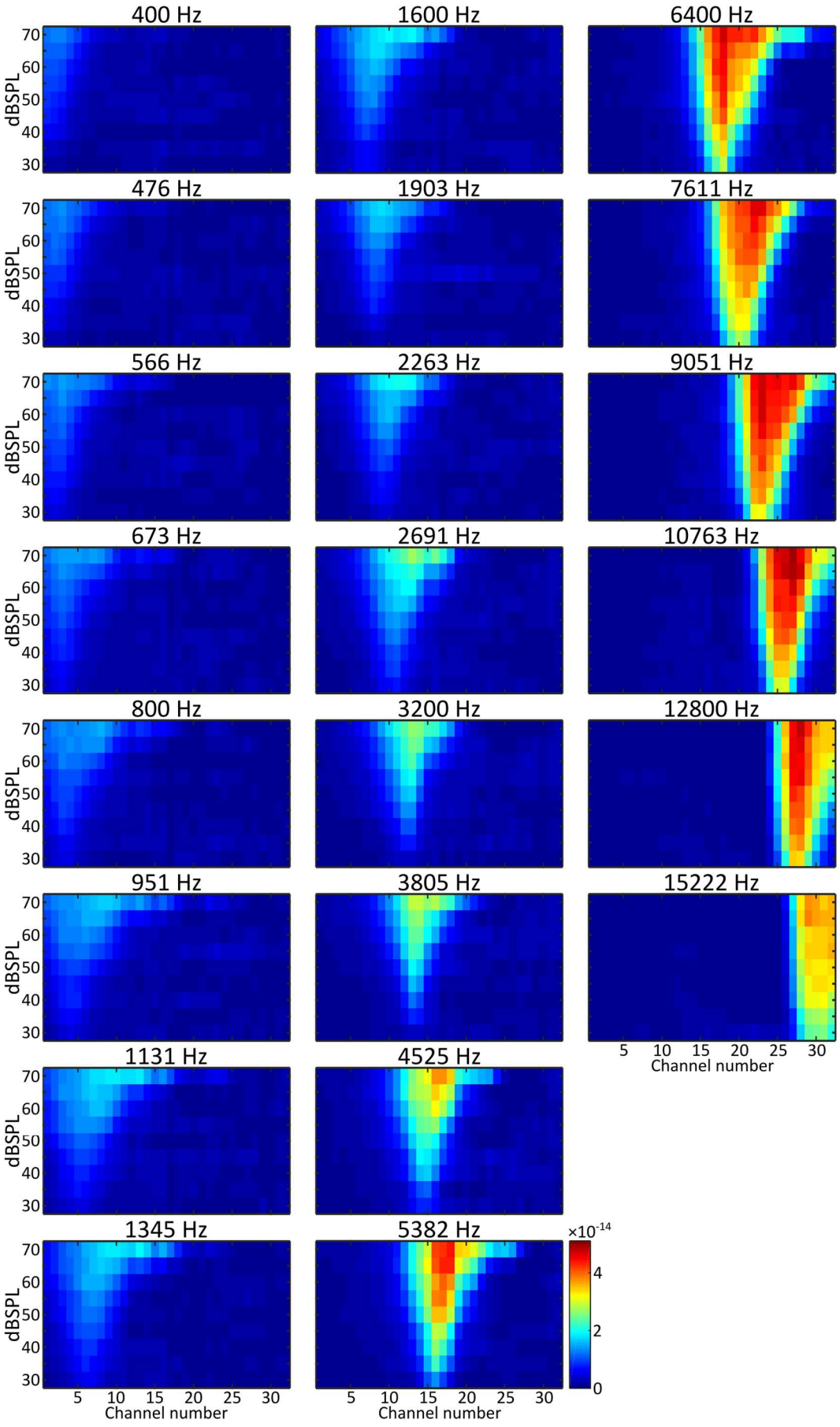

Figure B2.5 Example spatial tuning curve plots (362B1).

The abscissa of STCs represents the recording probe array that runs along the tonotopic axis of the IC. The progression of activity pattern along the recording array with increasing stimulus frequency is clearly visible. Also note the asymmetry of the patterns that can be related to the travelling wave on the basilar membrane. Similarly to the travelling wave envelope that gradually builds up from the base (high frequency part of the cochlea) towards the apex (low frequency part of the cochlea) until reaching its peak, the threshold of neural activity gradually decreases from the ventral electrodes (corresponding to the high frequency region in the IC) towards the dorsal electrodes (corresponding to the low frequency region in the IC) until reaching a minimum threshold. After the travelling wave reaches its peak, it decreases rapidly and likewise, the threshold of neural activity increases rapidly after its minimum.

The general goal of this study is to observe the various excitation patterns to acoustical and electrical stimuli along the tonotopically organised cochlea. It is however impossible to record the neural activity along the entire tonotopical range simultaneously directly at the output of the cochlea. Fortunately, the tonotopic organisation of the cochlea is preserved all along the auditory pathway, up to the cortex. The tonotopic map of the IC is easy to access. It is straight and more than 1 mm long and can for our purpose be used as a “proxy” of the cochlear activation. We are therefore not interested in space measured in millimeter, but expressed in characteristic frequency (CF), the frequency of a stimulus that excites the place with its lowest intensity. Such a CF-scale offers a way for mapping the STC of the IC to the STC of the cochlea. It is therefore necessary to determine accurately the CFs of the recording contacts, and this was done individually for each experiment. The CFs could as well be translated to positions along the cochlea in mm from the stapes, but the project aims to generalize the results from the guinea pig to the human cochlea, thus making this conversion superfluous.

Electrode frequency mapping can be approached by two methods. First, the CFs can be extracted from the threshold-tip of the response area of each electrode. The quantization error in mapping by this method depends on the frequency resolution of the applied test tones. This method is however prone to unavoidable imperfections in the frequency transfer function from the acoustic system to the acoustic input of the cochlea, the vibrations of the oval window. A notch present in the acoustic transfer function can lead to a jump in CF estimation and in turn falsify extraction of the tonotopy. The second method extracts the characteristic place (CP) of a single test frequency from the STCs. The CP would be here the electrode number, and the error in mapping in this case is determined by the spatial resolution of recording contacts. However, this method is independent of acoustic errors, as one STC corresponds to a single frequency, but might

be falsified by the variance in the sensitivity of the electrode contacts (both by the equipment as well as the number and proximity to the activated neurons).

Thus, in order to best estimate the tonotopic mapping of the IC to the electrode is obtained if the two methods are combined. First, the threshold tips (defining either stimulus frequency, or electrode number, here called CP) are extracted from both the response area (like Figure B2.3) and the STC plots (like Figure B2.5) following the method presented in [Snyder et al., 2004]. They defined the threshold of an electrode (or a stimulus frequency) by the lowest stimulus level that evoked an activity that exceeded 25% of the dynamic range of the recorded signal power. The CF of the electrode (or the CP of the stimulus frequency) is the frequency (or the electrode) at which the threshold is observed. If the lowest tested stimulus level evoked already an activity higher than 25% of the dynamic range, then this level is considered to be the threshold. In case of multiple frequencies leading to a threshold crossing, the one causing the highest activity is selected to be the CF (or CP).

In a second step a curve fitting method is applied, incorporating the data points obtained with both of these two methods. Figure B2.6 shows the CF estimates in blue and the CP estimates in green. First, the characteristic frequency map is roughly determined by a second order curve fitting (black solid line). A similar method is used by Dong and colleagues (2010). In a second step, the data points located more than 1/4th octave away from first fit are excluded and the curve fitting is repeated (red line) to obtain the final estimate of the CF mapping to the electrode contacts.

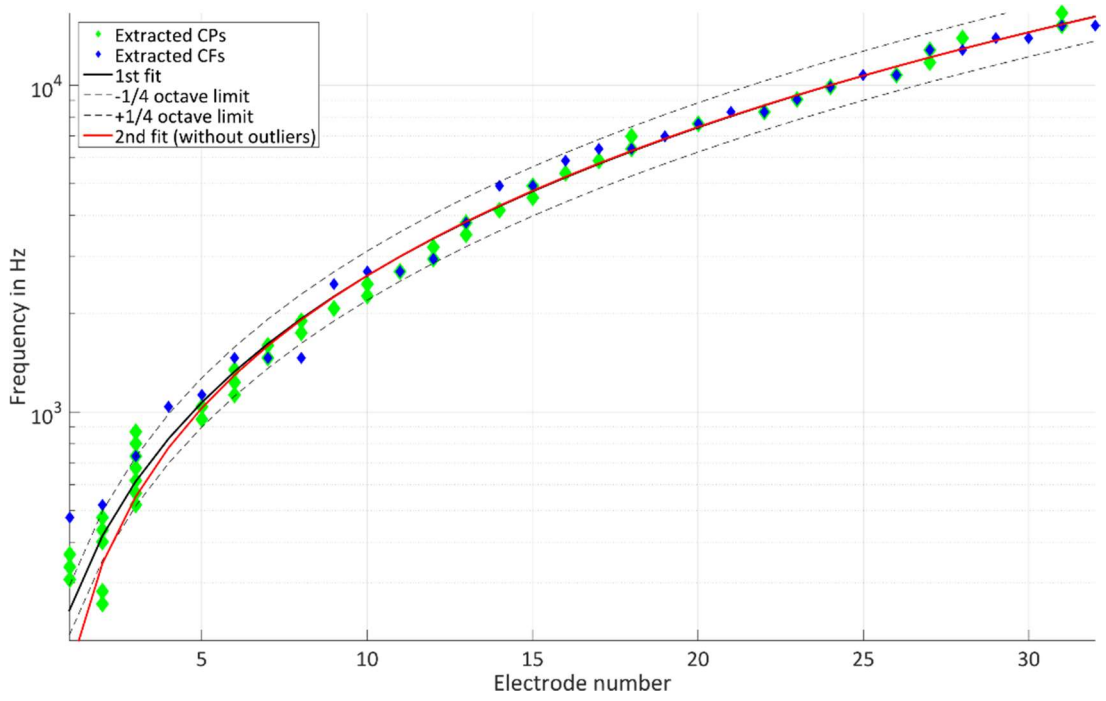

Figure B2.6 Electrode to CF mapping based on extracted CPs and CFs from frequency response are and spatial activity pattern plots.

Throughout the following chapters a double labelling of the x-axis (recording channel numbers and corresponding CFs) is used in plots where activity along the whole IC/cochlea is of interest. An example usage of double label is shown in Figure B2.7.

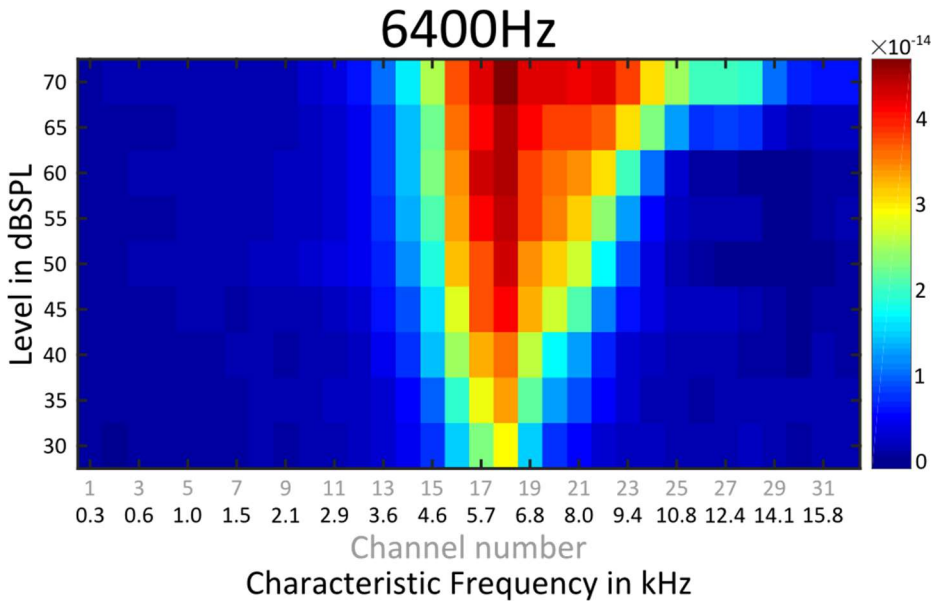

Figure B2.7 Double labelling example.

B3 Neural responses to electrical stimulation measured in the guinea pig mid-brain

To investigate the neural responses evoked by electrical stimulation in a healthy ear, experiments with electrical sinusoid stimulation were conducted. First, the characteristics of the electrophonic and direct electric responses were studied. Second, the electrophonic response properties were compared to the response properties to acoustic stimulation.

Electric stimulation was short, so that the electrical artefact could be separated from the neural response (latency >8 ms) in time. Electric sinusoid bursts of 8 ms including 2 ms on- and offset squared cosine ramps were presented in a bipolar mode at the two most apical electrodes of the CI. Stimuli consisted of a combination of various frequencies and levels and were repeated 50 times. Each repetition was presented in a new individually randomized order. Like in Sato et al. (2016), the stimulus amplitude was defined in dB relative to a 10 mA peak-to-peak signal.

B3.1 Direct electric and electrophonic response characteristics

Typical results from one animal are demonstrated in Figure B3.1. Spatial activation patterns are presented in panel A, where each sub-panel corresponds to a stimulus frequency indicated in the title. Panel B shows the response growth functions[4] as the stimulus level increased. Solid lines show response strength averaged across the three neighbouring electrodes that are most sensitive (threshold) to the electrophonic response and dashed lines show the average response strength across the three neighbouring electrodes most sensitive to direct electric stimulation. The stimulation frequencies are given in the colour legend. Panel C visualizes frequency-dependent (tonotopic) loci of electrophonic (blue dots) and fixed location of the direct electric (red dots) response.

[4] Note, that in order to observe the thresholds in response to the different stimulus frequencies more accurately, the step of background activity removal (for details see Appendix BA) is omitted for the curves in panel B.

In response to stimulation with frequencies from 1 to 5.6 kHz, a broad excitation pattern can be observed around at the characteristic place of 11kHz in the spatial activation patterns. This pattern is associated with the direct response. By having a closer look at the direct response, one can discover two distinct peaks around channel 24 and 30. It turned later out that these peaks are the result of the bipolar stimulation, forming a dipole and alternating the exciting current polarization across the two stimulation electrodes (see section B6.3.3 in chapter B6). It has been shown previously by Kral and colleagues (1998) that the two lobes of such dipole field by a bipolar CI stimulation can excite two distinct neural populations along the tonotopy of the spiral ganglion and it is therefore not surprising that it can excite two distinct neural populations in the IC. Response patterns to direct electrical stimulation with similar characteristics can also be seen in the data of Snyder and colleagues (2008).

The growth functions of direct electric responses (dashed lines in panel B) show that the threshold and response strength are inversely proportional to the stimulus frequency. Above threshold, the direct responses grow with a steep slope. Some of the growth functions that reach saturation (e.g. 1.4 kHz) have a dynamic range of less than 4 dB. Similar restricted electric dynamic range was also reported by others [Moxon, 1971; Sato et al., 2016]

Due to the proximity of the direct-electrical and electrophonic peaks in the 5.6 kHz condition, the response to direct electrical stimulation starts to merge with the basal tail of the electrophonic response, resulting in a slightly lower threshold, and shallower slope compared to the 4 kHz-condition. Above this frequency, the direct electric response cannot be clearly distinguished from the dominating electrophonic response.

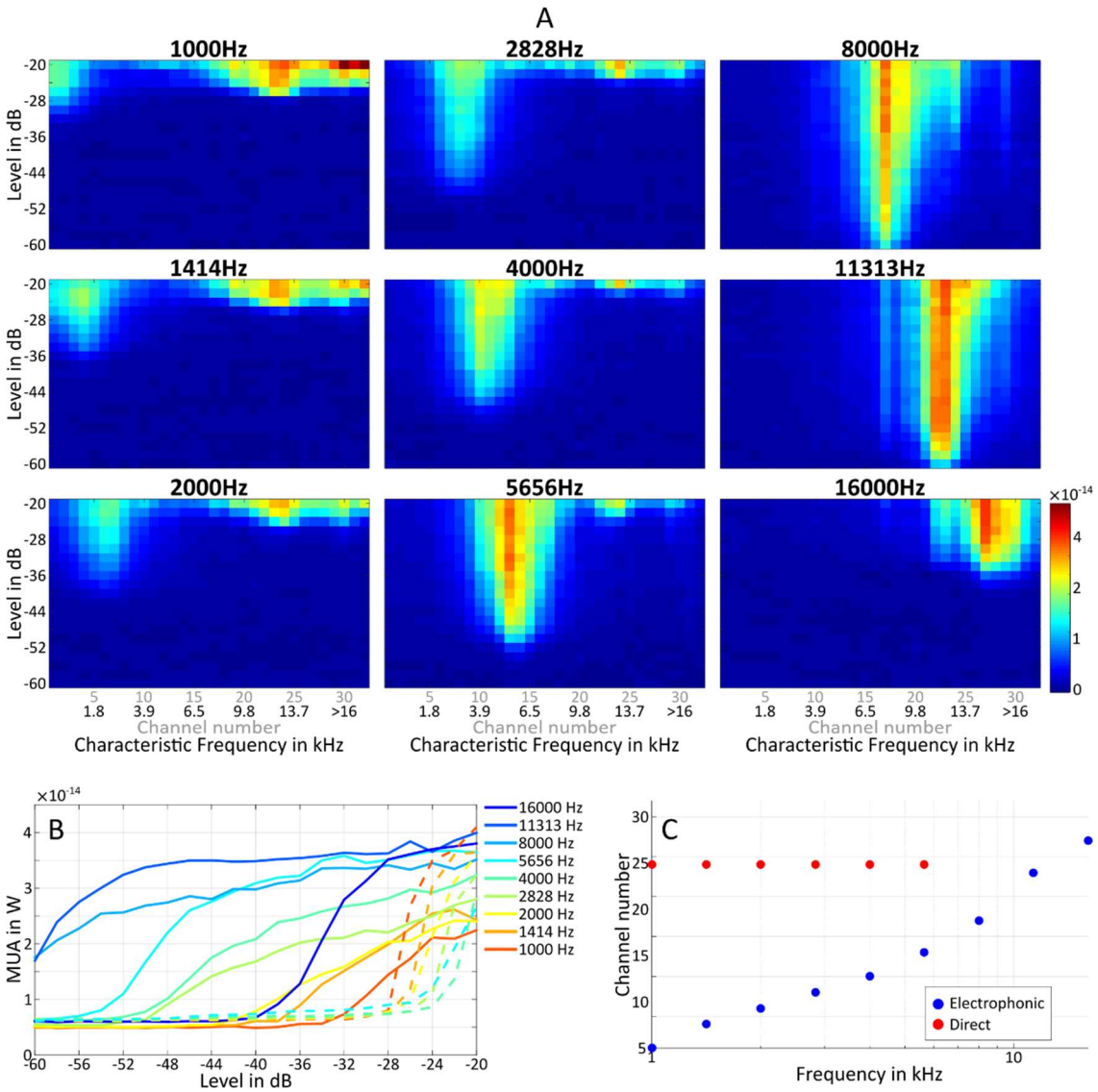

Figure B3.1 Response to electrical sinusoids in a normal hearing cochlea (355B13). A – Spatial activation patterns in response to electric sinusoids. B – Rate-level functions of electrophonic response (solid lines) and direct electric response (dashed lines); data obtained as the average response of 3 neighbouring electrodes that are most sensitive (threshold) to the electrophonic response and the direct electric stimulation (around the characteristic place of 11 kHz), respectively. Note that direct electrical responses could not be separated from the electrophonic at 8 kHz and above. C – Frequency-dependent (tonotopic) loci of electrophonic (blue) and fixed location of the direct electric (red) response.

The inverse relationship of the direct electric response threshold and response strength with stimulation frequency as shown in Figure B3.1 is in accordance with the literature that shows the proportionality of auditory nerve [Hartmann et al., 1984; van den Honert & Stypulkowski, 1984; Shepherd & Javel, 1999] or inferior colliculus neural [Lusted & Simmons, 1988] firing with the amount of delivered electrical charge rather than just the strength of the current. In our sinusoidal waveforms the amount of delivered charge is proportional the stimulus period. The lower the stimulus frequency, the longer the period thus more charge is delivered.

A second response, the electrophonic response, can be seen as a sharp peak at the best place of the stimulus frequency. The growth functions show that the electrophonic

thresholds decrease with increasing frequency up to 5.6 kHz, and although the 8 and 11.3 kHz curves are already above threshold for the lowest tested stimulus level, the sensitivity clearly increases further at these frequencies. Also, the strength of supra-threshold responses show proportionality to the stimulus frequency, with the exception of the 16 kHz stimulation, which is already above the characteristic frequency of the stimulation place (~11 kHz) and shows also a dramatically increased threshold. The response to this stimulus frequency is the result of a local resonance within the reach of the electrical spread, rather than the result of an electrically evoked travelling wave.

The tendency of increasing electrophonic response strength and decreasing threshold as the stimulus frequency approaches the characteristic frequency of the stimulation site was also demonstrated by Sato and colleagues [Sato et al., 2016]. Also EEOAEs show similar response characteristics [Murata et al., 1991; Kirk & Yates, 1996; Nuttall et al., 2001] as introduced in chapter B1. This frequency dependence can be explained mechanically. The origin of the electrically-evoked travelling wave of electrophonic responses is the site of electrical current injection, where presumably OHC electromotility displaces the basilar membrane. The mechanical impedance of the basilar membrane is frequency-dependent and has its minimum at the local characteristic frequency. It controls the velocity of the basilar membrane for a given OHC input force, which thus decreases as stimulation frequency departs from the characteristic frequency of the stimulation place, resulting in reduced energy transfer.

For stimulation frequencies higher than the characteristic frequency of the stimulation place, a travelling wave cannot develop. In this case, the electrophonic response is simply reflecting the local mechanical resonance at the characteristic place on the basilar membrane that gets probably excited directly by the electrical field of the stimulation that spreads to this place and drops exponentially with distance from the current injection site (e.g. [Black et al., 1981; Jolly et al., 1996; Kral et al., 1998; Tang et al., 2011; Dang et al., 2015]).

The slopes of the growth function in Figure B3.1-B vary across stimulus frequency, but in general are much shallower compared to the growth curves to direct electrical stimulation. Above 4 kHz, electrophonic growth functions reached saturation with a response limit similar to the strength observed at saturation of the direct-electric response. The dynamic range of electrophonic response, that is more than 30 dB at some stimulation frequencies, is much larger than the dynamic range of the response to direct electrical stimulation, similar to that seen for acoustic stimulation (see section B3.3).

Panel C shows that the response to the direct electrical stimulation stays locally fixed to the stimulation site that has a characteristic frequency of 11 kHz. In contrast, the place of the electrophonic response, like the response to acoustic stimulation (see section B3.3), changes with stimulus frequency according to the cochlear tonotopy, supporting the notion that it is evoked by an electrically induced mechanical travelling wave.

B3.2 Threshold of direct electric and electrophonic response

Thresholds of direct electric and electrophonic responses were analysed from 7 animals and plotted with respect to stimulus frequency in Figure B3.2.

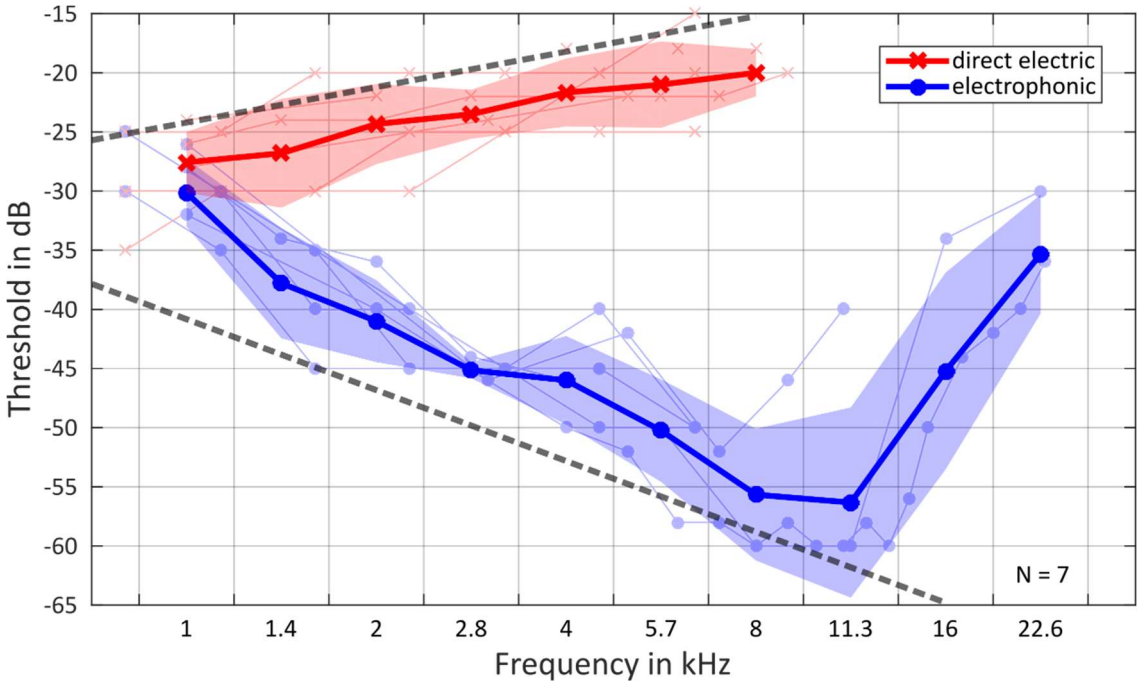

Figure B3.2 Threshold of electrophonic (blue) and direct electric response (red). Thin lines represent individual data; thick lines represent the average data across seven animals in half-octave bands with centre frequencies indicated on the x-axis and band borders shown by the grid lines; shaded area represents ±1 standard deviation from the average. Dashed grey lines indicate +3 and -6 dB/octave slopes.

The frequency-dependencies of the threshold reflect the observations made for the example in Figure B3.1. The threshold of the direct electric response increases with approximately 3 dB/octave until the electrophonic response becomes so close that it cannot be distinguished anymore. Electrophysiological studies with pulsatile electric stimulation show a direct electric threshold that decreases by 6 dB by doubling the pulse duration [Hartmann et al., 1984; van den Honert & Stypulkowski, 1984; Shepherd & Javel, 1999], that would be consistent with the theory of charge driven neural activity. However, psychophysical studies from the dawn of cochlear implants when devices

applied sinusoidal stimulation, demonstrated a detection threshold that also increases with approximately 3dB/octave above 300 Hz [Fourcin et al., 1979; Shannon, 1983, 1985] and suggest that the response threshold is not solely the function of the delivered electric charge. Indeed, firing threshold of neurons in the auditory pathway was additionally shown to be inversely proportional to the rate of change of the depolarizing current [Azouz & Gray, 2000; McGinley & Oertel, 2006; Ballestero et al., 2015], i.e. the firing threshold in response to a slowly increasing current is higher than the threshold in response to a rapidly changing signal. This phenomenon may be present during the application of sinusoidal waveforms and counteract the reduction of charge when increasing the stimulation frequency, leading to a threshold increase shallower than 6 dB/octave. An approximately 3 dB/octave direct electric threshold increase to sinusoidal stimulation can also be read from the results of Sato and colleagues [Sato et al., 2016].

The threshold of electrophonic response shows a decrease with approximately 6 dB/octave from 1 kHz to 11.3 kHz, the characteristic frequency of the stimulation site. Above this frequency, the thresholds increase sharply. The 6 dB/octave threshold decrease may, as mentioned above, reflect the increasing mechanical impedance that the outer hair cell forces face in moving the basilar membrane as the stimulation frequency departs from the characteristic frequency of the electrical stimulation site.

The opposing tendency of the direct electric and electrophonic thresholds below 11.3kHz results in an increasing gap between the curves. This gap is often called the “electrophonic advantage”, and was already observed and termed in 1971 by Moxon [Moxon, 1971] who also showed its frequency dependency i.e. the electrophonic advantage is larger for higher stimulation frequencies. The mean electrophonic advantage in our case at 1.4 kHz is 11 dB and increases up to an astonishing 36 dB at 8 kHz.

B3.3 Comparison of electrophonic and acoustic response

Electrophonic and acoustic responses were recorded to electric sinusoids and acoustic pure tones with identical temporal properties (8 ms in length, including 2 ms on- and offset ramps, and identical frequencies) and various levels that were presented in a randomized manner through 50 repetitions.

Electrophonic and acoustic response results can be compared in Figure B3.3, which shows a representative dataset from one experiment. Each row in the figure corresponds to a stimulus frequency indicated in the left-hand side of the rows.

The first column shows the spatial tuning curves to both kind of stimulation. Each line in a panel correspond to a different acoustic (solid lines) or electric (dotted lines) stimulus level. Lines with the same colour indicate acoustic and electric responses that are most similar in magnitude at the characteristic place of the stimulus frequency. The exact stimulus levels corresponding to the coloured lines can be read from the axes of the plots in the second column. Matching of responses of similar strength was done by visual judgement, and spatial tuning curves that did not exceed the noise floor, or show saturation are assigned a grey colour.

The second column relates the acoustic and electric stimulus levels that resulted in comparable acoustic and electrophonic responses. The marker colours in these panels are corresponding to the spatial tuning curves plotted in the first column.

The spatial tuning curves to electrophonic and acoustic stimulation show a strikingly similar shape at the characteristic place, which provides evidence that the mechanical electrophonic response travels along the basilar membrane like an acoustically evoked travelling wave. The plots relating electric current and acoustic stimulation levels giving similar neural activity at the characteristic place show a linear relationship with unit slope. This implies that the BM velocity, evoked by the OHC motility is proportional to the electrical stimulation current, a finding that is also supported by the linear growth function of EEOAE (e.g. [Murata et al., 1991; Ren & Nuttall, 1995; Nakajima et al., 1998] and own EEOAE measurements, reported in chapter B4 of this thesis).

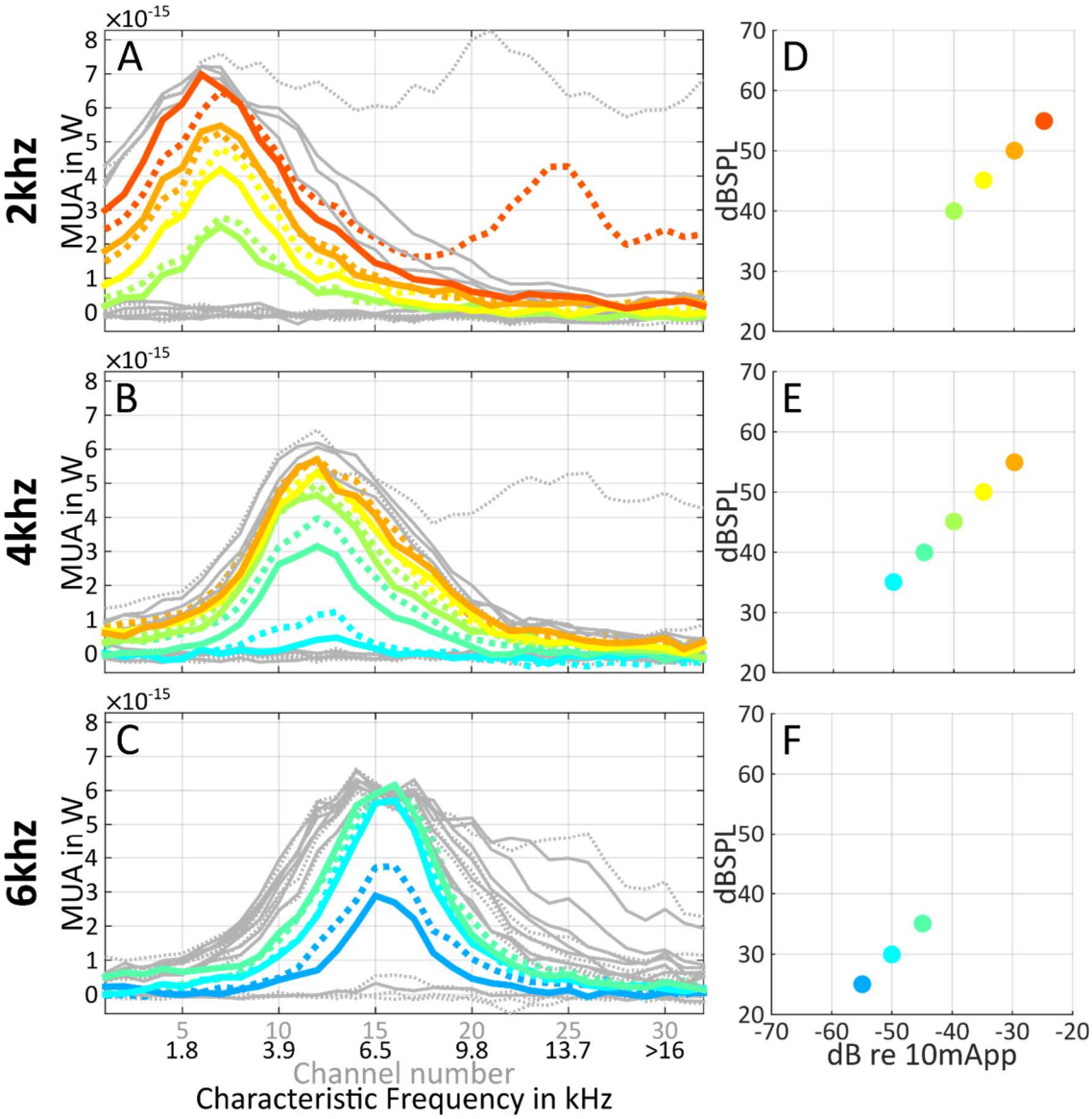

Figure B3.3 Comparison of electrophonic and acoustic responses; (355B29). First column: electrophonic (dotted lines) and acoustic (solid lines) spatial tuning curves; colours indicate responses with different levels, where electrophonic and acoustic response strengths were similar at the characteristic place of the stimulus frequency, for exact stimulus levels see the axes of the second column where the same colour coding is applied. Second column: Acoustic sound pressure levels and electric current levels eliciting similar neural response at the characteristic place of the stimulus are marked with dots

B3.4 Conclusions

It was shown, that in accordance with the study by Sato and colleagues (2016), electric stimulation of the hearing cochlea results in two separate stimulation sites: one related to the site of directly electrically stimulated auditory nerve fibres at the site of the stimulation electrode, and the other at the characteristic place of the stimulation frequency as an electrophonic response that is evoked by an electrically evoked basilar membrane movement.

For the first time in an electrophysiological study, it was shown that in response to sinusoidal stimulation, the direct electric response threshold increases with

approximately 3 dB/octave and the electrophonic response threshold decreases with approximately 6 dB/octave. In accordance with previous research [Moxon, 1971; Sato et al., 2016], the threshold of electrophonic response was shown to have an advantage over the threshold of the direct electric response. The electrophonic advantage increases as the stimulation frequency approaches characteristic frequency of the stimulation site where it can become as large as 36 dB.

Comparisons of acoustic and electrophonic tuning curves revealed a close resemblance that indicates the involvement of an electrically evoked travelling wave in the generation of the electrophonic response. Additionally, the pairing of acoustic and electric tuning curves allows for the assignment of an 'equivalent sound pressure level' to the electrophonic response. For example, the 2 kHz electric sinusoid at -25 dB re. 10 mA_{pp}, that is the threshold of the direct electric response, generates an electrophonic response that is equivalent to a 55 dB SPL tone.

The likely presence of OHC electromotility is suggested by the measurable cochlear microphonic responses in EAS patients [Choudhury et al., 2012; Haumann et al., 2019] also implies the presence of electrophonic response. A patient with good residual hearing thus may perceive the low-frequency content of basal electrical stimulation, e.g. the envelope information, acoustically as low-frequency disturbances in the apical part of the cochlea. Whether the envelope, modulating an electrical pulse-train carrier, gets demodulated by the OHC motility and travels up to the apex as an electrophonic response remains to be tested.

On the other hand, the electrophonic advantage could be utilised to evoke an acoustic-like stimulus for the residual hearing range of the cochlea, without yet evoking a direct electrical response. Unfortunately, the frequency-dependence of the electrophonic advantage is opposite than would be advantageous for this purpose because the residual hearing is usually in the low-frequency range where the electrophonic advantage is small. However, electrical stimulation was very basal in the experiments reported here, but in EAS patients a long electrode carrier may reach down to the 1 kHz characteristic place where mechanical impedance for the electromotile force transfer onto the BM and therefore the electrophonic threshold should be much lower.

There are some striking similarities between electrophonic responses and EEOAEs that suggest that their generation relies on the same mechanism. First, similarly to the stimulation site dependent band-pass characteristics of EEOAEs [Murata et al., 1991; Kirk & Yates, 1996; Nuttall et al., 2001], the electrophonic response was shown to have a threshold that increases as stimulation frequency departs from the characteristic frequency of the stimulation site. Second, the linear relationship between OHC

electromotility and stimulation current, as well as evoked BM velocity implied by a linear EEOAE growth function [Murata et al., 1991; Ren & Nuttall, 1995; Nakajima et al., 1998] was also supported here by showing linear relation between the current and acoustic sound pressure levels that evoke similar electrophonic and acoustic spatial activation patterns. These clues raised our interest to investigate the possibility of using EEOAEs as non-invasive markers for the presence of electrophonic response in human CI users. The following chapters (B4 and B5) report on my attempts to establish a direct link between EEOAEs and the electrophonic response.

B4 Biasing of OHC electromotility

The previous chapter pointed out the similar behaviour of EEOAEs and electrophonic responses. In EAS CI users with residual hearing, the electrophonic response may be present and interfere with the low-frequency acoustic hearing. An established link between the EEOAEs and the electrophonic response would allow for the usage of EEOAEs as a non-invasive diagnostic tool to identify the presence of electrophonics in patients. The putative driving source of both phenomena is OHC electromotility. A modification of the operational state of OHC electromotility is thus hypothesized to result in similar behaviour of both the EEOAEs and the electrophonic responses, the simultaneous observation of which would confirm the common source. The current chapter describes attempts to show such effects via OHC electromotility operating point biasing.

B4.1 The operating point of the electromotility

The normal operation point of OHC electromotility is defined by the resting membrane potential of the cell that is around -70 mV. In this state, the operation point is not in the most sensitive part of the motility curve as illustrated in panel A_1 and A_2 of Figure B4.1. An OHC pictogram in the left-hand side of the figure illustrates the cell in its resting state and the extreme, shortest and longest, states (indicated by dashed grey contour). Panel A_1 illustrates the characteristic curve of electromotility similarly to Figure B1.2, except that here, the change in length is expressed as the percentage of the maximum possible motility. The grey shaded area illustrates a possible stimulus induced membrane potential change and the corresponding change in the cell's length. Panel A_2 is the derivative of the curve in A_1, showing the sensitivity of electromotility expressed in dBs relative to the resting state. The vertical red dashed line indicates the -70 mV resting membrane potential and marks the operating point on the curves as a red dot, both in panel A_1 and A_2. The operating point is here clearly not at the maximum of the sensitivity curve.

Repositioning of the OHC electromotility operation point by changing the cell's resting membrane potential, i.e. the potential difference between the interior and the exterior of the cell, would result in a bias of the operation point and in turn, a change in sensitivity of the electromotility. Altering OHC motile responsiveness may either result in a reduced (panel B in Figure B4.1) or an increased (panel C in Figure B4.1) motility. OHC function

was studied by many by applying various biasing techniques and observing changes in EEAOEs.

A DC current injection into the cochlea may change the endolymphatic potential, the exterior potential surrounding the cell. The DC current can be both negative and positive, resulting in the increase or in the decrease of the resting membrane potential respectively. Electric DC biasing technique was first used by Roddy and colleagues (1994) who demonstrated enhanced or suppressed EEAOEs when additionally to the AC current stimulus they applied negative or positive DC currents into the scala media of the gerbil. Low frequency electric currents were also shown to modulate acoustically evoked DPOAEs [Frank & Kössl, 1997].

Similarly to the operating point of the electromotility, the operating point of the mechano-electrical transduction channels in the stereocilia can also be located asymmetrically along its transduction function (see Figure 1.4 in the main Introduction), causing an acoustic stimulus to be partially rectified and thus change the interior potential of the OHCs and consequently the operating point of the prestin electromotility. In 1989 Mountain and Hubbard showed that additional acoustic tone can enhance EEOAEs [Mountain & Hubbard, 1989]. Later Xue and colleagues (1993, 1995) identified that the acoustic enhancement is the largest if the frequency of the biasing tone is close to the characteristic frequency of the electric stimulation site and can be as large as 16 dB. These findings were complemented by Kirk and Yates (1996) who investigated the acoustic enhancement of EEOAEs at various cochlear turns of the guinea pig as shown in chapter B1. Kirk and Yates also showed that a low frequency acoustic tone, that slowly displace the basilar membrane position, and thus the operating point of the mechano-electrical transduction channels, can modulate EEOAEs [Kirk & Yates, 1998; Yates & Kirk, 1998]. Also Ren and Nuttall (1998) showed acoustic biasing effects on EEOAE that were evoked by extra-cochlear current injection.

During hybrid stimulation of patients with residual hearing, amplified intense acoustic stimulation is combined with electrical stimulation. As EEAOEs and electrophonic responses are thought to both be generated by OHC electromotility and EEOAEs are shown to get enhanced by as much as 16 dB [Xue et al., 1993] in the presence of a loud acoustic stimulus, also the electrophonic response may become enhanced leading to unwanted perceptual effects in EAS patients.

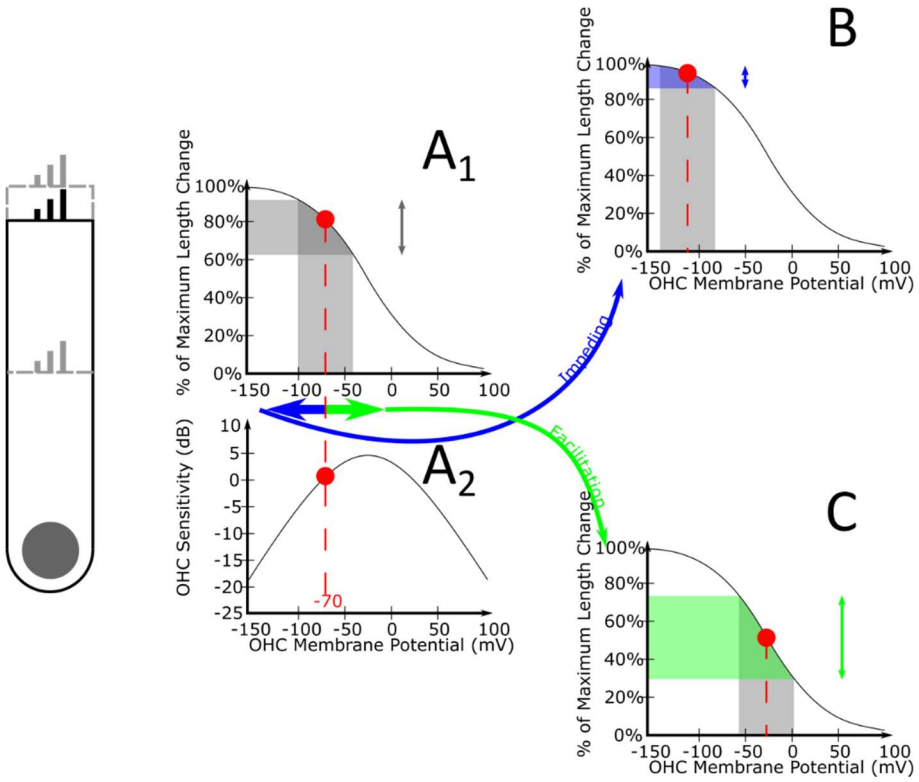

Figure B4.1 Changes in the membrane potential shift the operating point of OHC electromotility and results in a decreased or increased electromotile responsiveness. Adapted from [Roddy et al., 1994]. *An OHC pictogram in the left-hand side of the figure illustrates the resting and the extreme states of the cell (shortest and longest). Panel A_1 shows the OHC's electromotility curve with the length change expressed as percentage of the maximum possible length change. 0% corresponds to the shortest possible length. The vertical red dashed line corresponds to the natural -70 mV resting potential of the cell with a red dot on the curve marking the normal operating point. Grey shaded are below the curve illustrates a possible periodic membrane potential change around the resting state. The corresponding motility range can be read on the y-axis and is also marked by a grey double arrow. Panel A_2 shows the derivative of the curve in panel A_1 i.e. the sensitivity of OHC length change as a function of the operating point position. The sensitivity is expressed in dBs relative to the sensitivity in the natural state. Panel B illustrates the case with a resting potential of -110 mV. The operating point is in a shallower part of the motility curve compared to its natural position, thus a change in membrane potential equivalent to the one in panel A_1 results in less length change (indicated by the blue area and the blue double arrow). Panel C illustrates the case with a resting potential of -30 mV. The operating point is in a steeper part of the motility curve compared to its normal position, thus a change in membrane potential equivalent to the one in panel A_1 results in an increased length change (indicated by the green area and the green double arrow).*

B4.2 Acoustic biasing

First, the investigation of acoustic biasing of the electrophonic response is presented. Figure B4.2 illustrates the time course of the used stimuli. Acoustic and electric stimuli were presented simultaneously. Acoustic stimulation consisted of 100 ms long tones presented at the characteristic frequency of the direct stimulation place and at various sound pressure levels. Electric stimuli consisted of 8 ms long sinusoids with various frequencies at -30 dB re. 10 mA_{pp}. The level and frequencies of the electric stimuli were chosen such that electrophonic response was present for all electric stimulation and was also distinguishable from the direct electric response. Electric sinusoids were presented either 50 ms following (Case 1 in Figure B4.2) or preceding (Case 2 in Figure B4.2) both

the on- and offset of the acoustic tone. As shown in Figure B4.2, in the first case acoustic stimulation started at 0 ms and in the second case, the acoustic onset was at 100 ms. Both stimulation modalities included a 1 ms long on- and offset squared cosine ramp. Stimuli were presented every 400 ms in a randomized order and repeated 50 times.

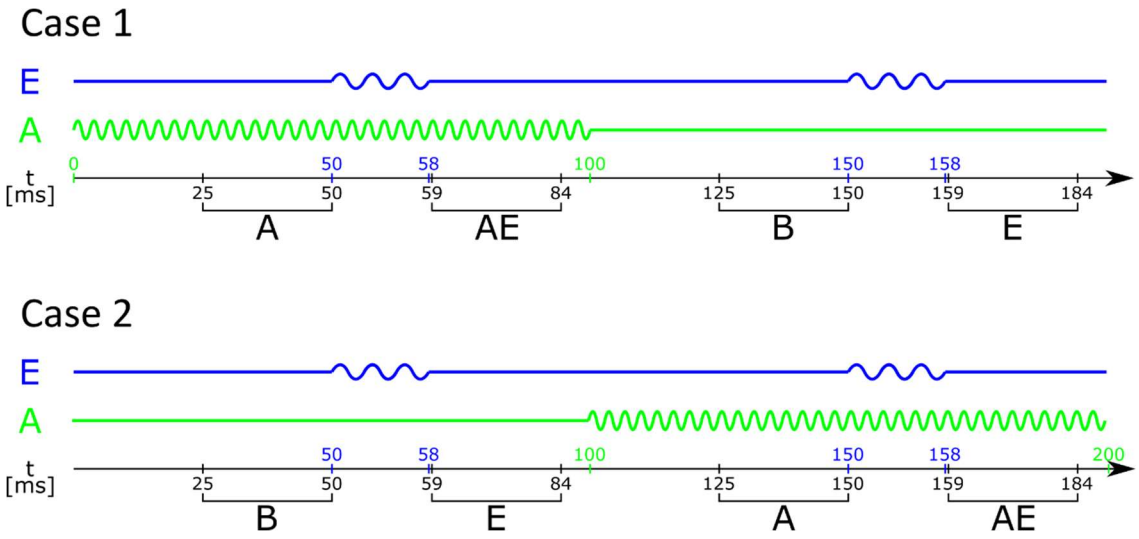

Figure B4.2 Acoustic biasing stimulus. Blue and green lines illustrate time course of the electric and acoustic stimulus. Numbers above the time axis with colours corresponding to the acoustic and electric stimuli show the on- and offset times. Numbers below the time axis show the limits of the windows used for extracting neural responses: A – Acoustic response window; AE – Acoustically biased electric response window; B – Background activity window; E – Electric response window

This procedure allowed for the observation of neural responses to various stimulus modality combinations. Neural responses were extracted in 25 ms windows for acoustic (A), electric (E), acoustically biased electric (AE) and spontaneous background activity (B) at positions shown in Figure B4.2. Acoustic biasing was tried in two animals.

B4.2.1 EEOAE artefact testing

To prove that the measured EEOAEs are not the result of electrical crosstalk between the stimulation and the acoustic recording path, the results of EEOAE measurements with open and blocked microphone tube were compared. Electrical sinusoids served as a test stimulus at various levels and frequencies. The growth functions of the EEOAEs for the recordings with open and blocked microphone tubes are shown in Figure B4.3. Measurements were conducted in the same animal in a healthy state. Obtaining clear growth functions only in the open tube condition demonstrate the physiological origin of EEOAEs. Note the typical linear nature of the growth functions that is in accordance with the work of other investigators [Ren & Nuttall, 1995; Nakajima et al., 1998].

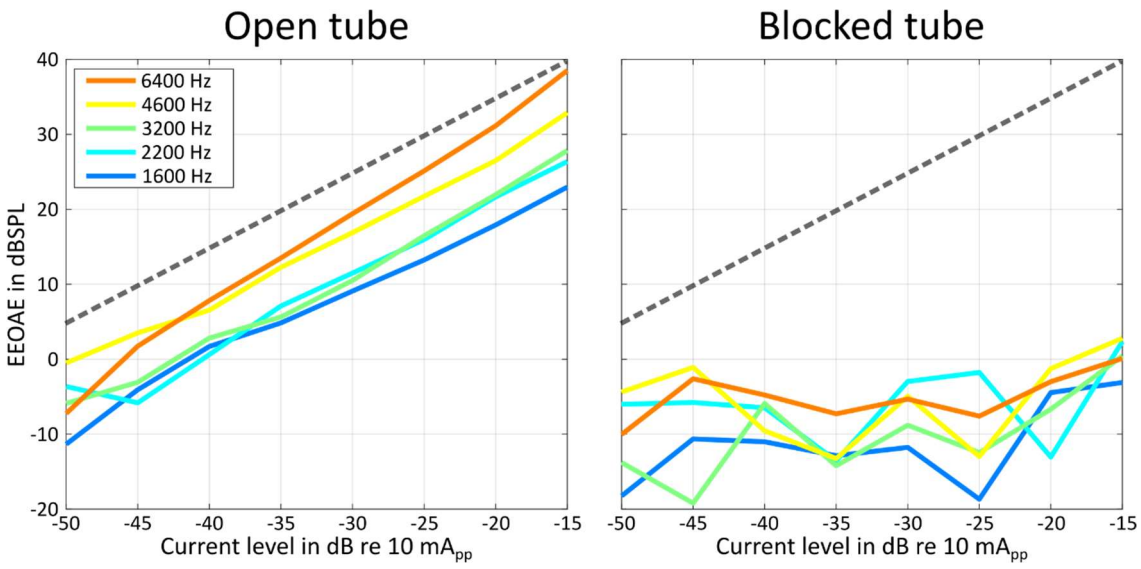

Figure B4.3 EEOAE growth functions measured with open (339B5) and blocked (339B37) microphone tube. The dashed grey line indicates 1 dB/dB linear growth.

B4.2.2 Results from animal #339

In this animal, the acoustic biasing effect was investigated on responses to electric sinusoids from 1.6 kHz to 6.4 kHz in half octave steps. The biasing tone was 8 kHz and based on previous literature results [Xue et al., 1995] the levels were selected to range from 50 to 80 dB SPL in 5 dB steps.

B4.2.2.1 Neural response

Figure B4.4 shows the spatial activation patterns obtained during the experiment. Panel A to E show the response of acoustically biased electric responses (window AE in Figure B4.2) with the electrical stimulus frequencies noted in the panel titles[5]. Coloured lines correspond to acoustic biasing levels from 50 to 80 dB SPL. Panel F shows the response to the 8 kHz acoustic biasing stimulus only (window A in Figure B4.2). Control responses to electric stimuli alone and background activity (window E and B in Figure B4.2) are shown as dotted lines in panel A to E and panel F, respectively.

The direct electric response is present for the 1.6, 2.3 and 3.2 kHz sinusoids. The direct electric response strength decays with increasing stimulation frequency due to the shortening stimulus periodicity as discussed in chapter B3. Albeit a clear peak is not visible, the decaying response pattern from high to low frequency regions in the right-hand side of the panels is indicative of a direct excitation place basal to the observed region.

[5] The indicated frequencies are rounded to the closest 100 Hz values. The exact electric stimulation frequencies were 1600, 2262, 3200, 4525 and 6400 Hz.

Electrophonic responses were present for all electric stimulus conditions at the characteristic place of the stimulus frequency. The peak of the electrophonic response to the 6.4 kHz electric stimulus shows no basal progression relative to the 4.5 kHz response and its strength is also reduced.

The acoustic response in panel F shows a clear peak at its characteristic place in response to 50 and 55 dB SPL stimulation levels. For higher stimulus levels, the neural excitation greatly widens towards more basal regions. Acoustic control experiments used for monitoring hearing sensitivity through the surgical procedure revealed that this phenomenon started to appear after preparing the cochleostomy. A small part of the cochlear wall may have fallen inside the scala tympani and may have resulted in restricted basilar membrane motion close to the insertion place. This may also explain the stop of basal progression of electrophonic response described in the previous paragraph.

In response to the 1.6, 2.3 and 3.2 kHz biased electric stimulation in panel A to C, the electrophonic response peaks are separate from the acoustic peak and show no change under biased conditions. In the 4.5 and the 6.4 kHz cases in panel D and E, the electrophonic response peak is inseparable from the acoustic peak under biasing condition and the common peak shows saturation with the same response strength for both cases. The saturation may have been caused by the aforementioned blockage of the basilar membrane.

No acoustic enhancement of the electrophonic response was shown in this experiment.

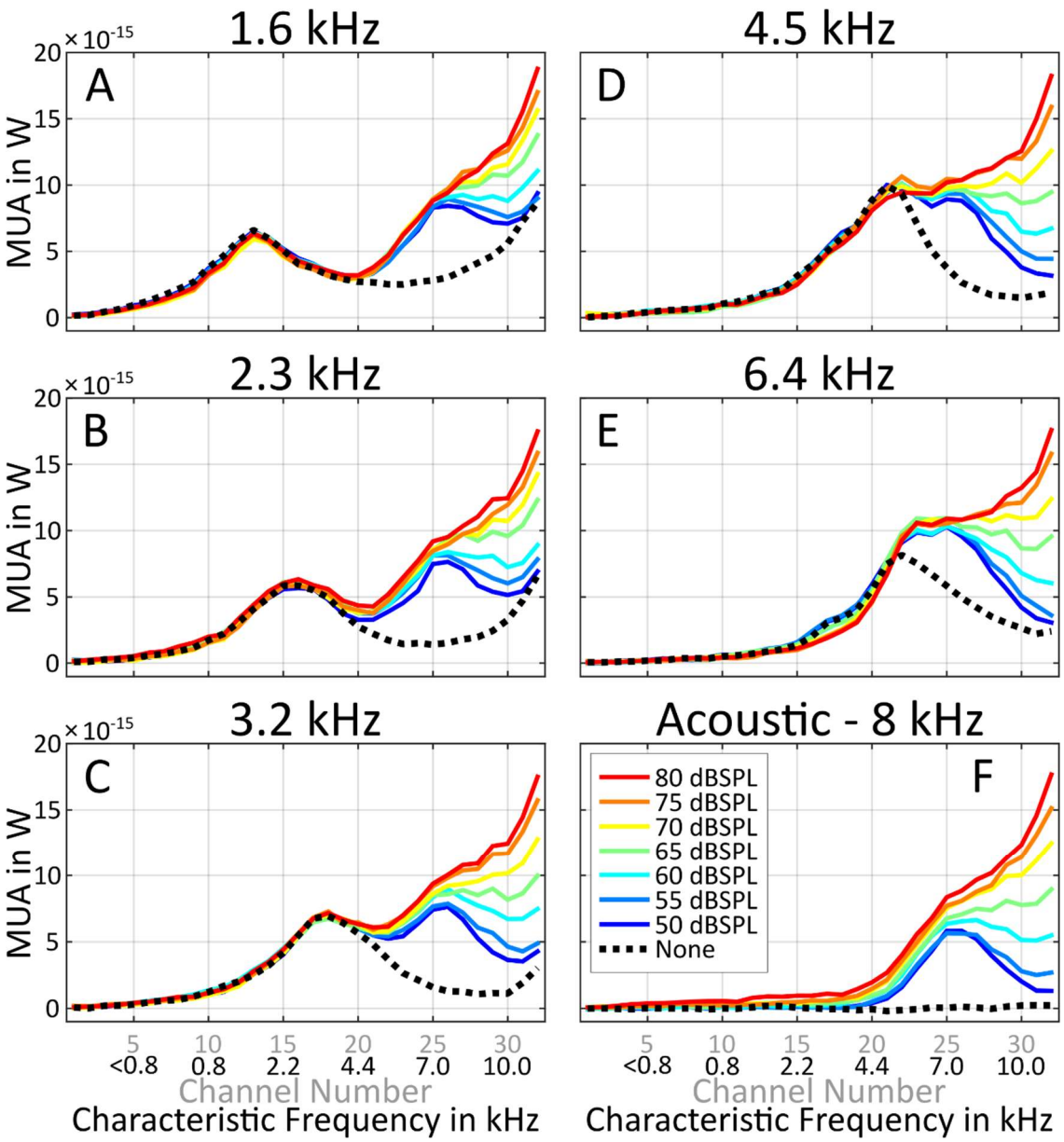

Figure B4.4 Effect of an 8 kHz acoustic biasing tone on the spatial activation patterns in response to -30 dB re. 10 mA_{pp} electric sinusoids of 1.6, 2.3, 3.2, 4.5 and 6.4 kHz (339B7). Panel A to E show response patterns to electric sinusoids (frequencies indicated in the panel titles) in the presence of the acoustic biasing tone. The 'Acoustic – 8 kHz' panel shows the spatial tuning curves in response to the biasing tone alone. Colours indicate the biasing tone level and black dotted lines show responses in the absence of the biasing tone.

B4.2.2.2 EEOAEs

Electrically evoked otoacoustic emissions were measured as a control and their spectrum is plotted in Figure B4.5. The columns represent the conditions with various frequencies of the electrical stimulation. Because EEOAE recordings have a shorter latency, they were extracted from a 5 ms window positioned 3 ms after the onset of the electric sinusoids.

The first row of Figure B4.5 shows the spectrum in response to the electric stimulation. The EEOAE is emphasized by blue colour and circle marker. To achieve a better signal

to noise ratio, these spectra are the average of the unbiased EEOAEs (window E in Figure B4.2) that were obtained during trials of all seven biasing levels.

The second row shows the spectrum during acoustic biasing with 70 dB SPL (window AE). Additionally to the EEOAEs and acoustic biasing tone components, the intermodulation products are also emphasized. The even order intermodulation products are coloured by green and the f_a-f_e and f_a+f_e components are differentiated by triangle and square markers. The odd order intermodulation products are coloured by red, and various markers are used to indicate the various components (f_a-$2f_e$ – triangle, f_a+$2f_e$ – square, $2f_a$-f_e – diamond and $2f_e$-f_a – star).

The third row shows the growth of EEOAEs and intermodulation products with respect to the level of the acoustic biasing tone. Only the components that were significantly different from background noise (shown by dotted lines) at least at one biasing level (ANOVA, $p<0.01$)[6] are plotted. The used colours and markers are identical to the ones used in the third row. The blue dots mark the unbiased EEOAEs.

EEOAE spectrum in response to purely electric stimulation shows a single peak at the stimulus frequency. The amplitude of the peak increases slightly with stimulation frequency as also revealed by the blue dots (unbiased) in the third row. This is in agreement with previous findings about the band-pass characteristics of EEOAE [Murata et al., 1991; Nakajima et al., 1994; Kirk & Yates, 1996; Nuttall et al., 2001], i.e. EEOAE grows as the stimulation frequency approaches the CF of the stimulation site.

The growth functions reveal, the EEOAEs in response to 1.6 and 6.4 kHz electric stimuli gradually increased with biasing levels by up to 4-6 dB. In the 3.2 kHz condition only the 80 dB SPL biasing condition resulted in increased EEOAE level by approximately 3 dB. No acoustic enhancement was observed for the 2.3 kHz and 4.5 kHz EEOAE. While the response peak of 1.6, 3.2 and 6.4 kHz EEOAE appears as a sharp spectral line, the corresponding spectral components of the 2.3 and 4.5 kHz EEOAs are spreading across the spectrum because the period of the 2.3 and the 4.5 kHz signals do not fit into 5 ms long analysis window. This imperfect resolution of the 2.3 and the 4.5 kHz primary components may have impeded the detection of an acoustic enhancement as compared to the perfectly resolved EEOAEs.

Interestingly, in the response spectra to combined acoustic and electric stimulation, additional intermodulation components appeared as an evidence of a nonlinear interaction between the electric and acoustic stimulation. The appearance of

[6] To be accepted as a significant response component, the acceptance criteria ($p<0.01$) must have been passed for any of the response-noise combinations. Noise at the component is measured at every biasing level.

intermodulation products was also shown by others at comparable levels [Hubbard & Mountain, 1983; Murata et al., 1991; Ren et al., 1996; Ren & Nuttall, 1998].

Additionally to the stimulus components (f_a and f_e), significant intermodulation products appeared mainly at the f_a-f_e frequency, and only with the 1.6, 2.3 and 3.2 kHz electric sinusoids. Above the noise floor, the level of these intermodulation products shows an approximately 1 dB/dB increase with increasing acoustic biasing levels. The $f_a \pm f_e$ intermodulation products probably reflect the electric modulation of the cochlear amplification of the acoustic tone causing a modulation of its stimulus frequency OAE (SFOAE). The proportionality of the increase of the $f_a \pm f_e$ intermodulation components with the biasing acoustic tone is indicative of a constant modulation strength that can be expected since the electric current that drives the modulation via the OHCs is constant.

In the 6.4 kHz condition, the $2f_e$-f_a intermodulation product appeared at 4.8 kHz and showed the highest response when the biasing tone was 55 dB SPL and gradually faded into the background noise with increasing biasing levels. The $2f_e$-f_a intermodulation product might be similar to an acoustically evoked distortion product otoacoustic emission (DPOAE) that is the result of the interaction of two mechanical waves. In our case, one wave was generated by the acoustic tone and the other is related to the electrophonic response that was generated by the electric stimulus. The mechanical origin of the $2f_e$-f_a component is further strengthened by the similarity of its level tuned characteristics to acoustic DPOAEs, that were also shown to possess an optimal primary tone level ratio to which the response is the strongest [Brown, 1987].

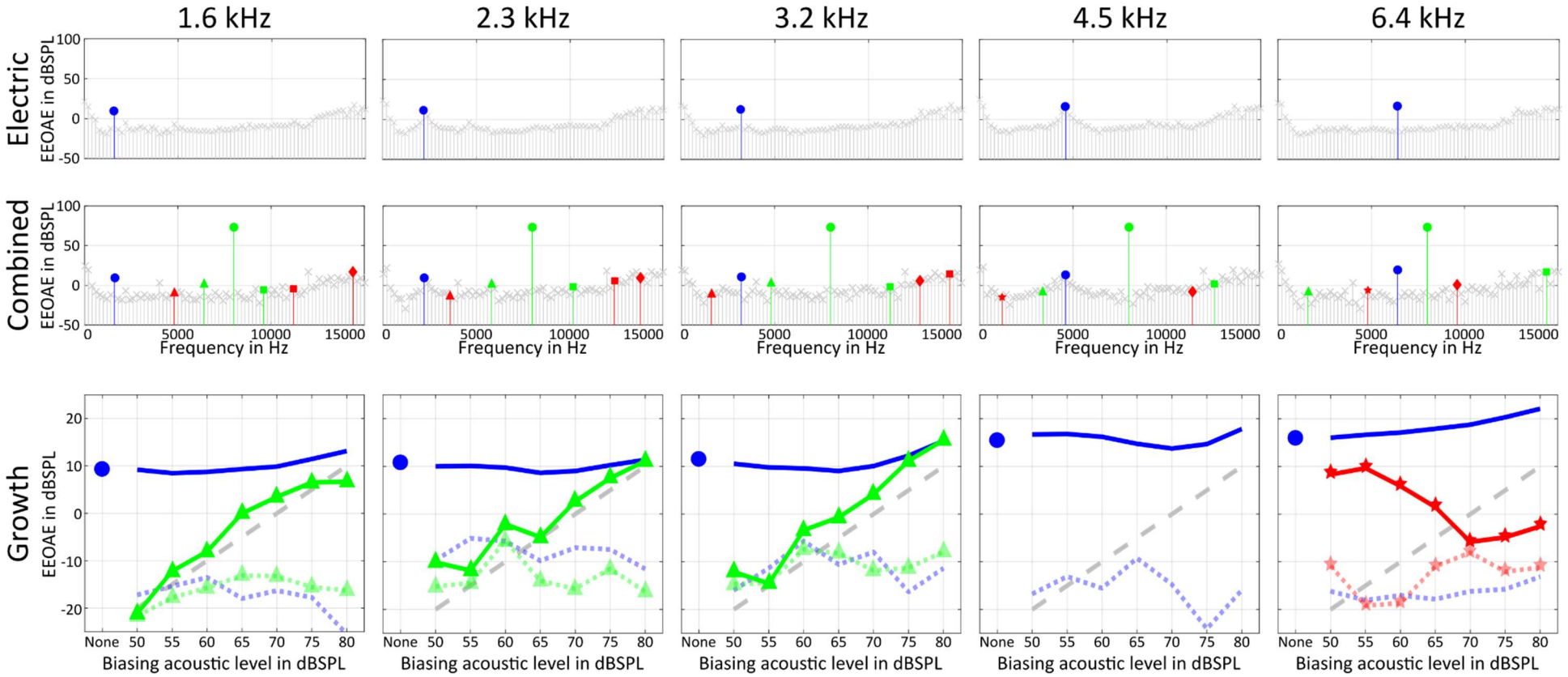

Figure B4.5 Acoustic biasing of EEOAE (339B7). Columns correspond to the applied electric stimulus frequencies.
1st row – EEOAE spectrum in response to the electric sinusoids alone, the EEOAE component is emphasized by blue colour.
2nd row – EEOAE spectrum during biasing with an 8-kHz acoustic tone of 70 dB SPL. Even harmonics are emphasized by green colour (f_a-f_e – triangle, f_a+f_e – square), odd harmonics are emphasized by red colour (f_a-2f_e – triangle, f_a+2f_e – square, 2f_a-f_e – diamond, 2f_e-f_a – star). Different markers aid the comparison to row 4.
3rd row – Growth function of EEOAE and the intermodulation products with acoustic biasing level. The intermodulation growth functions are plotted for the components that were significantly different from background noise at least at one biasing level (ANOVA, $p<0.01$). Colours and markers of the growth functions are matched to the components in the 3rd row. The dotted lines show the noise floor of the components matching in colour and markers. The noise floor is extracted from the spectrum of the acoustic-only response (5 ms window, 30 ms after the onset of the acoustic biasing tone). A blue circle marker notes the unbiased EEOAE level. Unit slope is shown by grey dashed line.

B4.2.3 Results from animal #349

Although, the well-tuned electrophonic responses in the previous chapter showed successful preservation of hearing sensitivity, that is essential for the investigation of the biasing effects, the possible mechanical obstruction in the basal cochlear region required the acoustic biasing experiment to be repeated.

Once positively tested for hearing preservation, the biasing tone was introduced, this time with a frequency of 10 kHz. Its levels ranged from 61 to 73 dB SPL in 3 dB steps. The lowest acoustic biasing level was chosen based on the experience that in the previous biasing experiment no enhancement of the electrophonic response or the EEOAE was observed below 60 dB SPL. The maximum 73 dB SPL acoustic biasing level was determined by the upper limit of the distortion free operation of the transducer at 10 kHz. Electric stimulation level was kept at 30 dB re 10 mA_{pp} and the frequency of the electric stimuli were this time chosen to be perfectly resolved as a single spectral line when a 4 ms long analysis window is applied for EEOAE extraction. (I.e., all frequencies were multiples of 250 Hz.)

B4.2.3.1 Neural response

Neural responses are shown in Figure B4.6 in the same way as Figure B4.4.

Similarly to the previous measurement, the electric-only control curves show the shift of the electrophonic response with stimulus frequency. Electric stimulus levels used in this preparation were below the direct electric threshold for all used frequencies. The acoustic control response shows a wide tuning and a relatively weak response in the high frequency range for all applied stimulus levels. Both are the result of a high frequency hearing loss that was probably caused by the insertion of the CI.

In the acoustically biased conditions, the electrophonic response increases slightly compared to the reference in the 2, 2.5 and 4 kHz electric stimulation cases. No enhancement of electrophonic response is visible at higher stimulation frequencies in panel D and E.

In panel A and B additional peaks appear in response to the biased electric stimuli around the 20^{th} and 19^{th} electrodes that are approximately located at the characteristic place of 8 and 7.5kHz, respectively, corresponding to the frequencies of the f_a-f_e intermodulation products.

The increase in response visible in panel A to C in Figure B4.6 is small and could be simply the superposition of the electrophonic and acoustic response. The acoustic response at the electrodes tuned to the electrophonic response is likely a “cross-talk”

activity from neurons tuned to the acoustic stimulus frequency that are located remotely from those recording electrodes but are still detectable by the electrodes tuned to the frequency of the electrophonic response. To better see whether there is a true increase of electrophonic level due to biasing, the difference between the biased responses and the sum of the corresponding acoustic and electric control responses was calculated and shown in Figure B4.7.

Clear differences only reflect the f_a-f_e intermodulation products, which only occur with simultaneous electric and acoustic stimulation, as seen also in the ear canal acoustic recordings in Figure B4.8. At the characteristic place of the electrophonic responses, however, there is no obvious increase in activity beyond what is expected by linear superposition of the responses to acoustic and electric stimulation alone. We conclude that there is again no evidence of an enhancement of the electrophonic responses.

Interestingly, panel D and E show a negative difference response in the overlapping region of the electrophonic and acoustic responses (approximately between channel 15 and 30), indicating that in these cases the neural response to the combined electric and acoustic stimulus is less than the superposition of the individually evoked responses. The same neurons respond to both electrical and acoustical stimulation in this cochlear region and it cannot be expected that the respective neural activity sums up linearly if both modalities are presented simultaneously.

B4.2.3.2 EEOAEs

EEOAEs are shown in Figure B4.8 and organized identically to the EEOAE results in the previous experiment. The careful selection of stimulation frequencies according to the 4 ms analysis window resulted in the appearance of EEOAEs as splatter-free single spectral lines.

Already under the lowest biasing condition, EEOAEs increased approximately by 4 dB in response to all electric frequencies. Following this initial enhancement, EEOAEs showed little further increase with increasing biasing levels. In contrast to the results obtained for electrophonic response, the enhancement of EEOAEs may indicate the biasing of the operating point of OHC electromotility. It turned out that the range of the biasing tone intensities was set too high in this experiment so that, unfortunately, a smooth increase from unbiased to biased EEOAE level could not be shown.

Similarly to the first experiment, intermodulation products are also visible in the EEAOE spectrum when electric sinusoids of 2, 2.5 and 4 kHz are presented together with the acoustic biasing tone. In these cases, the level of the f_a-f_e intermodulation products increases again with approximately 1 dB/dB with biasing tone intensity. In the biased 5

kHz response the even order intermodulation product coincides with the EEOAE frequency and could not be analysed. The odd order intermodulation products are like all the intermodulation products in the 6.5 kHz case, close or below the level of the background noise.

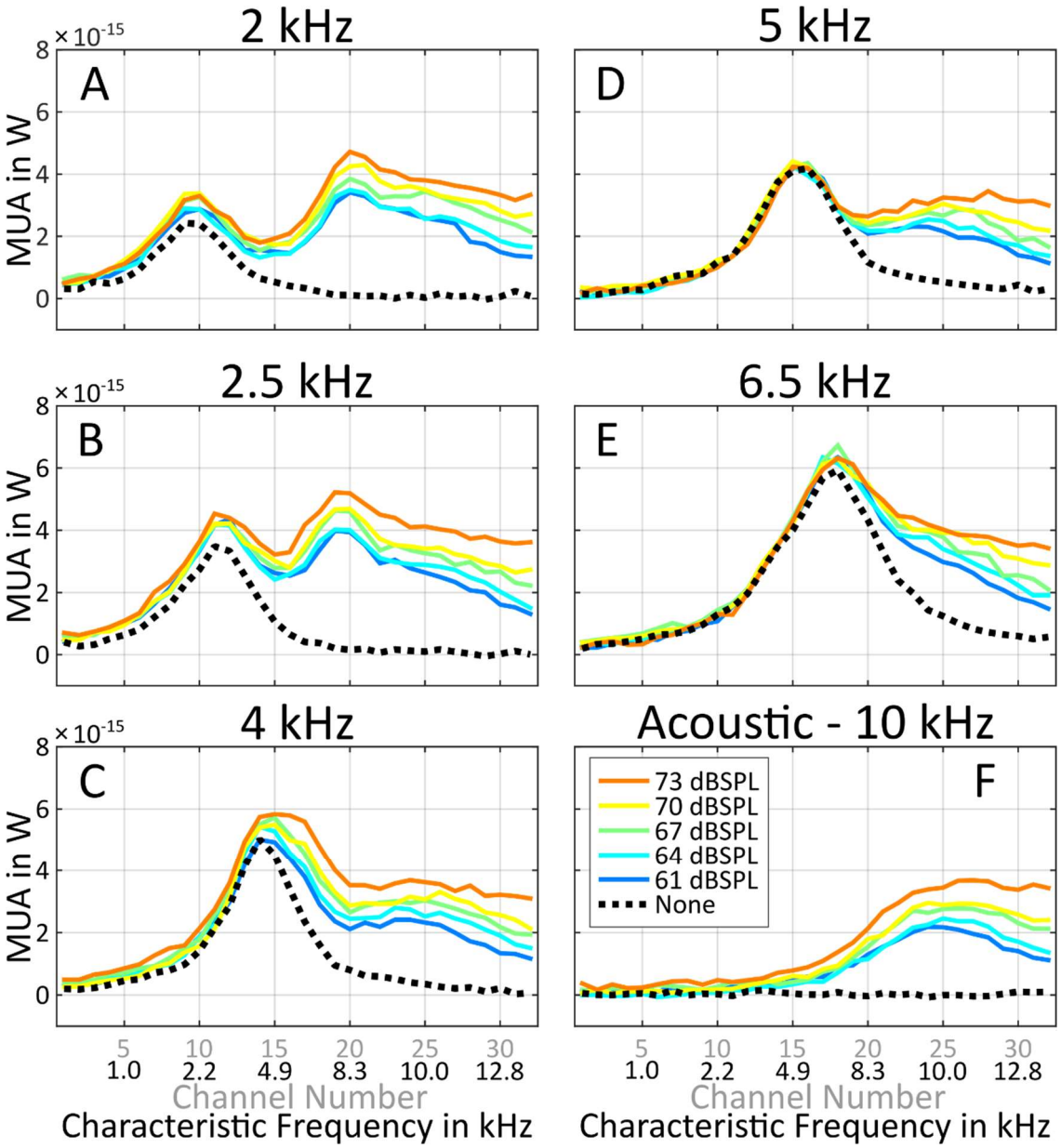

Figure B4.6 Same as Figure B4.4, but for electric stimulation with 2, 2.5, 4, 5 and 6 kHz (349B15).

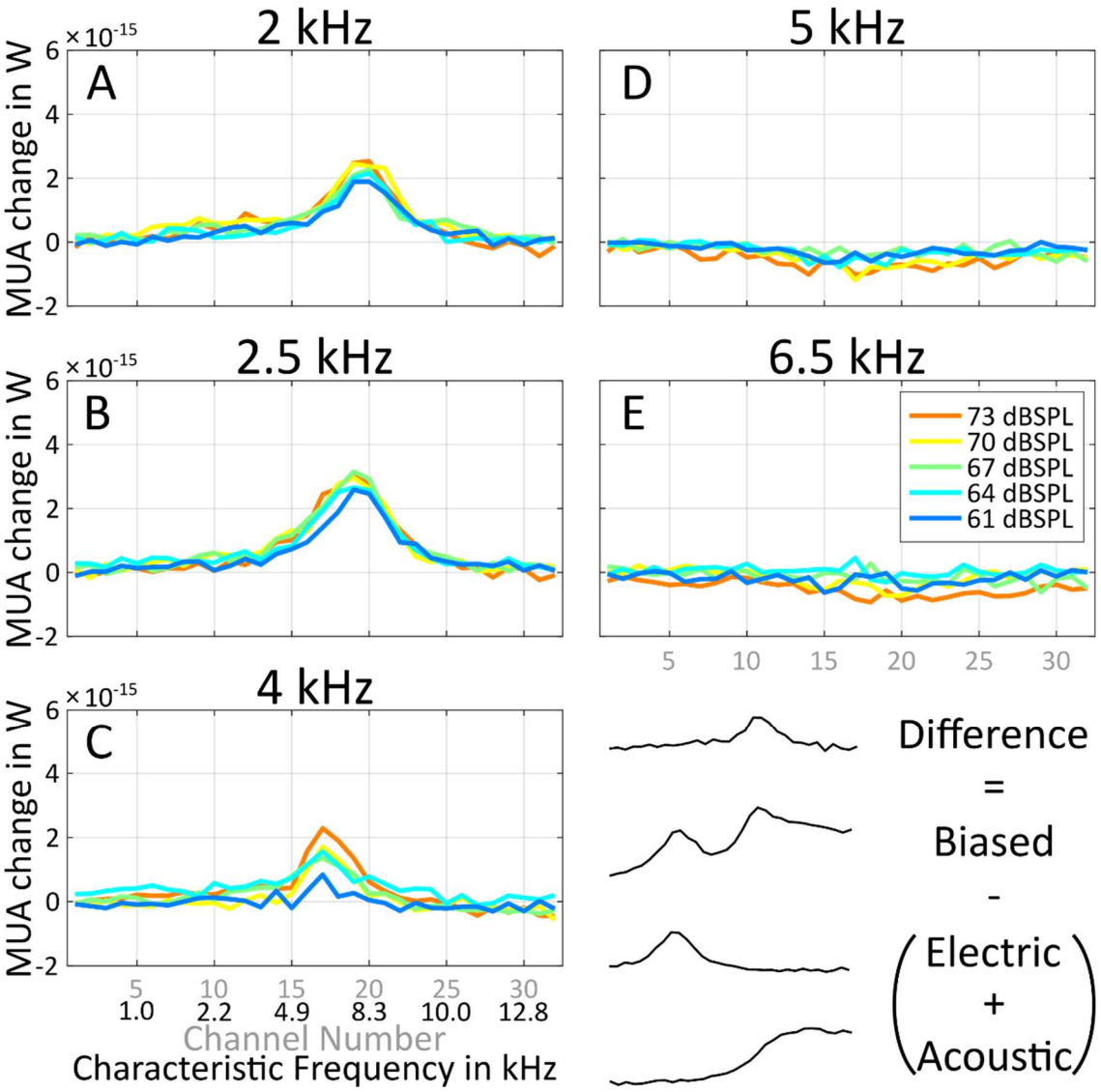

Figure B4.7. Difference between the biased responses and the sum of acoustic and electric responses. (349B15). Difference response is calculated by subtracting the acoustic and electric responses from the combined response. Each panel corresponds to an electric sinusoid with its frequency indicated in the titles. Colouring indicates the level of the applied biasing tone.

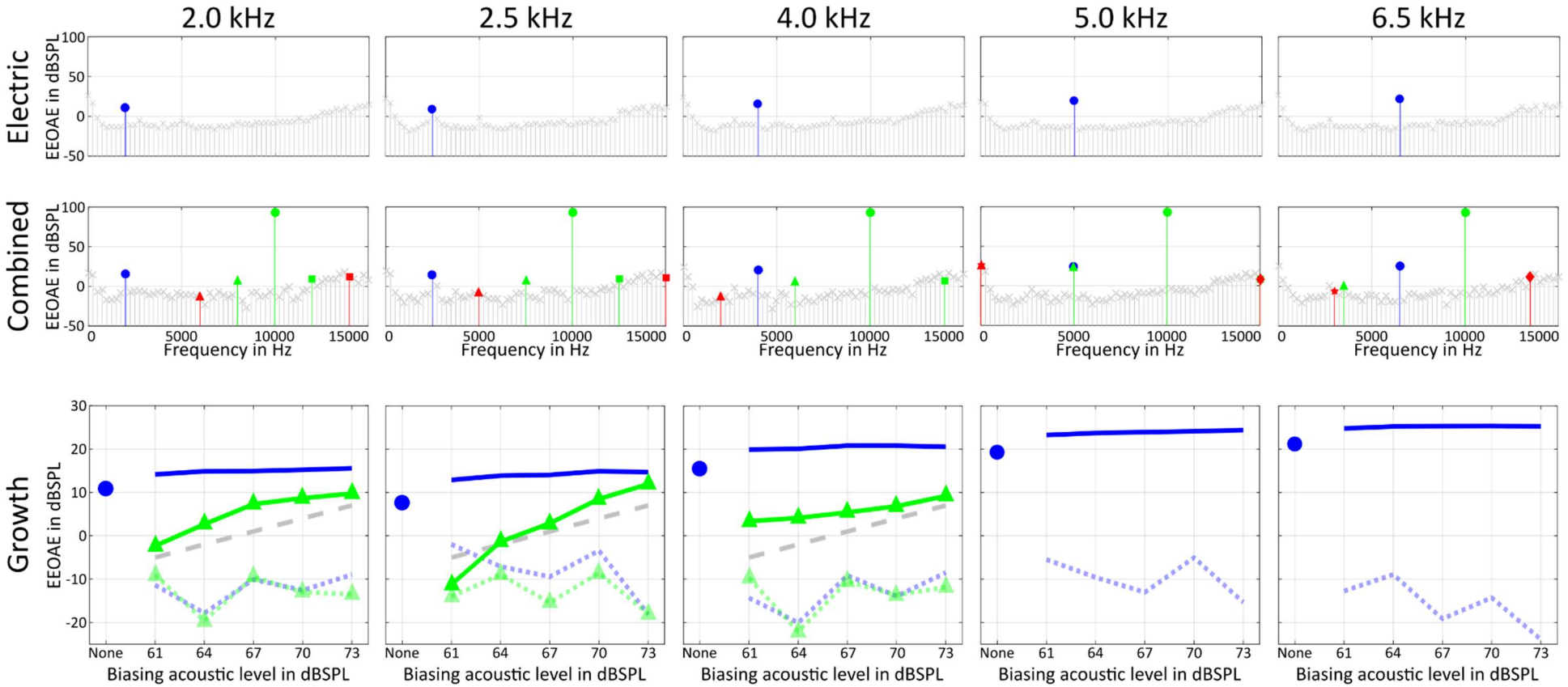

Figure B4.8. Same as Figure B4.5, but for animal #349 (349B15).

B4.2.4 Electrophonic and EEOAE acoustic biasing functions

To summarize the findings of the acoustic biasing experiments, the electrophonic response and EEOAE growth functions are compared in Figure B4.9 for both the first (339B7) and second (349B15) experiments.

To facilitate the comparison between neural responses and EEOAEs, the growth functions are referenced to the unbiased conditions and expressed in decibels. In panel A and C, neural responses are averaged across three neighbouring electrodes centred at the electrophonic response loci. Dashed lines in the same panels show the response growth of acoustic biasing tones at the electrophonic response place (acoustic only) added to the unbiased electrophonic responses (electric only).

The significance of acoustic biasing level on the electrophonic responses and EEOAEs was tested by ANOVA. Statistical significance was determined by a P-value below 0.01 and noted by a star at the right end of the corresponding lines in.

B4.2.4.1 Biasing of electrophonic responses

Panel A of Figure B4.9 shows that in the first experiment acoustic biasing had no significant effect on any of the tested electrophonic responses. The increased response strength at the electrophonic place in the 6.4 kHz condition is caused by the acoustic response that had a clear response at this location.

Panel C of Figure B4.9 shows that, similarly to the first experiment, acoustic biasing had no significant effect on the electrophonic responses in the second experiment, except in the case of the 4 kHz stimulation frequency. Applying the ANOVA test on the difference of the biased electrophonic and acoustic responses resulted in no significant effect by the acoustic biasing level. This negative result explains that the increase at the 4 kHz electrophonic place was caused by neural activity related to the acoustic stimulation and not by a genuine biasing effect. Note, that in the case of 4 kHz stimulation, the neural response related to the intermodulation product (see Figure B4.7) is in the proximity of the electrophonic place and most likely contributed to the observed increase of the electrophonic response.

B4.2.4.2 Biasing of EEOAEs

Panel B of Figure B4.9 shows that apart from the 2.3 kHz response, EEOAEs measured during the first experiment were significantly affected by acoustic biasing. EEOAEs in response to the 1.6, 3.2 and 6.4 kHz stimuli show a clear increase in response strength to biasing tones above 65 dB SPL. The lack of significant biasing effect on the 2.3 kHz

EEOAE and the lack of clear EEOAE increase with acoustic biasing level in the 4.5 kHz cases are probably caused by the imperfect resolution of the corresponding spectral components in the measured spectrum.

Panel D of Figure B4.9 also shows that acoustic biasing had a significant effect on the tested EEOAEs in the second experiment, except for the 2 kHz condition (still p=0.016). All EEOAE show an increasing tendency with acoustic biasing level, but the slope of increase is shallower when compared to the results from the first experiment. Note that the biasing effect is already present at the lowest biasing tone intensity. Xue fitted the EEOAE growth by a saturating sigmoidal function [Xue et al., 1995]. Thus, the present curves are probably within the saturating part of the biasing function.

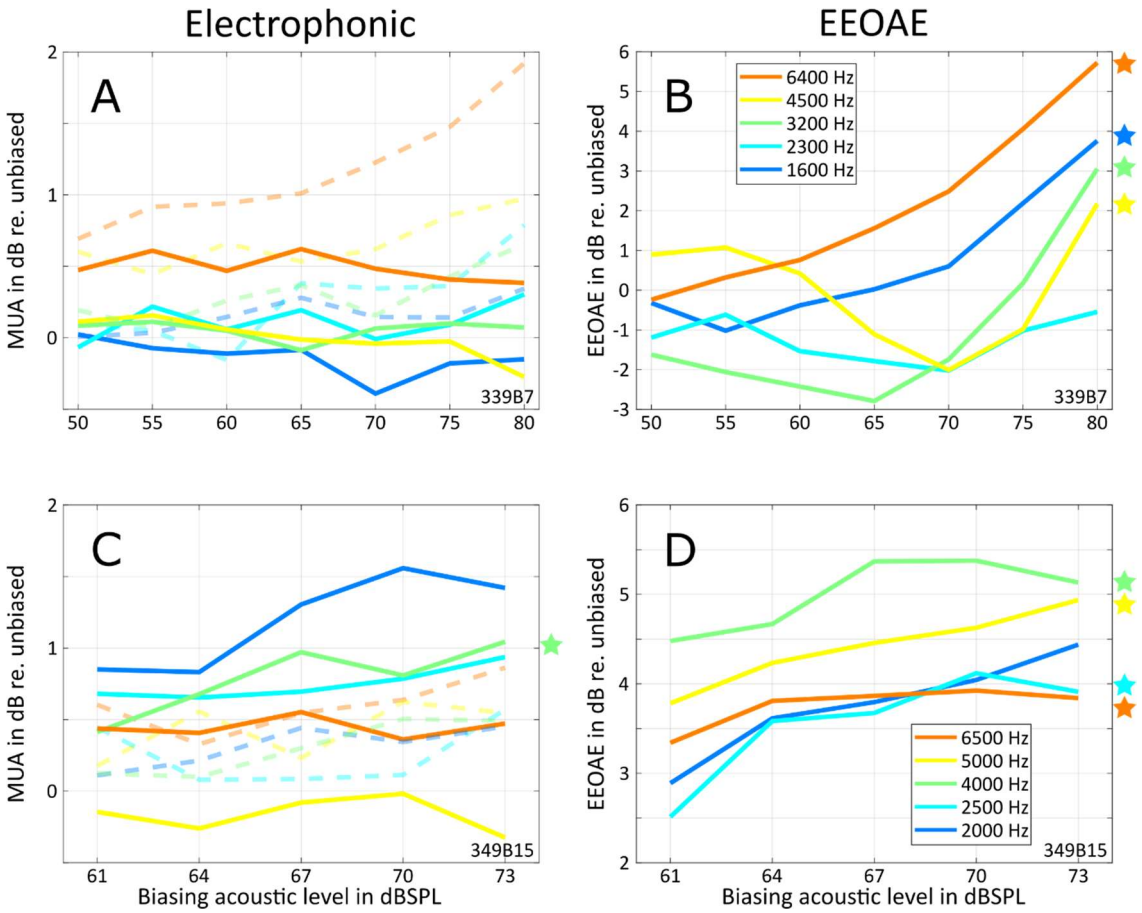

Figure B4.9 Change in electrophonic response and EEOAE with increasing biasing tone level (339B7 and 349B15). A, C) – Change in multi-unit activity in dB with reference to the unbiased response. Data is averaged across three neighbouring electrode sites at the electrophonic place (339B7: centre electrode 13, 16, 18, 21 and 22 for 1.6 to 6.4 kHz; 349B15: electrode 10, 11, 14, 15 and 18 for 2 to 6.5 kHz) in response to various electric sinusoids (differentiated by colours); Dashed lines represent the growth functions of the sum of the unbiased electrophonic response and the acoustic biasing tone response at the electrophonic place. B, D) EEOAE growth functions with reference to the unbiased response. Stars on the right side of the figure indicate if acoustic biasing level had a significant effect (ANOVA, p<0.01).

B4.2.4.3 Summary on acoustic biasing

No acoustic biasing of the electrophonic response was apparent in the first experiment and the small enhancement of electrophonic response in the second experiment was

shown to be solely the result of intermodulation products. In contrast, EEOAEs showed a small but significant dependency on the acoustic biasing level in both the first and second experiment. This finding suggests a dissociation of the electrophonic response and the EEOAEs.

Interestingly, acousto-electric intermodulation products appeared as detectable signals in the ear canal for both experiments, but only travelled down to their characteristic place in the second experiment. This difference might be due to the hypothesized mechanical blocking nature of the cochlear damage observed in the first experiment. The intermodulation products are evidence of a non-linear interaction between the two modes of stimulation.

B4.3 Electric biasing

The hypothesis of electric biasing is tested similarly to the acoustic biasing experiments. The applied stimulus waveform is visualized in Figure B4.10. Positive and negative DC currents are delivered in a monopolar mode using the same two most apical electrode contacts that are used for AC current delivery (which remained bipolar). Monopolar mode for DC current delivery was used in order to ensure effective DC biasing of OHC membrane potential at a wide spatial extent around the current injection site. To maintain charge balance within the 800 ms long presentation period, the polarity of the 100 ms long DC phases were altered within one stimulus condition. The onset of DC biasing currents was at 200 and 400 ms. The starting DC polarity was randomized, and the opposite DC polarities were separated by a 100 ms gap to avoid large artefacts that were observed at instantaneous phase switch during pilot experiments. The 8 ms long (including 1 ms on- and offset squared cosine ramps), -30 dB re. 10 mA_{pp}, 1.6 kHz electric sinusoids are presented 50 ms following the DC onsets. Control electric sinusoid stimuli with no DC were presented 50 ms following the start of a presentation.

To clearly dissociate the biasing effect on the electrophonic generation from simply affecting the cochlear amplification of the electrophonic travelling wave at its characteristic place, 60 dB SPL acoustic control tone pips of 1.6 kHz were also included in the procedure and presented instead of the electric sinusoids. In other words, this acoustic control tone was used to monitor if the current spread of DC biasing reaches the electrophonic place. The level of the control tone was selected such that the acoustic response is similar in strength to the electrophonic response to the electric probe. Another, 8 kHz acoustic control tone of 60 dB SPL was used to monitor whether delivery of DC current has an effect on cochlear amplification at the direct stimulation place.

The sets of electrical stimuli and the two acoustic control tones were presented in a randomized order and repeated 25 times.

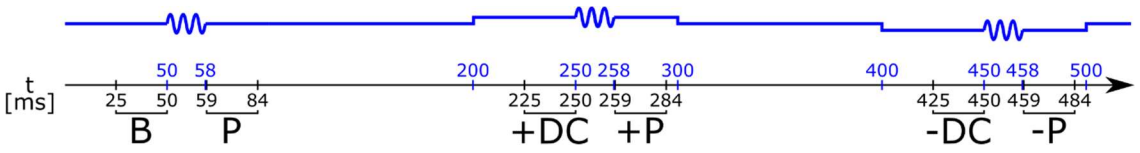

Figure B4.10 Electric biasing stimulus. Numbers above the time axis show the on- and offset times of DC biasing currents and the probes. Numbers below the time axis show the window limits used for neural response extraction. B – Background activity; P – Probe response; +DC – Positive DC response; +P – Response to Probe in positive DC phase; -DC – Negative DC response; -P – Response to probe in negative DC phase

B4.3.1 Neural response

Figure B4.11 shows the spatial activation patterns in response to the various stimulus conditions. Every column corresponds to a given probe condition and every row corresponds to different biasing conditions. Similarly to the acoustic biasing representation, within one panel, colouring represents the various biasing levels and dotted line corresponds to the biasing free condition.

Spatial activation pattern in response to probe-free positive DC biasing currents show that increasing biasing levels decreased the background activity at the direct stimulation place. Additionally, the largest biasing current resulted in a broad excitation pattern across electrode 5 to 25, representing neural responses that were apical to the current injection site. Negative biasing currents resulted in activity that increases with current level at the direct electric place. The response to the two highest biasing current also shows a broad excitation pattern that extends far apical into the cochlea. The broad excitation patterns of the largest applied DC currents may indicate a slight overstimulation, thus the results corresponding to these conditions should not be treated as responses that were directly stimulus-evoked, but as electrically evoked muscle activation that may have caused sound artefacts.

The response to the 1.6-kHz acoustic tone in unbiased condition shows a peak at its characteristic place. In positive-DC biasing conditions, the response pattern to the 1.6-kHz acoustic control stimulus at the electrophonic place remained unchanged, except for the highest biasing level. At the highest biasing level, the response peak was slightly reduced, indicating the direct effect of biasing current at the electrophonic place at this level. At the direct excitation place, neural response was suppressed below the background activity by increasing positive biasing currents. In negative-DC biasing conditions, the response pattern at the electrophonic place was unchanged. A minimal increase in neural activity is visible on both, the low and high frequency slopes of the peak, in the strongest biasing condition. This increase was similar to the ones observed

in the response to the negative DC current alone in panel L, thus can be associated with a muscle artefact. The response at the direct electric place increased with increasing biasing current. This control measurement showed that, except for the highest levels, the DC injection did not influence the cochlear transduction at the 1.6 kHz place, thus any effect on the electrophonic response would have had its origin at the electrophonic generation site near the current injection place.

The response to the 8-kHz acoustic tone in unbiased condition shows a clear peak at the corresponding characteristic place that is within the region of the direct electric stimulation. In the positive-DC biasing conditions, the activity at the peak only decreased at the highest biasing level. Basal to the response peak, the decreases of activity started already with lower biasing levels. In the negative-DC biasing condition, the neural activity at and basal to the response peak increased with increasing biasing levels. Except for the 3 lowest CF electrodes, neural activity was elevated across the whole recording region in response to the highest two DC biasing condition in a manner similar to the one in panel L. In conclusion, these control results show that at least the positive-DC biasing was strong enough to affect the transduction of the 8 kHz acoustic control tone at the direct injection site, thus should have also been potent enough to modify the OHC electromotility at this place.

Knowing that the acoustic controls show that the biasing conditions are as expected, let's now look at the biasing effect on the electrophonic response that had a clear response peak at the 1.6 kHz characteristic place. In positive-DC biasing condition, the electrophonic response slightly decreased across its whole peak region and the direct response completely diminished with increasing biasing levels. At the highest biasing level, the direct response even dropped below the background activity. In negative-DC biasing conditions, the change in electrophonic peak was negligible and the direct electric response increased with increasing negative-DC levels. Neural responses both at the low and high frequency slopes of the electrophonic peak were slightly increased in response to the highest biasing level. The small increase at the high frequency slope of the electrophonic response in the negative biasing case (panel C) can also be observed in the acoustic control cases (panel F and I) and was caused by the broad excitation of the largest biasing currents (panel L), probably due to a muscle artefact. The small increase at the low frequency slope of the electrophonic response at electrodes 5-10 is almost identical to the response to the biasing current alone (panel L) at these electrodes, thus it may also be linked to a muscle artefact.

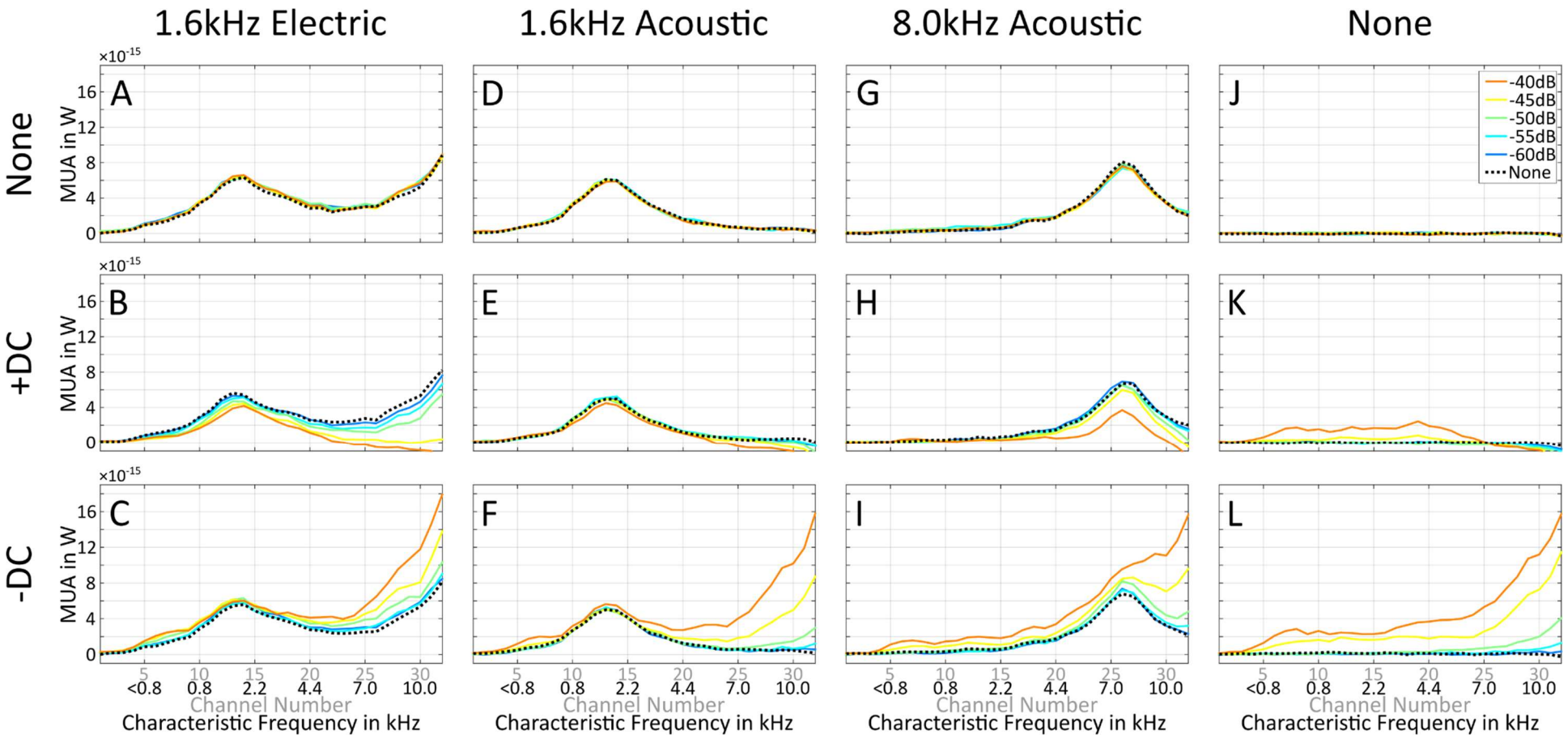

Figure B4.11 Effect of DC biasing currents on the spatial activation patterns in response to a 1.6 kHz electric sinusoid, a 1.6 kHz and an 8 kHz acoustic tone (339B10). Columns 1-3 show results with the probe stimuli and column 4 shows results without a probe. 1st row shows spatial activation pattern to unbiased stimuli. 2nd row shows spatial activation patterns in response to stimuli in +DC biasing currents with various levels (indicated by colours); response to the unbiased stimuli are shown by dotted lines. 3rd row shows spatial activation patterns in response to stimuli in -DC biasing currents with various levels (indicated by colours); response to the unbiased stimuli are shown by dotted lines.

B4.3.2 EEOAEs

EEOAEs are measured during electrical biasing and the results are shown in Figure B4.12. EEOAEs are extracted from 5 ms long windows positioned 3 ms after the onset of electric sinusoid stimuli. Rows of the figure represent the different biasing conditions as indicated in the labels on the left. The first column shows the response spectrum to the electric sinusoid presented alone and in a -50 dB re 10 mA_{pp} positive- and negative-DC conditions. The second column shows the change of the responses during DC injection. Statistical significance (ANOVA, $p < 0.01$) of DC-biasing on the EEOAE magnitude is noted by stars.

Panel A and D show the EEOAE in response to unbiased electric sinusoids. Since the stimulus is always the same in this condition, the response change function only illustrates the mean response to various repeats that had a standard deviation of 0.42 dB.

Results of the positive and negative DC biased EEOAEs show little changes from the unbiased condition. In positive biasing condition, the EEOAE shows a decrease of approximately by 1.26 dB, that also shows statistical significance. In negative biasing condition, the EEOAE shows a statistically significant increase up to 1.29 dB. Note that, without considering the EEOAEs measured during the strongest biasing condition that yielded muscle artefacts, only the positive-DC biasing effect remains statistically significant.

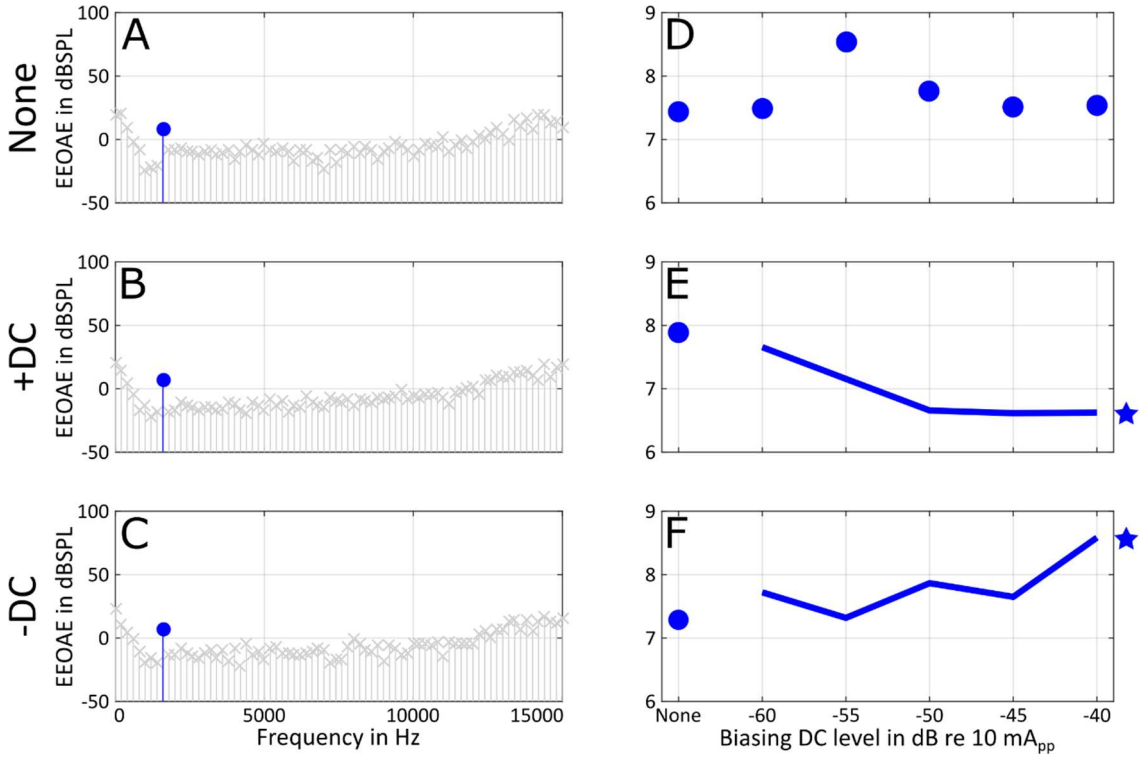

Figure B4.12 Effect of DC biasing currents on the EEOAE in response to a 1.6 kHz electric sinusoid (339B10). Rows correspond to biasing conditions with different polarities. The left column shows spectra of the microphone signal in the -50 dB re 10 mA_{pp} condition. The right column shows the EEOAE change as a function of DC current strength, except in the first row where no biasing current was applied, and the dots show the results of repeated measurements (std = 0.42 dB).

B4.3.3 Electrophonic and EEOAE electric biasing functions

The change in electrophonic response and EEOAEs during biasing conditions is summarized in Figure B4.13. Similarly to the acoustic biasing part, the change of electrophonic response and EEOAE is expressed in decibels with reference to the unbiased responses and statistical significance of electric biasing effect is noted by starts (ANOVA, $p < 0.01$) at the right end of the curves. Blue colour represents negative and red colour represents positive biasing conditions.

B4.3.3.1 Biasing of electrophonic responses

In panel A of Figure B4.13, solid lines show the change of electrophonic response strength and dashed lines show the change of response strength to the 1.6 kHz acoustic tone at the electrophonic place.

Positive-DC biasing in the -60 to -40 dB re. 10 mA_{pp} range had a significant effect on the electrophonic response strength that shows a monotonic decrease with increasing biasing level. Although the electric biasing shows no significant effect on the acoustic control tone, the sudden drop of the control curves at the highest biasing levels (in

conjunction with the symmetric increase for positive-DC) might be indicative of the direct effect of the biasing current at the electrophonic place. After omitting the results of the electrophonic response in the strongest positive biasing condition the effect of positive-DC biasing on the electrophonic response strength still remained significant.

In contrast to the positive-DC biasing, negative-DC biasing did not have an effect on the electrophonic response in the tested biasing level range.

B4.3.3.2 Biasing of EEOAEs

DC biasing showed no significant effect on the EEOAEs neither in the positive nor in the negative biasing conditions in the tested DC range ($p_{+DC} = 0.0439$, $p_{-DC} = 0.0105$). After disregarding the results during the largest DC biasing conditions based on its possible muscle artefact origin, the EEOAEs still show now significant dependence on the biasing level ($p_{+DC} = 0.0230$, $p_{-DC} = 0.5563$).

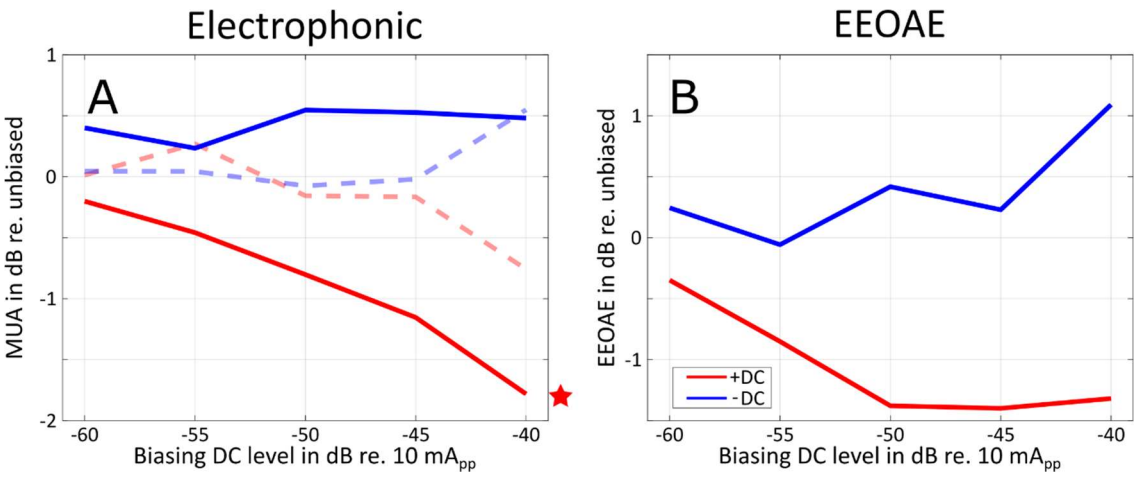

Figure B4.13 Change in neural activity and EEOAE with increasing positive and negative biasing current level (339B10). A) Multi unit activity is averaged across electrode 12, 13 and 14 at the electrophonic place in response to the electric sinusoid; Solid lines show the change in electrophonic response and dashed lines show the change in the acoustic response strength to the 1.6 kHz tone at the electrophonic place. Stars on the right indicate statistical significance of the electric biasing (ANOVA, $p < 0.01$). B) EEOAE biasing functions referenced to the unbiased EEOAE response.

B4.3.3.3 Summary on electric biasing

Both the electrophonic responses and the EEOAEs were shown to be unaffected by negative-DC biasing. Positive-DC biasing was shown to suppress both the electrophonic response and EEOAEs, although the effect on the latter was weaker and its significance remained slightly above the set criteria.

The presented electric biasing results were obtained from the same animal as the results of the first acoustic biasing experiment. In order to avoid any possible adverse physiological conditions induced by the biasing currents that could have distorted the

results of the acoustic biasing tests, the electric biasing measurements were always attempted last in the experimental procedure. Unfortunately, the animal of the second acoustic biasing experiment was not in state to start with the electric biasing experiment anymore.

B4.4 Discussion and Conclusions

Biasing of electrophonic response by shifting the operation point of OHC electromotility was attempted with the presentation of a simultaneous acoustic tone or constant current injection (DC) into the scala tympani. Biasing of EEOAEs was reported in previous studies and since they are hypothesized to share the same origin with electrophonic responses, EEOAE were also measured here, as a control response.

Acoustic biasing experiments showed no electrophonic enhancement and enhancement of EEOAEs only to a modest extent that was low compared to the 12-16 dB values reported by Xue and colleagues (1993) who applied scala media stimulation in the 2nd turn of the gerbil cochlea. The fact that the enhancement was only small is likely due to electric stimulus delivery into the first turn of the cochlea. Kirk and Yates [Kirk & Yates, 1996] tested acoustic enhancement of EEOAE, generated at several locations along the cochlea. They reported reduced acoustic enhancement efficiency for first turn electric stimulation in the guinea pig cochlea compared to more apical turns, and indeed, the less than 6 dB EEOAE enhancements observed in our experiments is in accordance with their findings. A likely explanation is that in the basal cochlear turn the OHC operating point is argued to be located more symmetrically, near the inflection point of the sigmoidal mechano-electrical transducer function [Russell et al., 1986], thus acoustically evoked alternating stereocilia displacement does not evoke a DC shift in the OHC membrane potential, and consequently, neither the expected operation point shift along the prestin motility curve.

The observed effects of electric biasing on the electrophonic response have to be interpreted carefully. The small decrease in electrophonic response strength in the positive biasing condition might not necessarily be the sole result of electromotility operating point biasing. Although the possible effect by the spread of direct electric excitation is ruled out by the help of the unaffected 1.6 kHz acoustic control tone, the very small change in electrophonic response strength may still be the result of the crosstalk from the activity of high-frequency neurons that respond to the direct electrical stimulation onto the electrodes tuned to the 1.6 kHz electrophonic response. In other words, the neural response at the electrophonic place in response to the unbiased electric sinusoid is possibly not only the result of the electrophonic response but also the neural crosstalk from higher frequency neurons. When biased by a positive DC current,

the contribution of neural crosstalk may be suppressed, and in turn, the electrophonic response may appear to be reduced.

The trend of EEOAE suppression by positive DC currents is in line with the results of Roddy and colleagues (1994), but the extent of measured changes in EEOAE are small compared to their approximately -2.5 dB. The small electric biasing effects in our experiment may be explained by our current injection method. In contrast to others who applied scala media current delivery [Roddy et al., 1994; Frank & Kössl, 1997], the biasing currents in the current experiment were delivered to the scala tympani in monopolar mode with the return electrode positioned on the neck muscle. This setup was probably inefficient for changing OHC operating point as the biasing current was likely drained away from the inner ear due to a low electrical resistance to the surrounding tissue. To obtain more localized biasing current delivery, the experiment was repeated with bipolar biasing stimulation, but DC effect were even less than with monopolar DC injection and were therefore not presented here. Because there was little project time left, with little hope of immediate surgical success of a locally unestablished technique for accessing the scala media, current injection using this route was not attempted.

In summary, the effects of outer hair cell electromotility biasing were either missing or very weak in the conducted experiments. Thus, whether electrophonic response and EEOAE share a common source could not be answered. Acoustic biasing experiments almost suggest a dissociation between the two phenomena, however, due to the first turn electric stimulation, the observed changes in EEOAE during acoustic biasing were small compared to the EEOAE enhancements from more apical turns reported in the literature [Kirk & Yates, 1996]. The effect of electric biasing on both the electrophonic response and the EEOAE was negligible. Although the faint, monotonically decreasing trend in both responses during positive DC biasing is indicative of a common source, the effect was statistically non-conclusive. In summary, the hypothesis of a common source cannot be rejected based in these results.

To establish a link between the electrophonic response and the EEOAE, the applied procedures proved to be insufficient without major change in the surgical approach. Application of the electrical stimulus in more apical turns would promise a larger acoustic biasing effect [Kirk & Yates, 1996] and bipolar stimulation across the cochlear partition e.g. one electrode in the scala tympani and the other in the scala media could provide a more localized and more efficient current delivery, thus may make the electric biasing effects more prominent as observed by others [Roddy et al., 1994]. Altering the surgical procedure is by no means straightforward and was not possible within the timeframe of the project, it was therefore decided to discontinue these biasing experiments of these types. As an alternative, the next chapter describes pharmacological manipulations in an

attempt to show that prestin motility drives both the electrophonic response and the EEOAE.

B5 Pharmacological blocking of OHC motility

The common source of the EEOAEs and the electrophonic responses could not be clearly demonstrated by the acoustic and electric biasing experiments in the previous chapter. The current chapter presents a different approach that, applies pharmacological blocking of the OHC electromotility in an attempt to establish a link between the EEOAEs and the electrophonic responses.

Prestin, a membrane protein, is the source of the electro-motile response of the outer hair cell as was shown by Zheng and colleagues [Zheng et al., 2000]. By the application of salicylate, a prestin-blocker agent, reduction in outer hair cell electromotility was shown in-vitro [Shehata et al., 1991; Mammano & Ashmore, 1993; Tunstall et al., 1995]. Later, in in-vivo experiments, the temporary reduction in both electrically evoked basilar membrane movement [Grosh et al., 2004] and electrically evoked otoacoustic emissions [Drexl et al., 2008] was demonstrated.

If outer hair cell electromotility at the direct stimulation place is the source of the electrophonic response, then salicylate injection at the stimulation site should reduce such mechanical responses along the entire cochlea at the same time. A simultaneous drop in EEOAEs and the electrophonic responses would strengthen the hypothesis of their common electromotile source, of which weak indications were already presented in chapter B4. At the same time, acoustic responses that are distant from the salicylate injection site should, at least initially, remain unaffected. Thus, acoustic responses are expected to only reflect a slow diffusion of the drug along the cochlea by a reduction in the response strength due to reduced cochlear amplification at the characteristic place of the stimuli. Additionally, the effect of salicylate on the acoustic responses are also expected to become weaker from basal to apical regions due to a gradually decreasing salicylate concentration along the cochlear duct.

B5.1 Methodology

Salicylate administration into the cochlea was performed as the final step of an experimental procedure because contamination of the fragile cochlear environment made further experimentation impossible.

Preceding experimentation, salicylate solution with a concentration of 10 mM[7] was prepared in phosphate buffered saline (artificial perilymph). For administration, the tip of a fine, plastic micro-capillary was positioned just inside the cochleostomy, adjacent to the cochlear implant electrode array, near the direct stimulation site. A 2 µl Hamilton syringe attached to the micro-capillary was used for slow manual delivery of salicylate over a few minutes. Care was taken to avoid air bubbles in the system.

Stimulation consisted of 100 or 120 ms (including 10 ms on- and offset ramps) long electric sinusoids or acoustic tones / tone pairs. A new stimulation started every 250 ms. Acoustic stimuli served for monitoring salicylate diffusion along the cochlea. To obtain a sampling of the salicylate effect with a resolution of 8 seconds, only 4 frequencies were combined with 4 levels, both for the acoustic and electric stimuli, and presented every 250 ms (2*4*4*0.25 = 8 second). The order[8] of stimulation was fixed to ensure identical intervals between the repeats of a stimulation type. Stimulation frequencies were selected to observe acoustic and electrophonic response changes along most of the cochlear tonotopy. Stimulation level selection was based on acoustic and electric spatial activation patterns obtained just preceding the salicylate application to cover the steepest part of the response growth function for the selected frequencies.

To show the changes of the electrophonic and acoustic responses, as well as that of the EEOAEs, neural activities and microphone signals are extracted by the method presented in chapter B4. The time-course was smoothed by a moving 80-second-long window that averaged ten sample measurements.

B5.2 Results from animal #354

Spatial tuning curves in response to 8 ms long (including 1 ms on- and offset ramps), 2, 6, 10 and 14 kHz acoustic and electric stimuli were obtained just before the salicylate injection and are shown in Figure B5.1.

[7] Salicylate solution of this concentration was shown to efficiently reduce electrically evoked basilar membrane movement when injected into the scala tympani by Grosh and colleagues (2004).

[8] First, the 16 acoustic stimuli were presented from low to high frequencies and from low to high levels within one frequency group, i.e. 2 kHz at levels from 40 to 70 dB SPL, then 6 kHz from 20 to 55 dB SPL, then 10 kHz from 30 to 65 dB SPL and 14 kHz from 25 to 60 dB SPL. Electric stimulation ordered in an identical manner started after the last acoustic trial.

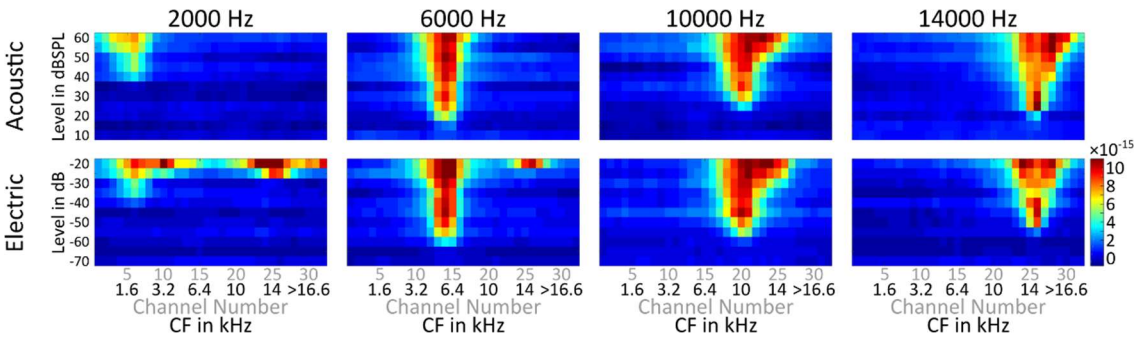

Figure B5.1 Spatial activation patterns in response to acoustic and electric stimuli with frequencies used in the subsequent pharmacological blocking experiment (354B29).

Acoustic responses confirmed the normal hearing state of the animal. Electrophonic response was present at all selected frequencies. Electrophonic response to the 2 and 6 kHz stimuli was distinct from the direct electric response that had a characteristic place of approximately 14 kHz. The electrophonic response to the 10 and 14 kHz stimulations were overlaying the direct electric stimulation response. The 10 kHz electrophonic response peak was slightly apical, and the 14 kHz response peak was on the direct stimulation place.

For the OHC motility blocking experiment, acoustic stimulation levels were selected for each stimulation frequency to be above threshold by 5, 15, 25 and 40 dB and electric stimulation levels were selected to be 0, 3, 6 and 9 dB relative to the electrophonic response threshold. Note that the range of applied current levels was compressed compared to the acoustic level range to avoid muscle responses. Exact sound intensity and electric stimulation levels can be read from the legend of Figure B5.3.

Figure B5.3 shows the time course of the neural responses at the characteristic place of the various applied stimuli. The data is also shown as a relative change compared to the initial response strengths in Figure B5.5.

The control responses to the 6, 10 and 14 kHz acoustic stimulation showed initial decrease while the response to the 2 kHz tone remained steady over time. As expected, the response to the 10 and 14 kHz stimuli were affected immediately after the application of salicylate because the corresponding tonotopic loci were near to the site of injection. Responses to the highest level 10 and 14 kHz tones also showed recovery, probably because the salicylate decreased at this location due to diffusion. In the case of the 6 kHz tone, a slow decrease in the response was observed that may be a sign that the salicylate diffusion reached the 6 kHz characteristic place. Thus, the extent of decrease in acoustic response strength depended on the characteristic place of the stimulus, more apical responses decreased less and with more delay (e.g. compare the 6, 10 and 14 kHz responses at the highest stimulation levels), that is in line with the initial hypothesis of the dilution of the salicylate solution by perilymph that yields a decreasing

concentration of the drug thus a weaker effect on the responses. The suppression of the acoustic responses also exhibited dependency on the applied stimulation level. The responses to higher acoustic levels tended to become suppressed later (e.g. 6 kHz at 30 and 40 dB SPL) and also recovered earlier (e.g. 14 kHz at 45 and 60 dB SPL). In general, the change in acoustic responses demonstrate that the drug injection and diffusion behaved according to the expectation.

Differences in the origins of acoustic and electrophonic responses are well reflected in the time courses of their response strengths following the salicylate injection. The initial electrophonic response strengths to 6 kHz electric sinusoids at -60 and -51 dB re 10 mA_{pp} levels were comparable to the response strength to 6 kHz tones at 20 and 30 dB SPL respectively. In both cases, the electrophonic response decayed faster than the acoustic response. The generator of the electrophonic response is the outer hair cell electromotility at the current injection site, where salicylate injection also takes place. The blocking of the outer hair cell motile response at the current injection site is therefore almost immediately apparent as a decrease in the electrophonic response. On the other hand, the acoustic response is the result of the stapes movement generated travelling wave that is unaffected by the reduced OHC motility at the basal region. Therefore, the slow decrease of the acoustic response solely shows that salicylate gradually reached the characteristic place by diffusion.

Electrophonic response decreased below the level of background activity (indicated by grey line in Figure B5.3) over time in all cases except for the 2 kHz electrophonic response. The time required for the cessation of electrophonic activities with similar initial strength e.g. response to 14, 10 and 6 kHz sinusoids at -49, -49 and -60 dB re. 10 mA_{pp} took approximately 2, 3 and 6 minutes. Additionally, in agreement with the results of Stypulkowski (1990), electrophonic responses to higher stimulus levels tend to be more robust to salicylate, i.e. a response to a stimulus with higher level requires more time to be suppressed (e.g. the electrophonic response to the 6 kHz stimuli in Figure B5.3). Note that electrophonic response is only partially reduced to stimulation with 2 kHz at -37, -34 and -31 dB re 10 mA_{pp}, the highest current levels applied in this experiment (see Figure B5.3). Salicylate was shown to only reduce, but not abolish electromotility completely [Kakehata & Santos-Sacchi, 1996]. Thus, these high current levels appear to have been sufficient to keep the hair cells moving during the salicylate exposure.

Electrically evoked otoacoustic emissions (EEOAE) were also measured throughout the experiment. The spectra of the recorded ear canal sound pressure at t_0, in response to the highest applied current levels at the various frequencies are shown in Figure B5.2. Clear EEOAEs were only present in response to the 2 and 10 kHz cases and EEOAEs remained below the background noise level for 6 and 14 kHz. The courses of the

EEOAEs over time are shown in Figure B5.4, and the changes relative to their initial strength in Figure B5.5. The observable responses to the 2 and 10 kHz electric sinusoids displayed a rapid decay at a similar point in time, quite immediately after salicylate application. If different at all, then in contrast to the electophonic responses to these stimulation frequencies, the 2 kHz EEOAE was affected slightly earlier than the 6 kHz EEOAE. The time of diminution of the 10 kHz EEOAEs roughly corresponded to that of the 10 kHz electrophonic responses. In contrast, the decay of the 2 kHz EEOAE was much earlier compared to that of the 2 kHz electrophonic response (see Figure B5.5). As opposed to the changes seen in the electrophonic responses, there was also no level dependence visible in the time-courses of the EEAOEs.

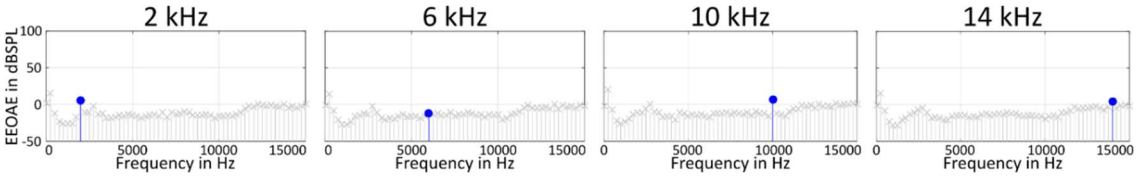

Figure B5.2 Spectrum of ear canal recordings during electric stimulation (354B30). The response to the highest electric stimulation levels are shown (for exact values see Figure B5.4).

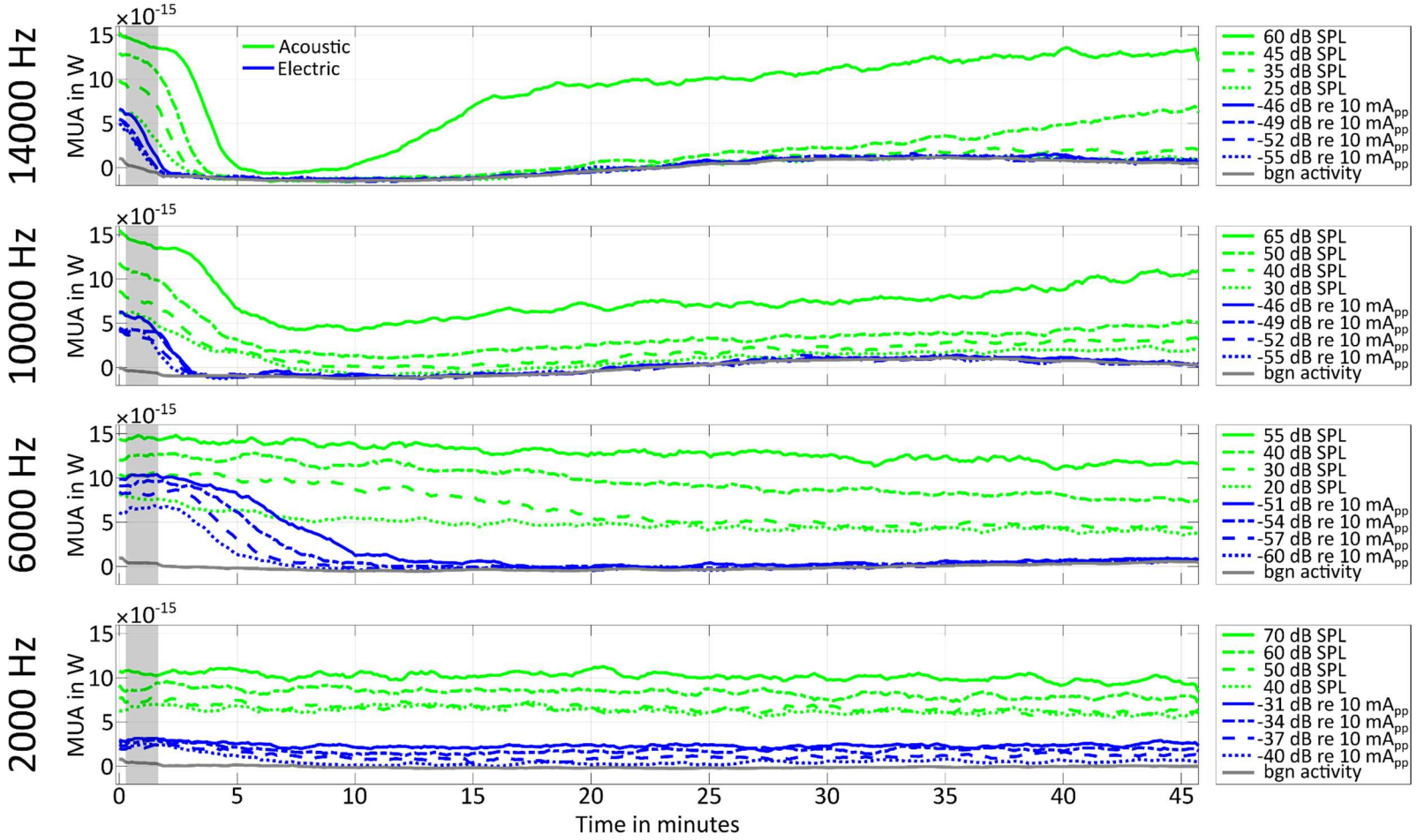

Figure B5.3 Effect of salicylate injection into the cochlea (over the period indicated by grey shaded area) on the neural responses to various acoustic tones and electric sinusoids over time (354B30). Neural responses are extracted at three adjacent electrodes centred at the CP (electrode 7, 15, 22 and 27) of the stimulation frequency (left labels) and a smoothing window of 10 stimulus repetitions (80 seconds) is applied. Acoustic and electric responses are indicated by green and blue colours respectively and grey line shows the background activity. Stimulus levels are differentiated by line styles.

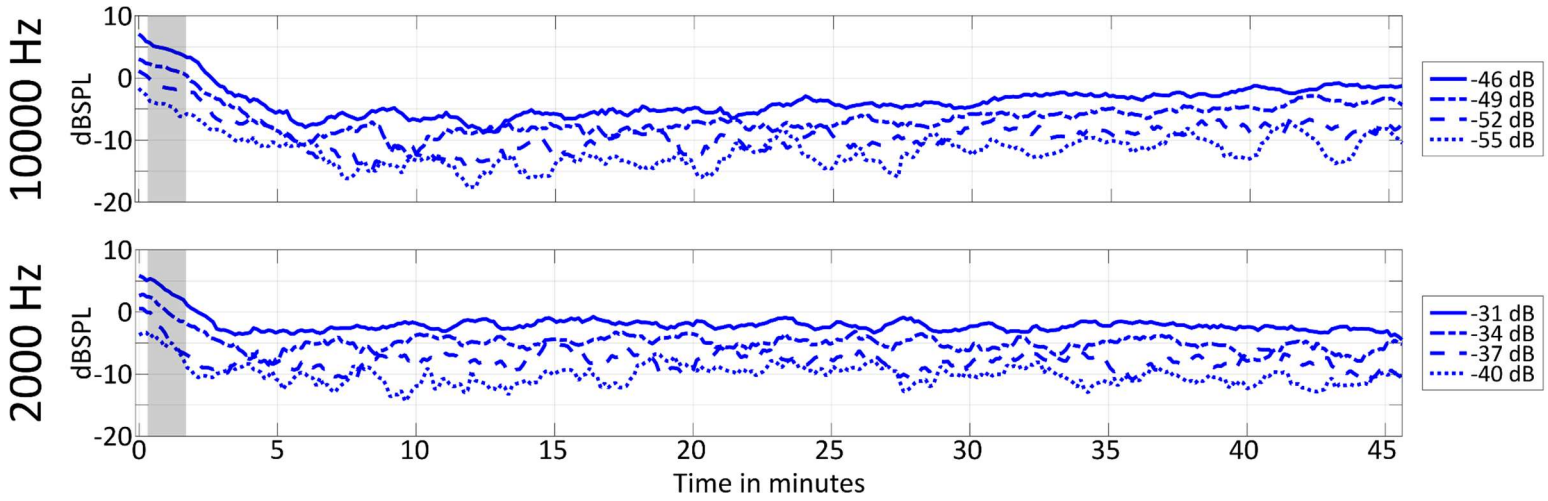

Figure B5.4 Effect of salicylate injection into the cochlea (over the period indicated by grey shaded area) on the EEOAEs to various electric sinusoids over time (354B30). A smoothing window of 10 stimulus repetitions (80 seconds) is applied on the curves. Stimulus levels are differentiated by line styles

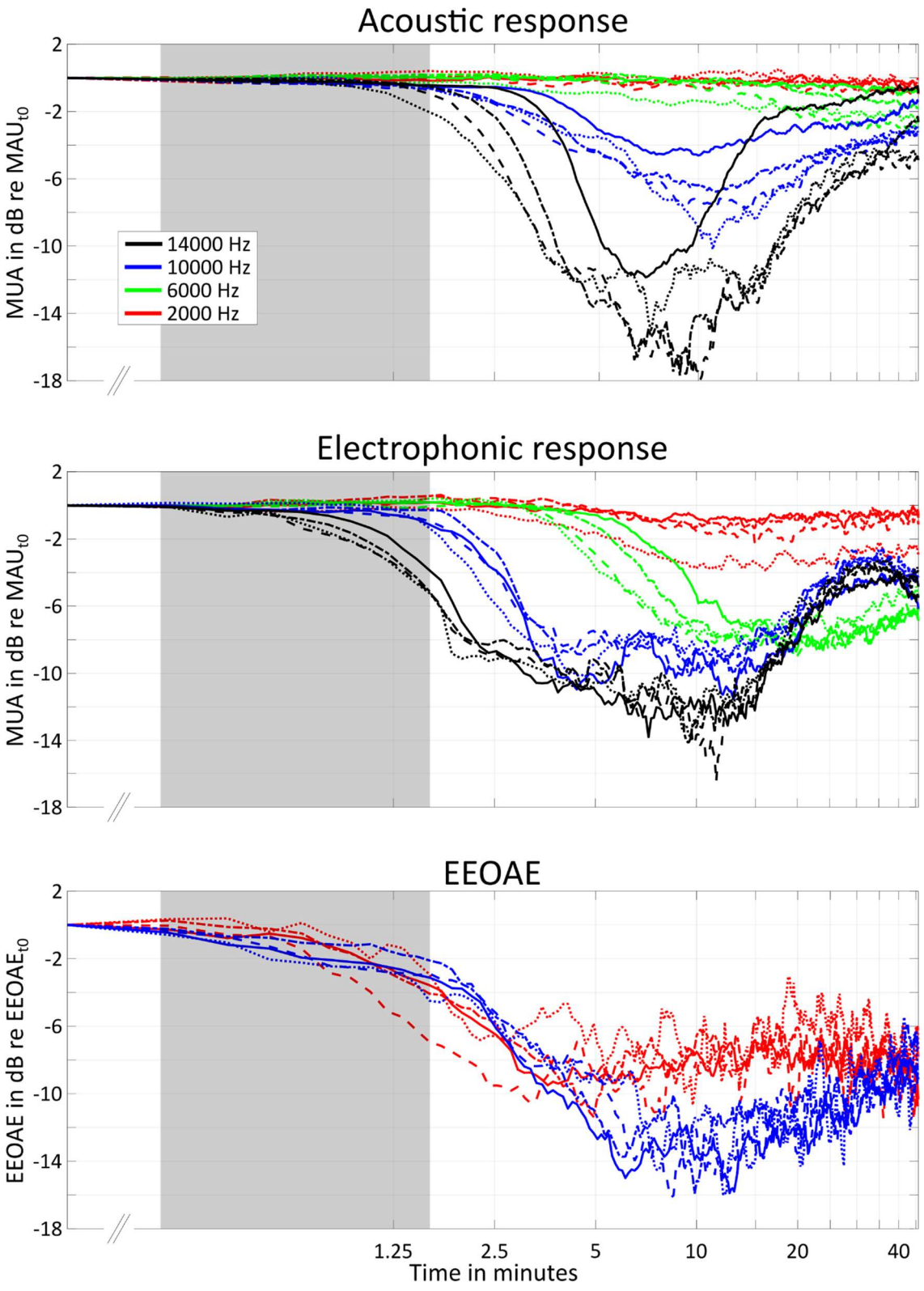

Figure B5.5 Relative change in neural responses and EEOAE due to OHC blocking (354B30). Responses are referenced to the datapoints obtained at t_0. Note, that EEAOEs are only plotted if the initial response was distinguishable from the background noise. Line styles are indicating the stimulation levels that can be read from Figure B5.3.

B5.3 Results from animal #355

The experiment described in B5.2 was repeated in another preparation. As it turned out that the amount and delay of the suppression is stimulus level dependent, the applied range of acoustic and electric stimulus was adjusted such that the initial response strengths were more similar. The acoustic stimuli consisted of 2, 4, 6 and 10 kHz tones at levels 5, 10, 20 and 30 dB SPL above threshold. Electric sinusoids were presented at the same frequencies and at levels 0, 5, 10 and 15 dB re 10 mA_{pp} above the threshold of the electrophonic response.

Acoustic and electric spatial activation patterns obtained just before the commencement of the OHC motility blocking experiment are shown in Figure B5.6 and demonstrate good acoustic sensitivity and clear electrophonic responses. In this experiment, the direct electric stimulation place was at the 13 kHz characteristic place.

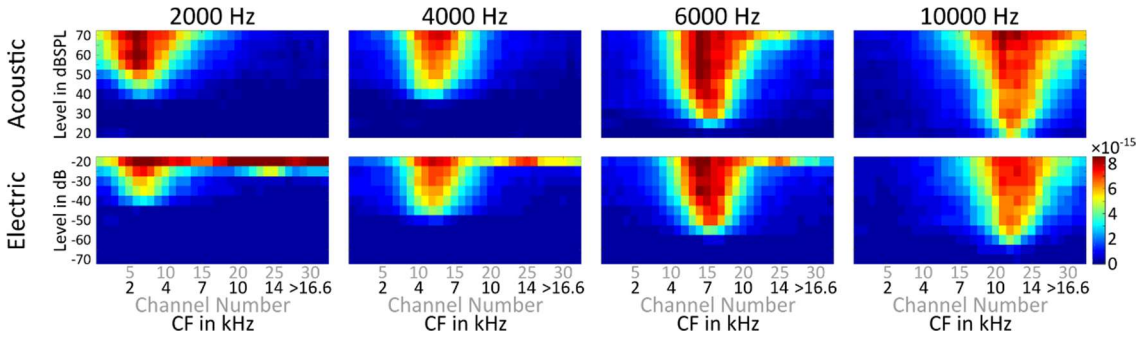

Figure B5.6 Same as Figure B5.1, but for animal #355 (355B29).

The time courses of acoustic and electrophonic response at their characteristic place are shown in Figure B5.8, and Figure B5.10 shows the relative change to their initial strength. Observations similar to the ones taken in B5.2 can be repeated here. Electrophonic responses to higher stimulus frequencies decayed earlier (see the 10 and 6 kHz responses). Also note the little effect on the 4 and 2 kHz electrophonic responses. Again, electrophonic responses to higher stimulation levels were more robust to salicylate i.e. dropped later and decreased less (see level series of 6 kHz response). EEOAEs were this time above noise level in response to all applied frequencies, as shown in Figure B5.7, and Figure B5.9 and lowest panel of Figure B5.10 shows that their decay curves demonstrated again only little frequency and level dependency. The acoustic responses reflect the diffusion of salicylate and also show level dependent robustness as seen in the experiment above. Interestingly, the acoustic responses to higher levels show a small increase (see the response to 4 and 6 kHz stimuli in Figure B5.8), whereas the electrophonic response and EEOAEs always decrease.

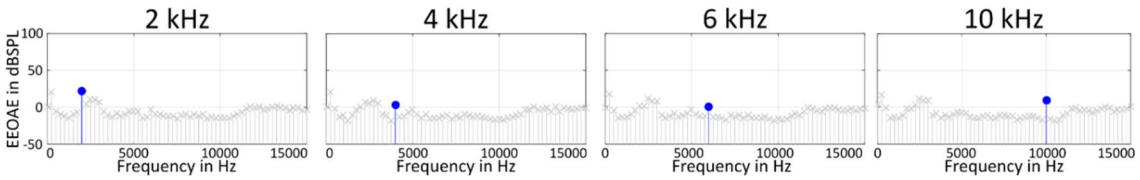

Figure B5.7 Same as Figure B5.2, but for animal #355 (355B30).

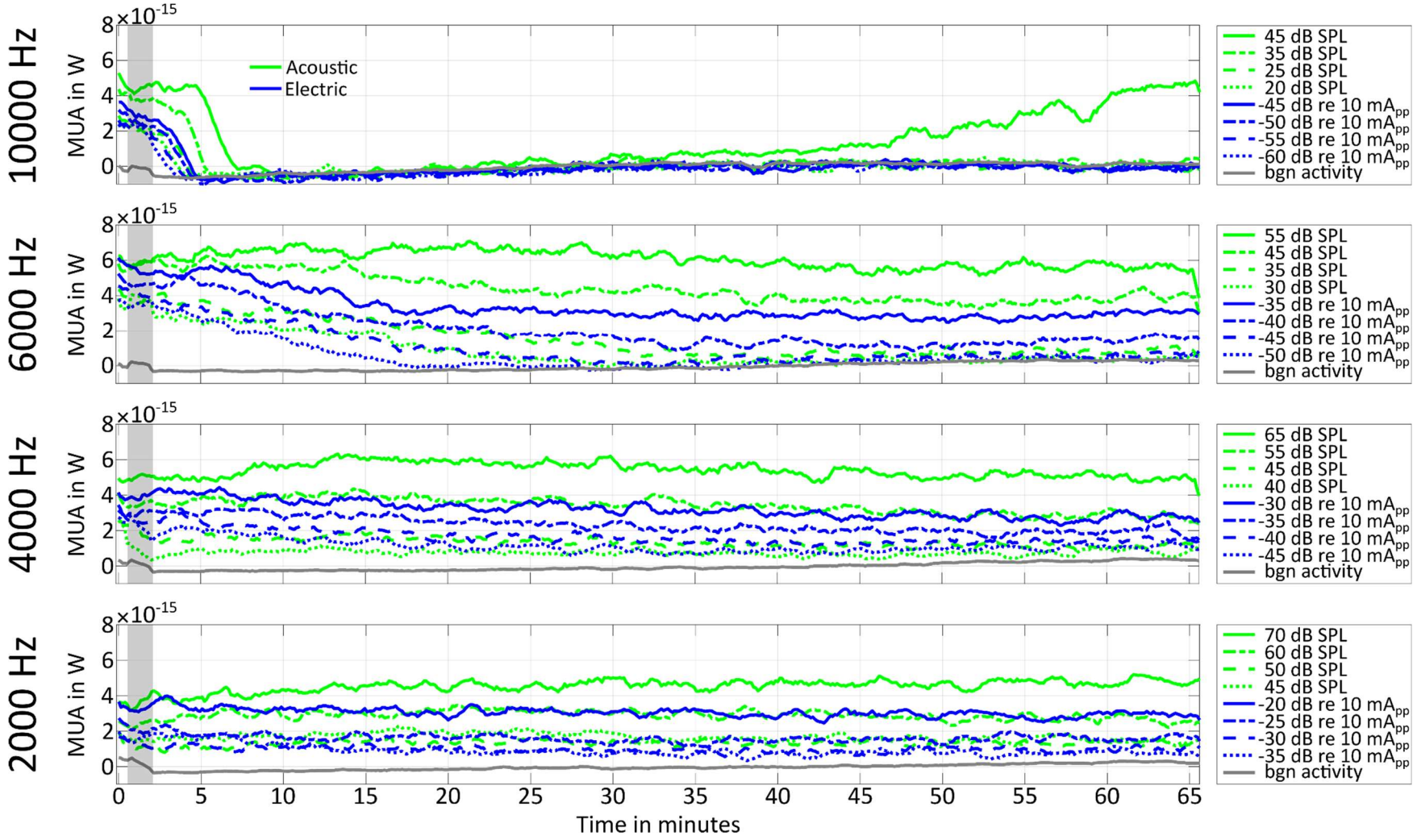

Figure B5.8 Same as Figure B5.3, but for animal #355 (355B30). Neural extraction is centred around electrode 7, 12, 15 and 22.

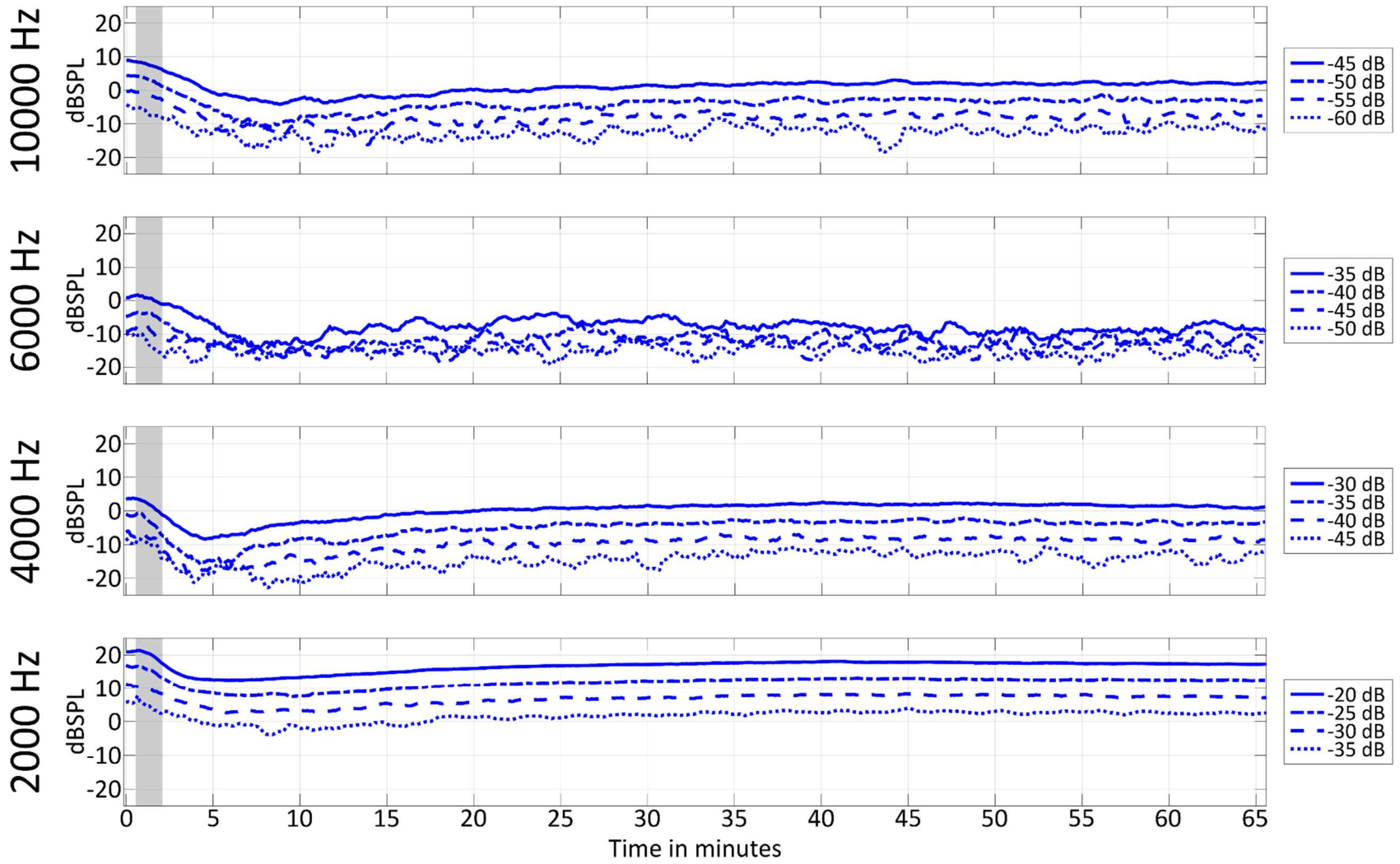

Figure B5.9 Same as Figure B5.4, but for animal #355 (355B30).

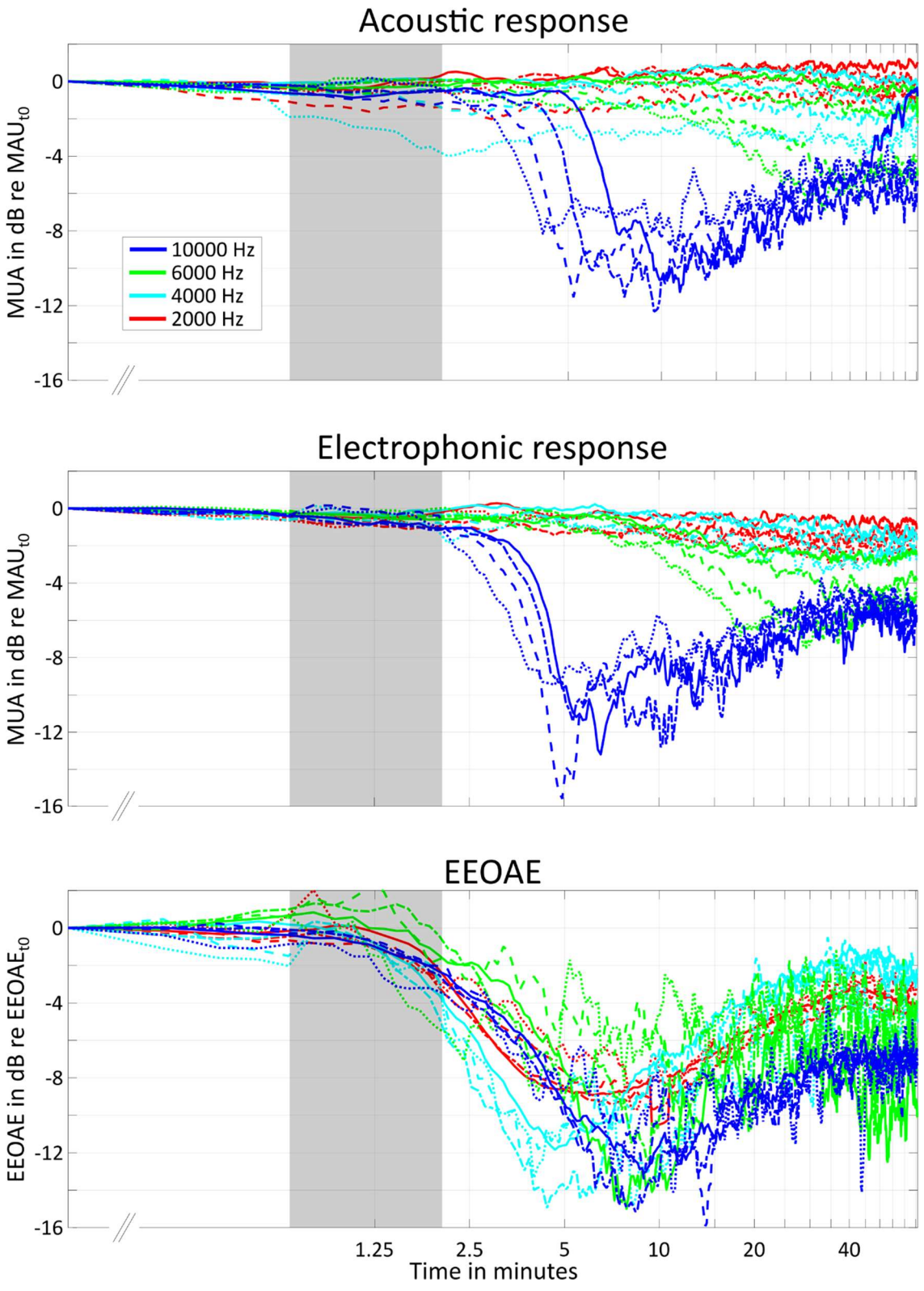

Figure B5.10 Same as Figure B5.5, but for animal #355 (355B30).

B5.4 Discussion and conclusions

Current results showed that the electrophonic response is dependent on the state of outer hair cells within the spread of electric excitation. This finding complements the results of Stypulkowski (1990), who showed that electrophonic response to biphasic electric pulses reduces after systemic application of salicylate in cats. Compared to the systemic administration, the direct infusion of the drug into the inner ear made it possible to observe localized effects on the outer hair cell motility during diffusion of the drug. Furthermore, the usage of electric sinusoids instead of pulses offered the observation of frequency specific changes in electrophonic response.

Since the generation site of the electromotile response is thought to be at the current injection site, we expected simultaneous drop in electrophonic responses after salicylate injection for all electrical stimulation frequencies. Instead, the decay was shown to appear later for lower stimulation frequencies, but the behaviour of the response over time was different from that of the acoustic response that were very little affected (e.g. see the 6 kHz responses with identical initial strength in Figure B5.3 or the 6 kHz response to the highest stimulation levels in Figure B5.8). An explanation for the frequency dependent electrophonic decay could be that the spatial spread of electric excitation covers basilar membrane loci with varying mechanical impedances. The electrically evoked travelling wave generation site may thus be a compromise between the decaying electrical field with distance from the injection site and the decreasing resonance frequency along the basilar membrane to the stimulus in apical direction. Although the former is frequency-independent, frequency-dependent mechanical impedance of the basilar membrane might cause the most effective generation site of the electrically evoked travelling wave to move more apical for lower stimulation frequencies, and thus, explain the observed delay of the electrophonic suppression time as stimulation frequency decreased. Salicylate requires more time to diffuse to more apical regions in the cochlea. In the future, this hypothesis could be easily addressed by simulating the electrically evoked generation of the travelling wave with a finite-element model. The generation of the electrically evoked travelling wave could be mimicked by modelling the OHCs as a spatially distributed force input, according to the spread of electric excitation, to the basilar membrane.

Electrophonic response was also shown to be more robust against the blocking of OHC electromotility when higher stimulations levels are applied. In the first place, the level dependence of electrophonic suppression may be explained by a larger required salicylate concentration at the excitation place to suppress a larger electromotile response. Alternatively, the larger delivered current also results in a lager spread of

excitation and in turn an increased number of recruited OHCs thus, to spatially cover the larger OHC population by the blocker agent, a longer diffusion time may be required.

The time courses of EEOAE suppressions were different from the time courses of electrophonic suppressions, indicating a difference in the most effective generation site of the two responses. The level independent suppression of EEOAEs commences almost immediately following the administration of salicylate, showing that their generation site is at the place of current injection. Thus, unlike the electrophonic generation site that may be governed by a balance between the strength of the electrical field and the local resonance frequency of the basilar membrane, the most efficient site for EEOAE generation appears to be the place where the electrical field is the strongest, i.e. the current injection site.

B6 Acousto-electric beats – a test for interaction between electrical and acoustical stimulation

In chapter B3 it was shown that in response to sinusoidal electrical stimulus, OHC motility can generate an acoustic like response, the electrophonic response, which travels in the cochlea to the characteristic place of the stimulus frequency. If the electrophonic response is present in a CI user with residual hearing, it may disturb the perception of acoustic stimulation that is aimed at stimulating low frequency residual hearing at the apex as illustrated in Figure B6.1. This potentially unfavourable interaction calls for a test to evaluate the presence of electrophonic response in EAS users. Since both the acoustic and electrophonic response are originating from the mechanical travelling wave on the basilar membrane, a beating phenomenon may be evoked by appropriate stimulus combinations. This acousto-electric beat may be used to test for electrophonic responses in CI patients.

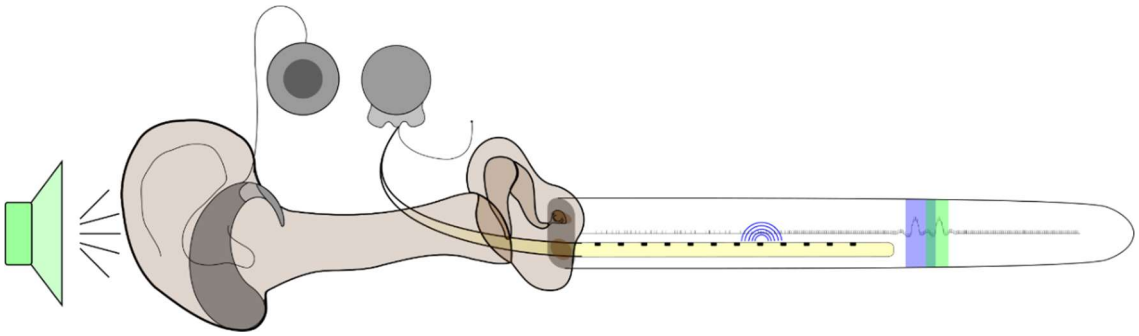

Figure B6.1 Illustration of the interaction of the acoustic and electrophonic response in the cochlea with residual hearing. At the apical part of the cochlea, the acoustically evoked travelling wave (highlighted by green) may interfere with the electrophonic response (highlighted by blue) that is generated by a basal electric stimulation.

B6.1 Beating phenomenon

Beating is the interference pattern of two sinusoidal waveforms that are slightly different in frequency. In Figure B6.2, panel A shows a pair of sinusoids with 10 (blue) and 11 Hz (green). The summation of these sinusoids results in the interference pattern shown in Panel B. The interference pattern displays a periodic amplitude change, with the periodicity corresponding to the frequency difference of the original signals. Maximum amplitude of the beat is the result of the summation of the sinusoids when they are in phase e.g. around 0 and 1 second. Minimum amplitude of the beat is the result of the

summation of the sinusoids when they are out phase e.g. around 0.5 second. The periodic nature of the beat allows for the translation of timing values to phases related to the beating period. In the current example, the maximum beat amplitude occurs at 0 and 360˚ and the minimum beat amplitude at 180˚. Complete cancellation in the beating pattern only occurs if the amplitude of the original sinusoids were equal. Panel C shows an example where the amplitude of the 11 Hz sinusoid is half of the amplitude of the 10 Hz signal. The resulting beating pattern in panel D illustrates the lack of perfect cancellation.

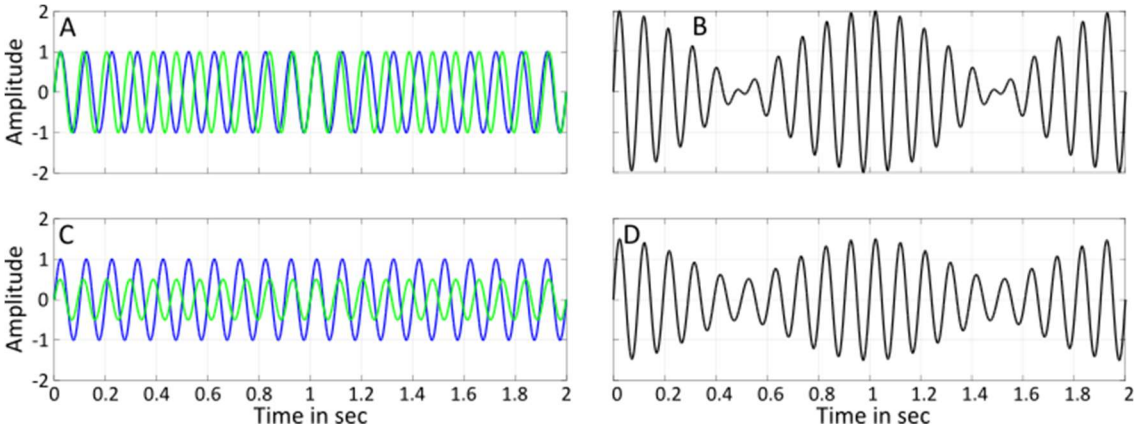

Figure B6.2 Beating pattern of sinusoids with slightly different frequencies – 10 Hz (blue) and 11 Hz (green). The summation of sinusoids with equal amplitudes (A) results in a beating pattern with perfect cancellation (B). The summation of sinusoids with non-equal amplitudes (C) results in a beating pattern without perfect cancellation (D).

The phase of the beating pattern is dependent on the relative phase of the input signals. Figure B6.3 illustrates the change in beating phase when the phase of the 11 Hz (green) sinusoid is systematically increased compared to the 10 Hz (blue) sinusoid from 0 to 360 degrees as noted in the top right corner of the panels. The difference in the starting phase of the input signals is reflected in the beat e.g. the maximum cancellation occurs at 180˚ when the input signals are in phase (panel A and B) and shifts by 90˚ to the negative direction (from 180˚ to 90˚) as the 11 Hz signal starts to lead by 90˚ (panel C and D).

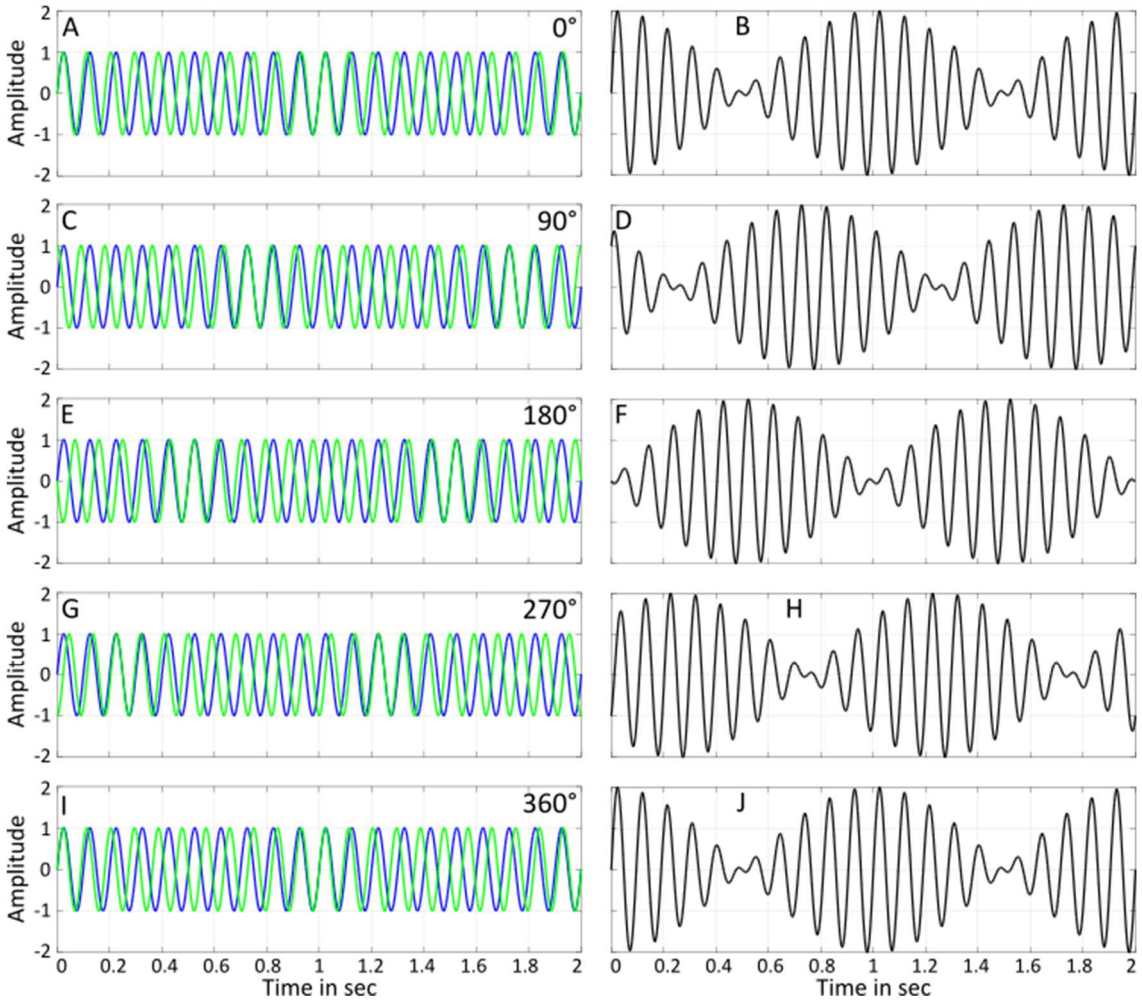

Figure B6.3 Beating pattern of equal amplitude sinusoids with 10 Hz (blue) and 11 Hz (green) with various phase differences.
A, B – 0˚ phase difference; maximum cancellation at 180˚ (0.5 s)
C, D – 90˚ phase difference; maximum cancellation at 180˚-90˚ (0.25 s)
E, F – 180˚ phase difference; maximum cancellation at 180˚-180˚ (0 s)
G, H – 270˚ phase difference; maximum cancellation at 180˚-270˚ (0.75 s)
I, J – 360˚ phase difference; maximum cancellation at 180˚-360˚ (0.5 s)

B6.2 Periodogram and beating strength

A spatial activation pattern captures the neural response along the tonotopy to a given stimulus at an instance. To visualize beating, the spatial activation patterns have to be presented over time.

In the experiments that aimed at observing acousto-electric beats, the stimuli were presented over multiple beating periods. Recording segments corresponding to the first and last beating period were discarded during analysis to avoid on- and offset effects. If not otherwise stated, the neural response was extracted from the remaining recording by a 25 ms sliding window with a step size of 1 ms. These settings allow for the clear visualization of a 5 Hz beat. The 25 ms long window captures a good amount of neural response without smoothing away the beat that has a 200 ms period length and the 1

ms step size results in a fine temporal resolution. In a final processing step, to visualize the response over one beating period i.e. to obtain a periodogram, the neural response was averaged across consecutive periods corresponding to the beating frequency.

In Figure B6.4, panels A and B show the time course of the neural response to a 2005 Hz acoustic tone and a 2000 Hz electric sinusoid respectively. The 2000 Hz electric stimulation was selected because, as demonstrated earlier in Figure B3.1, it evokes a strong electrophonic response that is clearly separated from the direct electric response. Note that the x-axis displays phase values as the plots correspond to one beating period (1/(5 Hz) = 200 ms). Both plots show a steady response with a peak at the characteristic place of the input stimuli. Panel B shows also a weak response at the place corresponding to the direct stimulation (15 kHz or electrode 28). Panel C shows the periodogram of the response when both stimuli are applied simultaneously. The plot reveals the beating pattern with a period of 1/(5 Hz) = 0.2 second. Maximum activity corresponding to perfect summation of the inputs when they were in phase can be observed around 340˚. Minimum activity corresponding to maximum cancellation of the inputs when they were out of phase is at 160˚.

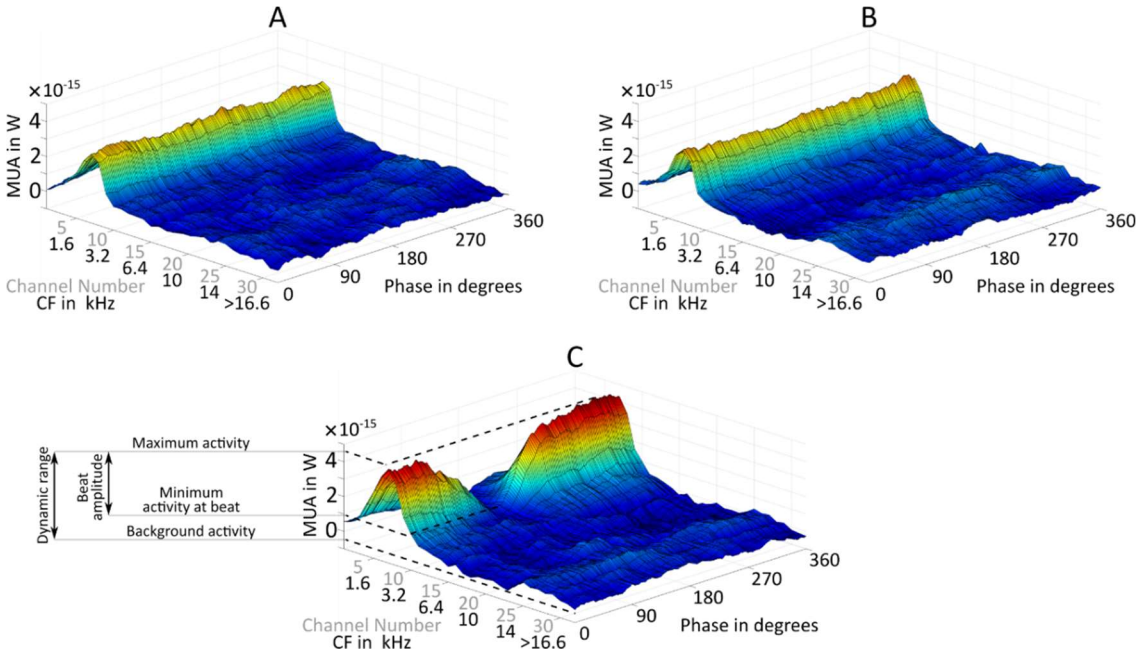

Figure B6.4 Example periodograms in response to a 2000 Hz electric sinusoid at -30 dB re. 10 mA_{pp}, a 2005 Hz acoustic pure tone at 47 dB SPL and to the combination of these (354B17). Panel A and B show the neural response to the acoustic pure tone and to the electric sinusoid over a 200 ms duration that corresponds one beating period (1/(5 Hz) = 200 ms), thus the time axis is expressed as phase. Panel C shows the periodogram of the neural response to the combination of the acoustic pure tone and the electric sinusoid.

To quantify the beat, the beating strength can be defined at every recording channel as follows:

$$Beat\ strength = \frac{Beat\ amplitude}{Dynamic\ range}$$

Where $Beat\ amplitude$ is the difference between the maximum and minimum activity at a given recording channel and the $Dynamic\ range$ is the difference between the maximum activity across all channels and the average background activity (i.e. zero since the 'real' background activity is removed by the analysis algorithm see Appendix BA).

For more compact presentation, only the x-y plane of the periodograms are shown further on, thus the strength of the response will only be represented by the colour-scale in these plots as shown in Figure B6.5. If not otherwise stated, the y-axis of this plot type always represents the beating phase from 0 to 360˚ thus later on labels will be omitted.

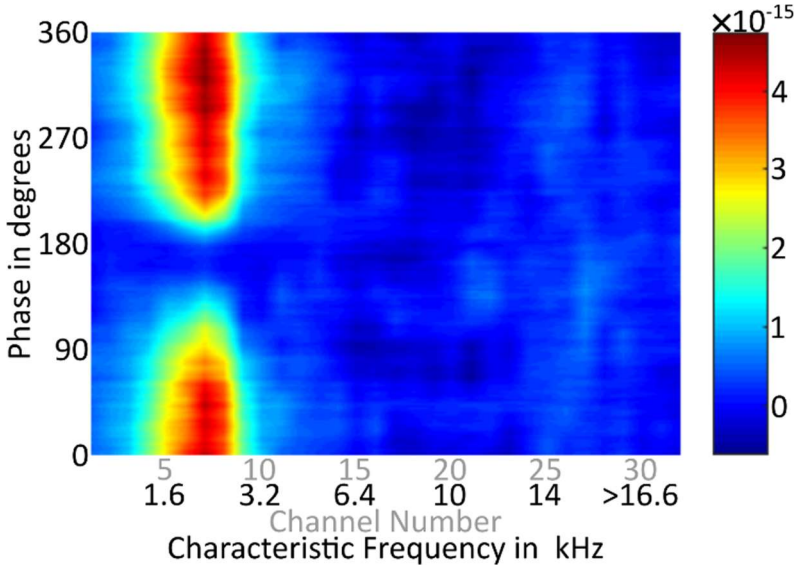

Figure B6.5 Example beating pattern in the cochlear place – time plane (354B17). This plot is the two-dimensional equivalent of panel C in Figure B6.4.

B6.3 Beating Response to Combined Electric Sinusoids and Acoustic Tones

As a first approach, acousto-electric beating effect is examined by the application of acoustic pure tones and electric sinusoids. Although modern cochlear implants do not utilize sinusoidal electric stimulation, the well-defined and understood excitation pattern (see chapter B3) of this stimulation type gives the opportunity to understand the principles of acousto-electric interactions in a clear environment without having to deal with complexities arising from the stimulation waveform. Readers more interested in clinical applicability of acousto-electric beats are referred to section B6.4 that introduces

experimental results with electric square waves and to section B6.5 that discusses clinical relevance.

B6.3.1 Stimulus level tuning for maximum beating strength

Theory shows that beating of two sinusoids is the strongest when the amplitude of the sinusoids is equal. The input signals in the cochlea are the acoustically and electrically evoked travelling waves. These travelling waves are hypothesized to evoke a beating response at their characteristic place if their amplitude is closely matched. Is this acousto-electric beat present in the cochlea? How is the strength of this beat affected by the level of the input stimuli? The first set of experiments was conducted to find an answer to these questions.

All beating experiments in this set were conducted with 2000 Hz electrical sinusoids and 2005 Hz acoustic pure tones. The level of the electric stimulus differed across experimental procedures (-40, -35, -30, -25 and -20 dB re. 10 mA_{pp}). Since acousto-electric beat was expected at equal acoustic and electrophonic responses, the acoustic levels resulting in a similar response strength as the electrophonic response (see chapter B3) were determined by a procedure conducted before the commencement of the beating experiments. Table B6.1 shows the identified equivalent acoustic levels of electrophonic responses evoked at various electric levels. The acoustic levels for the beating experiment were selected to cover a ±12 dB SPL range around these levels in 3 dB steps. The length of the stimulus was 1 or 2 seconds including 10 ms on- and offset squared cosine ramps and the stimuli pairs were presented in a randomized order. Control stimuli of solely electric or acoustic stimulation with parameters that were identical to the ones used for the beating, were randomly presented throughout the procedure.

	-40 dB	**-35 dB**	**-30 dB**	**-25 dB**	**-20 dB**
2 kHz	45 dB SPL	55 dB SPL	60 dB SPL	70 dB SPL	78 dB SPL

Table B6.1 Acoustic levels resulting in an electrophonic like response at various electric levels that are given in dB re. 10 mA_{pp} for animal #352.

Periodograms in response to the beating stimuli are presented in Figure B6.6. Each column corresponds to an electric stimulation level and each row corresponds to a paired acoustic stimulus level. The last row depicts the response to the electric control stimuli. The 0 dB row corresponds to a beating response where the acoustic stimulus levels were set to the ones shown in Table B6.1. The acoustic levels in rest of the rows can be calculated by adding the dB value of the row to the acoustic level corresponding to the 0

dB row, e.g. the periodogram in response to a -30 dB re. 10 mA_{pp} electric level in the -9 dB row was elicited by an additional 51 dBSPL (60 dBSPL + -9 dBSPL) acoustic tone.

The 2 kHz electrophonic response, spatially separated from the direct electric response, is visible in the electric control plots around channel 10 in response to -40 to -25 dB re 10 mA_{pp} and its response strength is increasing with stimulus level. In the -20 dB re 10 mA_{pp} control plot the electrophonic response merges into the direct response.

The predicted beating of the electrophonic response with an additional acoustic tone can indeed be observed at every applied electric stimulation level. The most prominent electrophonic beats can be found in the 6, -3, -3, -9 and -12 dB rows for the increasing electric levels. The notch of the electrophonic beat occurred approximately at 180˚ in all cases, indicating a level-independent electrophonic beating phase.

In response to electric stimuli at and above -35 dB re. 10 mA_{pp} , the direct electric response is visible around electrodes 25 and 30 with the CF of 11 and 15 kHz. The distinct direct excitation loci are characteristic to the bipolar electric stimulation (see chapter B3). The direct response strength increased, and its pattern widened with increasing electric stimulus level. In response to the -20 dB re. 10 mA_{pp} electric stimulus the excitation loci of the bipolar lobes were becoming less distinguishable due to the wider spread of excitation caused by the high stimulation level.

Surprisingly, a beating pattern also appeared at the direct stimulation place as the level of the acoustic tone increased. In the periodograms with -35 to -25 dB re 10 mA_{pp} electric levels, beating of the direct response at the 11 kHz characteristic place appears with a peak approximately at 270˚. In the -25 dB re. 10 mA_{pp} case beating of the direct response at the characteristic place of 15 kHz also appears with a peak around 90˚. Lastly, In the case of periodograms with -20 dB re. 10 mA_{pp} electric stimulus, the direct beat shows a peak around 90˚ at both the 11 and 15 kHz characteristic place. The roughly similar phase of the direct beat in this case was probably caused by the large electrical spread and hence the less distinguishable excitation loci.

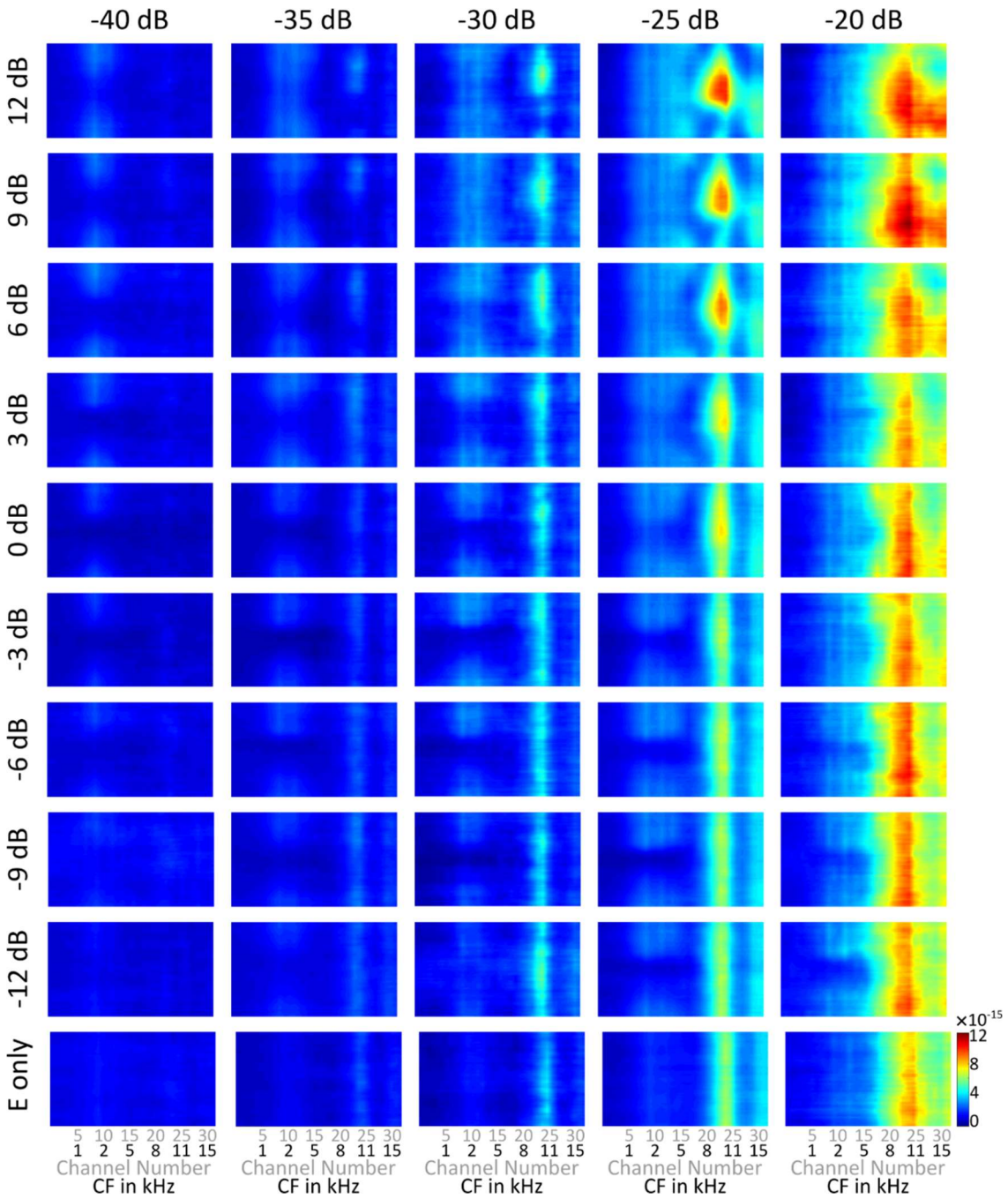

Figure B6.6 Periodograms in response to simultaneously presented 2000 Hz electric sinusoids and 2005 Hz acoustic tones. Each column corresponds to a single experiment in the same animal with the electric level (referenced to 10 mA_{pp}) indicated above the column (-40 to -20 dB re. 10 mA_{pp} – 352B14, 352B10, 352B25, 352B12, 352B19). Each row corresponds to a different applied acoustic level. The 0 dB row corresponds to conditions where the acoustic level from Table B6.1 is used. The acoustic levels in the rows above and below the 0 dB row can be calculated by adding the value in the row title to the predetermined 0 dB level. E.g. In the 6 dB row in the -35 dB re. 10 mA_{pp} column the acoustic level was 55+6=61 dB SPL. The last row contains the response to electric sinusoidal stimulation only. Beating effect at the 2 kHz electrophonic place is apparent for all used electric levels (columns) and additionally a beating pattern can also be observed at the direct stimulation place (around electrode 25 with the CF of 11 kHz).

B6.3.1.1 Beat strength and tuning

Figure B6.7 shows the beating strength and tuning curves for all stimulus conditions. Note, to visualize the direct electric peaks, the spatial tuning curve scale in the -20 and -

25 dB re. 10 mA_{pp} conditions cover a larger range compared to the conditions with lower electric levels.

In the beating strength plots in panel B, C, D and E an acoustic level dependent peak can be seen at the electrophonic place, indicating the electrophonic beat. The strongest electrophonic beats occurred at acoustic levels that resulted in approximately the same neural response as the electrophonic response, see the corresponding spatial tuning curves in panels G to J. This is in line with the theoretical basis that maximum cancellation, thus the strongest beat, occurs when the input signals are equal in amplitude, see Figure B6.2. Panel A shows a faint electrophonic beat in response only to the weakest acoustic stimulus, although in Figure B6.6 an electrophonic beat is observable at least for two more acoustic levels (69 and 72 dB SPL). The beating strength is calculated relative to the total dynamic range of the periodogram. In the -20 dB re. 10 mA_{pp} electric condition, the dynamic range of the recording is considerably larger than the extent of modulation in the electrophonic beat. This makes the small electrophonic beat invisible in the beating strength plots.

In panel B, C and D, a peak also appears at the direct electric place, reflecting the direct beat observed in Figure B6.6. The strength of the direct beat increased with acoustic level without showing an optimal tuning. Spatial tuning curves in panel G to I also reveal that beating at the direct electric place did not require a comparable acoustically and electrically evoked neural activity. Panel A shows similar increasing beat strength tendency in the high frequency region without a distinct peak. The lack of peak in this case was probably the result of the wide excitation pattern caused by the large current spread at this electric level. The unexpected appearance of the direct-electric beat with response properties in stark contrast to that of the electrophonic beat leads us to continue our investigation on separate branches dedicated to the different beat types.

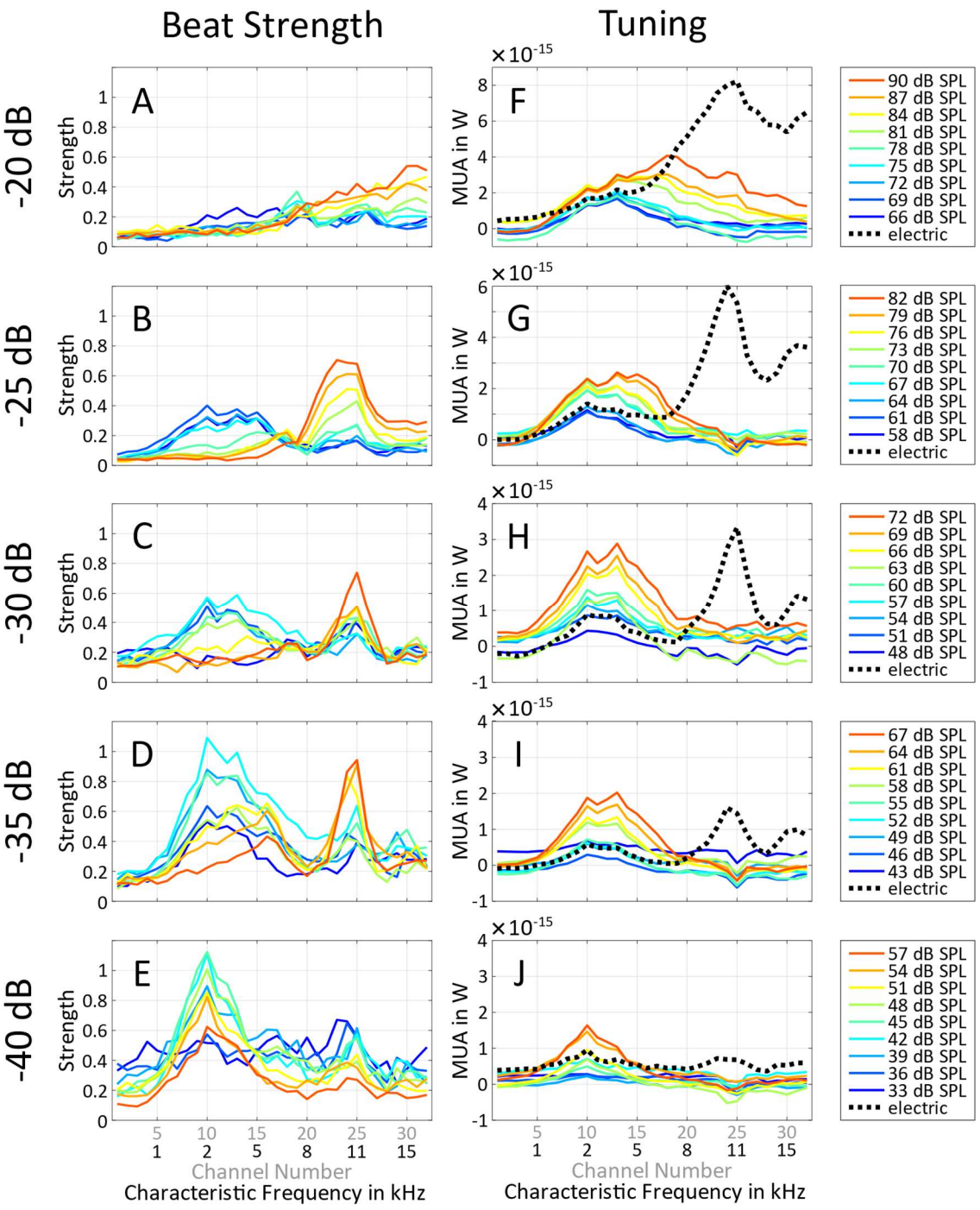

Figure B6.7 Beating strength (first column) and spatial tuning curves (second column) of a 2 kHz electric sinusoid at stimulus levels from -40 to -20 dB re. 10 mA_{pp} (rows) and a 2005 Hz acoustic tone at various levels (colour of the curves). Spatial activation patterns of the electric sinusoids are shown by dotted lines in the tuning curve plots. Note, to allow for the visualization of the direct electric peak, the scale of panel F and G covers a wider range compared to the rest of the tuning curve plots. (-40 dB – 352B14, -35 dB – 352B10, -30 dB – 352B25, -25 dB – 352B12, -20 dB – 352B19).

B6.3.2 Beating at the electrophonic place

Building on the experience collected by studying the acousto-electric beat tuning and its dependence on electric and acoustic levels, we first set out to expand our knowledge about the electrophonic-beat. We started by adding a new dimension to the investigated parameter space by studying the electrophonic beat in response to various stimulation

frequencies. This was followed by investigating the probable differences in the beating pattern upon the usage of inverted difference frequency. At last, the persistence of electrophonic beating with increasing difference frequencies was tested.

B6.3.2.1 Frequency dependency of electrophonic beat

Electrophonic beat may arise in different patterns at various stimulation frequencies due to the differences in the generation of the acoustically and electrically evoked travelling waves. To shine light on these differences, the parameter space of beating experiments was extended in the spectral dimension.

The used stimuli were similar to the ones described in B6.3.1, with the additional variation of the stimulus frequency. Electric sinusoids were presented at 2, 6, 10 and 14 kHz with an additional acoustic tone being 5 Hz higher. In this example the electric levels were -35, -30 and -25 dB re. 10 mA_{pp} . The stimuli were 1.2 second long including 10 ms on- and offset squared cosine ramps. Stimuli pairs and additional acoustic and electric control stimuli are presented in a randomized order.

Example periodograms in response to stimuli resulting in clear electrophonic beating patterns at -30 dB re. 10 mA_{pp} electric level are shown in Figure B6.8. The first two rows show the electric and acoustic control stimuli and the last row shows the beating patterns in response to the combined stimulation.

The electrophonic and acoustic responses are visible as continuous vertical stripes at the characteristic place of the stimuli. The direct electric response is only faintly visible in the 2 kHz electric control plot approximately at the 14 kHz characteristic place. In the periodograms of the combined responses, beating patterns are visible at the characteristic place of stimulation. The notch of the beat shows a phase of approximately 150, 60, 150 and 330˚ for the frequencies from 2 to 14 kHz.

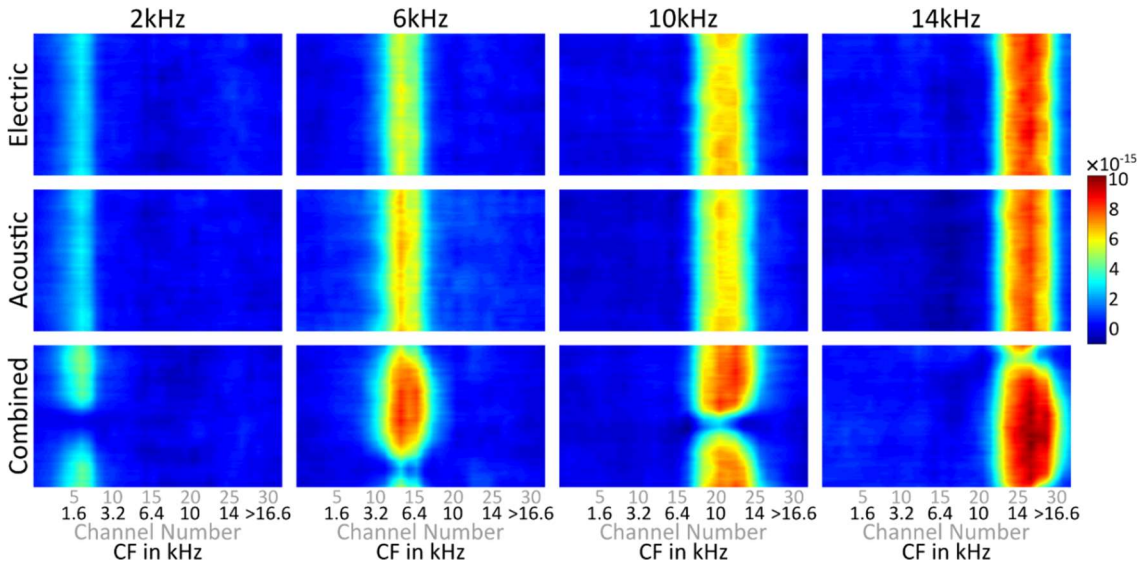

Figure B6.8 Example periodograms in response in response to electric, acoustic and combined stimuli with various frequencies (354B17). The first row shows electric responses to 2, 6, 10 and 14 kHz stimuli, presented at -30 dB re. 10mA$_{pp}$. The second row shows acoustic responses to 2005, 6005, 10005 and 14005 Hz presented at 47, 45, 47 and 43 dB SPL. The third row shows periodograms in response to the combination of the stimuli in the first two rows.

So where does the frequency dependent phase of the electrophonic beat come from? The phase of beating pattern was shown to be determined by the phase difference at the start of the input signals in Figure B6.3 in section B6.1. The input signals of the electrophonic beat are the acoustically and electrically evoked travelling waves. The phase accumulation of the acoustic travelling wave up to the characteristic place, i.e. the number of cycles in the travelling wave up to the characteristic place, is independent of stimulation frequency according to the review by Robles and Ruggero (2001) and as seen in the modelling results of this thesis in Part A, e.g. in Figure A4.1. On the other hand the phase of the acoustic travelling wave at the basal part of the cochlea is frequency dependent [Robles & Ruggero, 2001]. Furthermore, the propagation of vibrations through the middle ear is also frequency dependent [Dancer & Franke, 1980]. In contrast, outer hair cell electromotility possess a relatively flat phase response in the frequency range applied in the current experiment [Frank et al., 1999]. Based on the identical phase of electromotility, the phase of the electrically evoked travelling wave at the generation site can be assumed to be frequency independent. This suggests, the phase difference between the acoustically and electrically evoked travelling waves varies at the electric stimulation site due to the frequency-dependent phase accumulation of the acoustic travelling wave to this site and consequently gives rise to a frequency dependent phase of the electrophonic beat.

B6.3.2.1.1 Beat strength and tuning

Beating strength and spatial tuning curve plots are shown in Figure B6.9. Data for the 6 kHz condition at -25 dB re. 10 mA$_{pp}$ is discarded because the acoustic stimulus level was

set too high in this case, thus no electrophonic beat was present. In the rest of the conditions, beating at the electrophonic place was present and acoustic-electric level tuning could be shown.

The beating strength peak at high acoustic levels in the -25 dB re. 10 mA_{pp}, 2 kHz case gradually shifted towards the base of the cochlea. The shift of the beat remained within the range covered by the peaks of the spatial tuning curves. Looking at the corresponding tuning curves, strong neural activity can be seen at the basal slope of the electrophonic response. This high neural activity made the apparent basal shift of the strongest beat. Also note that, the basally shifting strongest beat appeared at acoustic stimulation levels that produced a travelling wave amplitude equal to the electrophonic response at the place of the strongest beat.

In the 6 kHz conditions at -30 dB re. 10 mA_{pp}, a beating strength peak first appeared at the electrophonic place, for low acoustic levels. As the acoustic level was increased, the electrophonic beat vanished, and at high acoustic levels a different beat appeared at a location basal to the electrophonic place, around channel 23 with the CF of approximately 12 kHz. This basal location was close to the direct excitation place at channel 28 (see the response in the -25 dB re. 10 mA_{pp} 2 kHz tuning curve panel), thus indicating the direct electric nature of the beat here. Channel 23 had a high sensitivity due to a close neural population (see Appendix BA) and this high sensitivity made the direct-beat visible. This case will be further discussed in section B6.3.3.

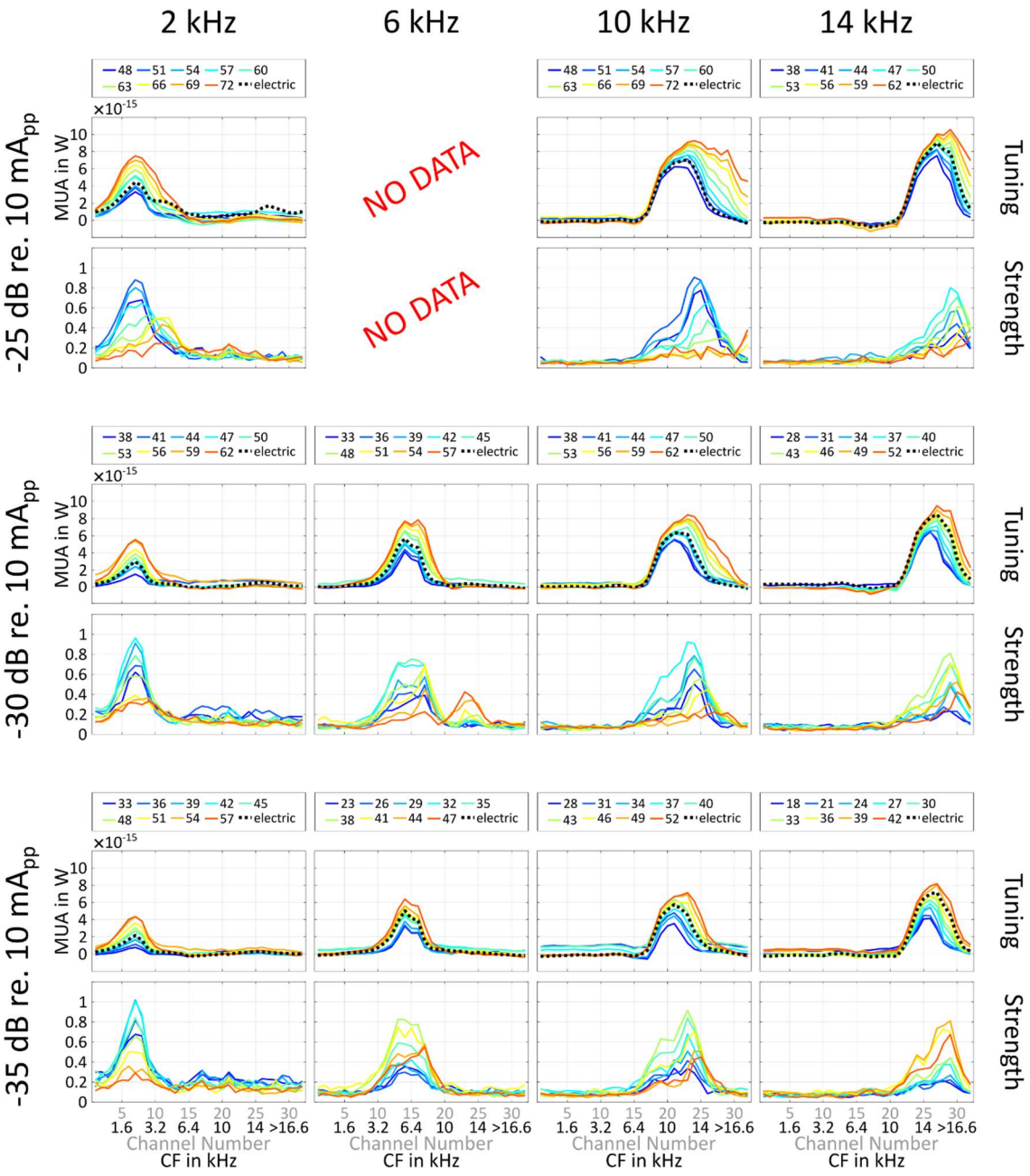

Figure B6.9 Spatial tuning curves of acoustic and electric stimuli and the corresponding beating strength curves (354B17). Every column corresponds to a condition that used an electric stimulus with the frequency indicated in the column title. Rows are organized in pairs: The upper row contains the spatial tuning curves and the lower row contains the beating strength plots. Row titles on the right-hand side of the figure aid the identification of the plotted data type. Each row corresponds to a different electric stimulus level, indicated left to the rows. Colouring of the curves identifies the applied acoustic level in dB SPL that is also shown in the labels above the spatial tuning curves (for compact representation the unit 'dB SPL' is omitted from the labels). Spatial tuning curve of the electric response is illustrated by dotted lines.

The maximum beating strength is plotted with respect to the used acoustic levels for all electric conditions in Figure B6.10. In general, all the curves show a peak corresponding to an acoustic level that gave a response close in strength to the electrophonic response. In all cases the higher electric level required a higher acoustic level to achieve the strongest beat. In accordance with the results of chapter B3, where similar growth functions for the electrophonic and acoustic responses were demonstrated, Figure B6.10

also demonstrates that a 5 dB increment in the electric stimulus level also required a 5 dB increment in the acoustic stimulation level to obtain the strongest beat.

Unit beating strength that correspond to the beat with maximum cancellation was not obtained in all conditions. This may have been caused by the coarse steps in the acoustic levels, that led to missing the strongest beats. Another factor could be the selectivity of the recording channels with cross-talk from non-beating surrounding neural population.

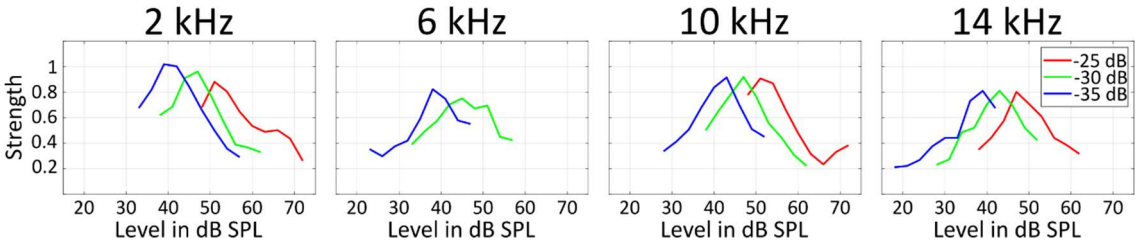

Figure B6.10 Maximum beating strength as a function of acoustic stimulation level (354B17). Electric stimulus frequency is indicated in the panel titles and the electric stimulus level, given in dB re. 10 mA_{pp}, is identified by the colour of the curves.

B6.3.2.1.2 Beating envelope

The envelopes of the electrophonic beats are shown in Figure B6.11 as the average response across the three electrodes at the electrophonic place. Each line in a plot represents a response at a different acoustic tone level. The colour code for their identification matches the one in Figure B6.9.

A theoretical beating envelope is superimposed on the plots as a grey line. The amplitude and offset of the theoretical beat envelope were determined by the strongest measured beat (emphasized by double linewidth). The phase of the theoretical beat envelope was set such that mean squared error between the theoretical beat envelope and the strongest measured beat is minimal.

In response to the 2 and 6 kHz stimuli the beat envelopes closely matched the theoretical curve. Saturation of the neural response was present in the 10 and 14 kHz conditions. In these cases, the beating was only present as a notch in the response as the maximum in stimulus superposition was not able to drive the neurons above saturation.

An asymmetry in the falling and rising slopes of the measured beat envelopes can also be noticed, with the most prominent one in the 10 kHz, -30 dB case. The rising slope of the beating envelope usually exhibits a slope that is steeper compared to the theoretical slope. This phenomenon was probably caused by spike rate adaptation following the notch in the beat. Note that, this asymmetry also caused a small mismatch between the notch positions of the theoretical and the measured data.

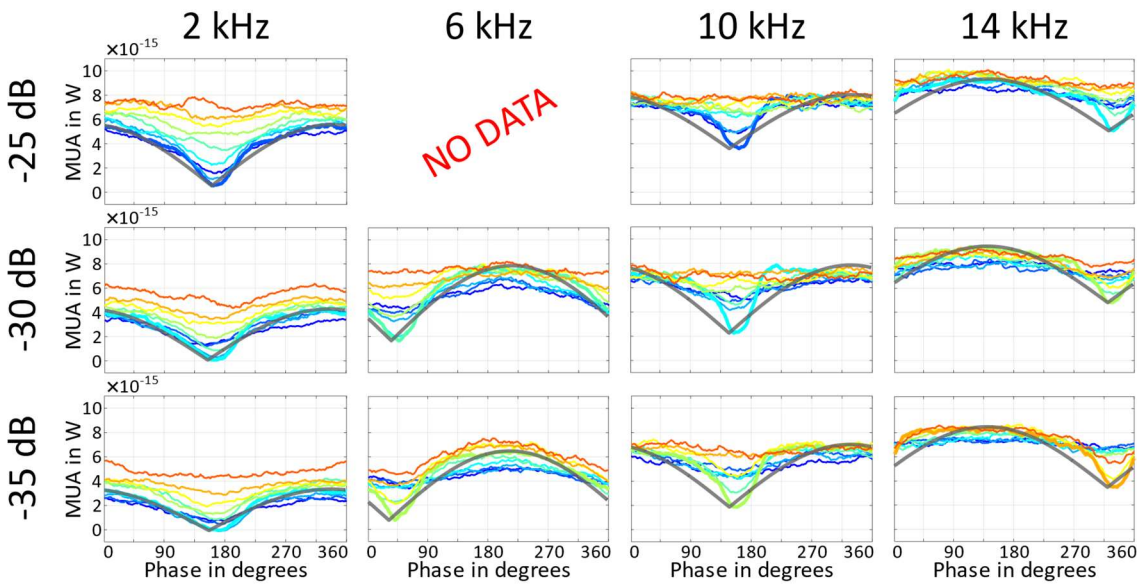

Figure B6.11 Electrophonic beat envelopes (354B17). Beat envelopes obtained by averaging the neural response at 3 neighbouring channels at the electrophonic response place. Each panel corresponds to a condition with the electric stimulus frequency indicated in the column titles and the electric stimulus level, given in dB re. 10 mA_{pp}, in the left label. Line colouring indicates the applied acoustic level, and it is identical to the one used in Figure B6.9. In each panel, the line with double width corresponds to the strongest beat. Theoretical beat envelope is shown in all panels as a grey line. See text about the determination of the theoretical beat.

B6.3.2.2 Dependency of electrophonic beat on the sign of the difference frequency

The presented beating results so far included stimuli where the acoustic stimulus frequency was always 5 Hz higher compared to the electric stimulus frequency. The sign of the difference frequency determines whether the acoustic or the electophonic signal leads before the beat maximum. Depending on the modality of the leading signal, the shape of the beat envelope may be different. In the present section the differences between electrophonic beats generated by a 5 Hz lower (-5 Hz difference frequency) and 5 Hz higher (+5 Hz difference frequency) acoustic stimulus are investigated.

The used stimuli were like the ones described in B6.3.2.1, but both -5 and +5 Hz were used as difference frequencies for defining the acoustic stimulus. The used electric levels were -44, -40 and -36 dB re. 10 mA_{pp}.

Example periodograms with clear beating patterns are shown in Figure B6.12. In all cases, a beating pattern appeared at the electrophonic place. An approximately 60˚ change in the phase is apparent between the -5 and +5 Hz beating patterns. However, due to the lack of knowledge about the phase of the stimuli at the site of interaction, the change of beating phase carries little information.

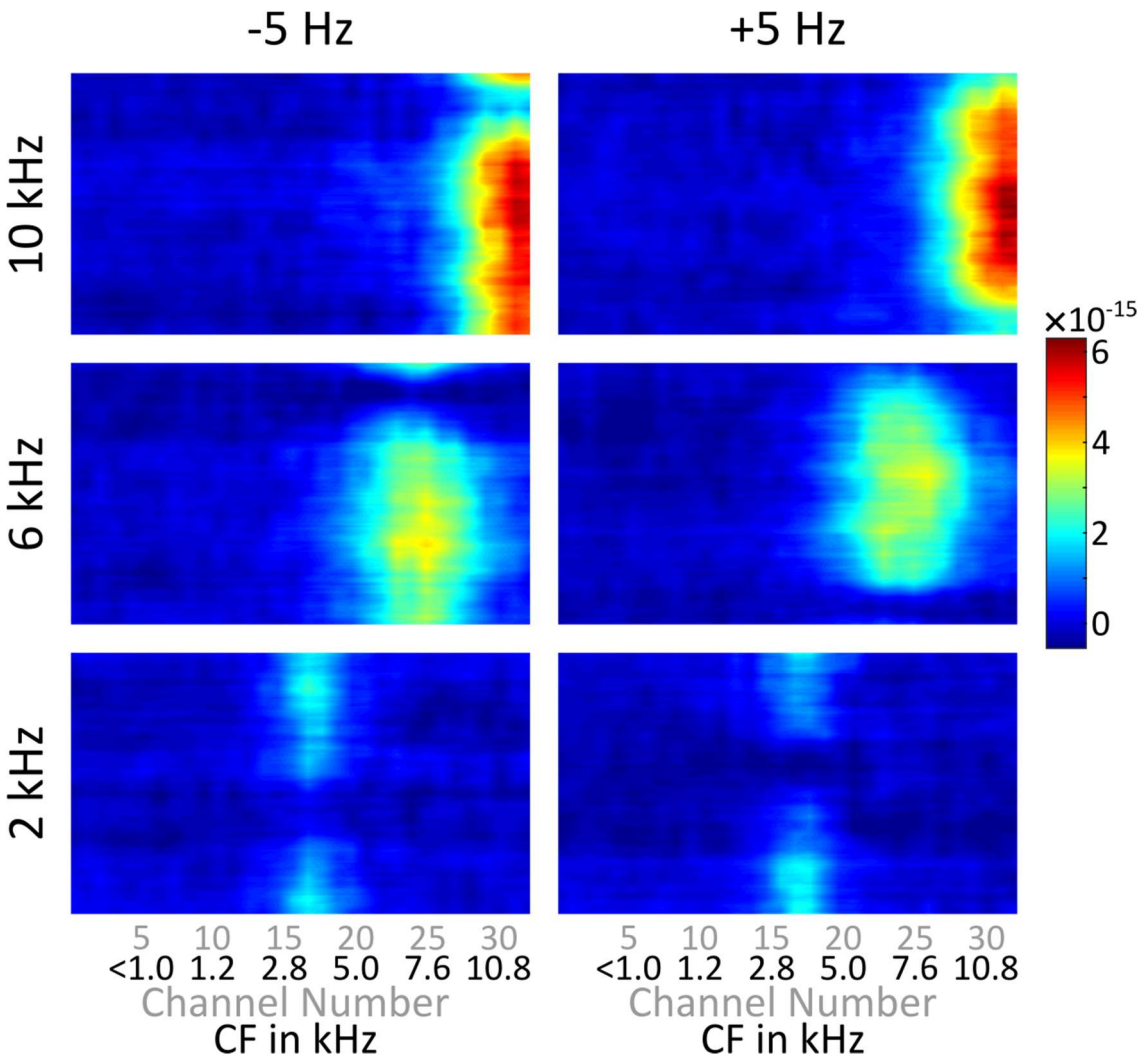

Figure B6.12 Example acousto-electric beat periodograms with -/+5 Hz difference frequencies (359B25). Examples obtained with -36 dB re 10 mA_{pp} electric stimuli and 42, 44 and 43 dB SPL acoustic stimuli in the 2, 6 and 10 kHz conditions. Each row corresponds to conditions with the electric stimulus frequency shown in the row title. The first column contains example periodograms where the acoustic stimulus frequency was 5 Hz lower than the electric, hence the difference frequency (noted in the column title) was -5 Hz. The second column contains example periodograms with where the difference frequency was +5 Hz.

The electrophonic beat envelopes in response to the +5 Hz and -5 Hz conditions are shown in Figure B6.13. Every trace corresponds to a stimulus condition and is obtained by averaging the response across 3 channels at the electrophonic place. To be comparable, traces corresponding to the -5 Hz conditions (red) are shifted by +66˚ to be aligned with the traces corresponding to the +5 Hz conditions (blue).

Traces corresponding to +/-5 Hz conditions show no systematic difference. This implies that, it does not matter which modality leads at the rising slope of the beat envelope.

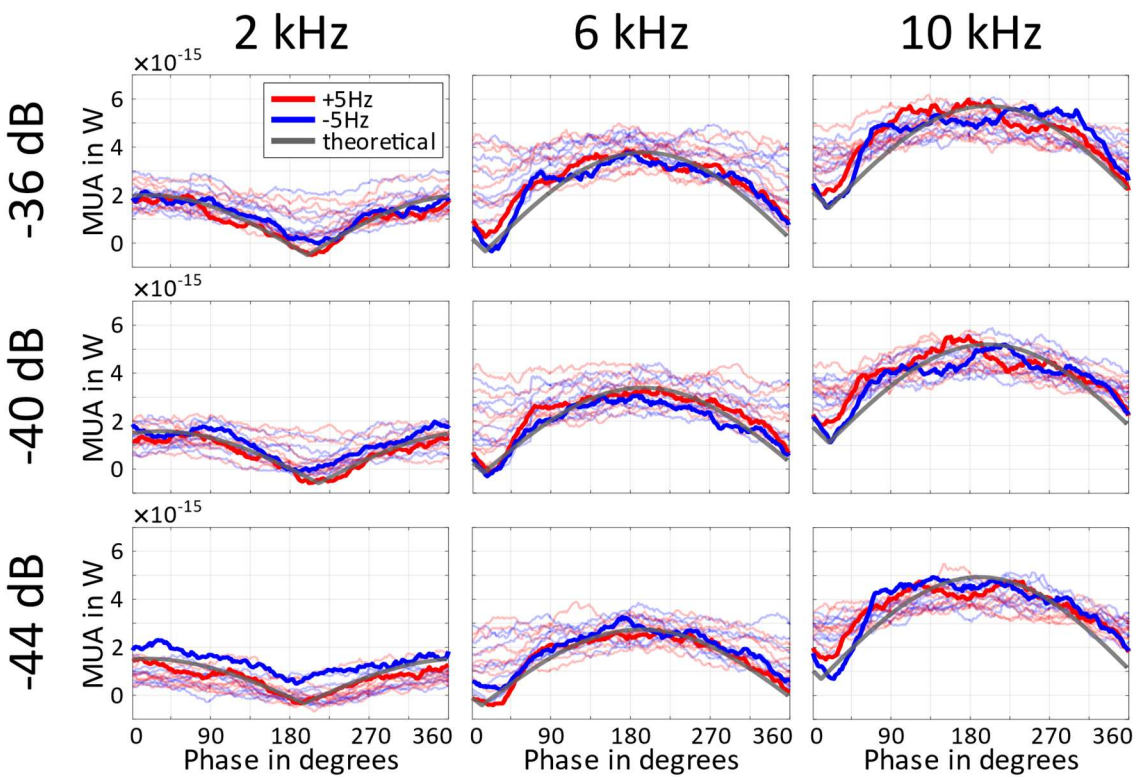

Figure B6.13 Beat envelope comparison for beating elicited by a +5 Hz (red) and -5 Hz (blue) difference frequency (359B25). Theoretical beat envelope is shown as a grey line and +/-5 Hz traces, showing the largest beat strength, are emphasized. For more efficient comparison, the curves corresponding to the -5 Hz beats are shifted by +66 degrees (+37 ms) to be aligned with the +5 Hz curves.

B6.3.2.3 Variation in beating frequency

In the preceding sections, the electrophonic beat was investigated for a difference frequency of 5 Hz. This section shows that electrophonic beats can be evoked at higher rates.

The used stimuli are similar to the ones described in section B6.3.2.1, but the electric stimulus frequency is fixed at 6 kHz and the difference frequency is varied between 5 Hz and 80 Hz. The used electric level was -40 dB re. 10 mA_{pp}. To obtain these results, a 5 ms long sliding window was used (for all five beat frequencies). The shortening of the window size was necessary because the original 25 ms long window would have smeared the beats with comparable period length, making them invisible in the neural response.

Results in Figure B6.14 show that the neural population in the inferior colliculus can follow beats easily up to 80 Hz. Note that the y axis, instead of phases, now displays a fixed 200 ms time interval. The number of beating cycles appearing in the plots is following the increment in the difference frequency.

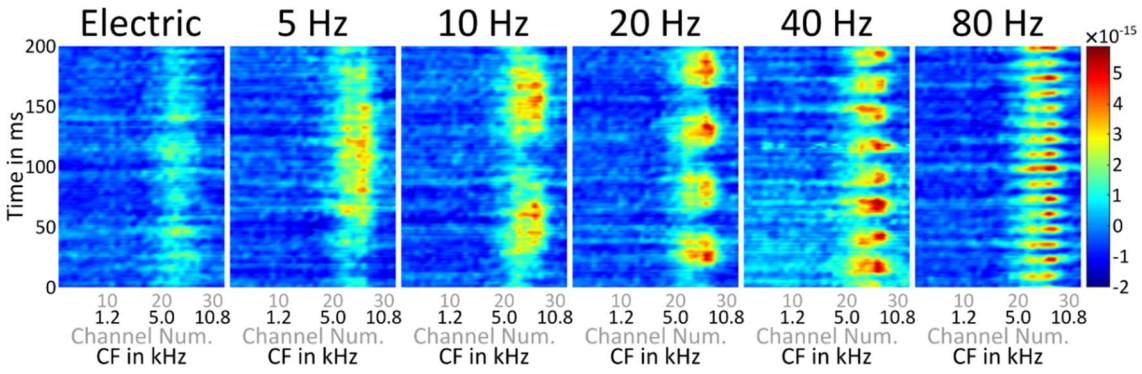

Figure B6.14 Excitation patterns of electrophonic beats at 6 kHz with various Δf difference frequencies (indicated in the panel titles) in a 200 ms time window (359B31). The electric sinusoid parameters were fixed at -40 dB re. 10 mA_{pp} level and 6 kHz frequency. The acoustic stimulus level was 48 dB SPL and the frequency was 6 kHz + Δf. The left-most panel illustrates the response to the 6 kHz -40 dB re. 10 mA_{pp} electric control condition. Note that the number of beating periods appearing in a plot increases according to the increment in the difference frequency.

B6.3.3 Beating at the direct electric place

In B6.3.1 the appearance of beating at the place of direct electric stimulation was shown. The phase of the direct-beat was different from the phase of the electrophonic beat and it did not require comparable response strengths evoked by the acoustic and electric components. Furthermore, in the previous section, beating at the direct place also appeared even if neither the acoustic nor the electric stimulus alone evoked an activity at the direct electric place (see the 6 kHz, -30 dB re. 10 mA_{pp} condition in Figure B6.9). These differences prompted us to regard the direct-beat as being different from the electrophonic beat and investigate it further in detail.

To study specifically the beat of the direct electric response, the electric stimulation had to be designed carefully. To be certain of the direct electric nature of the beat, the electric stimulus level had to be chosen high enough to elicit direct electric activity alone. To clearly distinguish the direct and electrophonic responses the electric stimulus frequency had to be low enough to spatially separate them from each other. Also, the electric stimulus level had to be kept moderate such that the spread of electric excitation does not reach the electrophonic place. On the other hand, electric stimulus frequency also had to be high enough to exclude the possibility of neural phase locking (upper limit of auditory nerve phase locking in guinea pigs is approximately 3.5 kHz [Palmer & Russell, 1986]), because the interaction of phase-locked neural responses to the acoustic stimulus and to direct-electrical stimulation may in some way by itself result in beat-like responses.

An experiment like the one in section B6.3.2.1, but with parameter settings dedicated to studying the direct beating phenomenon was conducted. Thus, a higher acoustic tone level was chosen, and keeping in mind the above-mentioned electrical stimulation

constraints and based on the results of a procedure with solely electric sinusoids that preceded the beating experiment, the electric stimulation parameters of 3 and 4 kHz and the level of -25 dB re. 10 mA_{pp} was selected.

Example periodograms grouped by electrophonic and direct electric beats are shown in Figure B6.15. For additional comparison, the results of the 6 kHz, -30 dB re. 10 mA_{pp} condition from section B6.3.2.1 is also included in the analysis[9]. The response to 3 and 4 kHz electric stimulation alone (shown both in the electrophonic and direct beat panel group) confirm the correct choice of stimulus parameters. Both the 3 and 4 kHz electric sinusoid evoked response patterns show the direct response at channel 23 and 30 characterised by the frequencies of approximately 12 and 16 kHz. As mentioned earlier, the double stripe in the direct excitation pattern is the result of the bipolar stimulation. The electrophonic response to these stimuli appears at channel 8 and 11 that are distinct from the direct response.

Clear electrophonic beat with a notch approximately at 120˚, 270˚ and 60˚ is visible in response to the combined response with 3, 4 and 6 kHz stimuli.

Direct electric beat appeared in response to the combined stimulation when the acoustic levels were raised to 72, 82 and 57 dB SPL for the 3, 4 and 6 kHz stimuli, respectively. Notably, the beating pattern is out of phase by 180 degrees at the responses corresponding to the side lobes of the bipolar electric stimulation, e.g. in response to the 3 kHz combined stimulation at channel 23 the beating pattern shows a peak at 180˚ while at channel 30 the notch of the beat is present approximately at the same phase. Besides being a neat demonstration of the opposing polarity of the current at the two stimulation electrodes, this direct beating pattern also indicates that the acoustic stimulus related component of the beat has the same phase across the whole region of direct electric excitation, i.e. it is related to the tail of the acoustic travelling wave, that is known to move in phase (see the review of [Robles & Ruggero, 2001] or the modelling results of Part A).

[9] Note that the scale of the figures corresponding to the experiment with 6 kHz is different from the other two as data is obtained from a different animal.

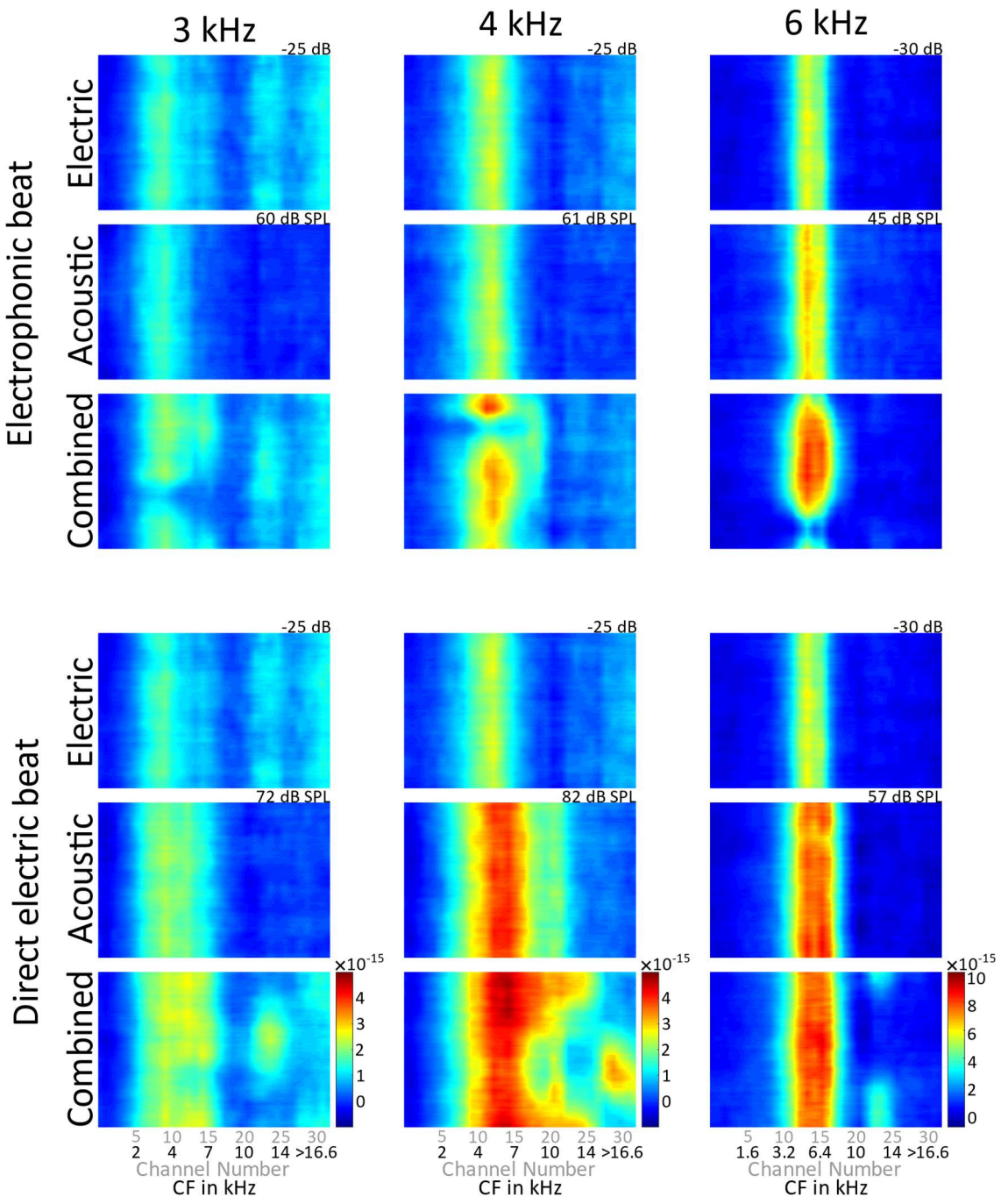

Figure B6.15 Beating pattern at the electrophonic and direct electric excitation place (355B25 – 3 and 4 kHz, 354B17 – 6 kHz). Rows 1 to 3 show examples of the electrophonic beat and rows 4 to 6 show examples where direct beating pattern is present. Acoustic and electric levels (in 10 dB re. 10 mA_{pp}) applied in the examples are noted in the upper right corner of the panels with acoustic- and electric-only responses.

B6.3.3.1 Beat strength and tuning

The spatial tuning curves of the applied acoustic and electric stimuli and the corresponding beating strength plots are shown in Figure B6.16. Observation similar to the ones drawn from the results presented in section B6.3.1.1 can also be repeated here. The electrophonic beat response requires a comparable excitation pattern evoked by the acoustic and electric stimulus at the electrophonic place. The direct beat does not require

comparable excitations and grows with acoustic stimulus level, without reaching and optimum point where beating strength is maximal.

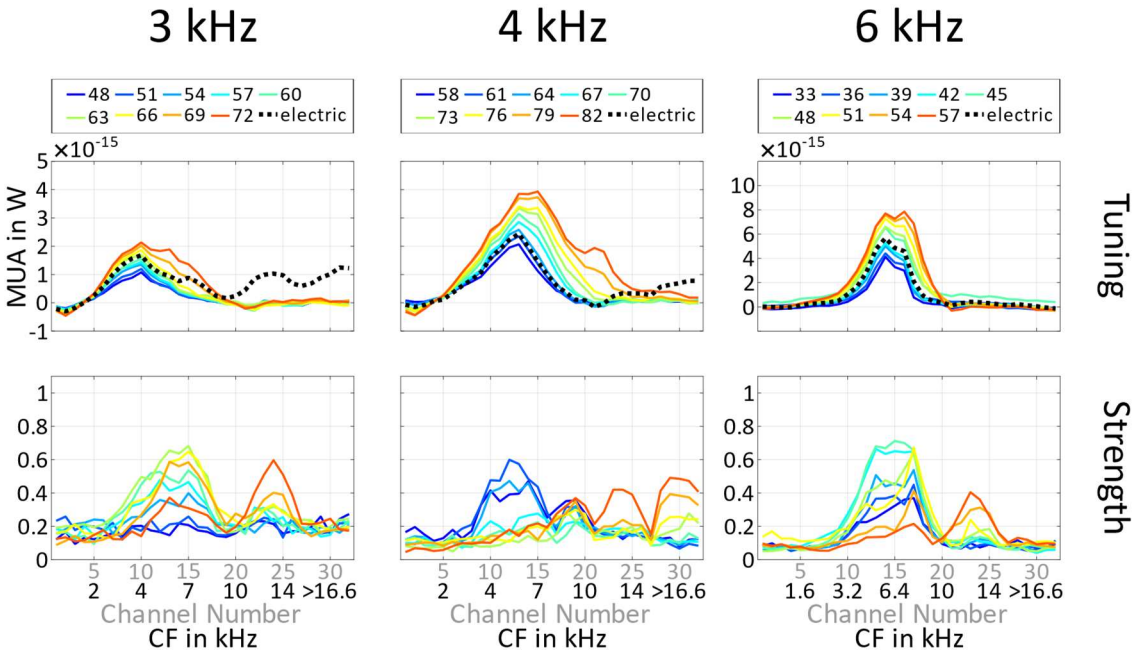

Figure B6.16 Spatial tuning curves of acoustic and electric stimuli and the corresponding beating strength curves (355B27 – 3 and 4 kHz at -25 dB re. 10 mA_{pp}, 354B17 – 6 kHz at -30 dB re. 10 mA_{pp}).

The evolution of maximum electrophonic and direct-electric beat strength with acoustic stimulation level is shown in Figure B6.17. Note that, in contrast to the electrophonic beat strength that shows a clear peak at all applied stimulation frequencies, the direct-electric beat strength does not reach an optimum point.

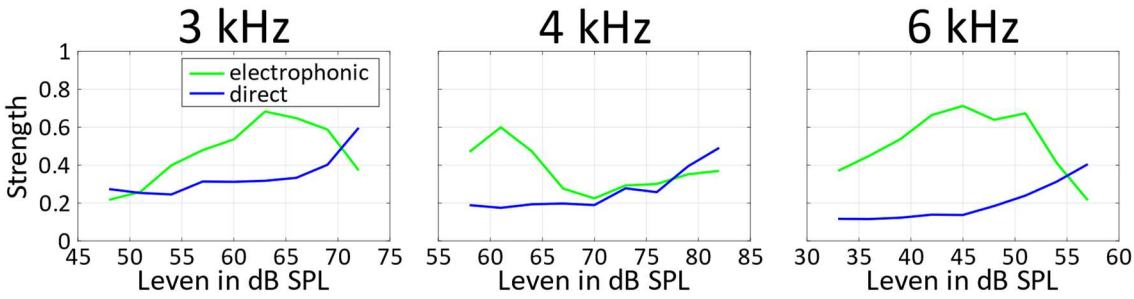

Figure B6.17 Maximum beating strength of at the electrophonic (green) and direct-electric (blue) places as a function of acoustic stimulation level. Stimuli were equivalent to the ones used in Figure B6.16. electrophonic beat strength is extracted from the responses at channels 1 to 20 and direct-electric beat strength is extracted from the responses at channels 21 to 32.

B6.3.3.2 Beating envelope at the electrophonic and the direct excitation places

Beating envelopes at the electrophonic place and the direct electric place are shown in Figure B6.18. To aid the observation of differences between the electrophonic and direct beat, the theoretical beat envelopes, that are calculated as described earlier in

B6.3.2.1.2., are also shown. In all cases, direct beat envelopes were extracted as the average of the response at channel 23 and the two neighbouring channels.

Electrophonic beat envelopes are similar to the ones observed in B6.3.2.1.2 and approximately follow the shape of the theoretical beat envelope. Envelopes corresponding to the strongest electrophonic beat at 3 and 4 kHz show saturation. In the 3 kHz case the saturation of the beat envelope is caused by reaching saturation in the neural responses. However, in the 4 kHz case, the beating envelope saturates well below neural saturation, that may be interesting for the interpretation of the beat, but the reason is unclear.

Compared to the electrophonic beat envelopes, direct beat envelopes show a different pattern. The notch, characteristic to the electrophonic beat, is not present in the envelopes of the direct beating patterns, that are rather sinusoidal. As can be seen in the example given in Figure B6.2, the beat envelope is more sinusoid-like if the input stimuli are not equal in amplitude. Thus, most likely the acoustic component related signal wasn't strong enough to cancel out the signal originating from the electric stimulus.

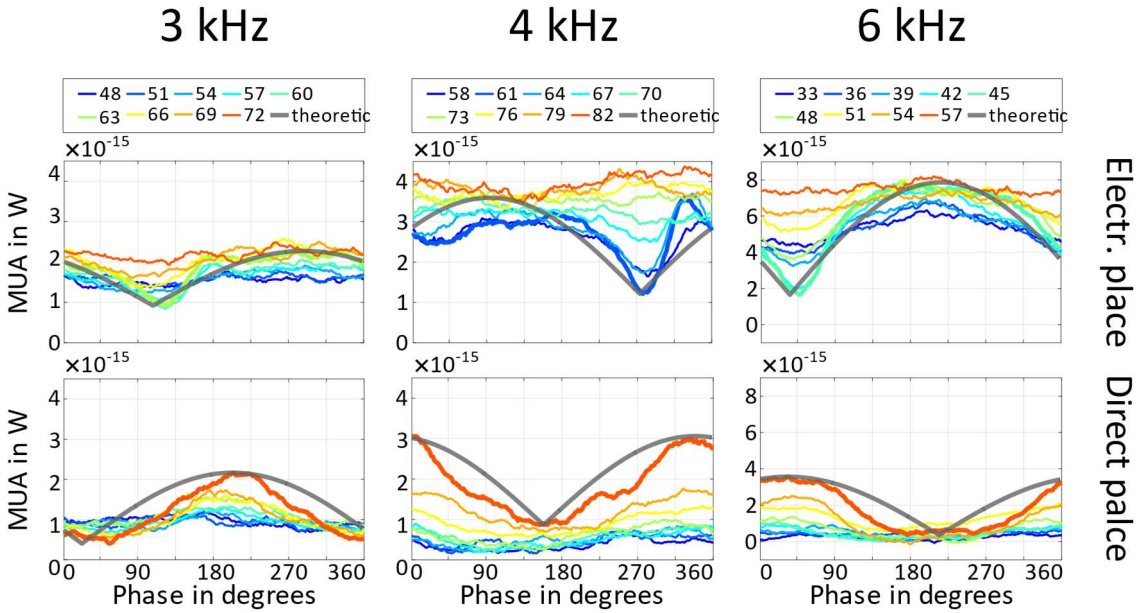

Figure B6.18 Beating envelopes at the electrophonic and direct electric excitation place (355B25 – 3 and 4 kHz at -25 dB re. 10 mA_{pp}, 354B17 – 6 kHz at -30 dB re. 10 mA_{pp}). First row displays beating envelopes at the electrophonic place. Second row displays beating envelopes at the direct electric place (data extracted at channel 22-24). Figures are to be read similarly to Figure B6.11.

In the case of the 6 kHz condition, due to the lack of direct response, the direct beat pattern shows enhancement only. Neural response only appears as the theoretical beat approaches its peak, indicating that the combined input signal was strong enough to cross neural threshold only at the beating peaks.

B6.3.3.3 Possible mechanisms evoking the direct beat

The distinct lack of a beat between the electrophonic place and the direct electrical place indicates that the direct electrical beat is not generated by the interaction of two travelling wave along the basilar membrane. Carrier resolution of the interacting signals is required to generate a beat. Thus, also an interaction via neural activation can be ruled out because the inner hair cells do not phase-lock to the high frequencies used in these experiments. It is however possible that the beat is generated by a micro-mechanical interaction within the organ of Corti. In the early 90s', Mammano and Ashmore demonstrated that in response to electrical stimulation, outer hair cell motility produces a reticular lamina (RL) displacement that is 5-10 times larger than the displacement of the basilar membrane [Mammano & Ashmore, 1993]. Due to the displacement of the RL the subtectorial space undergoes distortion that results in fluid movement capable of deflecting the inner hair cell stereocilia as modelled by Nowotny and Gummer [Nowotny & Gummer, 2006] and illustrated in Figure B6.19. This mechanism may be superposed by the shear motion caused by the tail of the acoustic travelling wave and generated the direct beating patterns. Apparently, the latter was still too small to fully cancel the stereocilia deflection due to the electrically evoked electromotility.

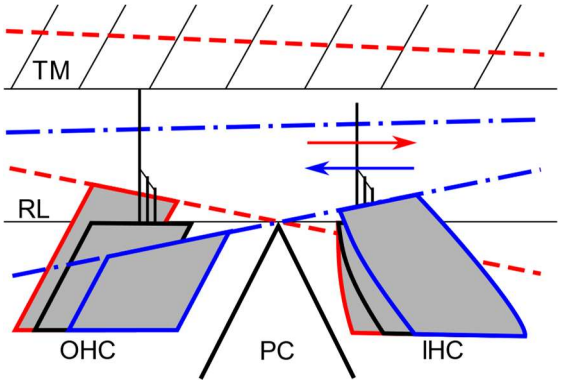

Figure B6.19 Distortion of the sub-tectorial space due to OHC electromotility results in IHC activation. Figure adapted from [Nowotny & Gummer, 2006]*. Blue lines indicate the condition with contracted outer hair cells and red lines indicate the condition with elongated outer hair cells. TM – tectorial membrane, RL – reticular lamina, OHC – outer hair cell, PC – pillar cells, IHC – inner hair cell*

Another possible explanation of the direct beat is an electrical interference. Acoustically evoked cochlear microphonic (CM) phase-locks across the entire hearing frequency range. Additionally, CM is argued to be the strongest at the base of the cochlea, i.e. at the current injection site, due to the in-phase displacement of the basilar membrane across a wide basal region, and in turn the synchronous membrane potential change of a large population of OHCs. These acoustically evoked electrical potentials superpose those generated by the current injection. It is possible that, at high acoustic levels, the CM become comparable to the potentials evoked by the current injection to have an impact on the net potential and cause the amplitude modulation by beating. Panel A of

Figure B6.20 illustrates an electric sinusoid (blue signal) that is just below threshold level (indicated by a red horizontal line) and the CM (green signal). Panel B shows that the threshold is exceeded by the peaks in the beat of the electric signal with the CM. Note that the lack of complete cancellation in the direct-beat also points towards an electrical interference caused by the CM. The CM response saturates (sigmoidal MET function, see Figure 1.4 in the main Introduction) and an acoustic tone has not been shown to be able to generate a CM strong enough to evoke an electrically induced AN response along the cochlea.

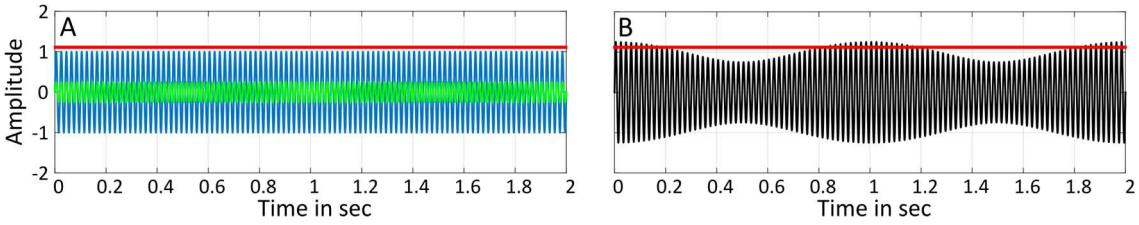

Figure B6.20 Interference of Cochlear Microphonic (CM) with the electric field of the CI. In panel A – Electric stimulation signal (blue) and cochlear microphonic signal (green) remain below the threshold of neural excitation (red). B – The combined electrical potential of current injection and tone-evoked CM exceeds periodically the neural excitation threshold.

One may test the proposed hypothesises by the application of DNQX, a pharmacological blocker that specifically targets IHC synapses. The presence of direct beating pattern after DNQX application would discard the possibility of our first hypothesis about sub-tectorial space distortion contributing to the beat since it requires the participation of IHCs. On the other hand, the CM related direct beat depends only on the presence of the OHCs, thus DNQX should not eliminate the direct beat if the second hypothesis stands. Unfortunately, the time frame of the current project did not allow for this test, so it remains to be an excellent opportunity for future research endeavouring in understanding the physiological mechanisms underlying the direct beat.

B6.4 Beating Response to Combined Electric Square Waves and Acoustic Tones

If an acousto-electric beat is present in an EAS user, it may be perceived as loudness modulation and could therefore serve for testing the existence of electrophonic response and its interaction with the acoustic stimulation. However, unlike analog devices in the past, contemporary cochlear implants are not designed to generate sinusoidal electrical waveforms anymore. To obtain a clearer view on the feasibility of evoking acousto-electric beats with modern commercial devices, beating with pulsatile electric waveforms

must be investigated. In this section, after presenting spatial activation patterns in response to electric pulse trains and square waves, beating patterns evoked by an electric square wave and acoustic pure tones will be shown.

B6.4.1 Spatial activation pattern of electric pulse trains

We have shown that electrophonic response to tonal electric stimulation produce a spatial activation pattern equivalent to an acoustic tone of the same frequency. McAnally and Clark have suggested that the spectral components of electric pulsatile stimuli also travel down to their respective characteristic places [McAnally & Clark, 1994]. With a sufficient resolution in the IC recordings, individual spectral components of a pulse train may thus appear as spatially separate peaks in the activation patterns.

In a first experiment, electric stimulation was delivered in the form of pulse trains consisting of charge balanced, biphasic pulses with 80 µs long phases. Electric stimulation level was varied from -50 to -25 dB re. 10 mA_{pp} in 5 dB steps. To obtain distinct peaks in the IC recordings related to the harmonics of the stimulation, the rate of the pulse trains was set to 1.5, 3 or 6 kHz and contained 9, 18 and 36 pulses, respectively.

The obtained spatial activation patterns are shown in Figure B6.21 along with the spectrum of the stimulus waveforms. The spectrum of a pulse train consists of its fundamental frequency and its harmonics. The magnitude of the harmonics displays a complex pattern with the strongest components found around the frequency corresponding to the length of the biphasic pulse, i.e. 1/(160 µs) = 6250 Hz.

The response to the 1.5 kHz rate pulse train displays a wide excitation pattern with a peak around 9 kHz. Due to the close spacing of the spectral components, separate peaks are not visible in the response pattern. Electrophonic response threshold decreases with distance from the stimulation site, where the lowest threshold is observed (see chapter B3). Thus, the 9 kHz peak in this example indicates the proximal location of the direct electric stimulation.

The response to the 3 kHz rate pulse train shows the resolved harmonics at the 3, 6 and 9 kHz characteristic places. The threshold of an individual peak is determined by both, the energy in the corresponding spectral component and its distance from the stimulation site. This characteristic explains that even though the energy of the 3 kHz component is approximately the same as the energy of the 6 kHz component, the response threshold of the latter one is lower due to the shorter distance between its characteristic place and the stimulation site. Similarly, even if the 9 kHz component carries less energy than the

6 kHz component, the corresponding response thresholds are similar because the 9 kHz characteristic place is closer to the electrophonic generation site.

The response to the 6 kHz rate pulse train show only one peak corresponding to the fundamental frequency at the 6 kHz characteristic place. The response to the 18 kHz spectral component is missing from the response pattern as the corresponding characteristic place is basal to the stimulation site. Note that 12 kHz harmonic component is not visible neither in the response pattern, nor in the stimulus spectrum because the combination of the 6 kHz rate and the 160 µs pulse width results in almost a square wave, the spectrum of which contains only the odd harmonics.

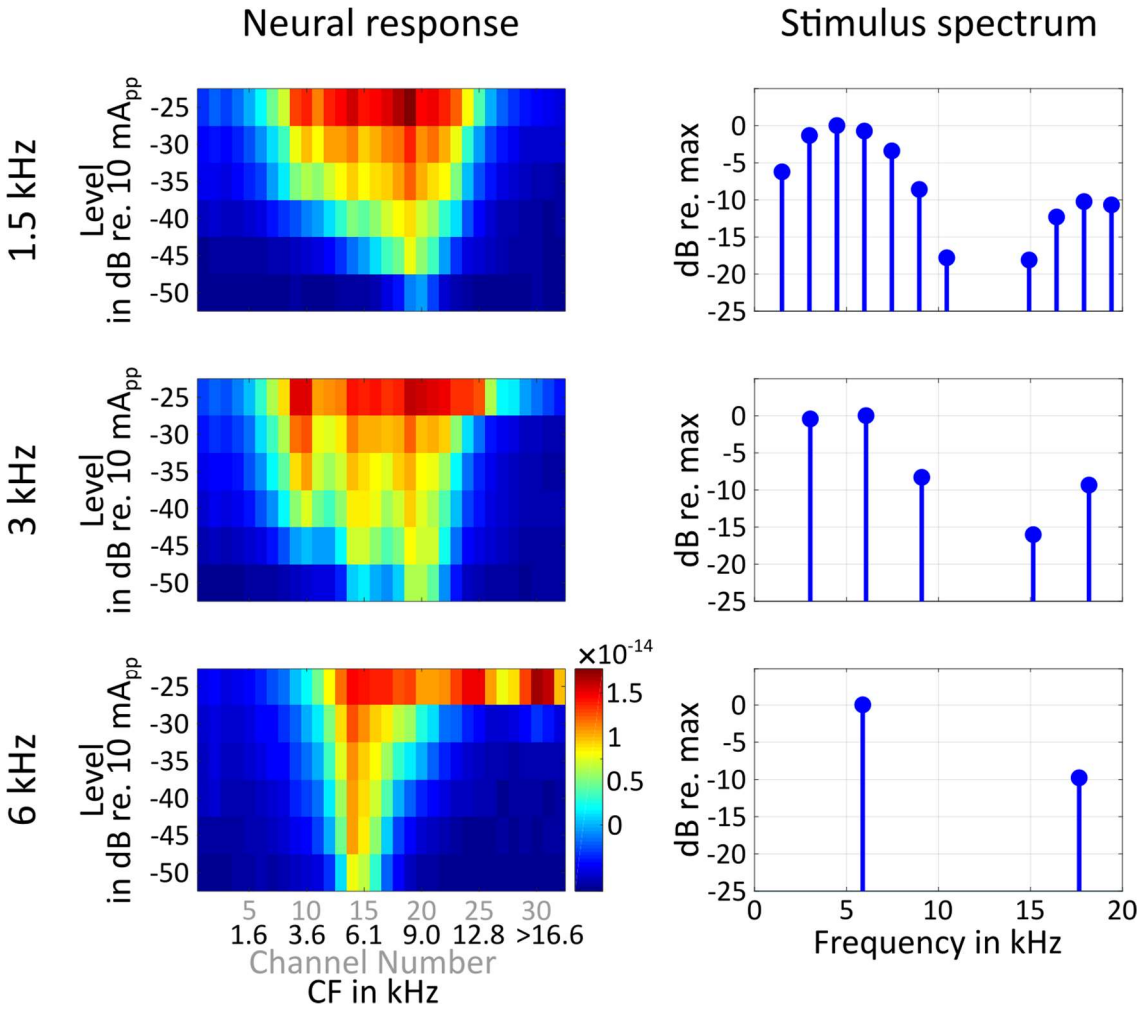

Figure B6.21 Spatial activation pattern in response to pulse trains with various rates and the corresponding spectrum of the waveforms (328B9).

B6.4.2 Spatial activation pattern of square waves

The spectrum of square waves is composed of the fundamental frequency of the wave and its odd harmonics. This attribute of the square wave stimulus makes it an optimal candidate for producing well separated peaks in the spatial activation patterns that can facilitate the observation of beating patterns later.

In the current experiment 6 ms long electric square waves of 2.5 and 5 kHz were used. Electric stimulation level was varied from -50 to -25 dB re. 10 mA_{pp} in 5 dB steps.

The spatial activation patterns in response to electric square waves are shown in Figure B6.22 along with the spectrum of the stimulus waveforms. The harmonic components are apparent in the response patterns as separate peaks. The response to the 2.5 kHz square wave shows nicely separated peaks at locations characterized by 2.5, 7.5 and 12.5 kHz. The response to the 5 kHz square wave shows the harmonic peaks at the 5 and 15 kHz places. The thresholds of the harmonic peaks are to be interpreted similarly as in section B6.4.1, i.e. the threshold decreases with shorter distance between the characteristic place and the stimulation site if the characteristic place is apical to the stimulation site.

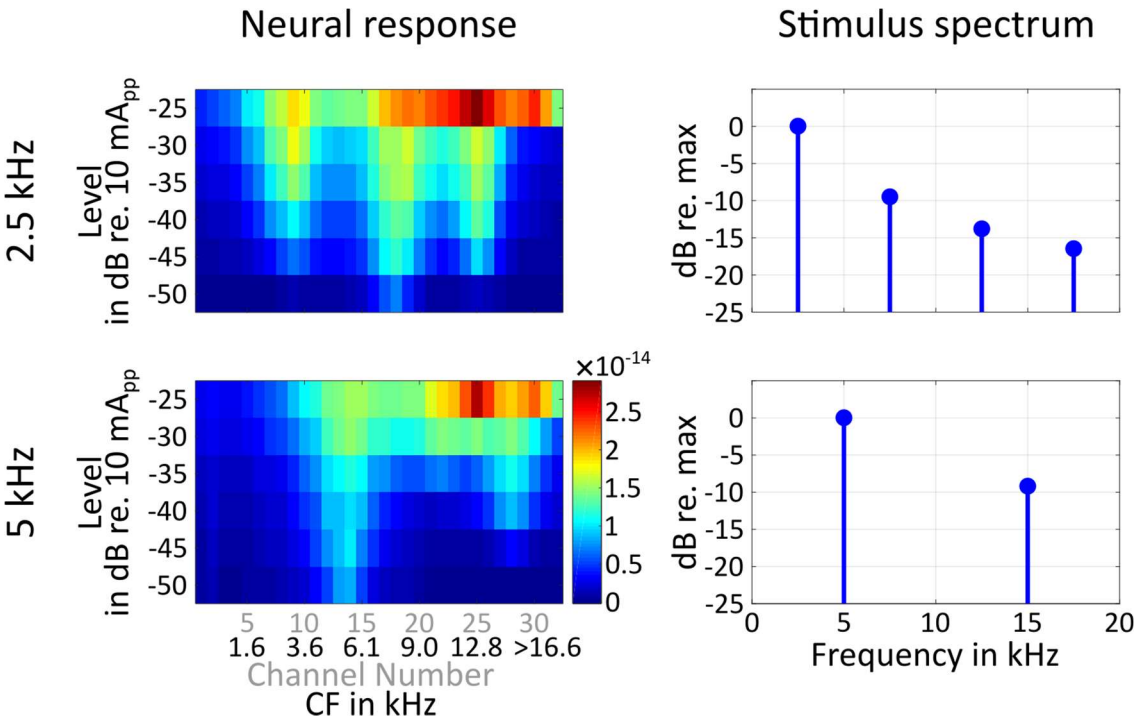

Figure B6.22 Spatial activation patterns in response to square wave stimuli and the corresponding spectrum of the waveforms (328B10, 328B11).

B6.4.3 Beating pattern examples with electric square waves

As the previous section demonstrated, the harmonic content of an electric square wave can be resolved by the cochlea and the corresponding electrophonic response appears in the form of distinct peaks in the spatial activation pattern. Here we will show that individual electrophonic components can beat with acoustic tones at the corresponding frequencies.

Electric stimulation was a 1.2 second, 2 kHz square wave at -35 dB re. 10 mA_{pp}. The used acoustic stimuli were identical to the ones paired with the -35 dB re. 10 mA_{pp} in section B6.3.2.1. Note that acoustic frequencies ([2 6 10 14] kHz + 5 Hz) are aligned with the harmonic content of the 2 kHz square wave.

Example periodograms in response to stimuli resulting in clear beating patterns are shown in Figure B6.23. Similarly to Figure B6.8, the first two rows show the electric and acoustic control stimuli and the last row shows the beating patterns in response to the combined stimulation. The pattern in response to the electric control stimulus is replotted in every column for easier comparison with the acoustic and beating responses.

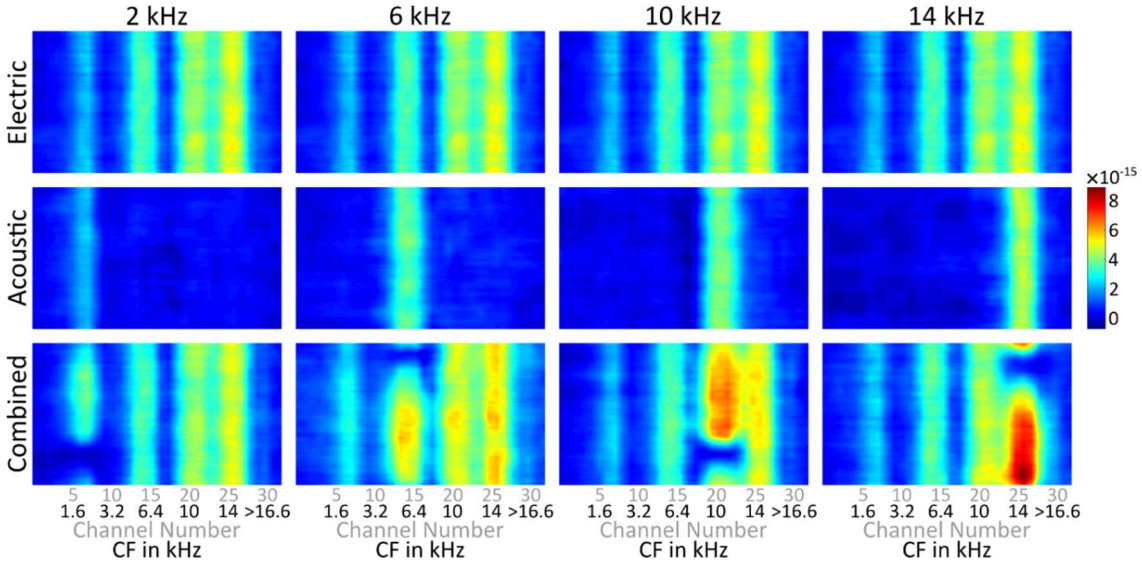

Figure B6.23 Same as Figure B6.8, but with electric square wave stimulation of 2 kHz at -35 dB re. 10mA_{pp} and acoustic tone levels of 45, 32, 31 and 18 dB SPL for the 2005, 6005, 10005 and 14005 Hz respectively (354B16).

In the electric control plots the harmonic content of the stimulus appears as vertical stripes at the relevant characteristic places i.e. 2, 6, 10 and 14 kHz. The acoustic control responses demonstrate that the acoustic response was nicely aligned with the harmonics in the electric responses and the acoustic response strength closely matched the response strength of the electric harmonic selected for beating. In the periodograms with the combined response, a beating pattern appeared for every stimuli pairs. The beating pattern was always located and confined around the characteristic place of the acoustic response (and the corresponding response to the harmonic component of the electric stimulus). The phase of the notch was leading the notch in the comparable periodograms in Figure B6.8 by approximately 90˚. This phase difference can be attributed to the phase

difference between the sinusoidal and the harmonic components of the electric square wave stimuli[10].

The tuning curves and the beating strength results are shown in Figure B6.24. Beating at the characteristic place of the harmonic electrophonic responses was tuned to the acoustic level eliciting equal response strength thus observations on beating strength are similar to the ones made in section B6.3.1.1 for the sinusoidal electrophonic beat.

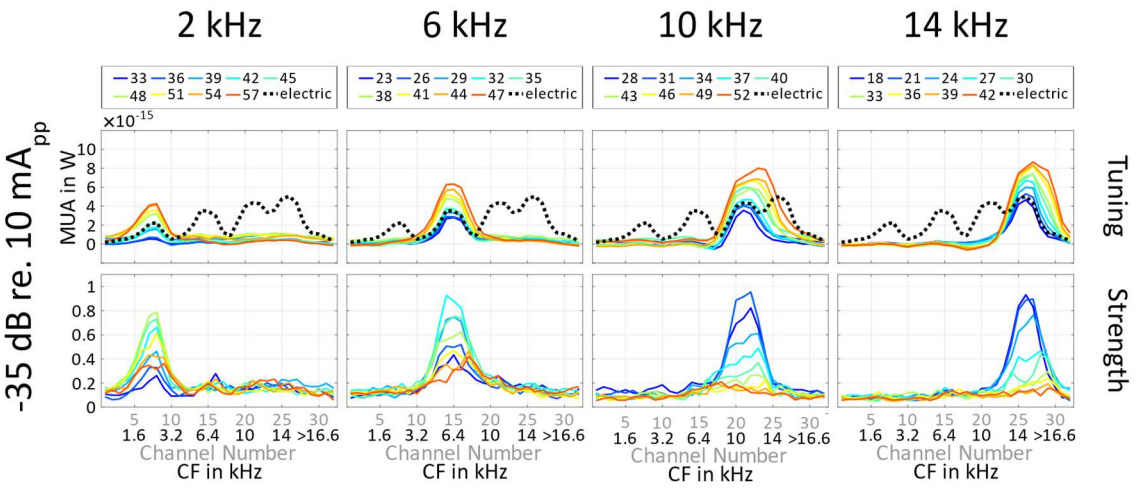

Figure B6.24 Tuning curves of input stimuli and resulting beating strengths for beating with electric square waves.

B6.5 On the applicability of beats to test acousto-electric interactions in CI users

We have seen that electrophonic response can beat with an acoustic tone in normal hearing guinea pigs. The typical audiogram of an EAS patient shows a ski-slope type hearing loss with preserved hearing only in the low frequency range. However, some patients have still relatively good thresholds [Koka & Litvak, 2017] and might be able to hear electrophonics that is completely unrelated to the perception that is intended to be restored by the electric stimulation. Furthermore, in EAS users, electrophonic response may also distort the acoustic signal stimulating the residual hearing range. To test the presence of electrophonic response in patients, acousto-electric beat at the electrophonic place may be used.

[10] Tonal stimuli are generated based on cosine functions that is the equivalent of a 90˚ phase shifted sinusoid. On the other hand, the harmonic components of the square wave are sinusoids with a phase of 0˚.

We have also demonstrated that an electrophonic beat requires an electrophonic response that is equivalent to the acoustically evoked response. This means, that to elicit an audible electrophonic beat, an electrophonic response that is strong enough to match the response to a high level the acoustic input is needed. As it was shown in chapter B3, strong electrophonic response also requires high electric stimulation levels. It may happen, that electric levels required for the electrophonic beat in EAS patients would exceed the most comfortable levels[11]. Additional obstacle arises due to the pulsatile stimulation implemented in modern commercial devices. A pulse train carries relatively little energy in the low frequency range (see Figure B6.21). Although the low frequency content of the stimulus could be enhanced by the application of long pulses, it would be of little use since extending the electric stimulation while keeping its amplitude constant would result in an increase of the delivered charge, thus would also increase the direct response strength resulting in uncomfortable electric stimulation for the patient.

Despite all the challenges of transferring the idea of electrophonic beat to human tests, the chance of its applicability still remains. We have demonstrated in chapter B3, that electrophonic response can have a stunning threshold advantage of 36 dB over the direct response. This electrophonic advantage was also shown to be inversely proportional to the distance between the stimulation place and the characteristic place of the stimulus frequency. Implantation in the guinea pig is restricted to the first half cochlear turn. However, by using the apical most electrodes of a human CI, which is usually positioned near the characteristic place of 1 kHz, the direct to electrophonic response distance can be greatly reduced, thus electric stimulus for evoking audible electrophonic beats may also be reduced to acceptable levels. This possibility calls for further research about the dependency of electrophonic response on the site of electric stimulation. Such investigation could be conducted both by electrophysiological animal experiments with a different cochlear approach that allows stimulation at more apical stimulation sites, or by computer simulation studies. Upon a confirmed feasibility of electrophonic beat at acceptable stimulation levels in EAS patients, a quick and easy to perform test could enrich the toolbox of the CI audiologists. The test could not only detect an electrophonic response, but, by maximizing the beat, an equivalent sound pressure level could be obtained to quantify the electrophonic response. Furthermore, as the electrophonic response requires residual hearing, testing with the electrophonic beat would could also implicitly serve for assessing the remaining hearing of the CI recipient.

The presented set of experimental results also shed light on the somewhat unexpected acousto-electric interaction at the electric stimulation site. This interaction type potentially

[11] Maximum current level that results in stimulation without causing discomfort for the CI patient.

bears high importance for EAS patients, who utilize low frequency sounds with high amplifications. Indeed, psychophysical studies showed the masking of electric probes by acoustic tonal stimulation across a wide frequency range [Lin et al., 2011; Krüger et al., 2017; Imsiecke et al., 2018]. The result of these studies is often argued to originate from neural interactions beyond the IC in the auditory pathway. It can be ruled out however that such interactions underlied the beating response observed in our study because they would require phase-locking to the stimuli, and our stimulus frequencies were deliberately selected to exceed the limit of neural phase locking. On the other hand, our results indicate that their findings might well have a cochlear origin, and a testing for a perceivable beating might be a suitable test to find this out.

In our experiments, high level acoustic stimulus could suppress or enhance the direct electric response depending on the phase relationship of the electric and acoustic stimuli. If our hypothesis, based on the interaction of cochlear microphonic and the electric stimulus stands, then the relevance of our finding may become relevant for most CI users as such interaction does not require remaining inner hair cells. These results gain even more weight in the light that, electrocochleography, a test that is becoming a routine during atraumatic CI surgery [Gibson, 2017; Dalbert et al., 2018; Page et al., 2018], shows cochlear microphonic response in CI recipients with severe or even profound hearing loss [Choudhury et al., 2012; Campbell et al., 2014; Fitzpatrick et al., 2014; Adunka et al., 2016; Riggs et al., 2017; Giardina et al., 2018; Fontenot et al., 2019].

To test the presence of cochlear microphonic related acousto-electric interaction at the direct stimulation place in human subjects, a procedure similar to the one presented by Zwicker [Zwicker, 1976] could be used. The proposed stimulus schematic is depicted in Figure B6.25. A low frequency acoustic tone could be presented simultaneously with a constant amplitude electric pulse train having a stimulation rate that is slightly different from the frequency of the acoustic tone so that its phase-position slowly changes. If acousto-electric interaction is present at the electric stimulation site, then the patient should perceive the electric stimulation as it was amplitude modulated with the period corresponding to the frequency difference. This principle is analogous to a beat.

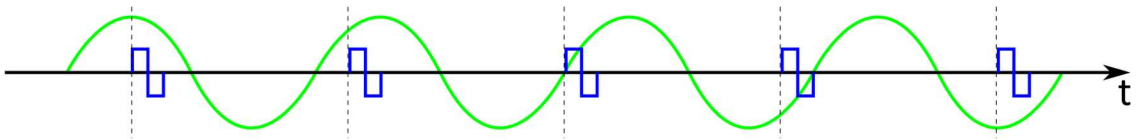

Figure B6.25 Proposal for stimulation paradigm to test for acousto-electric interaction at the direct place in human subjects. Green sinusoid curve illustrates the acoustic tone stimulus and blue pulses represent the electrical stimulus. If the electric stimulation rate is slightly different (in this example faster) from acoustic stimulation frequency, the subject may perceive a loudness modulation of the electrically generated sound because the phase-position of the electrical pulse slowly shifts along the sinusoidal acoustic stimulus.

B7 Summary of findings on acousto-electric interactions due to electromotility

Acousto-electric interactions were investigated using a normal hearing animal model. The main goal was to obtain a better understanding of the OHC originated electrophonic response and find methodologies that could serve as a basis for clinical applications for detecting the electrophonic response in patients.

Chapter B3 discussed experiments that were conducted in order to characterize the neural responses of a normal hearing ear to sinusoidal electric stimulation. Specifically, the electrophonic and direct electric responses were characterized and compared to acoustically evoked neural responses.

The electric stimulation was shown to evoke responses both at the site of excitation, i.e. the direct electric response, and at the characteristic place of the stimulation frequency, i.e. the electrophonic response. For the first time, the threshold of the direct electric response to sinusoidal stimulation was shown to increase with 3 dB/octave, while the threshold of the electrophonic response decreases with 6 dB/octave. The advantage of electrophonic threshold over the direct electric threshold was demonstrated to be able to increase up to 36 dB as the characteristic place of the stimulation frequency approaches the stimulation site. Additionally, the electrically evoked travelling wave origin of the electrophonic response was indicated by the resemblance of the electrophonic tuning curve to the acoustic tuning curve.

The likely presence of the electrophonic response in EAS patients was discussed on the one hand as a potential source of interference with the low-frequency acoustic hearing. On the other hand, electrophonic response was also argued to be possibility used for evoking acoustic like stimulation in EAS patients. These findings emphasized the necessity of determining the presence of the electrophonic response in patients. The chapter concluded by pointing out the similarity of the electrophonic response properties to that of the EEOAEs such as a stimulation site dependent band-pass characteristic and a linear growth function.

Chapter B4 and B5 set out to establish a link between the electrophonic response and the EEOAEs based on their putative common source i.e. OHC electromotility. Chapter B4 applied acoustic and electric biasing techniques to modify the operating point of OHC

electromotility and chapter B5 applied a pharmacological methodology to change the OHCs' operating state. The observation of a simultaneous change in the electrophonic responses and EEOAEs due to the modification of OHCs' operating state could confirm their common source. An established link could promote the usage of EEOAEs as a non-invasive diagnostic tool to detect the electrophonic response in EAS patients.

Acoustic biasing experiments showed no change in the electrophonic response and only a modest enhancement of EEOAEs. The small observed effects were argued to be due to the electric stimulation of the basal cochlear turn where OHC operating point is located symmetrically on the mechano-electric transfer function. Electric biasing effects were small, likely due to the current delivery into the scala tympani where the current may easily be drained away by the surrounding tissue. Biasing with positive DC current resulted in a monotonically decreasing trend in both the electrophonic responses and the EEOAEs that may be indicative of their common source, however, this effect was statistically non-conclusive. In summary, the hypothesis of a common source cannot be rejected based on the results of the biasing experiments.

Pharmacological blocking of OHC electromotility resulted in the suppression of both the electrophonic responses and the EEOAEs. However, the time course of the response suppressions was different, that is indicative of differences in the generation sites. The generation site of the electrophonic response is likely governed by the electrical spread and the mechanical impedance gradient of the basilar membrane, unlike the generation site of the EEOAE that appears to be at the site of electrical stimulation. A future research that applies finite-element modelling could be conducted to further investigate the differences in the generation sites.

Chapter B6 aimed at showing acousto-electric beats between the acoustic and electrophonic responses based on the knowledge that, both responses are the result of a mechanical travelling wave, thus, carefully selected stimulus conditions may evoke a beating phenomenon. Such an electrophonic beat may be perceived by EAS patients and may be used as a diagnostic tool for detecting the electrophonic response.

Beating of the electrophonic response with an acoustic tone was demonstrated in normal hearing guinea pigs using sinusoidal and also square wave electric stimulation. Additionally, the electrophonic beat was also demonstrated to require an equally strong electrophonic and acoustic response. It was pointed out that, in a typical EAS patient, an electrophonic response that is strong enough to match the acoustic response may require an electric stimulation that evokes an uncomfortable direct electric response. However, the stimulation site dependent electrophonic advantage may be in favour of the electrophonic beat during human testing due to the short distance between the most

apical CI electrode and the electrophonic place. These results are calling for further research to investigate the dependence of the electrophonic response on the stimulation site e.g. by animal studies using electrical stimulation in more apical cochlear turns or by computational modelling studies. An electrophonic beating test, that is feasible in humans, may allow for the detection and quantification of the electrophonic response in EAS patients.

Besides the electrophonic beat, an acousto-electric interaction at the direct electric place was also observed during experimentation. Based on the phase relationship of the electric and acoustic stimuli, the acoustic stimulus could enhance or suppress the direct electric response. This interaction was hypothesized to have a cochlear origin. The mechanism to explain the phenomenon was proposed to be either a pure mechanical interaction between the tail of the acoustic travelling wave and the OHC electromotility induced periodic micromechanical distortions at the stimulation site, or an electrical interaction between the cochlear microphonic and the electric stimulus. To test these hypothesises, a research method is proposed that applies DNQX, a pharmacological agent that blocks the IHC synapse, that would only affect the interaction if it is of mechanical origin because interaction of the cochlear microphonics and the electrical stimulation does not involve IHCs. The clinical relevance of an interaction between the cochlear microphonics and the electrical stimulation may be of great interest as such an interaction does not require residual IHCs at the electrical stimulation site, thus may be present in CI patients with extensive hearing loss. The hypothesis of this electric interaction is also proposed to be tested by further research in human subjects with a stimulation paradigm that is analogous to a beat.

Appendix BA Generation of spatial activation patterns along topological brain areas

BA.1 Background

The activity of the brain to a sensory input stimulus is formed by the activity of the individual units of neurons. Single units are communicating among each other by minuscule voltage discharges, usually referred as spikes. Often it is of interest to understand the response activity of a population of neurons within a topologically arranged brain region. Monitoring the spatially distributed population response is commonly done with multi-channel neural recording electrodes.

In auditory research the spatial activity along the cochlear tonotopy is often of interest. Direct measurement of cochlear activity e.g. basilar membrane mechanics [Nuttall et al., 1991] and auditory nerve fibre response [Liberman, 1982; Palmer & Russell, 1986; Tillein et al., 2015] is currently only feasible at individual loci due to difficulties of accessing the cochlea without causing major damage in it, thus the response of the complete organ remains hidden. A generally preferred technique to indirectly monitor the cochlear activity is to record the population response along the tonotopic axis of the Inferior Colliculus [Snyder et al., 2004; George et al., 2014; Sato et al., 2016]. Of particular interest is, here the tone evoked response pattern, first termed by Snyder and colleagues as the spatial tuning curve (STC) [Snyder et al., 1990].

The analysis of multi-channel neural recordings is by no means effortless. Main obstacles arise from across channel differences. The following sections detail the recording principles, specifies the underlying issues and proposes techniques to equalise the channels using various data examples.

BA.1.1 Idea behind the developed technique

The problem of a multi-channel neural recording is illustrated in panel A of Figure BA.1 in a simplified two-dimensional view. The probe's shank is represented by a blue line with the red diamonds being the recording contacts on it. Black dots indicate individual neurons that are randomly distributed in the x-y plane. The electrical field around a neuron has a dipole characteristics that falls off by 12 dB ($1/r^2$) with doubling the distance from the neuron [Buzsáki et al., 2012]. Although, the directionality of the dipole field could

be modelled by varying the strength of the electric field, for simplicity the qualitative description of the problem is not considered here, and the neural electrical field is assumed to be spherical. Based on this assumption, the rings in panel A represent regions around recording contacts in which the attenuation of the detected voltage signal from neurons is roughly similar, lighter colour corresponds to weaker detected signal i.e. more attenuation.

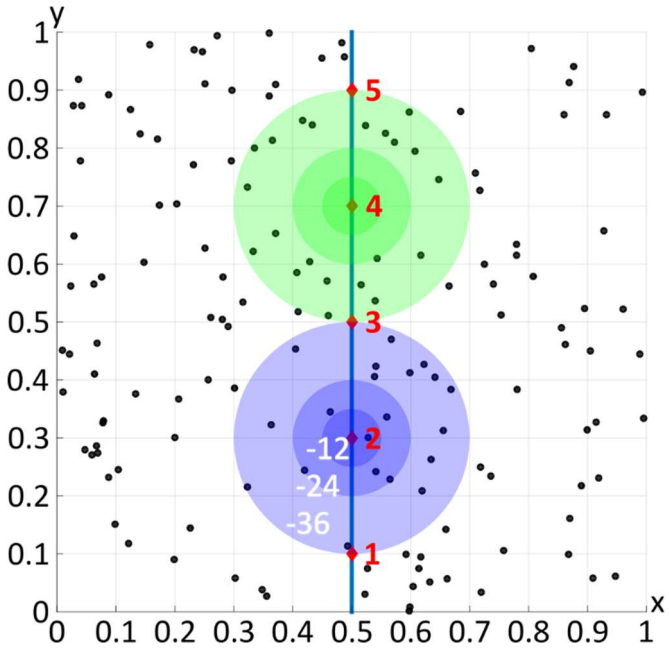

Figure BA.1 Two dimensional illustration of a neural recording. Electrodes on a shank are represented by red diamonds in an environment filled with randomly distributed neurons (black dots). The potential of neurons decreases with the increasing distance from a recording site as illustrated by the coloured rings around electrode 2 and 4.

There are two main approaches for quantifying the strength of the population response. The first method counts instances of neural spiking activity and usually referred to as spike-cutting or thresholding [Rey et al., 2015]. A highly simplified example of this method is shown in Figure BA.2. A threshold voltage value is defined (dashed horizontal line) and a spike is counted if the recorded signal crosses this value. The detected spikes (red markers) are then accumulated over several repeats of the stimulus and the mean response strength is quantified as the mean spike rate. The second method simply extracts the power in the signal (related to the area below the trace of the squared voltage signal, blue shadings in Figure BA.2). This method for neural activity quantification was first introduced by [Chung et al., 1987] and later termed as analog multi-unit activity (aMUA) by others [Kayser et al., 2007; Schnupp et al., 2015].

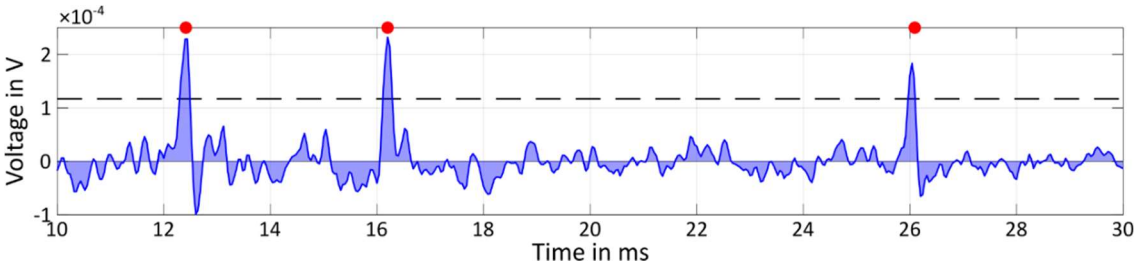

Figure BA.2 Methods for quantifying neural activity. The spike cutting method counts the events (red markers) when the signal (blue line) crosses a user defied threshold (dashed line). Analog multi-unit activity is related to the area below the squared signal (blue shading).

The two quantification methods are affected differently by the function of distance from the recording site. In the case of spike-cutting, the circles (outer edge of rings) in panel A of Figure BA.1 can represent different threshold settings. If the threshold at recording site 2 is set to be the closest -12 dB circle, the firing of only one neuron is captured. By decreasing the threshold level to -24 dB, 6 units are contributing to the measure. Naturally, to obtain a better estimate of the population response, it is preferred to capture the signal of many neurons. Unfortunately, the level of noise sets a limit for the lowest applicable threshold. A too low threshold would result in random voltage peaks being detected as spikes, thus eventually leading to false spike counts. To avoid the inclusion of false peaks, the threshold is usually set well above the noise level (3-5STD [Rey et al., 2015]). Using the aMUA approach, the increase of distance leads to a decreasing neural contribution until the signal of neurons from a certain distance onwards becomes negligible compared to the signal of the closer population.

Both techniques possess inherent drawbacks. The spike-cutting method counts the activity of only a few neurons near the recording electrode, and their number can vary largely across the electrode contacts e.g. 6 neurons within the -24 dB circle around electrode 2 as opposed to zero neurons within the -24 dB circle around electrode 4 in Figure BA.1. Furthermore, the constrained population of neurons, leads to the detection of only a few spikes during a recording trial. Due to the small number of detected spikes, the trial-by-trial variability of recordings can be high. To overcome this large variance, many repeats, resulting in an extended recording time, are required to obtain a representative average response. In case of the aMUA method, the activity is captured from a larger population size, thus the variance across trials is less and the recording time may be reduced. The problem with the aMUA method arises when the signal from a close neuron dominates the recording, thus the information about the population response is lost.

Recording from multiple channels imposes additional obstacles to the adequate representation of the population response. Differences among the channels should be accounted for to obtain a reliable result. Static, activity independent differences are

related to differences among the recording contacts, such as electrode impedance or background noise. Dynamic, activity related differences are caused by the irregularities in the neural distribution surrounding the recording sites. Consider the case when a stimulus activates all neurons in panel A of Figure BA.1 and neural activity is quantified either by aMUA or by spike cutting with a threshold at -24 dB. In an ideal situation all recording electrodes should show similar activity. However, comparing electrode 2 in the centre of blue rings to electrode 4 in the centre of green rings, it becomes obvious that the first electrode receives a larger input, regardless of being quantified as the number of spikes or the signal power, due to denser neural population in its vicinity.

To achieve a solution that is capable of genuinely representing the spatial activity of a neural population, the spike-cutting and aMUA methods may be united. The aMUA can serve as a basis for the devised method because it is inherently capturing population activity. Additionally, aMUA can be augmented by defining a limit, similar to the threshold used for spike-cutting, but instead of using this limit for counting events, it can be used for detecting the dominant neural activity that may later be eliminated. By applying this approach, the activity of close neurons will be excluded from the recording and only the activity of the distant population will contribute to the result. Furthermore, this combined method can also reduce the dynamic, activity dependent across channel differences, because the response dynamics is more homogeneous for the distant, larger population size than for the close, small groups of neurons.

Recording neural activity by multiple electrodes introduces a spatial smearing effect, that is illustrated in Figure BA.3. In panel A, the rings represent the decay of the electric field generated by a neuron at [0.44 0.61] and vertical dashed lines represent various positions of the recording shank. It is clearly seen that signal from the neuron is picked up by two electrodes when distance between the shank and the neuron is d_0. Panel B illustrates that a signal originating from a neuron distant to the recording electrode array is smeared over a larger section of the recording shank compared to the signal of a neuron that is near the recording contacts.

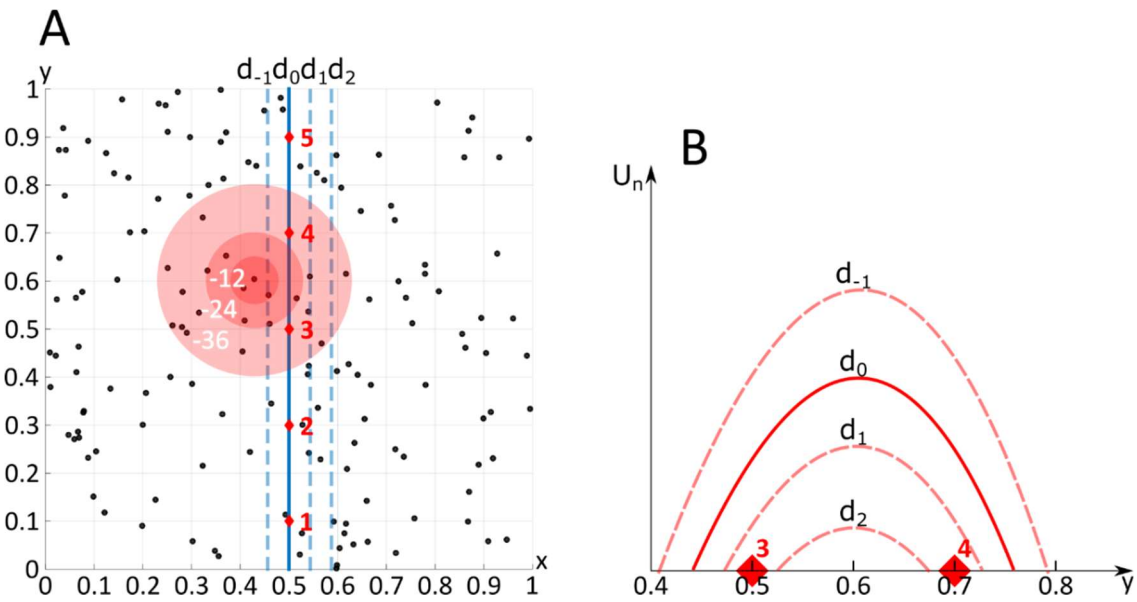

Figure BA.3 Illustration of spatial smearing. A - Electrical field of a neuron is illustrated as red rings; Vertical blue lines represent recording electrode shanks at various distances from the neuron at [0.44 0.61]. B – Sketch of explanatory spatial smearing profiles of neuron [0.44 0.61] in panel A for various neural to recording site distances; d is the distance of the recording shank from the neuron, U_n is the recorded voltage from the neuron

BA.2 Extraction of neural activity

The flow chart of the neural data processing steps is shown in Figure BA.4. The steps within the dashed rectangle are conducted on a channel-by-channel basis. Preceding the extraction of neural activity, the data is cleared of artefacts in a step that will be discussed in section BA.3. In the neural activity exclusion step, the clean, artefact free signal is first freed from dominant spiking activity originating from close neurons. This is followed by a spectral weighting step, that is responsible for calculating the power, i.e. aMUA, in the physiologically relevant spectral band. In the driven activity extraction step, the stimulus driven activity is obtained by removing the background activity form the recording.

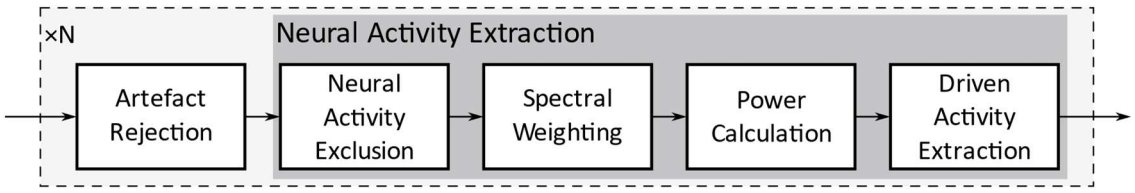

Figure BA.4 Flow chart of neural data processing. Processing is conducted for N recording channel independently.

BA.2.1 Selection of example data

To illustrate the processing steps, three example responses to acoustic pure tones were selected, each showing a distinct behaviour that was typically observed in the raw data. Spatial activation patterns of the examples (data extracted by the spectral weighting and

the power calculation step) are shown in Figure BA.5 and corresponding example raw recordings are shown in Figure BA.6. In the raw recording examples, signal parts exceeding 3 standard deviation of the background noise, i.e. the spiking activity, is distinguished by blue colour.

The response to a 9870 Hz tone shows a clear tuning curve. As expected, the neural activity was restricted to a few electrodes and gradually increased with stimulus level. The corresponding raw recording in panel A and B in Figure BA.6 show the activity at channel 23 in response to 70 and 35 dB SPL tones respectively. As expected, the response trace to the 35 dB SPL showed very little activity above the background level and continuous neural firing was present in response to the 70 dB SPL stimulus. In the rest of the chapter, this example will be referred as ‘clear’ pattern.

The response to the 16600 Hz tone resulted in a spatial activation pattern with two stripes at electrode 26 and 30 due to dominant neural activity. The corresponding raw recordings in panel C and D in Figure BA.6 show the activity at channel 26 in response to 70 and 30 dB SPL tones respectively. In response to the 70 dB SPL stimulus, spikes were apparent with magnitudes that greatly exceeded the background activity, thus dominated the recording. This example will later be referred as ‘dominant neuron’ spatial activation pattern.

The example response to the 2468 Hz tone shows a tuning curve with high background activity, especially at channel 17, caused by constant spiking. As the corresponding raw recording examples in panel E and F in Figure BA.6 illustrate, strong, stimulus level independent spiking activity was present at channel 17. This example will later be referred as spatial activation pattern with ‘high background activity’.

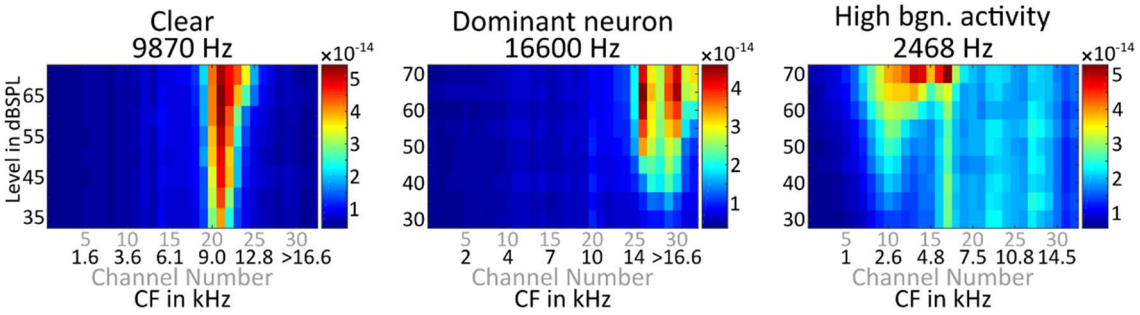

Figure BA.5 Spatial activation patterns, showing typical spiking behaviours (328B1, 355B12, 362B1).

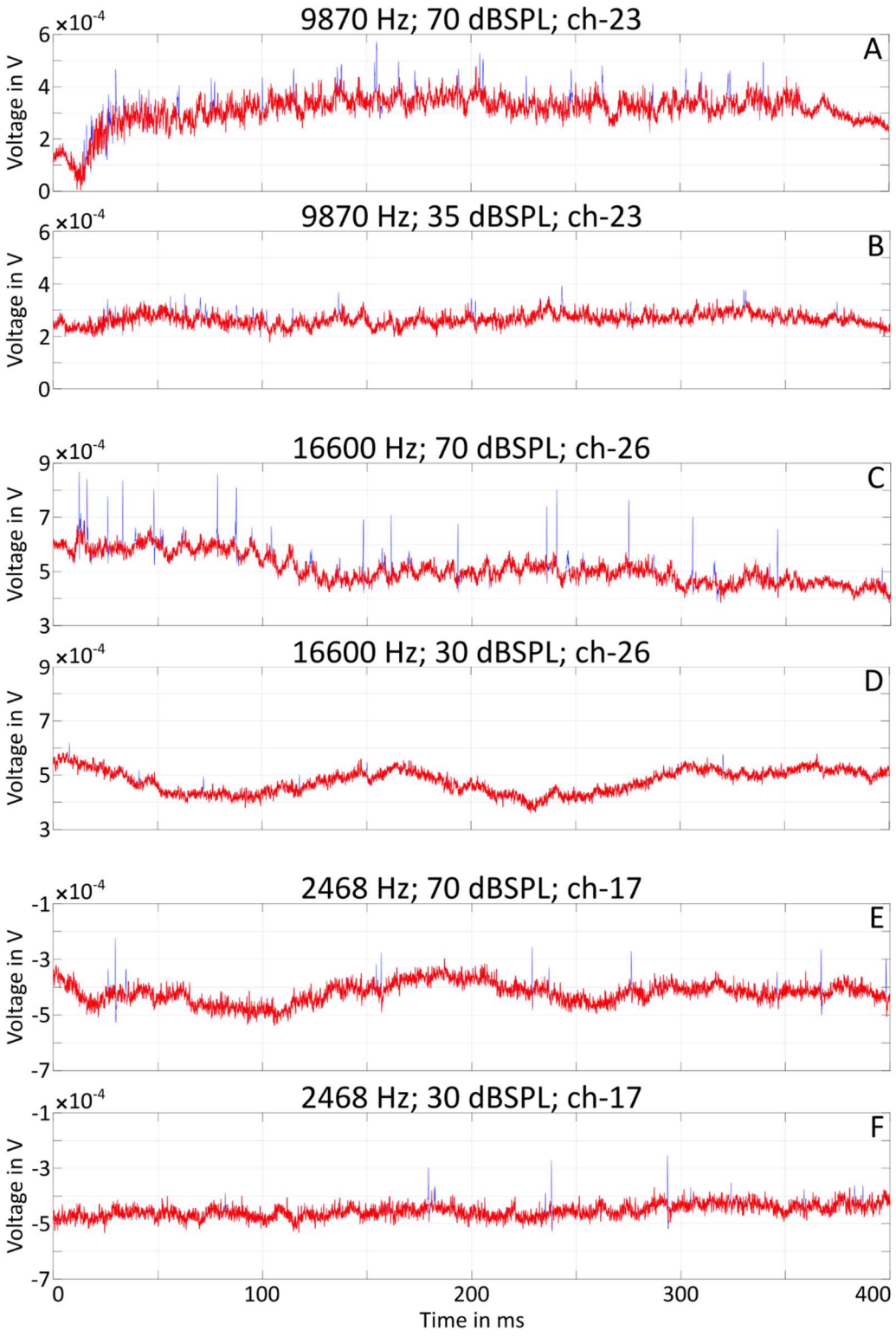

Figure BA.6 Spatial activation patterns, showing typical spiking behaviours (328B1, 355B12, 362B1). The panels are organized in pairs that show example recording traces during stimulation with low and high levels at a selected frequency and recording channel. Spiking activity is emphasized by blue colour. Panel A and B show an example of an expected spiking behaviour. Panel B shows little response to the 35 dB SPL stimulus and panel A shows increased and sustained spiking activity during stimulation by the 70 dB SPL tone. Panel C and D show an example of a dominating neural activity. Panel D show almost no spiking in response to the 30 dB SPL stimulus. Panel C displays large spikes, clearly sticking out of the background noise in response to the 70 dB SPL tone. Panel E and F shows an example of a neuron that was spiking even if the stimulus frequency was different from the neuron's characteristic frequency.

BA.2.2 Power calculation

To obtain aMUA, the power of the recorded signal was determined. The calculation was executed in the frequency domain to avoid an additional step of IFFT after spectrally shaping the signal. The used equation was as follows:

$$P = \frac{1}{F_s N^2} \sum |X|^2$$

Where P is the power of the signal, F_s is the sampling frequency, N is the number of samples in the signal (or the number of spectral components in the spectrum) and X is the Fourier transform of the signal.

BA.2.3 Spectral weighting

To emphasize the neural activity related part of the recoded signal's spectrum, a weighting vector was generated. To obtain the components of the vector, the spectra of response-free and neural activity rich recordings were compared in 74 acoustic response area measurements from 15 animals.

An acoustic response area measurement applied acoustic pure tone stimuli of various frequencies and levels with a stimulus duration of 350 ms that included 10 ms onset and offset squared cosine ramps. Stimuli were presented every 400 ms.

After the removal of the DC component from the raw signal, the power of the recorded data was extracted in 40 ms sections. The spectrum of the stimulated part was obtained as the average spectrum of the power in 8 consecutive windows from 7 to 327 ms. The power of the stimulus free condition was extracted from a window between 360 to 400 ms.

The average power at a recording channel in the stimulus free condition was used to set apart the response-free and activity-rich recordings during the stimulated part. The typical dynamic range of a recording was approximately 6 dB (see e.g. Figure BA.5), thus to capture the response already at threshold level, a recording was considered activity-rich if its power exceeded the average stimulus-free level by 0.5 dB or more.

The mean power spectrum of the active and the response-free recordings are plotted in Figure BA.7. The power spectrum of both parts show a low-pass characteristic. A small peak can be observed around 10.2 kHz in both curves. Other than its high frequency, the appearance of this peak in both curves shows that it is unrelated to the neural activity. As the high frequency region is excluded from the later analysis, this peak is not contaminating the results.

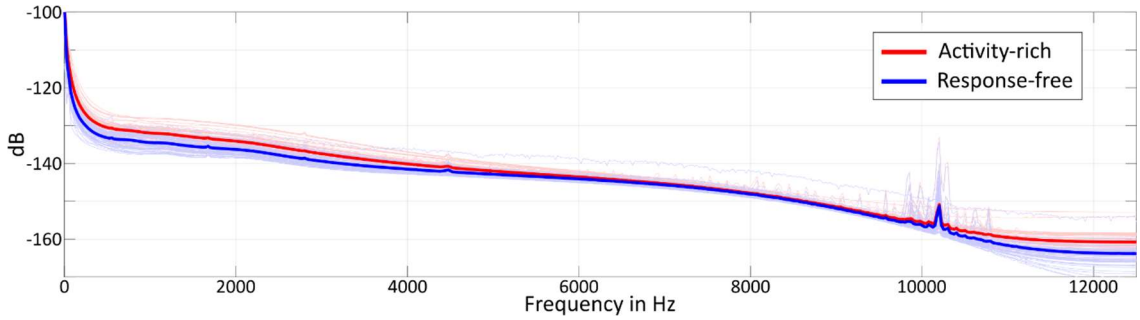

Figure BA.7 Spectrum of activity-rich (red) and response-free (blue) neural recordings. Thin traces show the spectrum of the individual recordings. Emphasized traces show the average spectrum.

To obtain the spectrum of the driven activity, the difference of the active and response-free spectra was calculated, and the result is shown in Figure BA.8. The difference spectrum revealed the low-pass characteristic of the neural activity with a cut-off frequency approximately at 6 kHz.

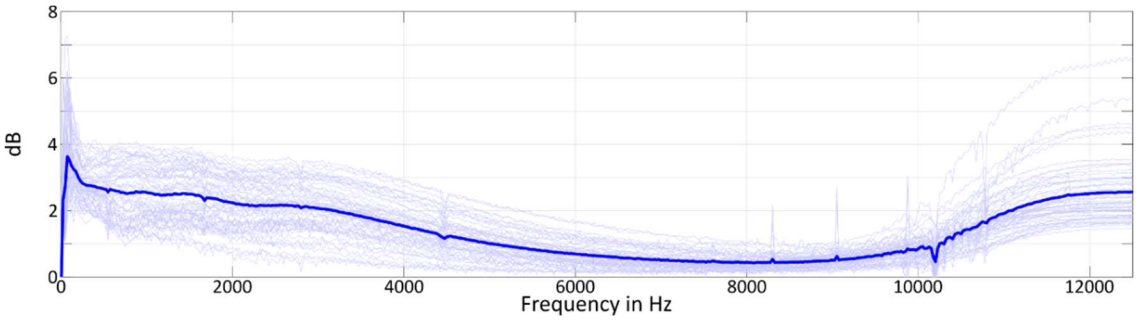

Figure BA.8 Difference between the activity rich and the response -free spectrum. Thin traces show the individual results and the emphasized trace indicates the mean.

Figure BA.9 summarizes the steps that were used to obtain spectral weights for emphasizing neural responses. The mean difference spectrum of the raw data is shown as a blue line. First, the raw data was smoothed with a 9-point rectangular window, the result of which is shown in red colour. In the second step, indicated by black colour, the points corresponding to less than 150 Hz[12] were set to zero. High frequency points are also set to zero above the frequency where the difference spectrum drops below 0.5 dB (the difference becomes negligible), around 7 kHz. In a third step, that is indicated by the magenta line, the frequency region around 800 Hz that is related to individual spiking activity [Chung et al., 1987] was emphasized. The points between 150 and 800 Hz were mirrored to the level of the 800 Hz point i.e. their new values were calculated as $y(x)' = y(x) - 2 \times (y(x) - y(800\,Hz))$. In a final step, the weighting vector was obtained by normalizing the shaped curve and the resulting weighting function is colour coded by green.

[12] According to Chung and colleagues [Chung et al., 1987], the lower limit of the physiologically relevant range is approximately 100 Hz and indeed, the difference spectrum in our case shows a sharp roll-off approximately around 150 Hz.

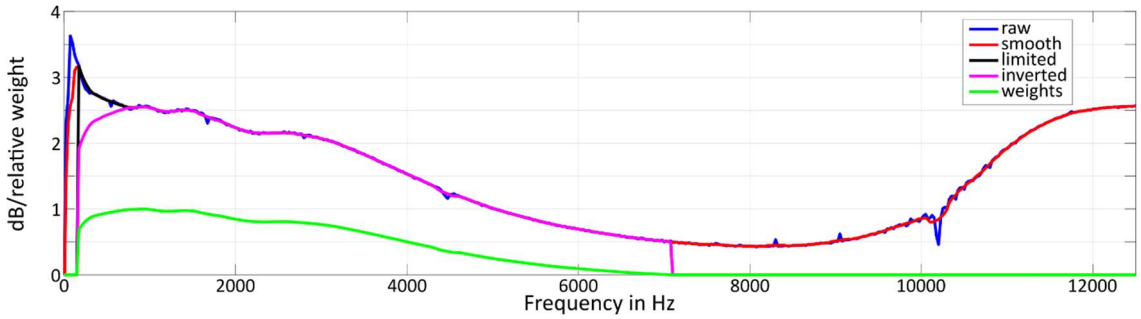

Figure BA.9 Generation of weighting vector for extracting neural activity. Blue line shows the raw difference spectrum of the activity-rich and response-free recordings. Red line shows the smoothed difference spectrum. Black line shoes the limited spectrum between 150 and 7000 Hz (see text for detailed explanation on choosing these limits). Magenta line shows the step of mirroring the components below 800 Hz (see text for detailed explanation). Green line shows the normalized magenta curve and represents the spectral weighting vector.

Figure BA.10 shows the effect of the spectral weighting by comparing spatial activation patterns generated by using the entire spectrum of the recording (except the DC component) to spatial activation patterns obtained after spectral weighting of the signal. In the case of the clear and the dominant neuron examples, the spatial activation patterns became more distinct from the background noise due to giving more weight to the physiologically relevant part. In the high background activity case, the noise at channels above 15 also got more emphasis, indicating its neural origin.

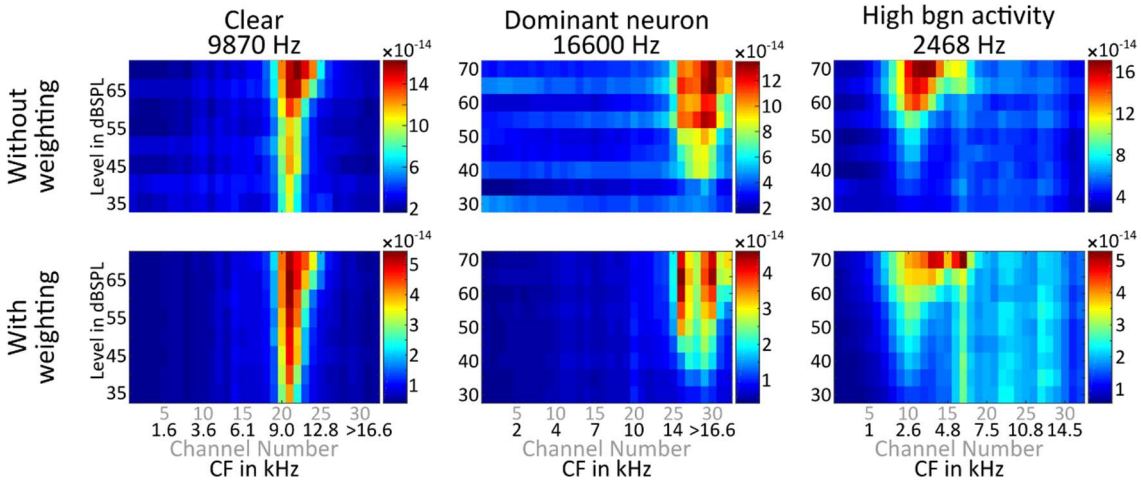

Figure BA.10 Effect of spectral weighting. The first row shows spatial activation patterns obtained by extracting aMUA based on the entire available frequency range (except the DC component). The second row shows spatial activation patterns obtained by extracting aMUA after the application of the weighting vector to emphasize the spectral components that are physiologically relevant.

BA.2.4 Exclusion of neural activity

To exclude the activity of close neurons, first the unwanted spikes must be identified. Figure BA.11 demonstrates the method used for spike detection. In the first step, the moving average of the signal was calculated using a 4 ms long window and subtracted from the raw signal to avoid the low frequency fluctuation in the recording. In a second

step the points that were exceeding, either in a positive or a negative direction, a user defined limit (dashed horizontal black lines) were identified. The limit was set individually for each channel, relative to the mean standard deviation in the background activity that was measured in the stimulus free parts of the recording. The identified outlier points are indicated by blue and points within the limits are shown by red colour.

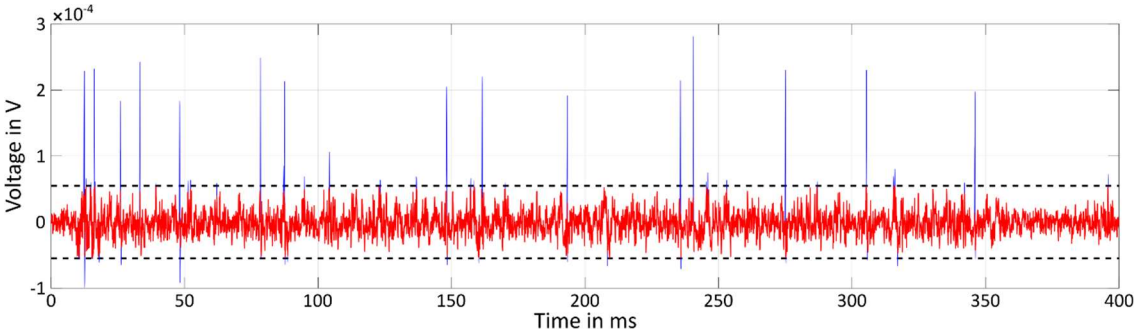

Figure BA.11 Illustration of dominant neural activity identification. The trace represents a single recording from the dominant neuron case at the 26th recording channel in response to 70 dB SPL stimulation level. Excessive neural activity is captured by setting the limit (dashed horizontal lines) to +/- 5 standard deviation of background activity (measured in the stimulus free part in the 360 to 400 ms window). The detected spikes are emphasized by blue colour.

Various techniques are available for removing the identified dominant spikes from the signal. Figure BA.12 shows the three tested methods on a spike detected at 148 ms in Figure BA.11. The raw recording trace and the trace after the processing step are indicted by solid blue and red lines respectively. The limits that were used for spike detection are shown as black dashed lines. The first method cuts off the tip of the spikes by setting the outlier points to the limit. The second method first identifies the whole spike by finding the zero-crossings before and after an outlier sequence. The identified spike is then shrinked by normalizing the spike to the limit. The third method eliminates the spikes by setting the outlier points to zero[13].

[13] These zero points are excluded from the step of power calculation.

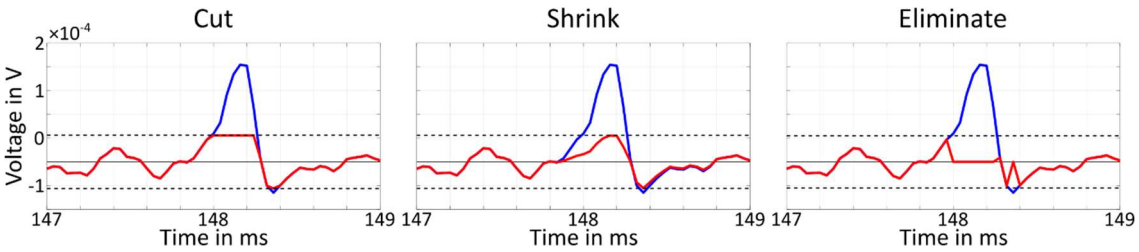

Figure BA.12 Comparison of spike removal methods. Data is identical to the one presented in Figure BA.11. Blue curve shows the raw data. Red curve shows the data after spike removal. Dashed horizontal lines indicate the limit used for detecting spikes. In the cutting method the outlier points of the data are set to be equal to the limit. In the shrinking method, the section corresponding to the spike is detected by identifying zero-crossings before and after the outliers and normalized to the limit. In the elimination method, the outlier points are set to zero (and later excluded from the aMUA calculation).

Figure BA.13 shows the effect of the different methods on the example with the dominant neuron by the application of a limit set to 5 standard deviation of the signal. The dominant neuron example is chosen to demonstrate the effectiveness of this computational step in the removal of across channel differences caused by dominant neural activity.

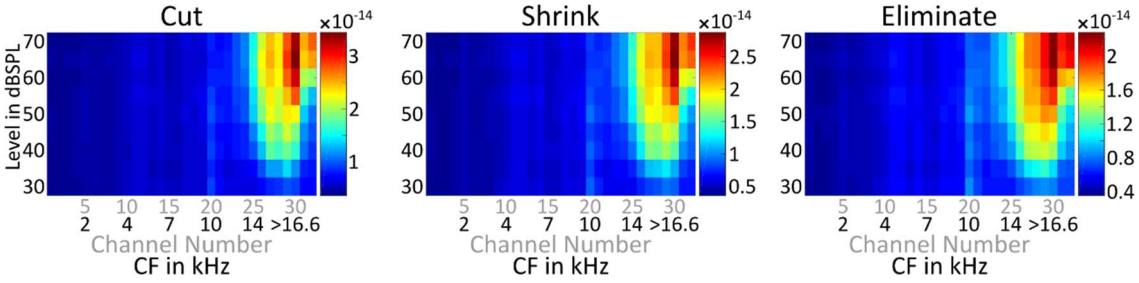

Figure BA.13 Comparison of the effect of dominant spike removal techniques on a spatial activation pattern that originally displayed strong neural response at channel 26 and 30.

The panels of Figure BA.12 and Figure BA.13 are organized from left to right based on the increasing amount of energy removed from the signal, that is the main difference between the methods. The spatial activation patterns obtained by the cutting and shrinking methods show that the activity at channel 26 and 30 remains dominant. On the other hand, the elimination technique successfully removes the dominant activity at channel 26. In the following steps the elimination method using a limit of 5 standard deviation of the background activity is going to be used as by visual observation this approach gave the most satisfactory results.

Figure BA.14 shows the effect of the neural activity exclusion step on the three example spatial activation patterns. In general, this processing step results in a driven activity that is less distinct from the background activity. The spatial smearing effect is also visible, and most prominent in the example of the clear spatial tuning curve. The width of the tuning curve became wider by approximately two electrodes. In the dominant neuron example, the method shows its power by removing the large across channel differences even in this extreme case. In the constant spiking case, the background activity got even

more enhanced than it was before, although the increased driven activity at channel 17 in response to the highest stimulus levels remained unaffected.

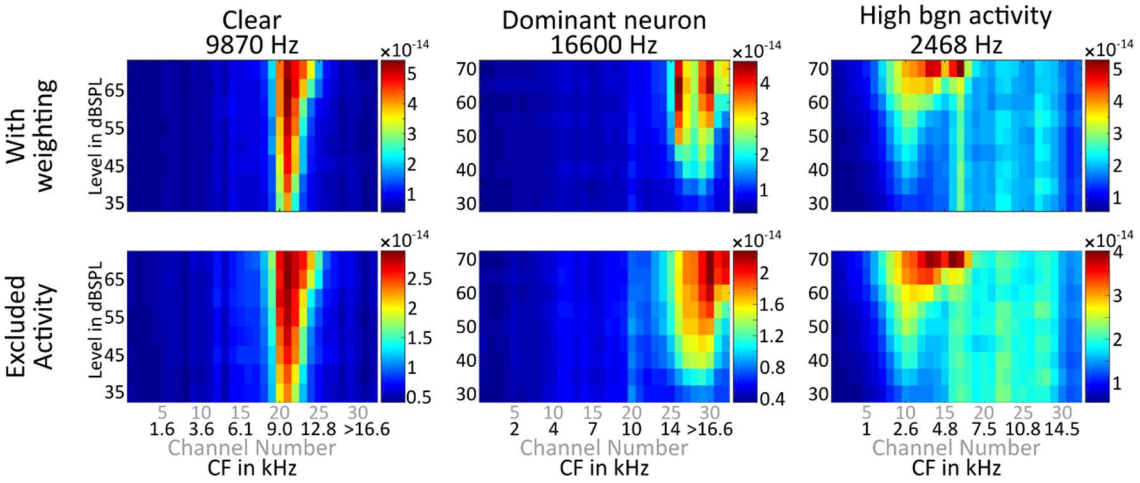

Figure BA.14 Effect of the neural activity exclusion step. The first row shows spatial activation patterns obtained by extracting aMUA after the application of the weighting vector. The second row shows spatial activation patterns that were obtained by using the neural activity exclusion step additionally to the spectral weighting. The excessive neural activity was removed by using the elimination method with a limit of 5 standard deviation of the background activity.

BA.2.5 Extraction of driven activity

To emphasize the stimulus driven activity, the background activity can be subtracted from all channels. To obtain the background activity at every channel, the power is extracted from the inter stimulus gaps.

Figure BA.15 shows the effect of the driven activity extraction step on the three examples, and it shows that the non-active part of the spatial activation patterns became more homogeneous in all cases. In the clear and the dominant neuron examples, the active part of the plots remained unaffected. In the high background activity case, the intense spontaneous neural activity at channel 15 and above was removed successfully, without affecting the stimulus driven response.

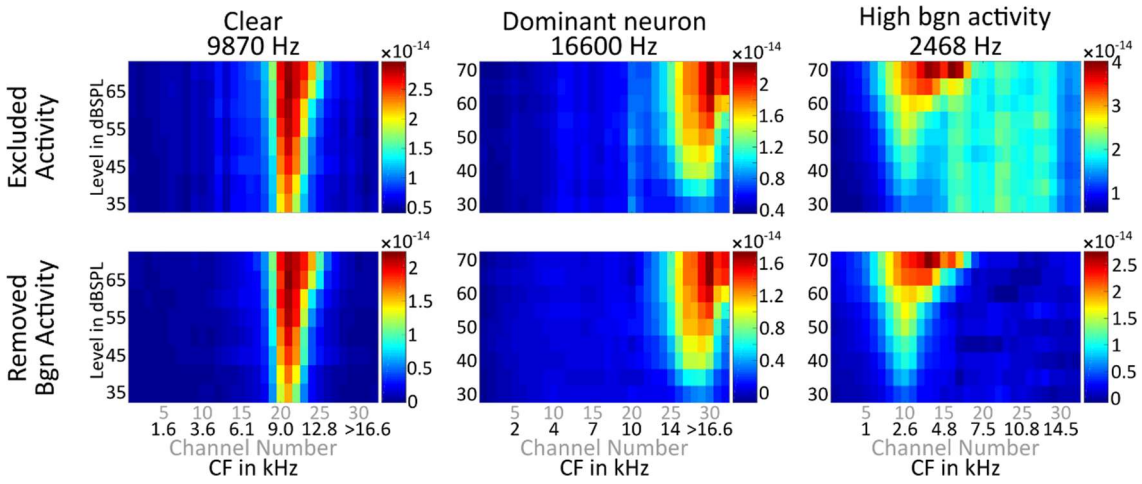

Figure BA.15 Effect of removing the background neural activity. The first row shows spatial activation patterns that were obtained by using the neural activity exclusion step. The second row shows the spatial activation patterns obtained by additionally removing the background neural activity.

BA.2.6 Step-by-step example

The effect of the processing steps applied throughout the spatial activation pattern extraction method are summarized in Figure BA.16. For comparison the result obtained by spike cutting alone, using a threshold of 3 standard deviation of the background activity, is also shown in the first row.

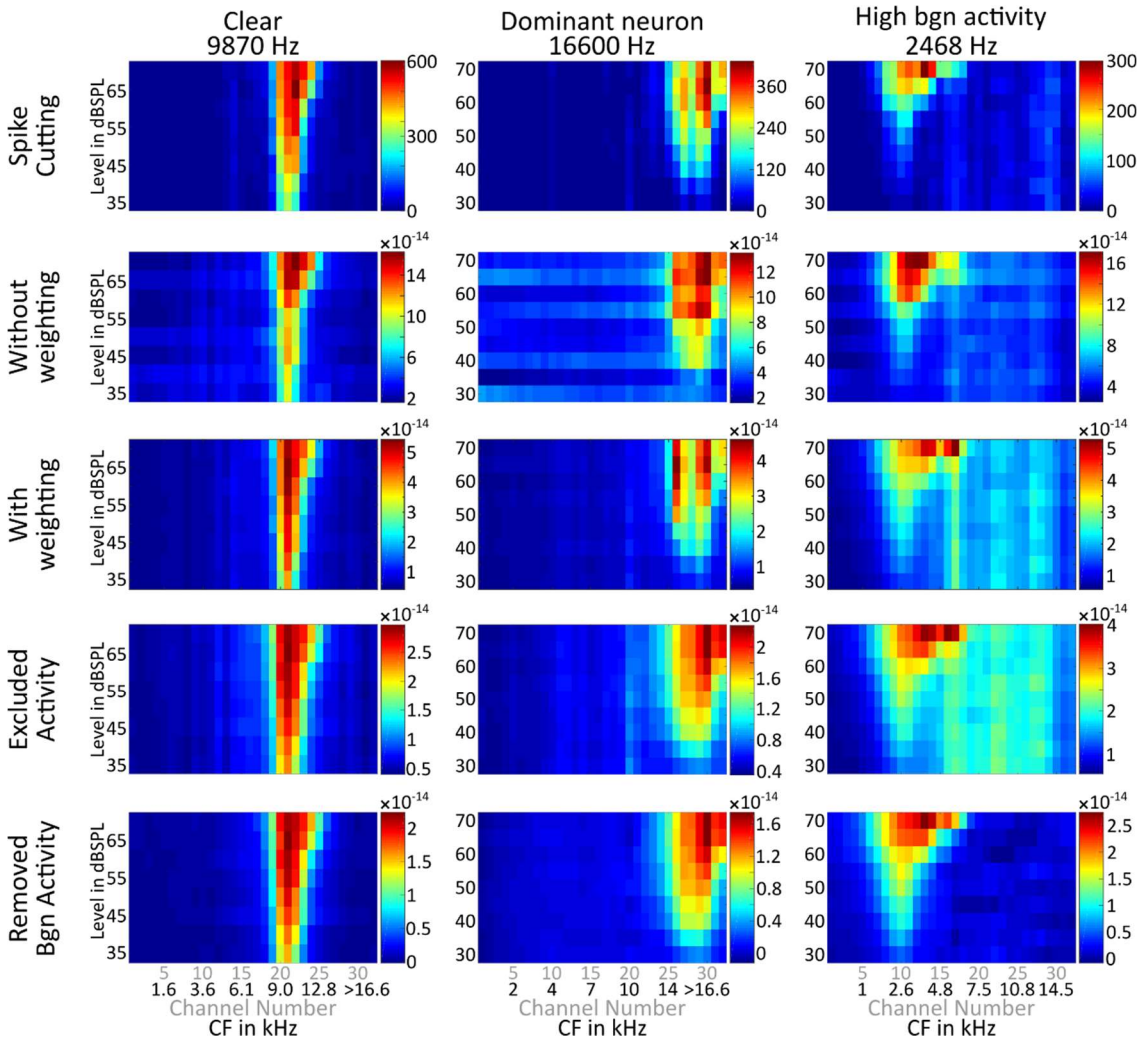

Figure BA.16 Step-by-step example of processing steps introduced in section BA.2.Spatial activation patterns obtained by spike cutting (3 std. threshold) are also shown for comparison in the first row.

BA.3 Artefact rejection techniques

Before working on the neural data, the raw recording must be cleaned of artefacts. Unwanted signal components may be indeterministic or deterministic. Indeterministic artefacts can originate from the imperfections of the recording hardware or some external noise. Deterministic artefacts are usually related to the applied stimulus e.g. the cochlear implant generated electrical field that is captured by the recording probe. In this project, the indeterministic artefacts were removed in the time domain, and the deterministic artefacts were either removed in time or the frequency domain.

The following sections are describing the artefact rejection methods that were automated and used throughout the project. Additionally to the automated methods, trials containing undetected, spurious signal were manually removed after visual inspection of the results.

BA.3.1 Rejecting indeterministic artefacts

The simplest way to detect a false signal in the time domain is to inspect the signal's amplitude. By setting an acceptance limit for valid signal amplitudes, the outliers can easily be identified. The limit can be set according to the standard deviation in every recording trace. In this project, the limit was set to the factor of 30 as it is large enough to avoid the detection of physiologically relevant spikes but not too large to miss static discharges that may have contaminated the measurements. In our recordings, the static discharge artefacts were characterized as spikes with only one sample, that were removed by linear interpolation between the points preceding and following the erroneous data point.

BA.3.2 Rejecting deterministic artefacts

If the artefact is non-overlapping with the neural response of interest, it can easily be discarded from the recording. This technique requires the design of short stimuli that precede the onset of the neural response.

An artefact with a well-determined spectrum can also be removed from the frequency domain. The applied spectral artefact rejection method is presented through an example where a 3 kHz electrical sinusoid was contaminating the signal. Figure BA.17 shows the recorded signal in both time and frequency domain after the steps of the artefact removal process. Panel A shows the 5 seconds long trace of the raw recording with an obvious artefact between 0 and 4.6 seconds. The frequency domain representation of the signal in panel B reveals the artefact's main 3 kHz component and its harmonics at 6, 9 and 12 kHz. The artefact does not cover the whole recording, thus spectral splatter is present around the harmonics of the artefact. To avoid spectral splatters, a rectangular window was applied to the signal with a length that equals to an integer multiple of the artefact's period. After windowing the signal between 0.2 and 4.2 seconds (panel C), the harmonic components of the artefact were appearing as single spectral lines in the frequency domain in panel D. As a last step, the artefact related spectral components were set to zero (panel F) to achieve a clean signal that can also be observed in the time domain (panel E).

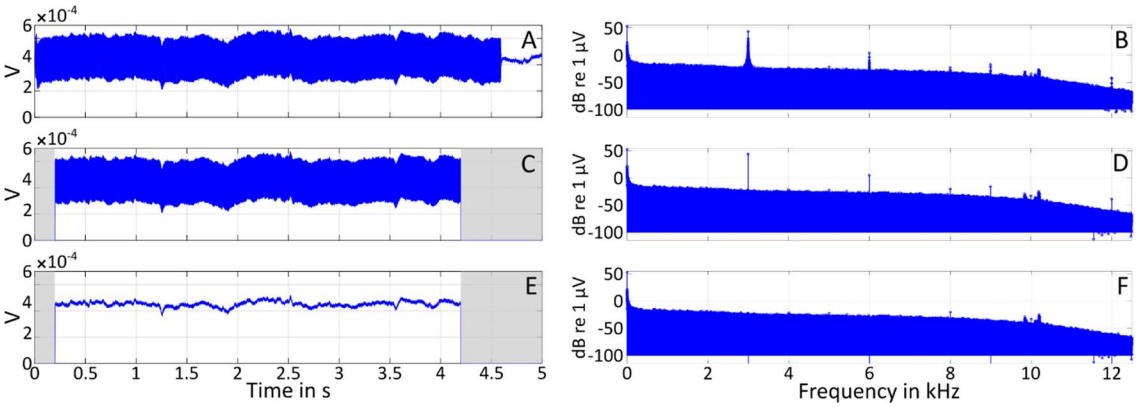

Figure BA.17 Steps of artefact rejection in the frequency domain. Left column illustrates the signal in time domain, right column shows the frequency domain representation of the signal. Panel A and B shows the raw signal with a 3 kHz electric artefact that dominates the signal between 0 and 4.6 seconds with spectral peaks at the harmonics of 3 kHz. Panel C and D shows the effect of rectangular windowing of the signal between 0.2 and 4.2 seconds. The artefact appears as single lines in the spectrum at the harmonics of 3 kHz. Panel E and F shows the signal after removal of the artefact related spectral components.

The application of artefact removal in the frequency domain requires an ensured common clock of the stimulating and recording hardware. Without synchronous stimulation and data acquisition, a drift may appear between the stimulation and recorded signals that would result in the imperfect resolution of the artefactual components and impede their removal.

BA.4 An example application

To illustrate the capability of the developed technique, the spectrogram of a speech signal is compared to its a neural response in panel B of Figure BA.18. For stimulation, a sentence, 'The true sense held the voice', was presented at 90 dB SPL and repeated 64 times. To obtain the neural spectrogram, i.e. the representation of neural activity over time, neural responses were extracted in 25 ms long consecutive analysis windows along the recording. To aid comparison, the neural spectrogram was time aligned to the spectrogram and its colour scale was limited between 0 and $6*10^{-14}$.

The neural spectrogram clearly follows the changes in the spectrum of the signal. The underrepresentation of activity in the low frequency region of the neural spectrogram is most likely caused by the imperfect positioning of the recording shank in the inferior colliculus.

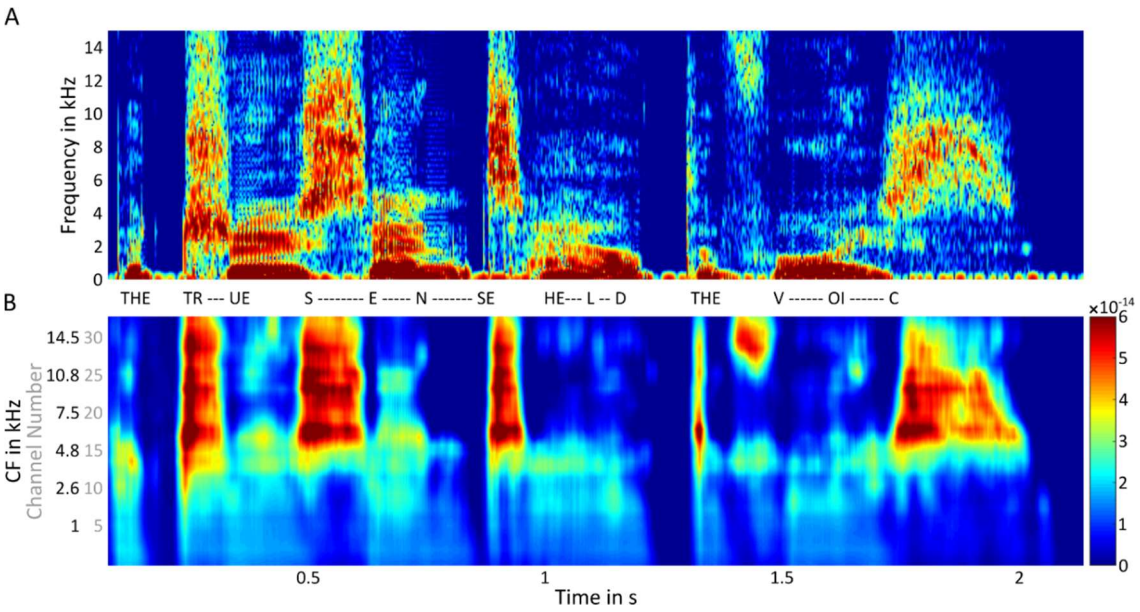

Figure BA.18 Comparison of to the spectrogram of a speech signal to its neural representation in the inferior colliculus (362B2).Panel A displays the spectrogram of the sentence 'The true sense held the voice', that was presented at 90 dB SPL. Panel B shows the neural response to the same sentence.

BA.5 Room for improvement?

The presented technique can be improved by including more complexity in the processing steps of neural activity exclusion and artefact rejection.

BA.5.1 Across-channel correlation-based spike removal

The neural activity was excluded on a channel-by-channel basis. This is a suboptimal implementation if the neurons close to the recording shank are wanted to be removed. As shown in an example in panel A in Figure BA.19, the signal of a neuron, that is in d_0 distance from the recording array, is detectable at electrodes e_{n-1}, e_n and e_{n+1}. The limit of spike elimination may be set such that at e_n, the spikes from the neuron are going to be eliminated, but the same spikes will still remain to be present at e_{n-1} and e_{n+1}. In this case the neighbouring electrodes may show higher neural activity, causing false peaks in the spatial tuning curves, like in the response to the 72 dB SPL tone at e_{13}, shown in panel B. The raw response to the 72 dB SPL tone at e_{12} (red) and e_{13} (blue) and their corresponding limits (dashed lines) are shown in panel C. Using these limits, a spike at 259.5 ms was eliminated at e_{12}, but the signal corresponding to the same spike at e_{13} remained intact.

To solve the described issue, cross-correlation of recordings across channels could be performed, and an identified dominant spike may be removed from all the channels where it appears.

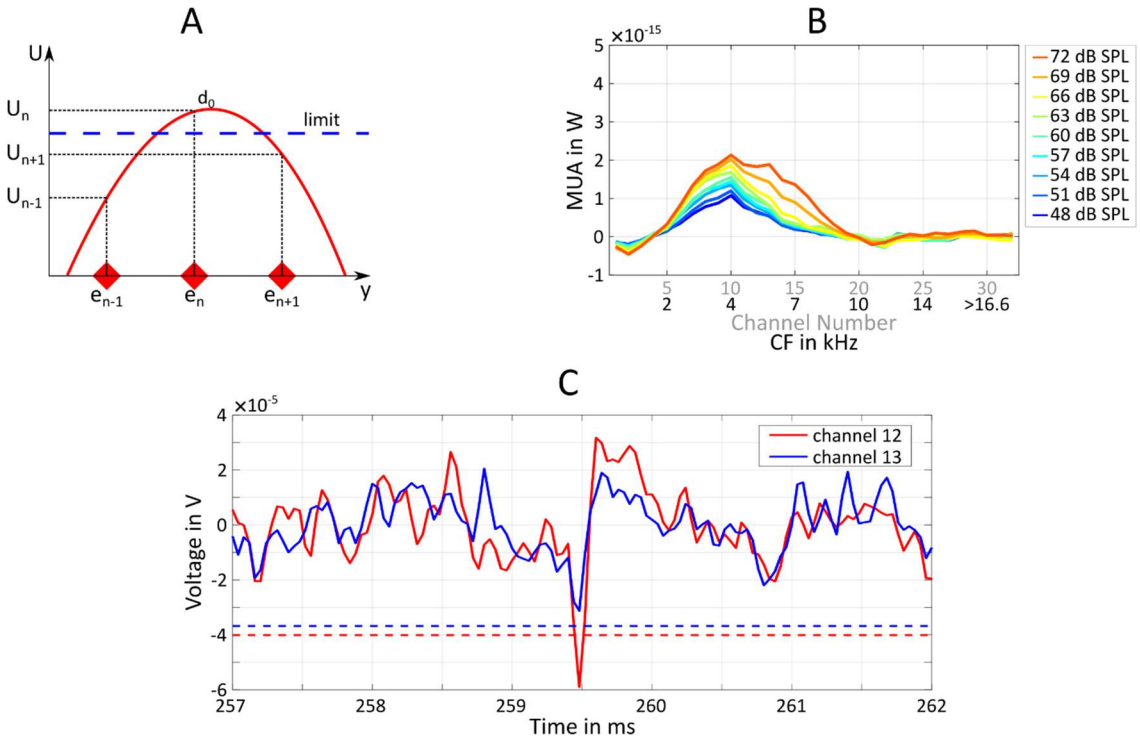

Figure BA.19 The signal of a dominant spike may appear at multiple recording channels, causing false peaks in the spatial tuning curves. Panel A illustrates the spatial smearing profile of a neuron that is in d_0 distance from the recording shank. A spike of this neuron would be eliminated at e_n, but not at e_{n-1} and e_{n+1} if the example limit (blue dashed line) is used for spike detection. Panel B shows the spatial tuning curves in response to acoustic tones (355B27). Note the double peak at the 10th and the 13th electrode in response to the 72 dB SPL tone. Panel C shows the raw recordings at electrode 12 and 13 in response to a 72 dB SPL tone in the same recording as in panel B (355B27). Horizontal dashed lines indicate the limits used at the electrodes.

BA.5.2 Across-channel correlation-based artefact rejection

Artefact rejection could also be improved by cross-correlating the extracted aMUA across channels. Recording similar response activity at the same time at all electrodes is highly unlikely, thus upon observation of a high correlation of aMUA across channels would indicate a false signal. To avoid erroneously detecting a wide band response e.g. a response to a plosive sound or wideband noise, a further test across trials with the same stimulus could be done. If high correlation is present in all trials, then the response can be considered valid as the chance of having the same artefact in many trials is low.

Bibliography

Addams-Williams, J., Munaweera, L., Coleman, B., Shepherd, R. K., & Backhouse, S. Cochlear implant electrode insertion: in defence of cochleostomy and factors against the round window membrane approach. *Cochlear Implants International*, *12:Sup2*: S36-s39, 2011.

Adunka, O. F., & Buchman, C. A. Scala Tympani Cochleostomy I: Results of a Survey. *The Laryngoscope*, *117*(12): 2187–2194, 2007.

Adunka, O. F., Dillon, M. T., King, E. R., Pillsbury, H. C., & Buchman, C. A. Hearing preservation and speech perception outcomes with electric-acoustic stimulation after 12 months of listening experience. *Laryngoscope*, *123*(10): 2509–2515, 2013.

Adunka, O. F., Giardina, C. K., Formeister, E. J., Choudhury, B., Buchman, C. A., & Fitzpatrick, D. C. Round window electrocochleography before and after cochlear implant electrode insertion. *Laryngoscope*, *126*(5): 1193–1200, 2016.

Adunka, O. F., Kiefer, J., Unkelbach, M. H., Lehnert, T., & Gstoettner, W. K. Development and evaluation of an improved cochlear implant electrode design for electric acoustic stimulation. *Laryngoscope*, *114*(7): 1237–1241, 2004.

Adunka, O. F., Pillsbury, H. C., & Buchman, C. A. Minimizing intracochlear trauma during cochlear implantation. *Cochlear Implants and Hearing Preservation*, *67*: 96–107, 2009.

Ashmore, J. F. A fast motile response in guinea-pig outer hair cells: the cellular basis of the cochlear amplifier. *The Journal of Physiology*, *388*(1): 323–347, 1987.

Azouz, R., & Gray, C. M. Dynamic spike threshold reveals a mechanism for synaptic coincidence detection in cortical neurons in vivo. *Proceedings of the National Academy of Sciences*, *97*(14): 8110–8115, 2000.

Ballestero, J., Recugnat, M., Laudanski, J., Smith, K. E., Jagger, D. J., Gnansia, D., & McAlpine, D. Reducing Current Spread by Use of a Novel Pulse Shape for Electrical Stimulation of the Auditory Nerve. *Trends in Hearing*, *19*: 1–12, 2015.

Békésy, G. Zür Theorie des Hörens: die Schwingungsform der Basilarmembran. *Physik*, *29*: 793–810, 1928.

Békésy, G. DC Resting Potentials Inside the Cochlear Partition. *The Journal of the Acoustical Society of America*, *24*(1): 72–76, 1952.

Békésy, G. *Experiments in Hearing*, 1960.

Black, R. C., Clark, G. M., & Patrick, J. F. Current Distribution Measurements Within the Human Cochlea. *Biomedical Engineering, IEEE Transactions On*, *BME-28*(10): 721–725, 1981.

Böhnke, F., & Arnold, W. 3D-finite element model of the human cochlea including fluid-structure couplings. *Orl*, *61*: 305–310, 1999.

Briggs, R. J. S., Tykocinski, M., Xu, J., Risi, F., Svehla, M., Cowan, R., … Lenarz, T. Comparison of round window and cochleostomy approaches with a prototype hearing preservation electrode. *Audiology and Neurotology*, *11*(SUPPL. 1): 42–48, 2006.

Brown, A. M. Acoustic distortion from rodent ears: A comparison of responses from rats, guinea pigs and gerbils. *Hearing Research*, *31*(1): 25–37, 1987.

Brownell, W. E., Bader, C. R., Bertrand, D., & de Ribaupierre, Y. Evoked mechanical responses of isolated cochlear outer hair cells. *Science (New York, N.Y.)*, *227*(4683): 194–196, 1985.

Büchner, A., Schüssler, M., Battmer, R. D., Stöver, T., Lesinski-Schiedat, A., & Lenarz, T. Impact of low-frequency hearing. *Audiology and Neurotology*, *14*(SUPPL. 1): 8–13, 2009.

Buzsáki, G., Anastassiou, C. A., & Koch, C. The origin of extracellular fields and currents--EEG, ECoG, LFP and spikes. *Nature Reviews. Neuroscience*, *13*(6): 407–420, 2012.

Campbell, L., Kaicer, A., Briggs, R., & O'Leary, S. Cochlear response telemetry: intracochlear electrocochleography via cochlear implant neural response telemetry pilot study results. *Otology & Neurotology*, *36*(3): 399–405, 2014.

Causon, A., Verschuur, C., & Newman, T. A. A Retrospective Analysis of the Contribution of Reported Factors in Cochlear Implantation on Hearing Preservation Outcomes. *Otology & Neurotology : Official Publication of the American Otological Society, American Neurotology Society [and] European Academy of Otology and Neurotology*, *36*(7): 1137–1145, 2015.

Choudhury, B., Fitzpatrick, D. C., Buchman, C. A., Wei, B. P., Dillon, M. T., He, S., & Adunka, O. F. Intraoperative round window recordings to acoustic stimuli from cochlear implant patients. *Otology and Neurotology*, *33*(9): 1507–1515, 2012.

Chung, S. H., Jones, L. C., Hammond, B. J., King, M. C., Evans, R. J., Knott, C., … Anson, M. Signal processing technique to extract neuronal activity from noise. *Journal of Neuroscience Methods*, *19*(2): 125–139, 1987.

Clark, J. G. Uses and abuses of hearing loss classification. *American Speech-Languag-Hearing Association*, *23*(7): 493–500, 1981.

Dalbert, A., Pfiffner, F., Hoesli, M., Koka, K., Veraguth, D., Roosli, C., & Huber, A. Assessment of cochlear function during cochlear implantation by extra- and intracochlear electrocochleography. *Frontiers in Neuroscience*, *12*(JAN): 1–9, 2018.

Dallos, P. The active cochlea. *The Journal of Neuroscience*, *12*(12): 4575–4585, 1992.

Dallos, P., & Cheatham, M. A. Production of cochlear potentials by inner and outer hair cells. *The Journal of the Acoustical Society of America*, *60*(2): 510–512, 1976.

Dancer, A., & Franke, R. Intracochlear sound pressure measurements in guinea pigs. *Hearing Research*, *2*(3–4): 191–205, 1980.

Dang, K., Clerc, M., Vandersteen, C., Guevara, N., & Gnansia, D. In situ validation of a parametric model of electrical field distribution in an implanted cochlea. *International IEEE/EMBS Conference on Neural Engineering, NER*, *2015-July*: 667–670, 2015.

Dong, S., Rodger, J., Mulders, W. H. A. M., & Robertson, D. Tonotopic changes in GABA receptor expression in guinea pig inferior colliculus after partial unilateral hearing loss. *Brain Research*, *1342*: 24–32, 2010.

Drexl, M., Lagarde, M. M. M., Zuo, J., Lukashkin, A. N., & Russell, I. J. The role of prestin in the generation of electrically evoked otoacoustic emissions in mice. *Journal of Neurophysiology*, *99*(4): 1607–1615, 2008.

Fitzpatrick, D. C., Campbell, A., Choudhury, B., Dillon, M., Forgues, M., Buchman, C. A., & Adunka, O. F. Round Window Electrocochleography Just Prior to Cochlear Implantation: Relationship to Word Recognition Outcomes in Adults. *Otology*, *35*(1): 64–71, 2014.

Fontenot, T. E., Giardina, C. K., Dillon, M. T., Rooth, M. A., Teagle, H. F., Park, L. R., … Fitzpatrick, D. C. Residual Cochlear Function in Adults and Children Receiving Cochlear Implants: Correlations With Speech Perception Outcomes. *Ear and Hearing*, *40*(3): 577–591, 2019.

Formeister, E. J., McClellan, J. H., Merwin, W. H., Iseli, C. E., Calloway, N. H., Teagle, H. F. B., … Fitzpatrick, D. C. Intraoperative round window electrocochleography and speech perception outcomes in pediatric cochlear implant recipients. *Ear and Hearing*, *36*(2): 249–260, 2015.

Fourcin, A. J., Rosen, S. M., Moore, B. C. J., Douek, E. E., Clarke, G. P., Dodson, H. C., & Bannister, L. H. External electrical stimulation of the cochlea: clinical, psychophysical, speech-perceptual and histological findings. *British Journal of Audiology*, *13*(85–107):, 1979.

Francart, T., & McDermott, H. J. Psychophysics, fitting, and signal processing for combined hearing aid and cochlear implant stimulation. *Ear and Hearing*, *34*(6): 685–700, 2013.

Frank, G., Hemmert, W., & Gummer, A. W. Limiting dynamics of high-frequency electromechanical transduction of outer hair cells. *Proceedings of the National Academy of Sciences of the United States of America*, *96*: 4420–4425, 1999.

Frank, G., & Kössl, M. Acoustical and electrical biasing of the cochlea partition. Effects on the acoustic two tone distortions f2-f1 and 2f1-f2. *Hearing Research*, *113*: 57–68, 1997.

Fraysse, B., Macías, Á. R., Sterkers, O., Burdo, S., Ramsden, R., Deguine, O., … James, C. Residual hearing conservation and electroacoustic stimulation with the nucleus 24 contour advance cochlear implant. *Otology and Neurotology*, *27*(5): 624–633, 2006.

Gantz, B. J., & Turner, C. W. Combined Acoustic and Electric Hearing. *The Laryngoscope*, *113*(10): 1726–1730, 2003.

Gantz, B. J., Turner, C. W., Gfeller, K. E., & Lowder, M. W. Preservation of hearing in cochlear implant surgery: Advantages of combined electrical and acoustical speech processing. *The Laryngoscope*, *115*(5): 796–802, 2005.

Gelfand, S. A. *Hearing: An Introduction to Psychological and Physiological Acoustics*, (5th ed.)2010.

George, S. S., Wise, A. K., Shivdasani, M. N., Shepherd, R. K., & Fallon, J. B. Evaluation of focused multipolar stimulation for cochlear implants in acutely deafened cats. *Journal of Neural Engineering*, *11*:, 2014.

Gfeller, K. E., Olszewski, C., Turner, C., Gantz, B. J., & Oleson, J. Music perception with cochlear implants and residual hearing. *Audiology and Neurotology*, *11*(SUPPL. 1): 12–15, 2006.

Giardina, C. K., Khan, T. E., Pulver, S. H., Adunka, O. F., Buchman, C. A., Brown, K. D., … Fitzpatrick, D. C. Response Changes During Insertion of a Cochlear Implant Using Extracochlear Electrocochleography. *Ear and Hearing*, *39*(6): 1146–1156, 2018.

Gibson, W. P. The clinical uses of electrocochleography. *Frontiers in Neuroscience*, *11*(MAY): 1–8, 2017.

Gifford, R. H., Dorman, M. F., Skarzynski, H., Lorens, A., Polak, M., Driscoll, C. L. W., … Buchman, C. A. Cochlear implantation with hearing preservation yields significant benefit for speech recognition in complex listening environments. *Ear and Hearing*, *34*(4): 413–425, 2013.

Greenwood, D. D. Critical Bandwidth and the Frequency Coordinates of the Basilar Membrane. *The Journal of the Acoustical Society of America*, *33*(10): 1344–1356, 1961.

Greenwood, D. D. A cochlear frequency position function for several species{\textemdash}29 years later. *The Journal of the Acoustical Society of America*, *87*(6): 2592–2605, 1990.

Grosh, K., Zheng, J., Zou, Y., de Boer, E., & Nuttall, A. L. High-frequency electromotile responses in the cochlea. *The Journal of the Acoustical Society of America*, *115*(5): 2178–2184, 2004.

Gstoettner, W. K., Heibig, S., Maier, N., Kiefer, J., Radeloff, A., & Adunka, O. F. Ipsilateral electric acoustic stimulation of the auditory system: Results of long-term hearing preservation. *Audiology and Neurotology*, *11*(SUPPL. 1): 49–56, 2006.

Gstoettner, W. K., Van De Heyning, P., Fitzgerald O'Connor, A., Morera, C., Sainz, M., Vermeire, K., … Adunka, O. F. Electric acoustic stimulation of the auditory system: Results of a multi-centre investigation. *Acta Oto-Laryngologica*, *128*(9): 968–975, 2008.

Gstöttner, W., Kiefer, J., Baumgartner, W. D., Pok, S., Peters, S., & Adunka, O. F. Hearing preservation in cochlear implantation for electric acoustic stimulation. *Acta Oto-Laryngologica*, *124*(4): 348–352, 2004.

Gudis, D. a, Montes, M., Bigelow, D. C., & Ruckenstein, M. J. The round window: is it the "cochleostomy" of choice? Experience in 130 consecutive cochlear implants. *Otology & Neurotology : Official Publication of the American Otological Society, American Neurotology Society [and] European Academy of Otology and Neurotology*, *33*(9): 1497–1501, 2012.

Hartmann, R., Topp, G., & Klinke, R. Discharge patterns of cat primary auditory fibers with electrical stimulation of the cochlea. *Hearing Research*, *13*(1): 47–62, 1984.

Haumann, S., Imsiecke, M., Bauernfeind, G., Büchner, A., Helmstaedter, V., Lenarz, T., & Salcher, R. B. Monitoring of the Inner Ear Function During and After Cochlear Implant Insertion Using Electrocochleography. *Trends in Hearing*, *23*: 1–18, 2019.

Havenith, S., Lammers, M. J. W., Tange, R. a, Trabalzini, F., della Volpe, A., van der Heijden, G. J. M. G., & Grolman, W. Hearing preservation surgery: cochleostomy or round window approach? A systematic review. *Otology & Neurotology : Official Publication of the American Otological Society, American Neurotology Society [and] European Academy of Otology and Neurotology*, *34*(4): 667–674, 2013.

Helbig, S., Adel, Y., Rader, T., Stöver, T., & Baumann, U. Long-term Hearing Preservation Outcomes After Cochlear Implantation for Electric-Acoustic Stimulation. *Otology & Neurotology*, *37*(9): e353–e359, 2016.

Helbig, S., Baumann, U., Hey, C., & Helbig, M. Hearing Preservation After Complete Cochlear Coverage in Cochlear Implantation With the Free-Fitting FLEXSOFT Electrode Carrier. *Otology & Neurotology*, *32*(6): 973–979, 2011.

Hochmair, I., Hochmair, E., Nopp, P., Waller, M., & Jolly, C. N. Deep electrode insertion and sound coding in cochlear implants. *Hearing Research*, *322*: 14–23, 2015.

Hubbard, A. E., & Mountain, D. C. Alternating current delivered into the scala media alters sound pressure at the eardrum. *Science (New York, N.Y.)*, *222*(4623): 510–512, 1983.

Hudspeth, A. J., & Corey, D. P. Sensitivity, polarity, and conductance change in the response of vertebrate hair cells to controlled mechanical stimuli. *Proceedings of the National Academy of Sciences of the United States of America*, *74*(6): 2407–2411, 1977.

Imsiecke, M., Krüger, B., Büchner, A., Lenarz, T., & Nogueira, W. Electric-acoustic forward masking in cochlear implant users with ipsilateral residual hearing. *Hearing Research*, 2018.

Incerti, P. V., Ching, T. Y. C., & Cowan, R. A systematic review of electric-acoustic stimulation: Device fitting ranges, outcomes, and clinical fitting practices. *Trends in Amplification*, *17*(1): 3–26, 2013.

Irving, S., Gillespie, L., Richardson, R., Rowe, D., Fallon, J. B., & Wise, A. K. Electroacoustic Stimulation: Now and into the Future. *BioMed Research International*, 1–17, 2014.

Ishiyama, A., Doherty, J., Ishiyama, G., Quesnel, A. M., Lopez, I., & Linthicum, F. H. Post hybrid cochlear implant hearing loss and endolymphatic hydrops. *Otology and Neurotology*, *37*(10): 1516–1521, 2016.

Ishiyama, A., Ishiyama, G., Lopez, I. A., & Linthicum Jr, F. H. Temporal Bone Histopathology of First-Generation Cochlear Implant Electrode Translocation. *Otology & Neurotology*, *40*: 1–11, 2019.

James, C., Blamey, P., Shallop, J. K., Incerti, P. V., & Nicholas, A. M. Contralateral masking in cochlear implant users with residual hearing in the non-implanted ear. *Audiology and Neuro-Otology*, *6*(2): 87–97, 2001.

James, C. J., Fraysse, B., Deguine, O., Lenarz, T., Mawman, D., Ramos, Á., … Sterkers, O. Combined electroacoustic stimulation in conventional candidates for cochlear implantation. *Audiology and Neurotology*, *11*(SUPPL. 1): 57–62, 2006.

Javel, E., & Shepherd, R. K. Electrical stimulation of the auditory nerve. III. Response initiation sites and temporal fine structure. *Hearing Research*, *140*(1–2): 45–76, 2000.

Jiefu, Z., Yuan, Z., Ren, T., & Nuttall, A. L. An Overview of Electrically Evoked Otoacoustic Emissions in the Mammalian Cochlea. *Journal of Otology*, *1*(1): 45–50, 2006.

Jolly, C. N., Spelman, F. A., & Clopton, B. M. Quadrupolar stimulation for cochlear prostheses: Modeling and experimental data. *IEEE Transactions on Biomedical Engineering*, *43*(8): 857–865, 1996.

Kakehata, S., & Santos-Sacchi, J. Effects of Salicylate and Lanthanides on Outer Hair Cell Motility and Associated Gating Charge. *The Journal of Neuroscience*, *16*(16): 4881–4889, 1996.

Kayser, C., Petkov, C. I., & Logothetis, N. K. Tuning to Sound Frequency in Auditory Field Potentials. *Journal of Neurophysiology*, *98*(3): 1806–1809, 2007.

Kiefer, J., Böhnke, F., Adunka, O. F., & Arnold, W. Representation of acoustic signals in the human cochlea in presence of a cochlear implant electrode. *Hearing Research*, *221*: 36–43, 2006.

Kiefer, J., Gstöttner, W., Baumgartner, W., Pok, S. M., Tillein, J., Ye, Q., & Von Ilberg, C. Conservation of low-frequency hearing in cochlear implantation. *Acta Oto-Laryngologica*, *124*(3): 272–280, 2004.

Kiefer, J., Pok, M., Adunka, O. F., Stürzebecher, E., Baumgartner, W., Schmidt, M., … Gstöttner, W. Combined electric and acoustic stimulation of the auditory system: Results of a clinical study. *Audiology and Neurotology*, *10*(3): 134–144, 2005.

Kirk, D. L., & Yates, G. K. Frequency tuning and acoustic enhancement of electrically evoked otoacoustic emissions in the guinea pig cochlea. *The Journal of the Acoustical Society of America*, *100*(6): 3714–3725, 1996.

Kirk, D. L., & Yates, G. K. Enhancement of electrically evoked oto-acoustic emissions associated with low-frequency stimulus bias of the basilar membrane towards scala vestibuli. *The Journal of the Acoustical Society of America*, *104*(September): 1544–1554, 1998.

Koka, K., & Litvak, L. M. Feasibility of Using Electrocochleography for Objective Estimation of Electro-Acoustic Interactions in Cochlear Implant Recipients with Residual Hearing. *Frontiers in Neuroscience*, *11*(337): 1–9, 2017.

Kral, A., Hartmann, R., Mortazavi, D., & Klinke, R. Spatial resolution of cochlear implants: The electrical field and excitation of auditory afferents. *Hearing Research*, *121*(1–2): 11–28, 1998.

Krüger, B., Büchner, A., & Nogueira, W. Simultaneous masking between electric and acoustic stimulation in cochlear implant users with residual low-frequency hearing. *Hearing Research*, *353*: 185–196, 2017.

Liberman, M. C. The cochlear frequency map for the cat: Labeling auditory-nerve fibers of known characteristic frequency. *The Journal of the Acoustical Society of America*, *72*(5): 1441, 1982.

Lim, H. H., & Anderson, D. J. Antidromic activation reveals tonotopically organized projections from primary auditory cortex to the central nucleus of the inferior colliculus in guinea pig. *Journal of Neurophysiology*, *97*(2): 1413–1427, 2007.

Lin, P., Turner, C. W., Gantz, B. J., Djalilian, H. R., & Zeng, F.-G. Ipsilateral masking between acoustic and electric stimulations. *The Journal of the Acoustical Society of America*, *130*(2): 858–865, 2011.

Loizou, P. C. Mimicking the Human Ear. *IEEE Signal Processing Magazine*, 101–130, 1998.

Lusted, H. S., & Simmons, F. B. Comparison of electrophonic and auditory-nerve electroneural responses. *The Journal of the Acoustical Society of America*, *83*: 657–661, 1988.

Mammano, F., & Ashmore, J. F. Reverse transduction measured in the isolated cochlea by laser Michelson interferometry. *Letters to Nature*, *365*: 838–841, 1993.

McAnally, K. I., & Clark, G. M. Stimulation of residual hearing in the cat by pulsatile electrical stimulation of the cochlea. *Acta Oto-Laryngologica*, *114*: 366–372, 1994.

McGinley, M. J., & Oertel, D. Rate thresholds determine the precision of temporal integration in principal cells of the ventral cochlear nucleus. *Hearing Research*, *216–217*(1–2): 52–63, 2006.

Miller, C. A., Abbas, P. J., Robinson, B. K., Nourski, K. V., Zhang, F., & Jeng, F. C. Electrical excitation of the acoustically sensitive auditory nerve: Single-fiber responses to electric pulse trains. *JARO - Journal of the Association for Research in Otolaryngology*, *7*(3): 195–210, 2006.

Miller, C. A., Abbas, P. J., Rubinstein, J. T., Robinson, B. K., Matsuoka, A. J., & Woodworth, G. Electrically evoked compound action potentials of guinea pig and cat: Responses to monopolar, monophasic stimulation. *Hearing Research*, *119*(1–2): 142–154, 1998.

Mountain, D. C., & Hubbard, A. E. Rapid force production in the cochlea. *Hearing Research*, *42*(2–3): 195–202, 1989.

Moxon, E. C. *Neural and Mechanical Responses to Electric Stimulation of the Cat's Inner Ear*, 1971.

Murata, K., Moriyama, T., Hosokawa, Y., & Minami, S. Alternating current induced otoacoustic emissions in the guinea pig. *Hearing Research*, *55*(2): 201–214, 1991.

Nakajima, H. H., Mountain, D. C., & Hubbard, A. E. Nonlinear characteristics of electrically evoked otoacoustic emissions. *Hearing Research*, *122*(1–2): 109–118, 1998.

Nakajima, H. H., Olson, E. S., Mountain, D. C., & Hubbard, A. E. Electrically evoked otoacoustic emissions from the apical turns of the gerbil cochlea. *Acoustical Society of America*, *96*(2): 786–794, 1994.

Ni, G., Elliott, S. J., Ayat, M., & Teal, P. D. Modelling Cochlear Mechanics. *BioMed Research International*, *2014*: 1–42, 2014.

Nourski, K. V., Abbas, P. J., Miller, C. A., Robinson, B. K., & Jeng, F.-C. Effects of acoustic noise on the auditory nerve compound action potentials evoked by electric pulse trains. *Hearing Research*, *202*: 141–153, 2005.

Nourski, K. V., Abbas, P. J., Miller, C. A., Robinson, B. K., & Jeng, F. C. Acoustic-electric interactions in the guinea pig auditory nerve: Simultaneous and forward masking of the electrically evoked compound action potential. *Hearing Research*, *232*: 87–103, 2007.

Nowotny, M., & Gummer, A. W. Nanomechanics of the subtectorial space caused by electromechanics of cochlear outer hair cells. *Proceedings of the National Academy of Sciences*, *103*(7): 2120–2125, 2006.

Nuttall, A. L., Dolan, D. F., & Avinash, G. Laser Doppler velocimetry of basilar membrane vibration. *Hearing Research*, *51*: 203–213, 1991.

Nuttall, A. L., & Ren, T. Electromotile hearing: evidence from basilar membrane motion and otoacoustic emissions. *Hearing Research*, *92*: 170–177, 1995.

Nuttall, A. L., Zheng, J., Ren, T., & de Boer, E. Electrically evoked otoacoustic emissions from apical and basal perilymphatic electrode positions in the guinea pig cochlea. *Hearing Research*, *152*: 77–89, 2001.

O'Connell, B. P., Holder, J. T., Dwyer, R. T., Gifford, R. H., Noble, J. H., Bennett, M. L., … Labadie, R. F. Intra- and postoperative electrocochleography may be predictive of final electrode position and postoperative hearing preservation. *Frontiers in Neuroscience*, *11*: 1–12, 2017.

Page, J. C., Cox, M. D., Hollowoa, B., Bonilla-Velez, J., Trinidade, A., & Dornhoffer, J. L. Trends in Intraoperative Testing during Cochlear Implantation. *Otology and Neurotology*, *39*(3): 294–298, 2018.

Palmer, A. R., & Russell, I. J. Phase-locking in the cochlear nerve of the guinea-pig and its relation to the receptor potential of inner hair-cells. *Hearing Research*, *24*(1): 1–15, 1986.

Prentiss, S., Sykes, K., & Staecker, H. Partial Deafness Cochlear Implantation at the University of Kansas: Techniques and Outcomes. *Journal of the American Academy of Audiology*, *21*(3): 197–203, 2010.

Ren, T., Guo, M., He, W., Miller, J. M., & Nuttall, A. L. Electrically evoked auditory nerve responses in the cochlea with normal outer hair cells. *Journal of Otology*, *4*(2): 71–75, 2009.

Ren, T., & Nuttall, A. L. Extracochlear electrically evoked otoacoustic emissions: a model for in vivo assessment of outer hair cell electromotility. *Hearing Research*, *92*: 178–183, 1995.

Ren, T., & Nuttall, A. L. Acoustical modulation of electrically evoked otoacoustic emission in intact gerbil cochlea. *Hearing Research*, *120*(1–2): 7–16, 1998.

Ren, T., Nuttall, A. L., & Miller, J. M. Electrically evoked cubic distortion product otoacoustic emissions from gerbil cochlea. *Hearing Research*, *102*(1–2): 43–50, 1996.

Revuelta, M., Santaolalla, F., Arteaga, O., Alvarez, A., Sánchez-del-Rey, A., & Hilario, E. Recent advances in cochlear hair cell regeneration—A promising opportunity for the treatment of age-related hearing loss. *Ageing Research Reviews*, *36*: 149–155, 2017.

Rey, H. G., Pedreira, C., & Quian Quiroga, R. Past, present and future of spike sorting techniques. *Brain Research Bulletin*, *119*: 106–117, 2015.

Riggs, W. J., Roche, J. P., Giardina, C. K., Harris, M. S., Bastian, Z. J., Fontenot, T. E., … Fitzpatrick, D. C. Intraoperative Electrocochleographic Characteristics of Auditory Neuropathy Spectrum Disorder in Cochlear Implant Subjects. *Frontiers in Neuroscience*, *11*(416): 1–16, 2017.

Robles, L., & Ruggero, M. A. Mechanics of the mammalian cochlea. *Physiological Reviews*, *81*(3): 1305–1352, 2001.

Roddy, J., Hubbard, A. E., Mountain, D. C., & Xue, S. Effects of electrical biasing on electrically-evoked otoacoustic emissions. *Hearing Research*, *73*(2): 148–154, 1994.

Roland, P. S., & Tobey, E. A tribute to a remarkably sound solution. *Cell*, *154*(6): 1175–1177, 2013.

Russell, I. J., Cody, A. R., & Richardson, G. P. The responses of inner and outer hair cells in the basal turn of the guinea-pig cochlea and in the mouse cochlea grown in vitro. *Hearing Research*, *22*: 199–216, 1986.

Sampaio, A. L. L., Araújo, M. F. S., & Oliveira, C. A. C. P. New Criteria of Indication and Selection of Patients to Cochlear Implant. *International Journal of Otolaryngology*, *2011*: 1–13, 2011.

Santos-Sacchi, J. Asymmetry in Voltage-Dependent Movements of Isolated Outer Hair Cells from the Organ of Corti. *The Journal of Neuroscience*, 1989.

Saoji, A. A., Koka, K., Litvak, L. M., & Finley, C. C. Pure-Tone Masking Patterns for Monopolar and Phantom Electrical Stimulation in Cochlear Implants. *Ear and Hearing*, *39*(1): 124–130, 2018.

Sato, M., Baumhoff, P., & Kral, A. Cochlear Implant Stimulation of a Hearing Ear Generates Separate Electrophonic and Electroneural Responses. *Journal of Neuroscience*, *36*(1): 54–64, 2016.

Sato, M., Baumhoff, P., Tillein, J., & Kral, A. Physiological Mechanisms in Combined Electric–Acoustic Stimulation. *Otology & Neurotology*, *38*(8): e215–e223, 2017.

Schnupp, J. W. H., Garcia-Lazaro, J. A., & Lesica, N. A. Periodotopy in the gerbil inferior colliculus: local clustering rather than a gradient map. *Frontiers in Neural Circuits*, *9*(37):, 2015.

Seligman, P., & McDermott, H. Architecture of the spectra 22 speech processor. *Annals of Otology, Rhinology and Laryngology*, *104*(suppl. 166): 139–141, 1995.

Semmelbauer, S., Böhnke, F., & Müller, J. M. Influence of a cochlea implant electrode on the traveling wave propagation. *AIP Conference Proceedings*, *1965*:, 2018.

Shannon, R. V. Multichannel electrical stimulation of the auditory nerve in man. I. Basic psychophysics. *Hearing Research*, *11*(2): 157–189, 1983.

Shannon, R. V. Threshold and loudness functions for pulsatile stimulation of cochlear implants. *Hearing Research*, *18*(2): 135–143, 1985.

Shehata, W. E., Brownell, W. E., & Dieler, R. Effects of salicylate on shape, electromotility and membrane characteristics of isolated outer hair cells from Guinea pig cochlea. *Acta Oto-Laryngologica*, *111*(3): 707–718, 1991.

Shepherd, R. K., Hatsushika, S., & Clark, G. M. Electrical stimulation of the auditory nerve: The effect of electrode position on neural excitation. *Hearing Research*, *66*(1): 108–120, 1993.

Shepherd, R. K., & Javel, E. Electrical stimulation of the auditory nerve. I. Correlation of physiological responses with cochlear status. *Hearing Research*, *108*(1–2): 112–144, 1997.

Shepherd, R. K., & Javel, E. Electrical stimulation of the auditory nerve: II. Effect of stimulus waveshape on single fibre response properties. *Hearing Research*, *130*(1–2): 171–188, 1999.

Skarzynski, P. H., Lorens, A., Piotrowska, A., & Anderson, I. Partial deafness cochlear implantation provides benefit to a new population of individuals with hearing loss. *Acta Oto-Laryngologica*, *126*(9): 934–940, 2006.

Skarzynski, P. H., Lorens, A., Piotrowska, A., & Anderson, I. Preservation of low frequency hearing in partial deafness cochlear implantation (PDCI) using the round window surgical approach. *Acta Oto-Laryngologica*, *127*(1): 41–48, 2007.

Skarzynski, P. H., Lorens, A., Zgoda, M., Piotrowska, A., & Szkielkowska, A. Atraumatic round window deep insertion of cochlear electrodes. *Acta Oto-Laryngologica*, *131*(7): 740–749, 2011.

Snyder, R. L., Bierer, J. A., & Middlebrooks, J. C. Topographic spread of inferior colliculus activation in response to acoustic and intracochlear electric stimulation. *JARO - Journal of the Association for Research in Otolaryngology*, *5*(3): 305–322, 2004.

Snyder, R. L., Middlebrooks, J. C., & Bonham, B. H. Cochlear implant electrode configuration effects on activation threshold and tonotopic selectivity. *Hearing Research*, *235*(1–2): 23–38, 2008.

Snyder, R. L., Rebscher, S. J., Leake, P. A., Kelly, K., & Cao, K. Chronic intracochlear electrical stimulation in the neonatally deafened cat. I: Expansion of central representation. *Hearing Research*, *50*(1–2): 7–33, 1990.

Stronks, H. C., Versnel, H., Prijs, V. F., Grolman, W., & Klis, S. F. L. Effects of electrical stimulation on the acoustically evoked auditory-nerve response in guinea pigs with a high-frequency hearing loss. *Hearing Research*, *272*: 95–107, 2011.

Stronks, H. C., Versnel, H., Prijs, V. F., & Klis, S. F. L. Suppression of the acoustically evoked auditory-nerve response by electrical stimulation in the cochlea of the guinea pig. *Hearing Research*, *259*: 64–74, 2010.

Stypulkowski, P. H. Mechanisms of salicylate ototoxicity. *Hearing Research*, *46*: 113–145, 1990.

Stypulkowski, P. H., & van den Honert, C. Physiological properties of the electrically stimulated auditory nerve. I. Compound action potential recordings. *Hearing Research*, *14*(3): 205–223, 1984.

Talbot, K. N., & Hartley, D. E. H. Combined electro-acoustic stimulation: A beneficial union? *Clinical Otolaryngology*, *33*(6): 536–545, 2008.

Tang, Q., Benítez, R., & Zeng, F. G. Spatial channel interactions in cochlear implants. *Journal of Neural Engineering*, *8*(4):, 2011.

The Ear Foundation Cochlear implants. 2016.

Tillein, J., Hartmann, R., & Kral, A. Electric-acoustic interactions in the hearing cochlea: Single fiber recordings. *Hearing Research*, *322*: 112–126, 2015.

Tunstall, M. J., Gale, J. E., & Ashmore, J. F. Action of salicylate on membrane capacitance of outer hair cells from the guinea-pig cochlea. *The Journal of Physiology*, *485*(3): 739–752, 1995.

Turner, C. W., Gantz, B. J., Vidal, C., Behrens, A., & Henry, B. A. Speech recognition in noise for cochlear implant listeners: Benefits of residual acoustic hearing. *The Journal of the Acoustical Society of America*, *115*(4): 1729–1735, 2004.

Turner, C. W., Reiss, L. A. J., & Gantz, B. J. Combined acoustic and electric hearing: Preserving residual acoustic hearing. *Hearing Research*, *242*(1–2): 164–171, 2008.

United Nations *World Aging Population 2017*, *United Nations New York*2017.

van den Honert, C., & Stypulkowski, P. H. Physiological properties of the electrically stimulated auditory nerve. II. Single fiber recordings. *Hearing Research*, *14*(3): 225–243, 1984.

Von Ilberg, C., Baumann, U., Kiefer, J., Tillein, J., & Adunka, O. F. Electric-acoustic stimulation of the auditory system: A review of the first decade. *Audiology and Neurotology*, *16*(SUPPL. 2): 1–30, 2011.

Von Ilberg, C., Kiefer, J., Tillein, J., Pfenningdorff, T., Hartmann, R., Stürzebecher, E., & Klinke, R. Electric-acoustic stimulation of the auditory system. New technology for severe hearing loss. *Orl*, *61*(6): 334–340, 1999.

Wada, H., Sugawara, M., Kobayashi, T., Hozawa, K., & Takasaka, T. Measurement of guinea pig basilar membrane using computer-aided three- dimensional reconstruction system. *Hearing Research*, *120*: 1–6, 1998.

Wilson, B. S., & Dorman, M. F. Cochlear implants: A remarkable past and a brilliant future. *Hearing Research*, *242*(1–2): 3–21, 2008.

Wilson, B. S., Finley, C. C., Lawson, D. T., Wolford, R. D., Eddington, D. K., & Rabinowitz, W. M. Better speech recognition with cochlear implants. *Letters to Nature*, *352*: 236–238, 1991.

World Health Organization *Multi-country assessment of national capacity to provide hearing care*, 2013.

Xue, S., Mountain, D. C., & Hubbard, A. E. Acoustic enhancement of electrically-evoked otoacoustic emissions reflects basilar membrane tuning: Experiment results. *Hearing Research*, *70*(1): 121–126, 1993.

Xue, S., Mountain, D. C., & Hubbard, A. E. Acoustic enhancement of electrically evoked otoacoustic emissions reflects basilar membrane tuning: a model. *Hearing Research*, *91*: 93–100, 1995.

Yates, G. K., & Kirk, D. L. Cochlear electrically evoked emissions modulated by mechanical transduction channels. *The Journal of Neuroscience : The Official Journal of the Society for Neuroscience*, *18*(6): 1996–2003, 1998.

Zahnert, T. The Differential Diagnosis of Hearing Loss. *Deutsches Ärzteblatt International*, *108*(25): 433–445, 2011.

Zheng, J., Shen, W., He, D. Z. Z., Long, K. B., Madison, L. D., & Dallos, P. Prestin, the motor protein of outer hair cells. *Nature*, *405*: 149–155, 2000.

Zwicker, E. A model for predicting masking--period patterns. *Biological Cybernetics*, *23*(1): 49–60, 1976.